Coden: JPLPAY
Volume 9, Part A-2, No. 10, October 1971

Journal of Polymer Science

Part A-2: Polymer Physics

Contents

Published by INTERSCIENCE PUBLISHERS a division of John Wiley & Sons, Inc.

Journal of Polymer Science **Part A-2: Polymer Physics**

The Journal of Polymer Science is published in four sections as follows: Part A-1, Polymer Chemistry, monthly; Part A-2, Polymer Physics, monthly; Part B, Polymer Letters, monthly; Part C, Polymer Symposia, irregular.

Published monthly by Interscience Publishers, a Division of John Wiley & Sons, Inc., covering one volume annually. Publication Office at 20th and Northampton Sts., Easton, Pa. 18042. Executive, Editorial, and Circulation Offices at 605 Third Avenue, New York, N.Y. 10016. Second-class postage paid at Easton, Pa. Subscription price, $325.00 per volume (including Parts A-1, B, and C). Foreign postage $15.00 per volume (including Parts A-1, B, and C).

JOURNAL OF POLYMER SCIENCE: PART A-2 VOL. 9, 1729–1745 (1971)

Radiation Chemistry of Poly(propylene Oxide)

G. P. ROBERTS* and M. BUDZOL, *Department of Chemistry and Materials Research Center, Northwestern University, Evanston, Illinois 60201* and MALCOLM DOLE,† *Department of Chemistry, Baylor University, Waco, Texas 76703*

Synopsis

Atactic, isotactic, and optically active poly(propylene oxides), PPOx, were irradiated with both γ-rays and electron beams. Up to a dose of 37 Mrad no change could be detected in the optical activity. G values for hydrogen evolution decreased as compared to polypropylene in about the same ratio as $G(H_2)$ of polyoxymethylene decreased as compared to polyethylene. G values for crosslinking and scission, estimated by means of gelation theories of Saito and Inokuti, were found to be greater for isotactic than for atactic PPOx. The behavior of transient infrared and ultraviolet absorption bands is discussed. Intrinsic viscosity data indicate a rapid initial chain degradation whereas CO gas and OH group production is linear with dose. Evidence for the conversion of one type of free radical to another on heating an irradiated sample from 77°K to room temperature is based on the behavior of transient infrared and ultraviolet absorption bands.

Poly(propylene oxide), which we shall designate as PPOx, can be synthesized in the atactic, isotactic, and optically active forms. As far as we are aware no study of the radiation chemistry of PPOx has hitherto been carried out. PPOx is interesting because it bears the same chemical relationship to polypropylene (PP) as polyoxymethylene (POM) does to polyethylene (PE). PP[1–4] and PE have both been studied radiologically by one of us and collaborators[5] and POM primarily by Fischer and Langbein[6] and by Neiman et al.[7]

EXPERIMENTAL

Materials

Propylene oxide was polymerized by the method of Furukawa et al.[8] Unfortunately, our centrifugal method for removing catalyst residues failed to remove all of the zinc from the isotactic sample. The zinc residue as zinc oxide was found by ignition to be 5.8% zinc in the isotactic sample, but only 0.2% zinc in the atactic. Therefore, it was decided to repurify the iso-

* Present address: Uniroyal, Inc., Chemical Division, Naugatuck, Connecticut 06770.

† To whom inquiries should be addressed.

tactic PPOx, but this decision was not made until some radiological experiments had been done on part of it. The purification procedure consisted of the following steps. The polymer was dissolved in benzene to make a 1–2% solution and the zinc impurity extracted by shaking with an equal volume of 10% aqueous hydrochloric acid. An aliquot of the aqueous layer was tested for zinc by making it alkaline and shaking with a carbon tetrachloride solution of dithizone to form the purple-red dithizonate of zinc. It was found that six to eight aqueous HCl extractions were necessary to remove all of the zinc. Actually, twelve extractions were used, and the benzene–polymer solution was washed five times with distilled water to remove acid before freeze drying from the benzene solution. This repurification process reduced the intrinsic viscosity between 10 and 15%.

The stability of the pure isotactic PPOx to light during a period of one month was studied by measuring the intrinsic viscosity of a sample stored uncovered on the laboratory bench and one stored in the dark, both in the presence of air. After 35 days the intrinsic viscosity of the uncovered sample had decreased from 3.28 to 2.15 dl./g, while that of the sample stored in the dark remained unchanged. As a result of these studies the PPOx samples were stored in the dark and *in vacuo*. Before the radiolysis studies were made on the isotactic PPOx, all of the samples were combined into one benzene solution, thoroughly mixed, and then freeze-dried. This was done to insure that all the samples used had the same average molecular weight initially. The weight-average molecular weight was estimated from eq. (1) of Allen, Booth, and Jones[9]

$$[\eta] = 1.12 \times 10^{-4} \bar{M}_v^{0.77} \tag{1}$$

valid for benzene solutions of PPOx at 25°C, to be 1.34×10^6 g/mole. The atactic molecular weights, two different samples, were 1.90×10^6 and 1.93×10^6.

Some optically active PPOx was prepared by the method of Shieh and Price,[10] but modified slightly. The resulting polymer had an intrinsic viscosity of 4.77 dl. g^{-1} and an optical activity, $[\alpha]_D^{25}$ equal to +18° in a 0.291% benzene solution. Inasmuch as no effect of the radiation on optical activity was observed, the details of the synthetic work will not be described here.

The gel and intrinsic viscosity studies were carried out on bulk PPOx as freeze-dried, but the spectroscopic observations required that the PPOx be prepared in a film form. The spinning technique of Kellö and Tkáč[11] was used to produce the films from a 1% solution of the polymer in spectral grade CCl_4. The film was spun on nickel mesh, 100 lines/in., 75% maximum transmission. In the spectroscopic calculations it is necessary to know only the ratio of the weight of the film to area. This weight to area ratio was measured using the infrared absorption bands at 2970, 935, and 835 cm^{-1}, as the absorption of these bands was found to be linear with the weight to area ratio. Absolute calibration was performed by measuring

the absorption of a known weight of film spun on a sodium chloride plate of known area.

As estimated approximately from the intensity of the 1016 cm^{-1} infrared band, the crystallinity of the PPOx in the spun film was calculated by the method of Hendus and Schnell[12] to be about 36%. Allen et al.[13] found that PPOx insoluble in methanol at 0°C had a density of 1.057 g/cm^3, from which a weight fraction of crystallinity equal to 39% can be calculated from their values of the density of amorphous and crystalline PPOx (1.002 and 1.157 g/cm^3, respectively). The maximum melting point of their sample of PPOx was 68°C and the glass transition temperature −75°C. Allen et al.[13] prepared their PPOx also by the catalytic method of Furukawa et al.[8]

Intrinsic Viscosity Measurements

Viscosity measurements were made by using an Ubbelohde inverted meniscus viscometer having a design similar to that of Desreux and Bischoff,[14] but modified in the case of the isotactic PPOx measurements so that an inert gas atmosphere was in contact with the dilute benzene solution of the PPOx. Kinetic energy corrections were applied and the intrinsic viscosity was calculated by a computer routine which averaged the values of both $(\eta_{rel} - 1)/c$ and $(\ln \eta_{rel})/c$ extrapolated to zero concentration. The curves used for the extrapolations were linear with concentration at least up to 0.16 g/dl.

A log–log plot was made of the intrinsic viscosity and slopes of the reduced viscosity versus concentration curves, in other words, a Huggins[15]

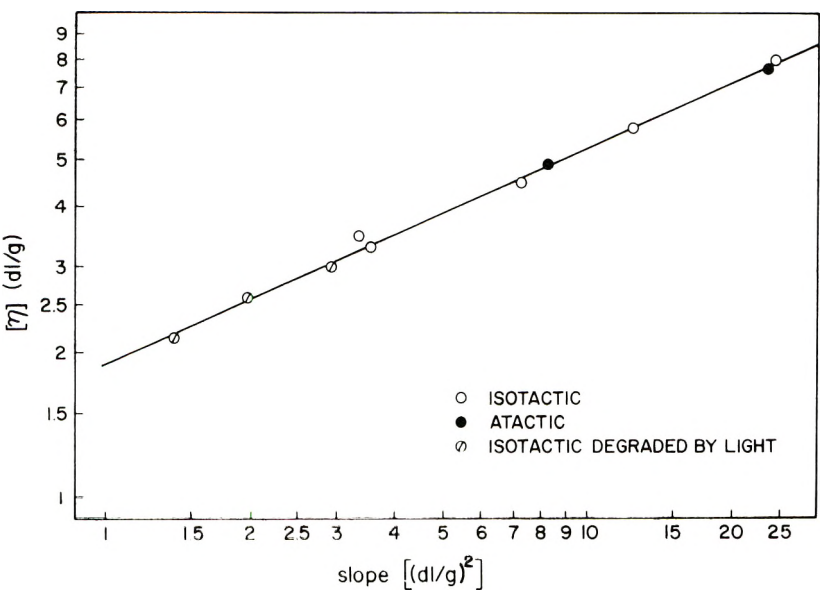

Fig. 1. Log plot of intrinsic viscosity slope of the reduced viscosity–concentration curves.

plot, for both the isotactic and atactic samples as well as the isotactic material degraded by light. All points fell on the same straight line (see Fig. 1) with a slope of 2.2, fairly close to the required Huggins slope of 2.0. However, the intrinsic viscosity of the irradiated PPOx samples did not agree with the relationship of Figure 1.

Irradiation Cells and Techniques

Both ^{60}Co γ-rays and electron beams were used for the irradiations, the γ-irradiation for the bulk samples and the electron beam for the films. The electron-beam dosimetry was accomplished by using thin films of PE at room temperature and measuring the rate of vinyl decay as a function of irradiation time. The G value for vinyl group disappearance had previously been determined by using ^{60}Co γ-rays whose dosimetry had been based on the Fricke dosimeter. For the irradiations at liquid nitrogen temperature in the combined irradiation-spectroscopic cell[16] the radiation rate was 34.5 Mrad/hr. The radiation intensity of the ^{60}Co source was measured by means of the Fricke dosimeter and varied from about 0.1 Mrad/hr before the source was restocked with fresh ^{60}Co to 0.9 Mrad/hr after restocking. These values were for 1962 and 1963, respectively; in the most recent work done in 1967 the dose rate was 0.4 Mrad/hr when the sample tubes were supported in channels cut into a solid copper block. All irradiations were carried out *in vacuo*.

In the case of the isotactic samples but not in the case of the atactic, free radicals could be detected by ESR measurements in the samples after the room temperature irradiations. To eliminate these free radicals be-

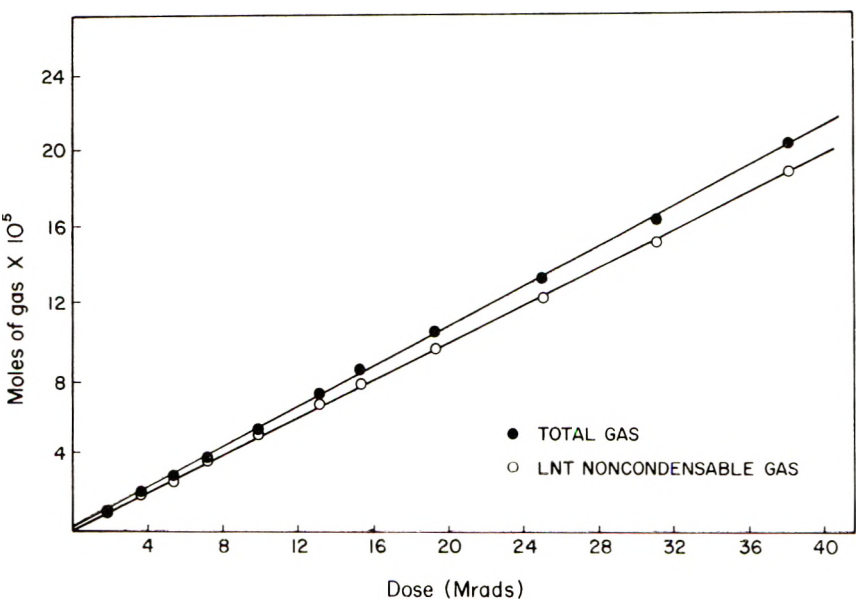

Fig. 2. Gas evolution as a function of dose.

fore exposing the samples to air, they were annealed at 58°C for 1/2 hr. This treatment effectively removed all of the free radicals.

Gas Measurement Techniques

Gas evolution studies were carried out on about 4 g of sample contained in a tube with a mercury manometer and a break-off seal so that samples could be taken for analysis in a Consolidated Electrodynamics 21–130 analytical mass spectrometer. The fraction of gas uncondensable at 77°K was determined by measurement with a Toepler pump. It was found that the evolution of gas was linear with dose at least up to 40 Mrad (Fig. 2).

Gel Studies

Benzene was used as a solvent at room temperature to extract the soluble fractions of the irradiated samples. In the case of the isotactic samples the extractions were performed in an atmosphere of helium to prevent degradation of the polymer during extraction. The irradiated samples were held in 200-mesh screen wire baskets made of stainless steel during the extractions. Although platinum mesh baskets are preferred[17], they were not used in this research. The samples were extracted for 24 hr, dried in a vacuum desiccator for 24 hr and then weighed. This process was repeated until a constant weight of gel was obtained. The same technique was used for the atactic samples, except that they were not extracted in an atmosphere of helium.

Spectroscopic Techniques

For the infrared measurements a polymer film was prepared on a sodium chloride plate by the spinning technique mentioned above, and then irradiated by electron beams in vacuum. The infrared spectrum of sodium chloride is not affected by the irradiation in the range of wave lengths of interest in this research. The spectra of both the isotactic and atactic samples agreed well with those of Kawasaki et al.[18] Most of the spectroscopic studies were carried out on films that had been deposited on nickel mesh.

ESR measurements were made on samples in quartz tubes with a Varian Model V 4500 spectrometer equipped with a Model V4560 100 kilocycle field-modulation and control unit. The tubes were annealed as previously described[5] after the irradiations to remove the ESR signals produced in the quartz by the irradiation.

The optical rotation of chloroform solutions of irradiated and unirradiated optically active isotactic PPOx were carried out using a Rudolph photoelectric spectropolarimeter. The irradiated sample was irradiated to a dose of 37.8 Mrad slightly less than the dose to the gel point and dissolved in chloroform to make a 0.3% solution. The specific optical rotations

were measured at 500 and 589 nm of both the irradiated sample and of an unirradiated control.

RESULTS AND INTERPRETATIONS

Gas Yields

Evolution of gas from both atactic and isotactic PPOx was linear with dose up to at least 40 Mrad, which is considerably beyond the dose to the gel point, at least in the case of atactic PPOx. The G values for hydrogen production were rather small, however. Table I compares $G(H_2)$ for PE, POM, atactic and isotactic PP, and PPOx.

TABLE I
G Values for Gases at Room Temperature

	Atactic		Isotactic			
	PPOx	PP[a]	PPOx	PP[a]	POM[b]	PE[c]
$G(H_2)$	0.97	2.34	1.12	2.78	1.7	3.7
$G(CH_4)$	0.06	0.10	0.07	0.07		
$G(CO)$	0.25		0.41		0.01	

[a] Data of Schnabel and Dole.[2]
[b] Data of Fischer and Langbein.[6]
[c] Data of Kang et al.[19]

The total amount of gas produced in the PPOx, which was condensable at 77°K, was equivalent to a G value of only 0.13 for the atactic and 0.12 for the isotactic samples. As the condensable gas was only 10% of the total, it was not studied further.

A qualitative study of the data of Table I reveals the following interesting correlations. The hydrogen yields from the isotactic PPOx and PP are slightly more than their atactic counterparts. Attachment of a methyl group to a linear chain reduces the hydrogen yields, even though in the case of the analogous pair POM and PPOx, POM contains less hydrogen per gram than the PPOx. It is interesting that the following ratios are roughly similar, $G(H_2)_{PPOx}/G(H_2)_{POM} = 0.66$ and $G(H_2)_{PP}/G(H_2)_{PE} = 0.75$ (isotactic samples in each case). Another correlation is to be seen in the effect of introducing oxygen into the chain in the reduction of the hydrogen yield; thus, $G(H_2)_{POM}/G(H_2)_{PE} = 0.47$, $G(H_2)_{PPOx}/G(H_2)_{PP} = 0.40$ (isotactic), and $G(H_2)_{PPOx}/G(H_2)_{PP} = 0.41$ (atactic). In the case of polyethylene, the reaction (1) has been suggested[2] as one source of the hydrogen:

$$-CH_2\overset{+}{C}H_2- \rightarrow H_2 + -CH{=}\overset{+}{C}H- \quad (trans)$$
$$\Delta E = -0.145 \text{ eV} \qquad (1)$$

This reaction could not occur in the case of POM. Schnabel and Dole[2] also pointed out that reactions similar to (1) in the case of PP were either

endothermic or only barely exothermic and thus less likely to occur than in the case of PE. With oxygen in the chain in the case of PPOx there would be even less likelihood of double-bond formation.

Turning now to the liberation of methane, it is interesting to note that the G values for methane liberation are the same in the case of isotactic PPOx and PP and nearly the same in the case of the atactic polymers. Because the concentration of methyl groups in units of moles per gram in PPOx is 0.72 that of the methyl group concentration in PP, one would expect $G(CH_4)$ to be that much less in PPOx. This is approximately the case for the atactic PPOx in comparison to the atactic PP.

The significant yield of carbon monoxide indicates an appreciable amount of chain scission. This will be discussed later in connection with estimates of chain scission from gel measurements. Rather surprisingly $G(CO)$ for PPOx was considerably greater than $G(CO)$ for POM.

Infrared and Ultraviolet Spectroscopic Data

By studying the changes in the infrared absorption band at 3480 cm^{-1} and using the extinction coefficient of 54 l./mole-cm given by Cross, Richards and Willis[20] it was possible to demonstrate that the amount of hydroxyl group grew linearly with the dose up to at least 200 Mrad and resulted in $G(OH)$ values at room temperature of 1.9 for isotactic PPOx and 1.8 for atactic. Fischer and Langbein[6] found $G(OH)$ to be 4.7 for POM; hence a large $G(OH)$ is not unusual for polymers containing oxygen in the chain. Fischer and Langbein explained the formation of $-OH$ by means of the reactions (2) and (3).

$$—CH_2OCH_2O— \rightarrow —CH_2O\cdot + \cdot CH_2O— \quad (2)$$

$$—CH_2O\cdot + \cdot CH_2O— + 2\ —OCH_2O— \rightarrow —CH_2OH + CH_3O— + 2—O\dot{C}HO— \quad (3)$$

Similarly in the case of PPOx we can write the reactions (4) and (5):

$$—O\overset{\displaystyle CH_3}{\underset{\displaystyle H}{C}}CH_2O\overset{\displaystyle CH_3}{\underset{\displaystyle H}{C}}CH_2— \rightarrow —O\overset{\displaystyle CH_3}{\underset{\displaystyle H}{C}}CH_2\cdot + \cdot O\overset{\displaystyle CH_3}{\underset{\displaystyle H}{C}}CH_2— \quad (4)$$

$$—O\overset{\displaystyle CH_3}{\underset{\displaystyle H}{C}}CH_2\cdot + \cdot O\overset{\displaystyle CH_3}{\underset{\displaystyle H}{C}}CH_2— + 2\ —O\overset{\displaystyle CH_3}{\underset{\displaystyle H}{C}}CH_2— \rightarrow —O\overset{\displaystyle CH_3}{\underset{\displaystyle H}{C}}CH_3 + CH_3CHOHCH_2— + 2\ —O\overset{\displaystyle CH_3}{\underset{\displaystyle }{C}}CH_2— \quad (5)$$

If this sequence of reactions is correct, then the G value for scissions should be at least equal to $G(OH)$. This point will be discussed later.

Carbonyl group formation at room temperature was investigated by observing the absorption band at 1730 cm^{-1}. However, no significant changes were observed. In the case of the isotactic PPOx the 1730 cm^{-1}

absorption band decreased slightly and then rose slightly with dose. The initial concentration was 3×10^{-4} mole/g. The COC stretching band at 1038 cm^{-1} and the CH_3 bending band at 1382 cm^{-1} both increased considerably on annealing at room temperature overnight after irradiation at 77°K although the original irradiation caused the first to decrease. These band intensities relative to their original intensities before irradiation are given in Table II.

TABLE II
Infrared Band Intensities of Isotactic Poly(propylene Oxide) Relative to Intensity before Irradiation[a]

Wave number of band, cm^{-1}	Band assignment[b]	Immediately after irradiation		After post-irradiation annealing	
		31.6 Mrad	63.2 Mrad	31.6 Mrad	63.2 Mrad
1038	COC stretch	0.86	0.83	1.14	1.26
1382	CH_3 bending	1.38	1.31	1.47	1.50

[a] All measurements and irradiations at 77°K.
[b] Data of Kawasaki et al.[18]

Both of these bands are crystallinity sensitive. Probably, the annealing increased the crystallinity of the samples although postirradiation annealing in the case of a highly crystalline PE decreased the crystallinity.[21] The difference between the two polymers may have been due to the low initial crystallinity of the spun-cast films of the PPOx. The enhancement of the crystallinity on annealing is also very probably promoted by the reduction of the average molecular weight (see below) on irradiation. Such a phenomenon has been previously postulated in the case of Teflon by Licht and Kline[22] and Bernier et al.[23]

Of more interest was our observation of a hitherto unobserved infrared band at 1210 cm^{-1} observed at 77°K in isotactic PPOx irradiated at 77°K. This band grows linearly with dose, (Fig. 3).

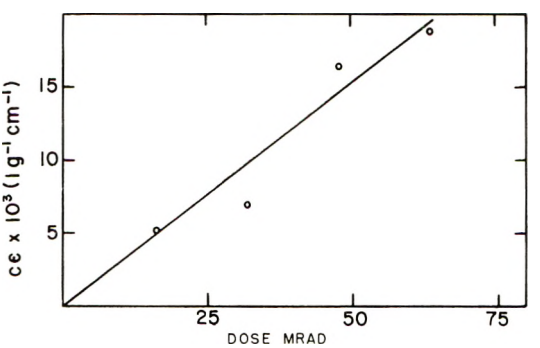

Fig. 3. Growth of the infrared absorption band in isotactic PPOx at 1210 cm^{-1} with dose. Irradiations and measurements at 77°K. The ordinate is the product of the concentration and extinction coefficient.

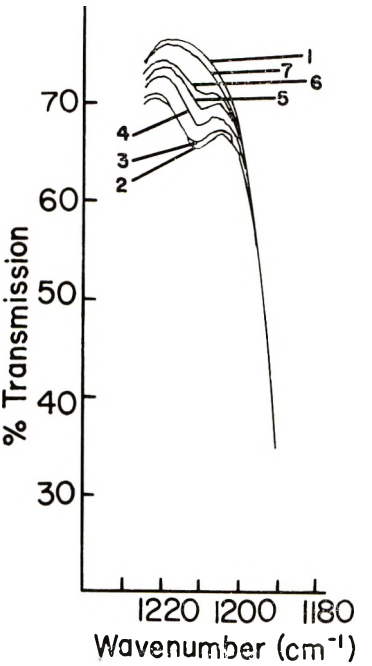

Fig. 4. Effect of postirradiation heat treatment on the intensity of the 1210 cm^{-1} infrared absorption band in isotactic PPOx after a dose of 63.2 Mrad at 77°K: (*1*) before the irradiation; (*2*) immediately after the irradiation at 77°K; (*3,4,5,6,7*) after heating slowly to −160, −120, −80, −40, or 0°C and immediately recooling to 77°K.

The effect of postirradiation heat treatment on the intensity of the band is illustrated in Figure 4. One interesting aspect of the data of Figure 4 is that this transient begins to disappear even before the glass transition temperature of PPOx, −75°C is attained. The band at 1210 cm^{-1} was not seen in atactic PPOx even after a dose of 94.8 Mrad; hence it must have been produced by some transient species in the crystalline regions of the isotactic PPOx. The discussion of the species responsible for this band is given below.

A similar phenomenon of a transient species is seen in the ultraviolet spectrum of isotactic PPOx illustrated in Figure 5. In this case the atactic PPOx behaved similarly. Although there was no change in the spectrum of PPOx from 250 to 2600 nm on irradiation at 77°K, the absorption band at about 286 nm grew as the sample irradiated to 63.2 Mrad was heated from 77°K to room temperature. The absorption reached a peak at 0°C of almost twice its initial value and then gradually decreased on standing at room temperature until after 48 hr it was down to 1.39 of its initial value.

A tentative assignment of the infrared transient at 1210 cm^{-1} may be made to the $-CH_2C(CH_3)HO\cdot$ free radical, and the 286 nm ultraviolet band may be assigned to the $-CH_2\dot{C}(CH_3)OH$ free radical to which the

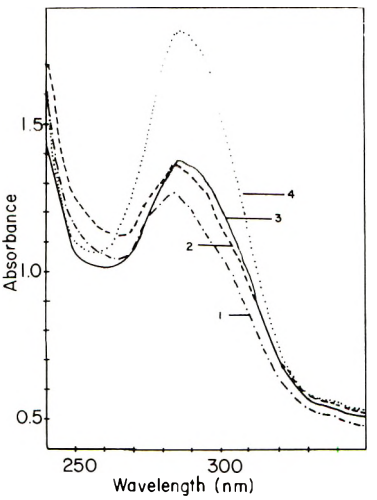

Fig. 5. Effect of postirradiation heat treatment on the intensity of the 286 nm band in the ultraviolet spectrum of isotactic PPOx irradiated to 63.2 Mrad at 77°K: (1) immediately after the irradiation at 77°K; curves (2,3,4) after heating slowly to −120, −40, or 0°C and recooling to 77°K.

former is converted by hydrogen atom migration as the sample is heated from 77°K to room temperature. A few preliminary ESR studies were made which showed that at 77°K the free radicals present consisted probably of a singlet and triplet. The triplet could have been the $-OC-(CH_3)HCH_2\cdot$ free radical. In the case of the atactic PPOx the ESR spectrum was a broad triplet; its decay rate at the temperature of solid CO_2 was found to be first-order with a half life of 14.8 hr.* More ESR work needs to be done to obtain quantitative decay data at different temperatures and to confirm, if possible, the free-radical structures suggested above.

Intrinsic Viscosity

The intrinsic viscosity of atactic PPOx decreased rapidly on irradiation, attained a minimum and then began to rise as the gel point was approached (Fig. 6). That of the isotactic PPOx decreased slightly more rapidly with dose. Geymer[24] has pointed out that if the irradiated polymer samples, specifically PP in his case, were exposed to air after the irradiation while the polymer still contained trapped radicals, oxidation followed by chain scission occurred with a pronounced drop in $[\eta]$ with dose. In the case of the data of Figure 6, the isotactic samples were annealed as mentioned above at 58°C for 30 min before exposure to air to remove the trapped free radicals which ESR measurements showed were absent in the irradiated atactic samples. An experiment using Geymer's technique of quenching the free radicals was tried in which the irradiated isotactic

* These experiments were performed by Dr. Pang-Nan Lee.

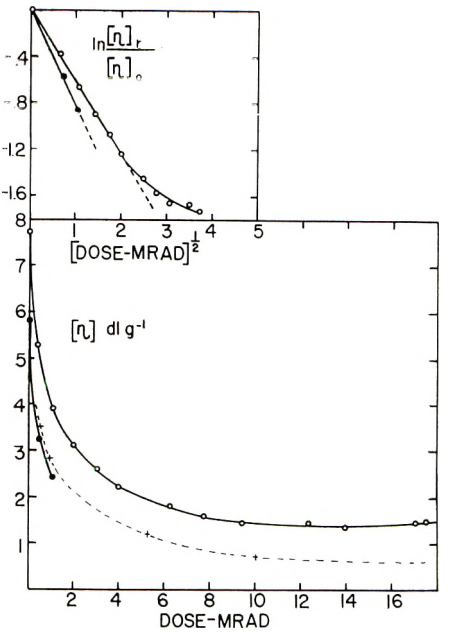

Fig. 6. Intrinsic viscosity of (○) atactic and (●) isotactic PPOx as a function of dose. The upper figure illustrates $\ln[\eta]_0/[\eta]_r$ values as a function of the square root of the dose.

sample was exposed to CH_3SH vapor at 1 atm pressure for 24 hr after a dose of 1.09 Mrad at room temperature and before exposure to air. The intrinsic viscosity was 2.30 dl/g, compared to 2.44 dl/g for a sample irradiated to 1.07 Mrad and annealed at 58°C for 30 min. Thus, the methyl mercaptan treatment did not eliminate the marked reduction in the intrinsic viscosity on irradiation.

In the upper part of Figure 6 is plotted $\ln [\eta]/[\eta]_0$ as a function of the square root of the dose; it can be seen that the relation is linear up to a dose of about 4 Mrad, i.e., over a dose range in which $[\eta]$ decreased by a factor of 3.3. In the case of PP, Keyser et al.[3] also found the $\ln [\eta] \propto r^{1/2}$ relationship to be valid with the curve for the isotactic PP having a steeper slope than that of the atactic. The slopes of the PPOx curves are about twice as great as those for PP.

If one ignores crosslinking, a plot can be made of $\bar{M}_v^{-1}$ versus the dose, and an idea of $G(S)$ obtained. From the initial linear portion of the curve, $G(S)$ was estimated in the case of isotactic PPOx to be $1.4b$, where b is $\bar{M}_w/\bar{M}_n$ (this assumes that $\bar{M}_v$ equals $\bar{M}_w$: the viscosity equation of Allen et al.[9] was calibrated in terms of $\bar{M}_w$).

For a constant slope of the plot of $\ln [\eta]/[\eta]_r$ versus dose, it was shown[3] that $G(X)$ must approximate $G(S)/2b$. If this is true, then the exact calculation of $G(S)$ from the slope of the $\bar{M}_v^{-1}$ dose plot should yield $1.4b\text{-}[1\text{-}(1/2b)]^{-1}$ instead of $1.4b$ when crosslinking is taken into account. Interpretation of the viscosity data is also complicated by the effect of the

chain branching produced by crosslinking on the intrinsic viscosity. An indication that this latter effect is important is seen in the fact that the viscosity of the irradiated PPOx samples did not follow the Huggins plot shown in Figure 1, whereas the viscosity of thermally degraded samples did.

Interpretation of the Gel Data

In radiation-chemical studies of polymers it is important to determine the dose r_g to the point of incipient gelation, i.e., to the gel point. If no degradation due to the irradiation occurs, and if the crosslinking G value, $G(X)$, is constant with dose, then $G(X)$ is readily calculated. However, as we have seen above, considerable degradation of the PPOx occurred during the irradiation. Furthermore, the interpretation of the data is complicated by a significant change with dose of $G(S)$, the G value for chain scissions, as will be demonstrated below. One important parameter, $\lambda = G(S)/G(X)$, can be evaluated rather unambiguously by extrapolation of the data to infinite dose.

TABLE III
Numerical Values Deduced from Gel Data for PPOx in Figures 7 and 8

	Atactic polymer	Isotactic polymer
r_g, Mrad	17.8	42.5
g_{max}	0.75	0.71
λ	1.5	1.64
b	3.0	5.05
y_g	0.281	0.266
$\bar{M}_{w,0}$	1.9×10^6	1.32×10^6
$\bar{M}_{w,t}$	1.86×10^5	3.62×10^4
$[\eta]_r/[\eta]$ at r_g dl/g	0.19	0.075
$[\eta]$ at r_g dl/g	1.5	0.44
$[\eta]$ corrected	1.65	0.46
$G(X)$	0.145	0.31
$G(S)$	0.22	0.51

The actually measured gel fractions are illustrated in Figure 7, where it can be seen that r_g for the isotactic sample is more than twice that of the atactic. More significantly, the product $r_g\bar{M}_{w,0}$ of the isotactic PPOx is 50% greater than that of the atactic. The various parameters deduced from the gel data are collected in Table III. The dose to the gel point and the limiting gel fraction at infinite dose were estimated two ways; r_g was obtained from a large-scale plot of the data of Figure 7 and by an extrapolation of the Charlesby-Pinner function, $s + s^{1/2}$, where s is the sol fraction, to the value 2, its value at the gel point. The maximum gel fraction, g_{max}, was estimated by plotting g versus r^{-1} and extrapolating to $r^{-1} = 0$.

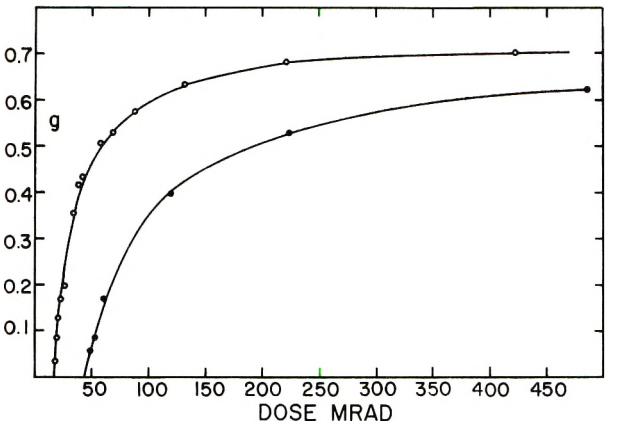

Fig. 7. Gel fractions as a function of dose for (○) atactic PPOx and (●) isotactic PPOx.

Another way of obtaining g_{max} is to extrapolate the function $s + s^{1/2}$ to infinite dose, at which point it is equal to $\lambda/2$; and then g_{max} can be calculated[25] from eq. (6):

$$g_{max} = (1/2)[1 - \lambda + (1 + 2\lambda)^{1/2}] \tag{6}$$

which is valid for any initial molecular weight distribution.

Charlesby and Pinner[26] some years ago derived the useful equation

$$s + s^{1/2} = G(S)/2G(X) + 100\, N_A/r2M_{n,0}G(X) \tag{7}$$

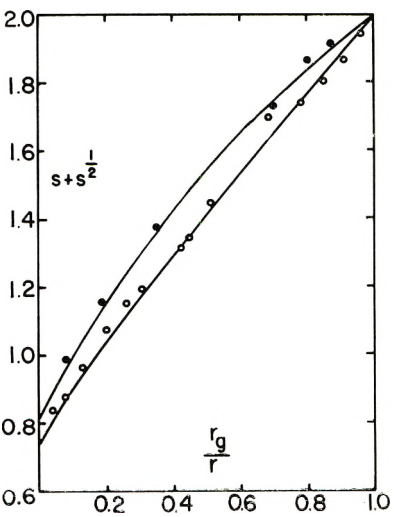

Fig. 8. Dimensionless Charlesby-Pinner plot for (○) atactic and (●) isotactic PPOx: (——) calculated from Inokuti's theory[25] for the atactic sample and from Saito's theory[27] for the isotactic sample.

in which N_A is Avogadro's number and the other symbols have been defined. In dimensionless units, eq. (7) can be written

$$s + s^{1/2} = (\lambda/2) + [2 - (\lambda/2)](r_g/r) \tag{8}$$

In Figure 8, $s + s^{1/2}$ is plotted as a function of r_g/r for both atactic and isotactic PPOx. Such a plot should eliminate any differences due to different molecular weights. Charlesby and Pinner derived eq. (7) for the case of a random initial molecular weight distribution; i.e., $b = 2$. However, the relation is not quite verified for the PPOx samples, in contrast[2] to PP.

The solid lines are theoretical curves calculated for the atactic sample on the basis of Inokuti's gel theory,[25] b and λ being taken equal to 3.0 and 1.5, respectively, while the theoretical curve for the isotactic sample, which shows greater curvature than that for the atactic, is based on the theory of Saito[27] with the parameters b and λ equal to 5.05 and 1.64, respectively. Excellent agreement is seen to exist; actually either theory could be applied to either curve, but the best agreement is obtained using the theories as described above. Table III includes values of y_g, the number of crosslinks at the gel point per initial number-average molecule, as taken from the tables of Inokuti and Saito for the λ and b parameters given above. If $G(S)$ and $G(X)$ were constant with dose, then $G(X)$ could be easily calculated from y_g and r_g.

A possible method of estimating $G(X)$ would be to calculate the value of $\bar{M}_w$ the PPOx would have at the gel point, denoted by $\bar{M}_{w,t}$, if only scissions and no crosslinking occurred. This theoretical $\bar{M}_{w,t}$ could then be used to calculate $G(X)$ from eq. (9):

$$G(X) = 4.82 \times 10^5/r_g\bar{M}_{w,t} \tag{9}$$

where r_g is in units of Mrad. To estimate $\bar{M}_{w,t}$, use has been made of the tables of intrinsic viscosities calculated by Katsuura[28] as a function of λ, radiation dose, and exponent α of the Mark-Houwink viscosity equation, eq. (1). Katsuura gives values of the ratio of the intrinsic viscosity after irradiation to that before the irradiation, $[\eta]_r/[\eta]_0$, both with and without the consideration of branching. From Table III, it can be seen that the measured intrinsic viscosity ratio at the gel point was only 0.19 in the case of the atactic PPOx and even smaller (0.075) in the case of the isotactic sample. Unfortunately, Katsuura carried his calculations only to λ = 7.0, and the lowest viscosity ratio calculated was 0.222 (for α = 0.8). This fact demonstrates that our initial λ must have been much greater than the final λ which was only about 1.5 (Table III). Katsuura's calculations were based on the assumption of an initial generalized Poisson distribution. Although the initial molecular weight distribution in our PPOx was probably not a Poisson distribution, by the time that the gel point was reached, it must have been close to this distribution because of the agreement of the gel data with the calculated Charlesby-Pinner function based on the Poisson distribution (Fig. 8). Katsuura's calculations show

that the ratio of the intrinsic viscosity of the unbranched molecules to that of the branched is greater, the greater the crosslinking and the less the chain scission. By a rather long and uncertain extrapolation of Katsuura's data we estimated that the intrinsic viscosities at the gel point should be raised by a factor of 1.11 in the case of the atactic PPOx and by a factor of 1.05 in the case of the isotactic in order to correct for the effect of branching on the intrinsic viscosity values. It is due to the extensive radiolytic degradation that these correction factors are so low.

With the above correction, $\bar{M}_w$ for the atactic sample was then estimated from eq. (1) to be 2.59×10^5. But this molecular weight had to be corrected for its increase due to crosslinking which had occurred during the irradiation up to the gel point. Inasmuch as the curve fitting of Figure 8 required b to be 3.0 for atactic PPOx, 2.59×10^5 was divided by 3.0 to obtain $\bar{M}_n$ at the gel point. From Inokuti's table[25] the crosslinks per initial number-average molecule for the values of λ and b required for the curve fitting of Figure 8 were obtained. This number was added to the number of molecules per gram at the gel point, after a series of successive approximations, and $\bar{M}_n$ was then recalculated. Multiplying this new value of $\bar{M}_n$ by 3 gave the desired value of $\bar{M}_{w,t}$. By inserting the latter into eq. (9), $G(X)$ for the atactic sample was found to be 0.15. A similar treatment yielded 0.31 for the isotactic PPOx. Multiplying each of these results by their respective λ values, gave 0.22 and 0.51 for the $G(S)$ values of the atactic and isotactic PPOx, respectively. These numbers are the same order of magnitude as the $G(CO)$ values, namely 0.25 and 0.41, respectively. However, they do not agree with the large $G(OH)$ values, 1.8 and 1.9 for the atactic and isotactic samples, respectively. At present we do not know how to resolve this discrepancy. These G values for crosslinking and scission are given in Table III.

Effect of the Irradiation on Optically Active Isotactic PPOx

It was thought that perhaps the radiation might cause racemization of solid optically active PPOx to occur. Table IV compares the optical activity of the unirradiated PPOx with that of a sample irradiated to a dose of 37.8 Mrad, just short of the gel-point dose. As can be seen from the data no significant change in the optical activity occurred. After a dose of 37.8 Mrad and assuming a $G(S)$ value of 0.50 there is only one

TABLE IV
Optical Rotations of Irradiated and Unirradiated Poly(propylene Oxide) in Chloroform

	Unirradiated (0.00301 g/ml)	Irradiated (0.00308 g/ml)
α_D^{25}	−0.058°	−0.060°
α_{5000nm}^{25}	−0.081°	−0.089°
$[\alpha]_D^{25}$	−19.3°	−19.5°
$[\alpha]_{5000nm}^{25}$	−26.9°	−28.9°

fracture per 862 repeating units; hence it is not certain that such a small fraction of fractures would measurably affect the optical activity.

Mechanisms and Material Balance

Although crosslinking could occur without the evolution of hydrogen by the mechanism demonstrated by Fischer and Langbein[6] in the case of POM, eqs. (2) and (3) given above plus the coupling of two free radicals formed, nevertheless, one would expect the evolution of hydrogen to result either in a crosslink (or an intramolecular link) or a double bond. Unfortunately, no double bonds were detected by means of the infrared spectra, but the double bond absorption bands may have been hidden by other bands. Hydrogen may also have come from the decomposition of excited $CH_2\overset{*}{O}$ split out of the main chain. From photochemical studies[29] formaldehyde is known to yield H_2 and CO on photolysis with light of wave-length shorter than 3130 Å. In this way the significant yield of CO can be explained as well as the production of H_2 without the formation of crosslinks or double bonds. However this could not be the only mechanism for H_2 formation, otherwise $G(H_2)$ would be equal to $G(CO)$.

The large yield of OH groups is difficult to explain. The yield was approximately linear with dose as was the yield of gases. For this reason the apparent large initial $G(S)$ value could not have been responsible in the main for either CO or OH group production. If the chain end $\cdot OCH(CH_3)CH_2-$ rearranged to $\cdot C(OH)(CH_3)CH_2-$ and then recombined, the OH group yield could have increased without a concomitant increase in $G(S)$.

This research was supported by the U.S. Atomic Energy Commission, first at Northwestern University and then at Baylor University, and by income from the chair in Chemistry at Baylor University endowed by a gift from The Robert A. Welch Foundation. We are also indebted for support provided by the Advanced Research Projects Agency of the Department of Defense through the Northwestern University Materials Research Center.

References

1. M. Dole and W. Schnabel, *J. Polym. Sci.*, **54**, S29 (1961).
2. W. Schnabel and M. Dole, *J. Phys. Chem.*, **67**, 295 (1963).
3. R. W. Keyser, B. Glegg, and M. Dole, *J. Phys. Chem.*, **67**, 300 (1963).
4. M. Inokuti and M. Dole, *J. Polym. Sci. A*, **1**, 3289 (1963).
5. D. C. Waterman and M. Dole, *J. Phys. Chem.*, **74**, 1913 (1970).
6. H. Fischer and W. Langbein, *Kolloid Z.* **216–217**, 329 (1967).
7. M. Neiman, T. S. Fedoseyeva, G. I. Chubarova, A. L. Buchachenko, and Ya. S. Lebedev, *Polym. Sci. USSR*, **5**, 421 (1964).
8. J. Furukawa, T. Tsuruta, T. Saegusa, and G. Kakogawa, *J. Polym. Sci.* **36**, 541 (1959); *Makromol. Chem.*, **36**, 25 (1959).
9. G. Allen, C. Booth, and M. N. Jones, *Polymer*, **5**, 195 (1964).
10. N. Shieh and C. C. Price, *J. Org. Chem.*, **24**, 1169 (1959).
11. V. Kellö and A. Tkáč, *Chem. Zvesti*, **7**, 129 (1953).
12. H. Hendus and G. Schnell, *Kunststoffe*, **51**, 69 (1961).

13. G. Allen, C. Booth, M. N. Jones, D. J. Marks, and W. D. Taylor, *Polymer*, **5**, 547 (1964).
14. V. Desreux and J. Bischoff, *Bull. Soc. Chim. Belges*, **59**, 93 (1950).
15. M. L. Huggins, *J. Amer. Chem. Soc.*, **64**, 2716 (1942).
16. M. Dole and G. G. A. Böhm, "Radiation Chemistry—II" (*Advan. Chem. Ser.*, No. **82**), American Chemical Society, Washington, D.C., 1968, p. 525.
17. M. Budzol and M. Dole, *J. Phys. Chem.*, **75**, 1671 (1971).
18. A. Kawasaki, J. Furukawa, T. Tsuruta, T. Saegusa, G. Kakogawa, and R. Sakata, *Polymer*, **1**, 315 (1960).
19. H. Y. Kang, O. Saito, and M. Dole, *J. Amer. Chem. Soc.*, **89**, 1980 (1967).
20. L. H. Cross, R. B. Richards, and H. A. Willis, *Discussions Faraday Soc.*, **9**, 235 (1950).
21. F. Williams, H. Matsuo, and M. Dole, *J. Amer. Chem. Soc.*, **80**, 2595 (1958).
22. W. R. Licht and D. E. Kline, *J. Polym. Sci. A-2*, **4**, 313 (1966).
23. G. A. Bernier, D. E. Kline, and J. A. Sauer, *J. Macromol. Sci.* **B1**, 335 (1967).
24. D. O. Geymer, *Makromol. Chem.*, **100**, 186 (1967).
25. M. Inokuti, *J. Chem. Phys.*, **38**, 2999 (1963).
26. A. Charlesby and S. H. Pinner, *Proc. Roy. Soc.* (London) **A249**, 367 (1959).
27. O. Saito, H. Y. Kang, and M. Dole, *J. Chem. Phys.*, **46**, 3607 (1967).
28. K. Katsuura, *Introduction to Radiation Chemistry*, Vol. II, A. Amemiya, Ed., Maruzen, Tokyo, 1962, p. 631 (in Japanese).
29. J. G. Calvert and J. N. Pitts, Jr., *Photochemistry*, Wiley, New York, 1966, p. 369.

Received December 21, 1970
Revised March 11, 1971

JOURNAL OF POLYMER SCIENCE: PART A-2 VOL. 9, 1747–1761 (1971)

Scattering of Light by Disordered Spherulites. II. Effect of Disorder in the Magnitude of the Anisotropy

T. HASHIMOTO and R. S. STEIN,* *Polymer Research Institute and Department of Chemistry, University of Massachusetts, Amherst, Massachusetts 01002*

Synopsis

The contribution to the disorder scattering by imperfect spherulites resulting from fluctuations in the magnitude of the anisotropy is analyzed for two-dimensional spherulites. The fluctuations are described in terms of a parameter characterizing the mean-square amplitude of the fluctuation and a correlation function describing the distance over which the correlation occurs. Cases considered are those where the correlation depends on either the radial or the angular separation of the scattering volume elements. As with the case of disorder in orientation, one finds that disorder in anisotropy may result in a nonzero value of intensity at $\mu = 0°$ and 90°, a decrease in the higher-order variation of scattered intensity with θ, and an increase in the intensity of scattering at higher values of θ over that for a perfect spherulite. In addition, disorder in the angular direction leads to an increase in the scattered intensity at small values of θ as compared with the zero intensity of scattering from a perfect spherulite at $\theta = 0°$.

INTRODUCTION

In part I of this work,[1] the scattering of light from a disordered two-dimensional spherulite was analyzed where the anisotropy $\delta = \alpha_1 - \alpha_2$ of the scattering volume element was held constant but the orientation of its optic axis vector **a** was allowed to deviate from its average orientation angle β_0 with respect to the spherulite radius. In this part we shall consider the consequences of holding the optic axis orientation angle β constant at β_0 but allowing the magnitude of the anisotropy to fluctuate from its average value δ_0.

THE CALCULATION

For a two-dimensional spherulite of radius R lying in a plane perpendicular to the incident light beam with scattering optic axes lying in the plane of the spherulite and at a constant angle β_0 to the radius (Fig. 1), the amplitude of H_V scattering is given by[1,2]

$$E_{HV} = \frac{1}{2} C_2 \cos \rho_2 \int_{r=0}^{R} \int_{\alpha=0}^{2\pi} \delta(r,\alpha)(\cos 2\beta_0 \sin 2\alpha + \sin 2\beta_0 \cos 2\alpha) \times \cos k(\mathbf{r}\cdot\mathbf{s}) d\alpha r dr \quad (1)$$

* To whom correspondence should be sent.

The term C_2 is a combination of physical constants whose value is immaterial to these considerations and is related to C of Part I[1] by $C = C_2\delta$, the terms α and r are the circular coordinates of the scattering volume, while the angle ρ_2 is a function of the scattering angles θ and μ defined by

$$\cos \rho_2 = \cos \theta / [\cos^2\theta + \sin^2\theta \sin^2\mu]^{1/2} \tag{2}$$

It is to be noted that at large values of the scattering θ, H_V and V_V do not strictly represent cases of crossed and parallel polarizers but require somewhat different values of the polarization angles as discussed by Prins et al.[3]

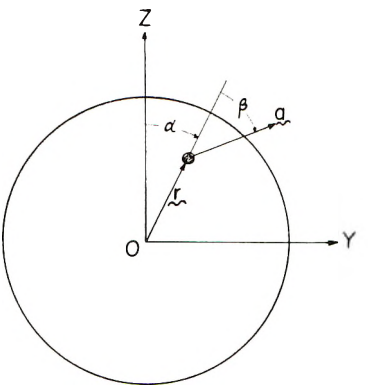

Fig. 1. Coordinates of the scattering element in a two-dimensional spherulite.

As in Part I, k denotes $2\pi/\lambda$, λ is the wavelength in the medium, and $\mathbf{s}$ is equal to $\mathbf{s}_0 - \mathbf{s}_1$ where $\mathbf{s}_0$ and $\mathbf{s}_1$ are unit incident and scattered ray vectors. The anisotropy $\delta(r,\alpha)$ must be included within the integral because it is a function of position in the disordered spherulite. As in Part I, we shall use the correlation function technique to evaluate the scattered intensity, which involves squaring eq. (1) prior to integration. Since the general case would lead to a four-fold integral whose numerical evaluation would be prohibitive, we shall consider only special cases where $\delta(r,\alpha)$ is a function of α or of r only, but not of both together.

CASE OF RADIAL DISORDER

If $\delta(r,\alpha)$ only varies with r but not α, eq. (1) may be integrated over α to give

$$E_{HV} = C_2\pi \cos \rho_2 \sin 2\xi_0 \int_{r=0}^{R} \delta(r) J_2(x) r dr \tag{3}$$

where

$$\xi_0 = \mu + \beta_0$$

$$x = kr \sin \theta$$

and $J_2(x)$ is the second-order Bessel function of x. Therefore, upon squaring, and introducing Poynting's vector to obtain the intensity, one obtains

$$I_{HV} = K \cos^2\rho_2 \sin^2 2\xi_0 \int_{r_1=0}^{R} \int_{r_2=0}^{R} \delta(r_1)\delta(r_2)J_2(x_2)J_2(x_1)r_1r_2dr_1dr_2 \quad (4)$$

where $K = C_2^2\pi c'/4$ and c' is the velocity of light. We shall now consider $\delta(r_i)$ to fluctuate from its average value by an amount $\Delta(r_i)$ defined by

$$\delta(r_i) = \delta_0 + \Delta(r_i) \quad (5)$$

Then, we have

$$\langle\delta(r_1)\delta(r_2)\rangle_{r_{12}} = \delta_0^2 + 2\delta_0\langle\Delta(r_1)\rangle + \langle\Delta(r_1)\Delta(r_2)\rangle_{r_{12}} \quad (6)$$

where the average is found at constant $r_{12} = r_2 - r_1$. Now, since positive and negative fluctuations are equally probable, it follows that

$$\langle\Delta(r_1)\rangle_{r_{12}} = 0 \quad (7)$$

Let us define a correlation function of anisotropy like that introduced by Stein and Wilson[4]

$$\Psi_r(r_{12}) = \langle\Delta(r_1)\Delta(r_2)\rangle_{r_{12}}/\langle[\Delta(r_1)]^2\rangle_{av} \quad (8)$$

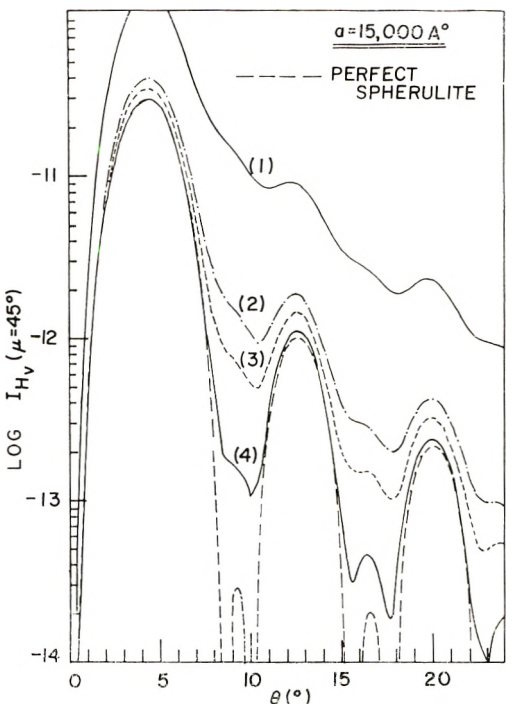

Fig. 2. Calculated variation of H_v scattered intensity with θ at $\mu = 45°$ for 2 mμ spherulites having radial disorder correlation distance of a = 15,000 Å and λ = 364 mμ and values of $\langle[\Delta(r_i)]^2\rangle_{av}/\delta_0^2]$ of (*1*) 1×10^{-3}, (*2*) 1×10^{-4} (*3*) 5×10^{-5}, and (*4*) 1×10^{-5}.

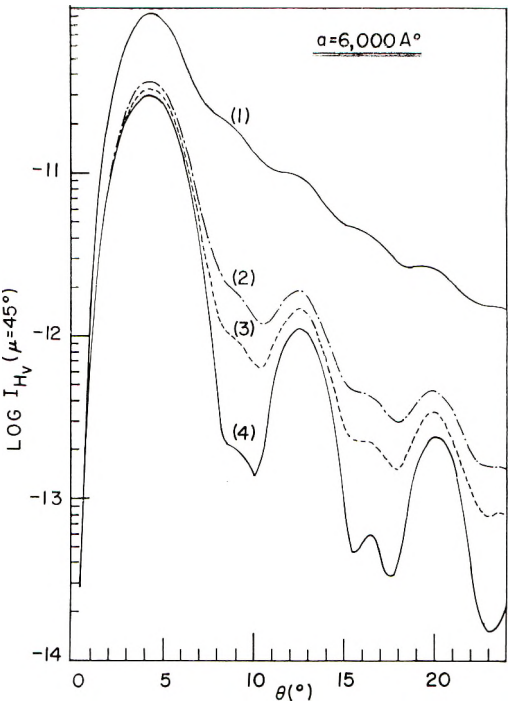

Fig. 3. Calculated variation of H_v scattered intensity for the case of Fig. 2 for a = 6000 Å. Values of $\langle[\Delta(r_i)]^2\rangle_{av}/\delta_0^2$ are (*1*) 1×10^{-3}, (*2*) 1×10^{-4}, (*3*) 5×10^{-5}, and (*4*) 1×10^{-5}.

Then eq. (4) becomes

$$I_{H_v} = K \cos^2\rho_2 \sin^2 2\xi_0\delta_0^2 \left\{ \int_{r_1=0}^{R} \int_{r_2=0}^{R} J_2(x_1)J_2(x_2)r_1r_2dr_1dr_2 + \frac{\langle[\Delta(r_i)]^2\rangle_{av}}{\delta_0^2} \int_{r_1=0}^{R} \int_{r_2=0}^{R} \Psi_r(r_{12})J_2(x_1)J_2(x_2)r_1r_2dr_1dr_2 \right\} \quad (9)$$

The first term represents the scattering from a perfect spherulite, whereas the second term represents the excess scattering from the anisotropy fluctuations. Thus

$$I_{H_v} = K \cos^2 \rho_2 \sin^2 2\xi_0\delta_0^2 \left\{ \frac{R^4}{w^4} [2 - 2J_0(w) - wJ_1(w)]^2 + \frac{\langle(\Delta(r_i))^2\rangle_{av}}{\delta_0^2} \int_{r_2=0}^{\infty} \int_{r_1=0}^{\infty} \Psi_r(r_{12})J_2(x_1)J_2(x_2)r_1r_2dr_1dr_2 \right\} \quad (10)$$

where

$$w = kR \sin\theta$$

As in Part I, an exponential correlation function is assumed, of the form

$$\Psi_r(r_{12}) = e^{-|r_{12}|/a} \quad (11)$$

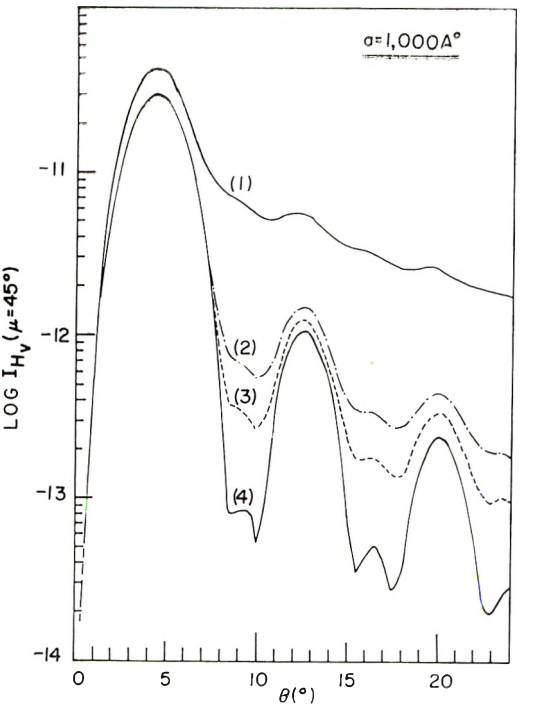

Fig. 4. Calculated variation of H_v scattered intensity for the case of Fig. 2 for a = 1000 Å. Values of $\langle[\Delta(r_t)]^2\rangle_{av}/\delta_0^2$ are (*1*) 1×10^{-3}, (*2*) 1×10^{-4}, (*3*) 5×10^{-5}, and (*4*) 1×10^{-5}.

where a is a radial correlation distance of anisotropy disorder. The integral in the second term of eq. (10) is identical with that appearing in Part I for radial disorder of orientation so that the results of the numerical integrations of that part may be employed here.

Numerical results have been obtained for $\beta_0 = 90°$ (or 0°), $R = 3\ \mu$, $\lambda = 364$ mμ, and for $a = 1000$ Å, 6000 Å, and 15,000 Å. The arbitrary constant in the scattering intensity equation is chosen such that $K\delta_0^2 = 10^5$ for convenience in plotting. The absolute value of the scattered intensity is not pertinent to the considerations of this paper. A plot of the H_v intensity at $\mu = 45°$ is given in Figure 2 for $a = 15{,}000$ Å and $\langle(\Delta r_t)^2\rangle/\delta_0^2$ of 0, 1×10^{-5}, 5×10^{-5}, 1×10^{-4}, and 1×10^{-3}. It is seen that with an increasing amplitude of anisotropy fluctuation, the fine structure of the higher-order intensity variation with θ is lost, and also there is an increasing intensity of scattering at larger values of θ. The even-order intensity maxima tend to smear out while the odd-order maxima tend to be broadened and enhanced in intensity.

As with orientation fluctuations in the radial direction, the zero intensity at $\theta = 0$ which arises from the angular symmetry is preserved. The intensity varies with $\sin^2 2\xi_0$ so that the variation of intensity with the azimuthal angle μ characteristic of a perfect spherulite remains.

Plots of the variation of the scattered H_v intensity at $\mu = 45°$ for a variety of values of $\langle[\Delta(r_i)]^2\rangle/\delta_0^3$ are given in Figure 3 for $a = 6000$ Å and Figure 4 for $a = 1000$ Å. It is noted that as the correlation distance becomes shorter, the build-up of intensity at larger scattering angles becomes greater.

CASE OF ANGULAR DISORDER

In this case, $\delta(r,\alpha)$ only varies with α but not r, so that eq. (1) may be integrated over r to give

$$E_{H_v} = \frac{1}{2} C_2 \cos \rho_2 R^2 \int_{\alpha=0}^{2\pi} \delta(\alpha) \sin (2\alpha + 2\beta_0) f(\gamma) d\alpha \tag{12}$$

where $\gamma = \alpha - \mu$ and

$$f(\gamma) = \frac{\cos (w \cos \gamma) - 1}{(w \cos \gamma)^2} + \frac{\sin (w \cos \gamma)}{(w \cos \gamma)} \tag{13}$$

Thus, if $\beta_0 = 0^0$ or 90^0

$$I_{H_v} = \frac{K \cos^2 \rho_2 R_4}{4\pi^2} \int_{\alpha_1=0}^{2\pi} \int_{\alpha_2=0}^{2\pi} \delta(\alpha_1)\delta(\alpha_2) \sin 2\alpha_1 \sin 2\alpha_2 f(\gamma_1) f(\gamma_2) d\alpha_1 d\alpha_2 \tag{14}$$

If, as in Part I, we assume that $\langle\delta(\alpha_1)\delta(\alpha_2)\rangle_{\alpha_1,\alpha_2}$ depends only upon the angular separation of the scattering elements and is random, and we define a fluctuation in $\delta(\alpha)$ by

$$\delta(\alpha_i) = \delta_0 + \Delta(\alpha_i) \tag{15}$$

so that

$$\langle\delta(\alpha_1)\delta(\alpha_2)\rangle]_{\alpha_1,\alpha_2} = \delta_0^2 + \langle\Delta(\alpha_1)\Delta(\alpha_2)\rangle_{\alpha_{12}} \tag{16}$$

where $\alpha_{12} = \alpha_2 - \alpha_1$, then we may define an angular correlation function

$$\Psi_\alpha(\alpha_{12}) = \langle\Delta(\alpha_1)\Delta(\alpha_2)\rangle_{\alpha_{12}}/\langle[\Delta(\alpha_1)]^2\rangle_{av} \tag{17}$$

so that eq. (14) becomes, as shown in Part I

$$I_{H_v} = \frac{1}{4} K \cos^2 \rho_2 R^4 \delta_0^2 \left\{\frac{1}{w^4} [2 - 2J_0(w) - wJ_1(w)]^2 \sin^2 2\mu + \frac{\langle[\Delta(\alpha_1)]^2\rangle_{av}}{\delta_0^2} [\sin^2 2\mu g_1 + \cos^2 2\mu g_2]\right\} \tag{18}$$

where

$$g_1 = \int_{\gamma_2=0}^{2\pi} \int_{\gamma_1=0}^{2\pi} \Psi_\alpha(\gamma_{12}) \cos 2\gamma_1 \cos 2\gamma_2 f(\gamma_1) f(\gamma_2) d\gamma_1 d\gamma_2 \tag{19}$$

and

$$\mathcal{I}_2 = \int_{\gamma_2=0}^{2\pi} \int_{\alpha_1=0}^{2\pi} \Psi_\alpha(\gamma_{12}) \sin 2\gamma_1 \sin 2\gamma_2 f(\gamma_1) f(\gamma_2) d\gamma_1 d\gamma_2 \qquad (20)$$

where

$$\gamma_{12} = \gamma_2 - \gamma_1 = \alpha_{12}$$

The angular correlation function may be represented by an exponential function

$$\Psi(\alpha_{12}) = e^{-|\alpha_{12}|/c} \qquad (21)$$

where $|\alpha_{12}|$ is the absolute value of α_{12} with the additional restriction that if $\alpha_{12} > 180°$, $\Psi_\alpha(\alpha_{12}) = \Psi_\alpha(\alpha_{12} - 180°)$.

The results of the numerical calculations of Part I may then be used. A calculated variation of I_{H_v} with θ at $\mu = 45°$ is given in Figure 5 for a 3 μ spherulite and $\lambda = 364$ mμ for $c = 0.7\pi$ and various values of $\langle[\Delta(\alpha_i)]^2\rangle/\delta_0^2$. The arbitrary constant is so chosen that $K\delta_0^2R^4/4\pi^2 = 10^5$. Similar plots are given in Figure 6 for $\langle[\Delta(\alpha_i)]^2\rangle_{av}/\delta_0^2 = 5 \times 10^{-3}$ and $c = \pi$, 0.7π, and 0.5π. It is evident from the figures that angular disorder produces a

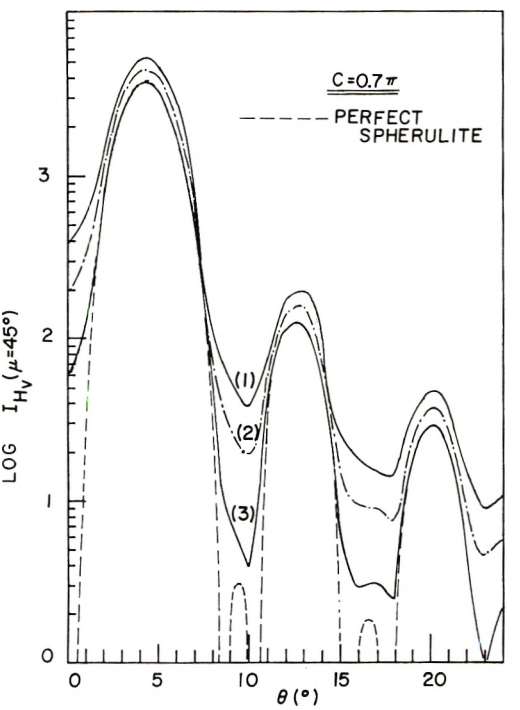

Fig. 5. Calculated variation of H_v scattered intensity with θ at $\mu = 45°$ for 3 μ spherulites having angular disorder with $c = 0.7\ \pi$ radians and $\lambda = 364$ mμ and various values of $\langle[\Delta(\alpha_i)]^2\rangle_{av}/\delta_0^2$. Values of $\langle[\Delta(\alpha_i)]^2\rangle/\delta_0^2$ are (*1*) 1×10^{-2}, (*2*) 5×10^{-3}, and (*3*) 1×10^{-3}.

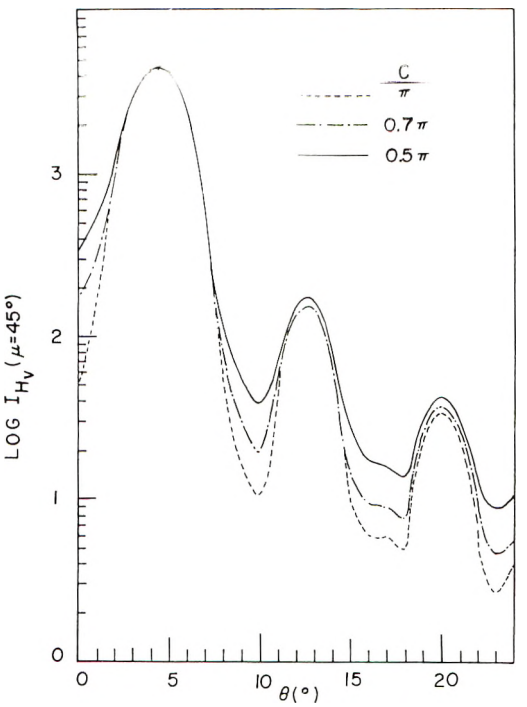

Fig. 6. Calculated variation of H_v scattered intensity for the case of Fig. 5 for $\langle[\Delta(\alpha_t)]^2\rangle_{av}/\delta_0^2 = 5 \times 10^{-3}$ and $c = \pi$, $0.7\ \pi$ and $0.5\ \pi$ radians.

somewhat similar effect as does radial disorder, with the higher-order maxima and minima becoming more diffuse with an increase in the mean-square amplitude of the anisotropy fluctuation $\langle[\Delta(\alpha_t)]^2\rangle_{av}/\delta_0^2$, and with a decrease in the correlation distance c. An important difference between the effects of radial and angular disorder is that with angular disorder, there is an increasing intensity at angles less than that of the maximum intensity θ_{max}, with increasing amplitudes or decreasing correlation distances whereas this region is not much affected by radial disorder. On the other hand, the intensity at angles greater than θ_{max} is more affected by radial disorder.

While the azimuthal dependence of H_v intensity is not affected by radial disorder of anisotropy, so that the intensity remains zero at $\mu = 0^0$ and $\mu = 90°$ (for $\beta_0 = 0°$ or $90°$), there is an appreciable effect on this μ dependence due to angular disorder of anisotropy. Thus, it is possible to distinguish between such radial and angular disorder from an examination of this μ dependence. It is noted that radial disorder of orientation of optic axes does affect the μ dependence of scattered intensity in contrast to the effects of radial disorder in the magnitude of the anisotropy.

The effect of angular disorder in anisotropy is demonstrated in the contour diagrams in Figures 7*a*, 7*b*, and 7*c*, where a perfect spherulite is compared with disordered spherulites having angular correlation distances of 0.7π radian and mean-square fluctuations of anisotropy characterized by

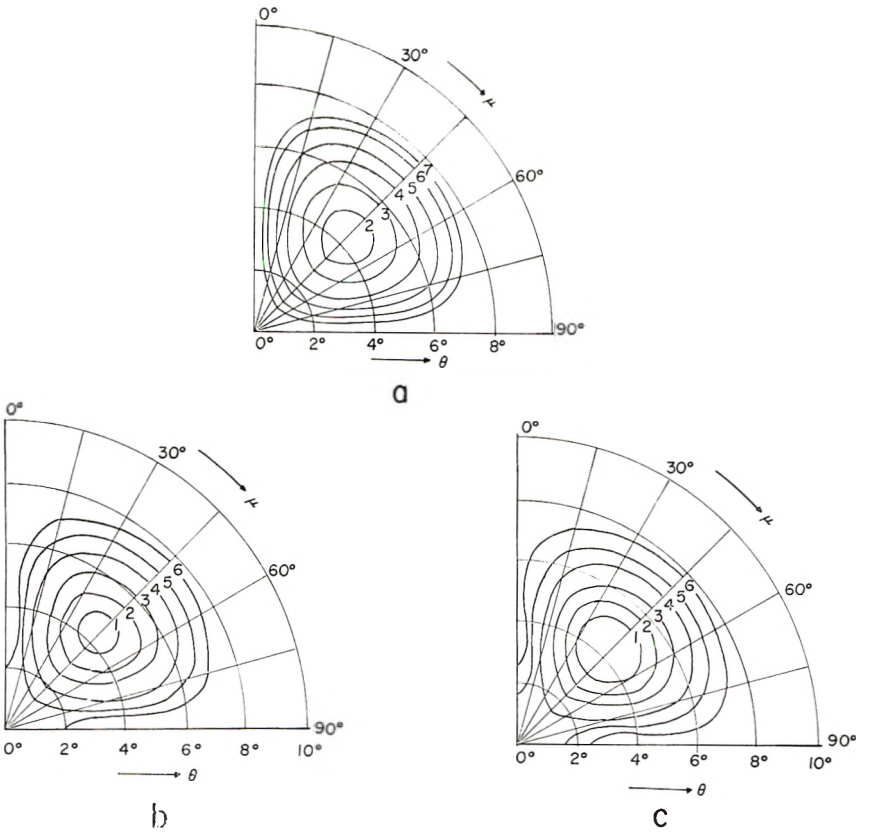

Fig. 7. Intensity contour diagrams for H_v scattering for a 3 μ spherulite with angular disorder in the magnitude of the anisotropy characterized by angular correlation distance of 0.7 π radians and $\langle[\Delta(\alpha_i)]^2\rangle_{av}/\delta_0^2$ of (*a*) 0, (*b*) 0.005, and (*c*) 0.01. The numbers on the contour lines refer to relative intensities enumerated in Table I.

$\langle[\Delta(\alpha_i)]^2\rangle/\delta_0^2$ of 0.005 and 0.01. It is seen that increasing disorder leads to patterns of the "tennis-racket" type described by Kawai and co-workers.[5] The numbers on the contour lines refer to relative intensities given in Table I. With increasing disorder, there is a buildup of a connecting link of scat-

TABLE I
Designation of Contour Lines of Constant Intensity

Line no.	Relative intensity
1	4×10^3
2	3×10^3
3	2×10^3
4	1×10^3
5	5×10^2
6	2×10^2
7	1×10^2

tered intensity between the center of the pattern and the typical H_n scattering maximum.

CASE OF COMBINED DISORDER IN ORIENTATION AND ANISOTROPY

Radial Disorder

If both the angle β and the anisotropy δ are dependent upon r, one must use, instead of eq. (3), the equation

$$E_{H_v} = C_2\pi \cos \rho_2 \int_{r=0}^{R} \sin 2\xi(r) \cdot \delta(r) J_2(x) r dr \tag{22}$$

where $\xi(r) = \mu + \beta(r)$ and is a function of r which must be included in the integral. The intensity is then

$$I_{H_v} = K \cos^2 \rho_2 \int_{r_1=0}^{R} \int_{r_2=0}^{R} \langle \delta(r_1)\delta(r_2) \sin 2\xi(r_1) \sin 2\xi(r_2) \rangle_{r_1,r_2} \times J_2(x_1) J_2(x_2) r_1 r_2 dr_1 dr_2 \tag{23}$$

It is assumed that fluctuations in angle are independent of fluctuations in the magnitude of the anisotropy. Thus, it follows that

$$\langle \delta(r_1)\delta(r_2) \sin 2\xi(r_1) \sin 2\xi(r_2) \rangle_{r_1,r_2} = \langle \delta(r_1)\delta(r_2) \rangle_{r_1,r_2} \langle \sin 2\xi(r_1) \sin 2\xi(r_2) \rangle_{r_1,r_2} \tag{24}$$

Now from Eqs. (6), (7) and (8) we have

$$\langle \delta(r_1)\delta(r_2) \rangle_{r_1,r_2} = \delta_0^2 + \langle [\Delta(r_i)]^2 \rangle_{av} \Psi_r(r_{12}) \tag{25}$$

We may adopt the procedure of Part I[1] to show that

$$\langle \sin 2\xi(r_1) \sin 2\xi(r_2) \rangle_{av} = f(r_{12}) (\sin^2 2\xi_0 \langle \cos^2 2\Delta\beta_1 \rangle_{av} + \cos^2 2\xi_0 \langle \sin^2 2\Delta\beta_1 \rangle_{av}) \tag{26}$$

where

$$f(r_{12}) = \langle \cos 2\beta_{12} \rangle_{r_{12}} \tag{27}$$

and, as in Part I, $\Delta\beta_1 = \beta(r_1) - \beta_0$ and $\beta_{12} = \beta(r_2) - \beta(r_1)$. Therefore, from eqs. (23)–(27), we obtain

$$I_{H_v} = K \cos^2 \rho_2 \{ \sin^2 2\xi_0 \langle \cos^2 2\Delta\beta_1 \rangle_{av} + \cos^2 2\xi_0 \langle \sin^2 2\Delta\beta_1 \rangle_{av} \} \times \delta_0^2 \int_{r_1=0}^{R} \int_{r_2=0}^{R} \left[1 + \frac{\langle [\Delta(r_i)]^2 \rangle_{av}}{\delta_0^2} \Psi r(r_{12}) \right] f(r_{12}) J_2(x_1) J_2(x_2) r_1 r_2 dr_1 dr_2 \tag{28}$$

This equation reduces to eq. (28) of Part I when $\langle [\Delta(r_i)]^2 \rangle_{av} = 0$ and when an exponential correlation function is assumed for $f(r_{12})$ and to eq. (10) of this paper when $\Delta\beta_1 = 0$ and $f(r_{12}) = 1$.

If there is a large amplitude fluctuation, $\langle \cos^2 2\Delta\beta_1 \rangle_{av}$ and $\langle \sin^2 2\Delta\beta_1 \rangle_{av}$ approach each other and approach 1/2. Also, under these conditions, the

correlation distance associated with the correlation function $f(r_{12})$ is small compared with the radius of the spherulite, so that the limits of integration may be extended to infinity without appreciable error to give

$$I_{Hv} = \frac{1}{2} K \cos^2 \rho_2 \delta_0^2 \int_{r_1=0}^{\infty} \int_{r_2=0}^{\infty} \left\{1 + \frac{\langle [\Delta(r_i)]^2 \rangle_{av}}{\delta_0^2} \Psi_r(r_{12})\right\} f(r_{12}) J_2(x_1) J_2(x_2) r_1 r_2 dr_1 dr_2 \quad (29)$$

This result is a two-dimensional analog of the Stein-Wilson random orientation correlation theory.[4] In this case, there is sufficient randomness that the effect of the spherulitic superstructure is smeared out, and the scattered intensity becomes independent of the azimuthal angle μ and is cylindrically symmetrical about the incident beam. Furthermore, the scattering pattern becomes independent of the spherulite radius R but depends only upon the correlation distances associated with the disorder in anisotropy and orientation.

Angular Disorder

An analogous treatment applies to the case of a combination of anisotropy and orientational disorder in the angular direction which leads to the equation

$$I_{Hv} = (K/4\pi^2) K \cos^2 \rho_2 R^4 \delta_0^2 \{ [\sin^2 2\xi_0 \langle \cos^2 2\Delta\beta_1 \rangle_{av} + \cos^2 2\xi_0 \langle \sin^2 2\Delta\beta_1 \rangle_{av}] g_1 + \sin^2 2\xi_0 \langle \sin^2 2\Delta\beta_1 \rangle_{av} + \cos^2 2\xi_0 \langle \cos^2 2\Delta\beta_1 \rangle_{av}] g_2 \} \quad (30)$$

where

$$g_1 = \int_{\gamma_1=0}^{2\pi} \int_{\gamma_2=0}^{2\pi} \left\{1 + \frac{\langle [\Delta(\alpha_i)]^2 \rangle_{av}}{\delta_0^2} \Psi_\alpha(\gamma_{12})\right\} G(\gamma_{12}) \cos 2\gamma_1 \cos 2\gamma_2 \times f(\gamma_1) f(\gamma_2) d\gamma_1 d\gamma_2 \quad (31)$$

and

$$g_2 = \int_{\gamma_1=0}^{2\pi} \int_{\gamma_2=0}^{2\pi} \left\{1 + \frac{\langle [\Delta(\alpha_i)]^2 \rangle_{av}}{\delta_0^2} \Psi_\alpha(\gamma_{12})\right\} G(\gamma_{12}) \sin 2\gamma_1 \sin 2\gamma_2 \times f(\gamma_1) f(\gamma_2) d\gamma_1 d\gamma_2 \quad (32)$$

where $G(\gamma_{12})$ is an orientation correlation function in the angular direction defined by

$$G(\gamma_{12}) = \langle \cos 2\beta_{12} \rangle_{\gamma_{12}} \quad (33)$$

the average being evaluated for all pairs of scattering elements at the same radial distance from the center of the spherulite but at a fixed angular separation γ_{12}. As with the case of radial disorder, it is seen that the intensity is the sum of two terms, one of which arises from orientational disorder and the other from both orientational and anisotropy disorder.

THE V_v COMPONENT OF SCATTERING AND THE SEPARATION OF DENSITY AND ORIENTATION FLUCTUATIONS

In previous work on the scattering from media with random fluctuations,[4] it was shown that the H_v scattering arises primarily from orientation fluctuations but that the V_v scattering also contains a contribution from density (or average refractive index) fluctuations. Thus from a combination of measurements of V_v and H_v scattering, it is possible to separate the two contributions. For a perfect spherulite, the H_v scattering arises from the anisotropy δ_0 of the spherulite, whereas the V_v scattering also depends upon the refractive index of the surroundings.[2] Thus, it is expected that the H_v scattering from a disordered spherulite will depend upon the anisotropy of the spherulite and upon the fluctuations of anisotropy and optic axis orientation, while the V_v scattering also depends upon the refractive index of the environment and upon the fluctuation of the density of the spherulite from the average.

From previous results,[2] one obtains the expression for the amplitude of the V_v scattering

$$E_{V_v} = C_2 \cos \rho_1 \left\{ \int_{r=0}^{R} \int_{\alpha=0}^{2\pi} \alpha_2(r,\alpha) \cos [x \cos (\mu - \alpha)] d\alpha r dr + \int_{r=0}^{R} \int_{\alpha=0}^{2\pi} \delta(r,\alpha) \cos^2 \gamma \cos [x \cos (\mu - \alpha)] d\alpha r dr \right\} \quad (34)$$

where

$$\cos \rho_1 = \cos \theta / [\cos^2 \theta + \sin^2 \theta \cos^2 \mu)^{1/2}$$

We shall first consider the case of only radial disorder where eq. (34) may be integrated over angle to give

$$E_{V_v} = -C_2 \pi \cos \rho_1 \left\{ 2 \int_{r=0}^{R} \alpha_2(r) J_0(x) r dr + \int_{r=0}^{R} \delta(r) [J_0(x) - J_2(x) \cos 2\xi] r dr \right\} \quad (35)$$

Upon squaring to calculate the intensities, one obtains

$$I_{V_v} = K \cos^2 \rho_1 (4I_1 + 4I_2 + I_3) \quad (36)$$

where

$$I_1 = \int_{r_1=0}^{R} \int_{r_2=0}^{R} \langle \alpha_2(r_1) \alpha_2(r_2) \rangle_{r_1,r_2} J_0(x_1) J_0(x_2) r_1 r_2 dr_1 dr_2 \quad (37)$$

$$I_2 = \int_{r_1=0}^{R} \int_{r_2=0}^{R} \langle \alpha_2(r_1) \delta(r_2) \rangle_{r_1,r_2} J_0(x_1) \times [J_0(x_2) - J_2(x_2) \langle \cos 2\xi_2 \rangle_{r_1,r_2}] r_1 r_2 dr_1 dr_2 \quad (38)$$

and

$$I_3 = \int_{r_1=0}^{R} \int_{r_2=0}^{R} \langle \delta(r_1)\delta(r_2)\rangle_{r_1,r_2} [J_0(x_1)J_0(x_2) - 2J_0(x_2)J_2(x_1)\langle \cos 2\xi_1\rangle_{r_1,r_2} + \langle \cos 2\xi_1 \cos 2\xi_2\rangle_{r_1,r_2} J_2(x_1)J_2(x_2)]r_1 r_2 dr_1 dr_2 \quad (39)$$

It has been assumed that anisotropy and density fluctuations are independent of orientation fluctuations. The integral I_1 depends upon density fluctuations, I_3 depends upon anisotropy and orientation fluctuations, while I_2 depends upon cross correlations of density and anisotropy fluctuations.

In eq. (38), $\langle \cos 2\xi_2\rangle_{\text{av}}$ depends only upon r_2 and

$$\begin{aligned} \langle \cos 2\xi_2\rangle_{r_1,r_2} &= \langle \cos 2\xi_2\rangle_{\text{av}} = \langle \cos (2\mu + 2\beta_2)\rangle_{\text{av}} \\ &= \langle \cos (2\mu + 2\beta_0 + 2\Delta\beta_2)\rangle_{\text{av}} = \langle \cos (2\xi_0 + 2\Delta\beta_2)\rangle_{\text{av}} \\ &= \cos 2\xi_0 \langle \cos 2\Delta\beta_2\rangle_{\text{av}} - \sin 2\xi_0 \langle \sin 2\Delta\beta_2\rangle_{\text{av}} \\ &= 0 \end{aligned} \quad (40)$$

since $\langle \sin 2\Delta\beta_2\rangle_{\text{av}} = \langle \cos 2\Delta\beta_2\rangle_{\text{av}} = 0$, as positive and negative values of $\Delta\beta_2$ are equally probable. Similarly, in eq. (39), $\langle \cos 2\xi_1\rangle_{r_1,r_2}$ is 0, so it follows that

$$I_2 = \int_{r_1=0}^{R} \int_{r_2=0}^{R} \langle \alpha_2(r_1)\delta(r_2)\rangle_{r_1,r_2} J_0(x_1)J_0(x_2) r_1 r_2 dr_1 dr_2 \quad (41)$$

and

$$I_3 = \int_{r_1=0}^{R} \int_{r_2=0}^{R} \langle \delta(r_1)\delta(r_2)\rangle_{r_1,r_2} [J_0(x_1)J_0(x_2) + \langle \cos 2\xi_1 \cos 2\xi_2\rangle_{r_1,r_2} J_2(x_1)J_2(x_2)]r_1 r_2 dr_1 dr_2 \quad (42)$$

As before, one may use

$$\langle \cos 2\xi_1 \cos 2\xi_2\rangle_{r_1,r_2} = [\cos^2 2\xi_0 \langle \cos^2 2\Delta\beta_1\rangle_{\text{av}} + \sin^2 2\xi_0 \langle \sin^2 2\Delta\beta_1\rangle_{\text{av}}] f(r_{12}) \quad (43)$$

In the Stein-Wilson theory, it is assumed that density and anisotropy fluctuations were independent. We shall not make this assumption here but shall consider a particular simplifying model where the density and orientation fluctuations both arise from the same origin, that is, the fluctuation in the number of crystals per unit volume. It is conceivable, of course, that anisotropy fluctuations could also arise, in part from fluctuations in the amorphous orientation but we shall not consider this possibility.

To interconnect the fluctuations in density and anisotropy, we shall consider the fluctuations in $\rho(r)$, the number of crystals at distance r from the origin (assuming only radial fluctuations). If the principal polarizabilities of the crystals are α_1 and α_2, the polarizability per unit volume at radius r is

$$\alpha_1(r) = \rho(r)\alpha_1$$

$$\alpha_2(r) = \rho(r)\alpha_2 = \left(\alpha - \frac{1}{3}\delta\right)\rho(r) \tag{44}$$

so that

$$\delta(r) = \alpha_1(r) - \alpha_2(r) = \rho(r)(\alpha_1 - \alpha_2) = \rho(r)\delta$$

where $\delta = \alpha_1 - \alpha_2$ and the average polarizability α is $(\alpha_1 + 2\alpha_2)/3$. Thus we write

$$\langle\alpha_2(r_1)\alpha_2(r_2)\rangle_{r_1,r_2} = \left(\alpha - \frac{1}{3}\delta\right)^2\langle\rho(r_1)\rho(r_2)\rangle_{r_1,r_2} \tag{45}$$

Now since $\rho(r_1) = \rho_0 + \Delta\rho_1$, where ρ_0 is the average number of crystals per cubic centimeter, it follows that

$$\langle\rho(r_1)\rho(r_2)\rangle_{r_1,r_2} = \rho_0^2 + \langle(\Delta\rho)^2\rangle_{\text{av}}\gamma(r_{12}) \tag{46}$$

where $\gamma(r_{12})$ is a correlation function defined as

$$\gamma(r_{12}) = \langle\Delta\rho_1\Delta\rho_2\rangle_{r_1,r_2}/\langle(\Delta\rho)^2\rangle_{\text{av}} \tag{47}$$

Thus we see that

$$\langle\alpha_2(r_2)\alpha_2(r_1)\rangle_{r_1,r_2} = \left(\alpha - \frac{1}{3}\delta\right)^2\rho_0^2\left[1 + \frac{\langle(\Delta\rho)^2\rangle_{\text{av}}}{\rho_0^2}\gamma(r_{12})\right] \tag{48}$$

Similarly, it follows that

$$\langle\delta(r_1)\delta(r_2)\rangle_{r_1,r_2} = \delta^2\rho_0^2\left[1 + \frac{\langle(\Delta\rho)^2_{\text{av}}}{\rho_0^2}\gamma(r_{12})\right] \tag{49}$$

and

$$\langle\delta(r_1)\alpha_2(r_2)\rangle_{r_1,r_2} = \delta\left(\alpha - \frac{1}{3}\delta\right)\rho_0^2\left[1 + \frac{\langle(\Delta\rho)^2\rangle_{\text{av}}}{\rho_0^2}\gamma(r_{12})\right]. \tag{50}$$

Upon substituting these values into eqs. (37), (38), and (39) for I_1, I_2, and I_3, one obtains

$$I_{V_v} = K\cos^2\rho_1\rho_0^2\left\{\left(4\alpha^2 + \frac{4}{3}\alpha\delta + \frac{1}{9}\delta^2\right)\int_{r_2=0}^{R}\int_{r_1=0}^{R}\left[1 + \frac{\langle(\Delta\rho)^2\rangle_{\text{av}}}{\rho_0^2}\gamma(r_{12})\right]J_0(x_1)J_0(x_2)r_1r_2dr_1dr_2\right.$$
$$+ \delta^2[\cos^2 2\xi_0\langle\cos^2 2\Delta\beta_1\rangle_{\text{av}} + \sin^2 2\xi_0\langle\sin^2 2\Delta\beta_1\rangle_{\text{av}}]$$
$$\left.\int_{r_2=0}^{R}\int_{r_1=0}^{R}\left[1 + \frac{\langle(\Delta\rho)^2\rangle_{\text{av}}}{\rho_0^2}\gamma(r_{12})\right]f(r_{12})J_2(x_1)J_2(x_2)r_1r_2dr_1dr_2\right\} \tag{51}$$

The first term is associated with density fluctuations while the second term is associated with both density and orientation fluctuations. The first term is independent of μ, while the second term is dependent upon μ.

The eq. (28) may be written in terms of these same variables as

$$I_{H_v} = K \cos^2 \rho_2 \{\sin^2 2\xi_0 \langle \cos^2 2\Delta\beta_1 \rangle_{av} + \cos^2 2\xi_0 \langle \sin^2 2\Delta\beta_1 \rangle_{av}\}$$
$$\times \delta^2 \rho_0^2 \int_{r_1=0}^{R} \int_{r_2=0}^{R} \left[1 + \frac{\langle (\Delta\rho)^2 \rangle_{av}}{\rho_0^2} \gamma(r_{12})\right] f(r_{12}) J_2(x_1) J_2(x_2) r_1 r_2 dr_1 dr_2 \quad (52)$$

It is possible to separate the contributions to scattering arising from density and orientation fluctuations by measurement of I_{V_v} and I_{H_v} at appropriate angles. Thus, it would be possible to obtain the parameters $\langle \cos^2 2\Delta\beta_1 \rangle_{av}$ and $\langle (\Delta\rho)^2 \rangle_{av}/\rho_0^2$, and the correlation functions $\gamma(r_{12})$ and $f(r_{12})$ required to specify the disorder in a given system. The means for separation depend upon the choice of the particular model of two-dimensional spherulites with random disorder in the radial direction. Analogous but different procedures may be developed for the more complex cases of angular disorder, a combination of radial with angular disorder, or for three-dimensional spherulites.

This study was supported in part by a contract with the Office of Naval Research and in part by grants from the American Chemical Society and the National Institutes of Health.

References

1. R. S. Stein and W. Chu, *J. Polym. Sci. A-*, *28*, 1137 (1970).
2. S. Clough, J. J. van Aartsen, and R. S. Stein, *J. Appl. Phys.*, **36**, 3072 (1965).
3. A. E. M. Keijzers, J. J. van Aartsen, and W. Prins, *J. Amer. Chem. Soc.*, **90**, 3107 (1968).
4. R. S. Stein and P. R. Wilson, *J. Appl. Phys.*, **33**, 1914 (1962).
5. M. Motegi, T. Oda, M. Moritani, and H. Kawai, *Polym. J.* (Japan), **1**, 209 (1970).

Received January 20, 1971
Revised March 11, 1971

JOURNAL OF POLYMER SCIENCE: PART A-2 VOL. 9, 1763–1776 (1971)

Effect of Molecular Weight on the Refractive Increment of Polyethylene and *n*-Alkanes

H. L. WAGNER and C. A. J. HOEVE,* *Institute for Materials Research, National Bureau of Standards, Washington, D. C. 20234*

Synopsis

As in the case with other polymers previously reported, the values of the refractive index increment dn/dc of polyethylene and the n-alkanes change with molecular weight. Most of the variation may be understood by examination of the role of density in the Lorentz-Lorenz mixing equation for specific refractivity, $R_{12} = p_1R_1 + P_2R_2$ used to calculate dn/dc. It may also be shown that as the absolute refractive index difference between solute and solvent becomes smaller, dn/dc becomes more sensitive to density change of the solute.

INTRODUCTION

Because the calculated value of the molecular weight of a high polymer determined by light scattering depends on the square of dn/dc, the derivative of refractive index with respect to concentration, small variations in this quantity have a significant effect on the calculated molecular weight. Although in the past it has been generally assumed that dn/dc is constant with molecular weight, exceptions, particularly at low molecular weights, have been reported for poly(ethylene oxide)[1–3] and *p*-oligophenylenes.[4] More recently, Barrall, Cantow, and Johnson[5] have shown a molecular weight dependence for molecular weights of up to 300,000 for the narrow molecular weight polystyrenes used for calibration of gel permeation chromatography. These differences can lead to errors of as much as 12% in molecular weight determinations.

In a forthcoming paper dealing with the NBS standard linear polyethylene sample, SRM 1475,[6] a similar variation of about 2% in dn/dc with molecular weights from 13,000 to 110,000 is found for polyethylene fractions. This effect could not be attributed to chemical differences, since the infrared spectra for the high and low molecular weight fractions were the same.

In an attempt to find the reason for this molecular weight effect, determinations of dn/dc were made for the *n*-alkanes, the low molecular weight homologs of polyethylene. Because of limitations imposed by solubility and

* Present address: Department of Chemistry, Texas A and M University, College Station, Texas 77843.

equipment, it was not possible for these *n*-alkanes to be measured in 1-chloronaphthalene, the solvent which has, in the past, been used for polyethylene. The measurements of dn/dc were performed instead at 60°C and 135°C in 1,2,4-trichlorobenzene.

EXPERIMENTAL

Differential Refractometer

This instrument is to be described in a forthcoming report.[6]

Absolute Refractometer

An Abbé refractometer manufactured by Bausch and Lomb, Inc.* was used for the determination of absolute refractive index. Water circulating at constant temperature was used in the refractometer to obtain 60°C data for 1,2,4-trichlorobenzene at 5893 Å. Since this instrument also measures dispersion, it is possible to correct by interpolation to 5460 Å. Measurements at 135°C, which would have been very desirable, could not be made with available equipment.

Solvents

Reagent grade 1-chloronaphthalene was doubly distilled, center cuts being taken each time. Impurities observed by gas–liquid chromatography were less than 0.5%.

Since the previous determinations[6] of dn/dc of polyethylene fractions were carried out with technical grade 1,2,4-trichlorobenzene (Eastman) and these are compared with the measurements for the *n*-alkanes in this paper, this same grade of solvent was used for the latter measurements. As before, 0.05% Ionol (2,6-*di-tert*-butyl-4-methyl phenol) was added as an antioxidant. Gas–liquid chromatography showed only a single major peak containing at least 99% of the material.

Normal Alkanes

These were obtained from the LeChat Chemical Company, Chicago, Illinois and used without further purification. The purities were stated by the manufacturer to be as follows: *n*-eicosane ($C_{20}H_{42}$), 99.5% pure; *n*-octacosane ($C_{28}H_{58}$), 99.0% pure; *n*-hexatriacontane ($C_{36}H_{74}$), 99.0% pure.

Polymers

SRM 1475 is a linear polyethylene and SRM 1476 a branched polyethylene provided by the National Bureau of Standards as standard reference materials. Their characterizations are described elsewhere.[7,8]

*Certain commercial equipment, instruments, or materials are identified in this paper in order to adequately specify the experimental procedure. In no case does such identification imply recommendation or endorsement by the National Bureau of Standards, nor does it imply that the material or equipment identified is necessarily the best available for the purpose.

Fraction R1201-7 is a linear polyethylene fraction supplied by Allied Chemical Corporation. AC-6 is a polyethylene wax supplied by the Monsanto Chemical Co. Fractions 12x, 7y, PE 15, PE 120, and 12 AC are fractions of SRM 1475 obtained by the column elution method. The number-average molecular weights $\bar{M}_n$ were obtained by methods indicated in Tables I and II. For a more complete description of the methods used to characterize the fractions, reference should be made to the series of papers describing the characterization of SRM 1475.[7]

Density Determinations

The values of ρ_2, the density of polyethylene for different molecular weights, were obtained by extrapolation of the *n*-alkane data of Doolittle[9] to high molecular weights. Although these values for polyethylene do not agree precisely with any of the measured values which have been reported,[10-12] (and which are not in complete agreement among themselves), Doolittle's data were used because it was possible to make some assessment of the change in density with molecular weight.

The partial specific volume $\bar{v}_2$ of polyethylene SRM 1475 in 1-chloronaphthalene at 135°C was determined from the change in density of this solvent when polyethylene was dissolved. The density was measured with a pycnometer. Since a large enough supply of fractionated material was not available, this measurement could not be done as a function of molecular weight. The partial specific volumes of the *n*-alkanes at 60°C and 135°C were also determined by pycnometry and the method of intercepts.[13] Specific volumes were plotted against weight fraction and the limiting low-concentration tangent was extrapolated to its intercept on the 100% solute axis.

RESULTS

The values of dn/dc for polyethylenes and polyethylene fractions in 1-chloronaphthalene and 1,2,4-trichlorobenzene previously reported[6] are listed in Tables I and II, together with their number-average molecular weights $\bar{M}_n$. Those for the *n*-alkanes in 1,2,4-trichlorobenzene at 60 and 135°C, measured at concentrations of from 0.008 to 0.025 g/ml, at 60 and 135°C, are shown in Table III. Standard deviations are also given.

Densities and partial specific volumes are shown in Tables IV and V. The densities of the *n*-alkanes were taken from the literature.[14] In the case of $C_{28}H_{58}$ and $C_{36}H_{74}$, which are crystalline at 60°C, the amorphous density was obtained by extrapolation to this temperature from somewhat higher temperatures. Nearly identical results are obtained by using Doolittle's[9] empirical relationship

$$\ln (1/\rho) = (a/M) + b$$

TABLE I
dn/dc of Polyethylenes in 1-Chloronaphthalene at 135°C

Sample	$\bar{M}_n$	dn/dc, ml/g	Standard deviation of dn/dc, ml/g[a]	No. of points[a]
SRM 1475	18,300[b]	−0.1932	0.00016	5
SRM 1476	25,200[c]	−0.1916	0.00028	5
Fraction R 1201-7	12,300[c]	−0.1931	0.00042	3
Fraction PE 15	13,500[d]	−0.1929	0.00035	3
Fraction 12x	110,000[c]	−0.1883	0.00088	2
Fraction PE 120	112,000[d]	−0.1879	0.00059	4

[a] The estimated standard deviation of the slope, calculated by linear regression of the refractive index difference, Δn, on the concentration c, assuming a zero intercept. The number of points in each regression line is shown in column 5. For convenience all standard deviations are given to two significant figures, with no implication that such precision is warranted.

[b] Value obtained from gel-permeation chromatography.[7]

[c] Value provided by manufacturer, Union Carbide Corp.

[d] Determined by osmometry.[26]

[e] Estimated from Mark-Houwink equation.[27]

TABLE II
dn/dc of Polyethylenes in 1,2,4-Trichlorobenzene at 135°C

Sample	$\bar{M}_n$	dn/dc, ml/g	Standard deviation of dn/dc, ml/g[a]	No. of points[a]
AC-6	2,000[b]	−0.1085	0.00028	3
SRM 1475	18,400[c]	−0.1085	0.00015	5
Fraction 12 AC	34,800[d]	−0.1082	0.00019	3
Fraction 7y	77,000	−0.1073	0.00038	3
Fraction 12x	110,000	−0.1063	0.00014	4

[a] The estimated standard deviation of the slope, calculated by linear regression of the refractive index difference, Δn, on the concentration c, assuming a zero intercept. The number of points in each regression line is shown in column 5. For convenience all standard deviations are given to two significant figures, with no implication that such precision is warranted.

[b] Approximate value, supplied by manufacturer.

[c] Estimated from Mark-Houwink equation.[27]

[d] Value obtained from gel-permeation chromatography.[7]

where ρ is the density, M is the molecular weight, and a and b are functions of the absolute temperature T:

$$\ln a = C_1 T + C_2$$

$$b = C_3 T^{C_4}$$

Doolittle found the values of the constants to be: $C_1 = 0.00275$, $C_2 = 2.303$, $C_3 = 0.000182$, $C_4 = 1.19$. The densities, at 135°C, of two linear polyethylenes differing about tenfold in molecular weight were also calculated from these relations.

TABLE III
Refractive Index Increment of Normal Alkanes in 1,2,4-Trichlorobenzene

Alkane	60°C			135°C		
	dn/dc, ml/g	Standard deviation of dn/dc, ml/g[a]	No. of points[a]	dn/dc, ml/g	Standard deviation of dn/dc, ml/g[a]	No. of points[a]
n-Eicosane, $C_{20}H_{42}$	−0.169	0.00018	4	−0.175	0.00055	5
n-Octacosane, $C_{28}H_{58}$	−0.154	0.00017	5	−0.153	0.0012	4
n-Hexatriacontane, $C_{36}H_{74}$	−0.146	0.00034	4	−0.143	0.0013	6

[a] The estimated standard deviation of the slope, calculated by linear regression of the refractive index difference Δn on the concentration c, assuming a zero intercept. The number of points in each regression line is shown in columns 4 and 7. For convenience all standard deviations are given to two significant figures, with no implication that such precision is warranted.

TABLE IV
Densities and Partial Specific Volumes

	Temp, °C	Density, g/ml	Partial specific volume, ml/g
Solvents			
1,2,4-Trichlorobenzene	60	1.405	
1,2,4-Trichlorobenzene	135	1.315	
1-Chloronaphthalene	135	1.095	
n-Alkanes			
$C_{20}H_{42}$	60	0.762[a]	
$C_{28}H_{58}$	60	0.782	
$C_{36}H_{74}$	60	0.792	
Polyethylenes			
$\bar{M}_n$ = 12,300	135	0.7905[b]	
$\bar{M}_n$ = 110,000	135	0.7922[b]	
Polyethylene SRM 1475 in 1-chloronaphthalene	135		1.29

[a] Data of Timmermans.[14]
[b] From calculations shown in text.

Refractive indices are listed in Table VI. The refractive indices of the normal alkanes were taken from the literature,[14] by interpolating between 40 and 70°C to obtain a value at 60°C for $C_{20}H_{42}$, and extrapolating back to 60°C for the other alkanes, since they are ordinarily crystalline at this temperature. It was also necessary to approximate a correction for dispersion. Since the refractive index of $C_{36}H_{74}$ had been measured[15] at both 5893 and 5460 Å, the ratio between the two, 1.0014, was applied to the values of n at 60°C and 5893 Å to give the values listed in Table VI.

DISCUSSION

Polyethylene

To determine whether the variation of dn/dc with molecular weight could be calculated by application of the Lorentz-Lorenz equation, the molar refractivity was calculated for a 12,300 and an 110,000 molecular weight polyethylene, the extremes of molecular weight in Table I. This was done by summing, over the entire molecule, the molar refractivity of the two methyl groups and the appropriate number of methylene groups. Vogel's[16] values of 4.643 cm^3/mole for the methylene group and 5.624 cm^3/mole for the methyl group at 5893 Å were used. Values at 5460 Å, the wavelength used to measure dn/dc, are not available, but should not differ significantly from those at 5893 Å.

From the values of molar refractivity and the density from Doolittle's data the indices of refraction for these two molecular weights were obtained by substitution in the Lorentz-Lorenz equation:

$$[R] = (M/\rho)\,(n^2 - 1)/(n^2 + 2) \qquad (1)$$

TABLE V
Partial Specific Volume $\bar{v}_2$ of the Normal Alkanes in 1,2,4-Trichlorobenzene

Normal Alkanes	60°C			135°C		
	$\bar{v}_2$, ml/g	Standard deviation, ml/g[a]	No. of points[a]	$\bar{v}_2$, ml/g	Standard deviation, ml/g[a]	No. of points[a]
n-Eicosane, $C_{20}H_{42}$	1.33	0.018	5	1.53	0.052	5
n-Octacosane, $C_{28}H_{58}$	1.287	0.0028	9	1.37	0.015	4
n-Hexatriacontane, $C_{36}H_{74}$	1.26	0.013	11	1.35	0.013	3

[a] Standard deviation of the slope calculated by linear regression of the specific volume vs. weight fraction of alkane. The number of points in each regression line is shown in columns 4 and 7.

TABLE VI
Refractive Indices

	Temp, °C	λ, A°	n
1-Chloronaphthalene	135	5460	1.5859[a]
1,2,4-Trichlorobenzene	60	5460	1.5577
$C_{20}H_{42}$	60	5460	1.4285[b]
$C_{28}H_{58}$	60	5460	1.4390[b]
$C_{36}H_{74}$	60	5460	1.4449[b]

[a] Data of Stacey and Arnett.[28]
[b] Adjusted from values of Timmerman.[14]

where $[R]$ is the molar refractivity, n the refractive index, ρ the density, and M the molecular weight, for which the number-average molecular weight was used. These indices of refraction are given in Table VII for these two polyethylenes.

TABLE VII
Calculated and Observed Values of dn/dc
of Polyethylenes in 1-Chloronaphthalene at 135°C

	Polymer $\bar{M}_n$ = 12,300	Polymer $\bar{M}_n$ = 110,000
Polymer density ρ_2, g/ml	0.7905	0.7922
Specific refractivity R_2, ml/g	0.3311	0.3310
Calculated refractive index n_2	1.4366	1.4375
dn/dc, ml/g		
Calculated, by eq. (3), 5893 Å	−0.200	−0.198
Calculated, Dale-Gladstone relation, 5893 Å	−0.189	−0.187
Observed, 5460 Å	−0.193	−0.188

To calculate dn/dc, we use the Lorentz-Lorenz mixture rule, which is an approximation[17] but often gives good results:[18]

$$R_{12} = p_1R_1 + p_2R_2 \tag{2}$$

where R is the specific refractivity defined as:

$$R = (1/\rho)(n^2 - 1)/(n^2 + 2)$$

and the subscripts 1, 2, and 12 refer to the solvent, solute, and solution respectively. The symbols p_1 and p_2 are the weight fractions of solvent and solute. In the limiting case at zero concentration, and assuming volume additivity, Heller[19] has shown that:

$$\left(\frac{dn}{dc}\right)_{c\to 0} = \left(\frac{3}{2\rho_2 n_1}\right)\left[\frac{(n_2^2 - 1)}{(n_2^2 + 2)} - \frac{(n_1^2 - 1)}{(n_1^2 + 2)}\right]\left[1 - \frac{(n_1^2 - 1)}{(n_1^2 + 2)}\right]^{-2} \tag{3}$$

where n_1 is the refractive index of the solvent and n_2 is the refractive index of the solute.

Although data for slightly different wavelengths are used in the computation of dn/dc, the values calculated from eq. (3) give surprisingly good agreement with the measured values at 5460 Å, as shown in Table VII. Certainly the relative values for the two molecular weights should be meaningful. The calculated change in dn/dc, about 1%, accounts for about half of the observed change.

It is interesting to compare these results with those obtained from the data of Bianchi, Luetzel, and Price[20] for Marlex 50 polyethylene. These are 0.3280 ml/g for the refractivity and 1.256 ml/g for the specific volume. Although the wavelength of the light is not given, there is a good possibility it was the green mercury line 5461 Å since the Brice-Halwer differential refractometer was used for the refractive index determination. From these data in eq. (3), dn/dc is -0.207 ml/g, which compares with an average of -0.199 ml/g calculated at 5893 Å as described above, and an average measured value of -0.190 at 5461 Å.

The empirical Dale-Gladstone relation

$$dn/dc = (n_2 - n_1)/\rho_2$$

also gives satisfactory results. These are shown in Table VII. For the data of Bianchi, Luetzel, and Price cited above, the relationship gives a dn/dc value of -0.195 ml/g for Marlex 50.

Since volume additivity is not always obeyed, however, eq. (2) may be applied without this assumption. We obtain from eq. (2) for the limit of zero concentrations:

$$dn/dc = (R_2 - R_1\bar{v}_2/v_1)/[6n_1/(n_1^2+2)^2] \quad (4)$$

where $\bar{v}_2$ is the partial specific volume of the solute and v_1 is the specific volume of the solvent. Equation (4) reduces to eq. (3) if $\bar{v}_2 = 1/\rho_2$.

Since the values of $\bar{v}_2$ were not determined for fractions, the change in dn/dc with molecular weight in 1-chloronaphthalene can not be calculated by using eq. (4), as was done by using eq. (3), in which the densities, extrapolated for two different molecular weights, are employed.

By using the value of $\bar{v}_2$ determined for the whole polymer, 1.29 ml/g in eq. (4), dn/dc is calculated to be -0.218 ml/g, somewhat lower than the observed value of -0.188. The result does not depend on which value of R_2 of Table VII is used. If instead, the reciprocal of the value of the density given by Doolittle in Table VI for a molecular weight of 12,300 is substituted for $\bar{v}_2$, eq. (4) necessarily gives the same value as eq. (3), -0.200 for dn/dc. It would be expected that eq. (4), in which no assumptions are made about volume additivity, as in the case of eq. (3), should give better results than the latter. Why this is not the case is not understood; perhaps some fortuitous cancellations occur in eq. (3), or, more likely, the value of $\bar{v}_2$ to which eq. (4) is very sensitive, is not known precisely enough. It should also be remembered that many approximations entered into the evaluation of these equations.

These calculations show that although there is practically no difference in the specific refractivity of these two polyethylenes, which differ by a factor of ten in molecular weight, the calculated value of dn/dc nevertheless changes by about 1%. Density, which also enters into eqs. (3) and (4), changes by about 0.2%, and this change may be shown to result in the much larger change in the calculated dn/dc.

This change in density with molecular weight has long been recognized[21] in the case of paraffin hydrocarbons to be due to the fact that the molal volume is an additive property, and that the volumes of the methyl and methylene groups are dissimilar. Doolittle's equation, used to compute the density of polyethylene for these two different molecular weights, may be shown to have the form expected for such molal additivity.

If eq. (3) is recast in terms of the specific refractivity, and partially differentiated with respect to the density of the solute, ρ_2, holding R_1, R_2 and ρ_1 constant, we obtain for the relative change in $(dn/dc)_{c\to 0}$

$$\frac{\delta(dn/dc)_{c\to 0}}{(dn/dc)_{c\to 0}} = \left[\frac{(R_1/R_2)(\rho_1/\rho_2)}{1 - (R_1/R_2)(\rho_1/\rho_2)}\right]\frac{\delta\rho_2}{\rho_2} \tag{5}$$

Thus the fractional change in dn/dc is proportional to the fractional change in density of the solute divided by a small number which decreases as $R_1\rho_1$ approaches $R_2\rho_2$. Hence the smaller the refractive index difference between polymer and solvent, the greater is the influence of the fractional change in density of the solute. This explains why only a 0.2% difference in density leads to a 1% difference in dn/dc and suggests a way of measuring molecular weight if more sensitive methods of measuring dn/dc were available.

n-Alkanes

The values of dn/dc for the alkanes computed by using eq. (4) are compared with the observed values in Table VIII. The calculated value depends on a small difference in the numerator of eq. (4), which in turn is very sensitive to the value of $\bar{v}_2$, the partial specific volume. The values for these are listed in Table V. These partial specific volumes are difficult to measure beyond three significant figures by pycnometry so that the agreement between observed and calculated dn/dc values is quite reasonable.

TABLE VIII
Comparison of Calculated and Experimental dn/dc of *n*-Alkanes in 1,2,4-Trichlorobenzene at 60°C

	$C_{20}H_{42}$	$C_{28}H_{58}$	$C_{36}H_{74}$
Density ρ_2, g/ml	0.762	0.782	0.792
Refractivity R_2, ml/g	0.3380	0.3365	0.3360
dn/dc, ml/g			
Calculated, eq. (4)	−0.187	−0.165	−0.140
Calculated, Dale-Gladstone	−0.169	−0.152	−0.142
Observed	−0.169	−0.154	−0.146

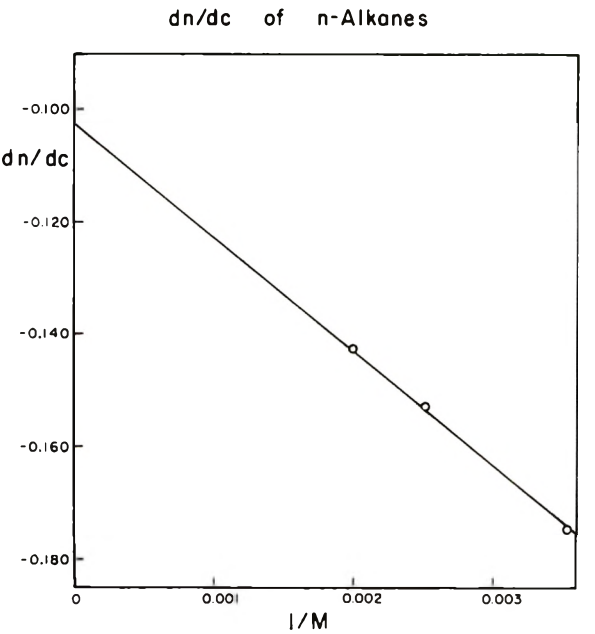

Fig. 1. Variation in dn/dc of the normal alkanes with the reciprocal of the molecular weight at 135°C. The solvent is 1,2,4-trichlorobenzene and the solutes are $C_{36}H_{74}$, $C_{28}H_{58}$, and $C_{20}H_{42}$.

The values of dn/dc calculated by using the empirical Dale-Gladstone relation are also shown in Table VIII and agree quite well with the observed data.

Equation (3) indicates that dn/dc should be proportional to specific volume, v_2 of the solute, which in turn is proportional to $1/M$ to a first approximation. If the 135°C trichlorobenzene data for the n-alkanes are plotted against $1/M$ (Fig. 1) and extrapolated to $M = \infty$, we obtain a dn/dc of -0.102. This compares well with the value of -0.106 value found for linear polyethylene of the highest molecular weight measured in Table II. The equation for the line shown in Figure 1 is:

$$-dn/dc = 0.1023 + 20.4(1/M)$$

If we now use this equation to estimate the effect of molecular weight for the polyethylenes of Table VII, we obtain for $M = 12{,}300$, $dn/dc = -0.1039$ ml/g; and for $M = 110{,}000$, $dn/dc = -0.1025$ ml/g. Thus a 1.5% difference in dn/dc is found for these two molecular weights, compared with an observed 2.5%, when an extrapolation is made from low molecular weight data.

Polystyrene

The question arises as to whether other data showing a variation of refractive index with molecular weight can be understood by the use of eq.

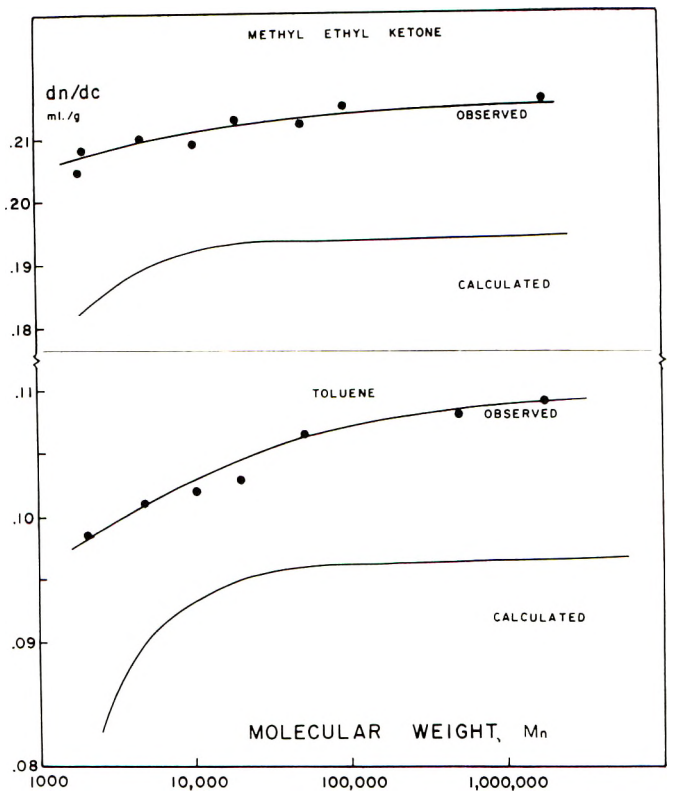

Fig. 2. Variation in dn/dc with the logarithm of number-average molecular weight at 25°C. The lower curves were calculated by using eq. (3), as described in the text. For data, see Hoeve, Wagner, and Verdier.[7]

(3). If we assume the specific refractivity of polystyrene is constant, and can be calculated from the refractive index and density at one molecular weight from the Lorentz-Lorenz equation, the refractive index may be calculated for any other molecular weight provided the density is known.

Values of the refractive index and specific volume for these calculations are obtained by extrapolation, using temperature coefficients found above T_g, from T_g to lower temperatures. This assumes that dn/dc found in this way approximates more closely that which occurs when two liquids are mixed than when data from the glassy state are employed to compute dn/dc. O'Mara and McIntyre[22] have found that using such a procedure gives good results.

For specific volume we use the equation of Fox and Flory:[23]

$$v_2 = 0.913 + 5.5\times10^{-4}t + 53/M \quad (160 \geq t \geq T_g)$$

For refractive indices we use the data of Jenckel and Hensch,[24] which above 85.5°C may be expressed by

$$n = 1.5820 - 35\times10^{-4}(t - 85.5)$$

for 5890 Å, giving a value of 1.6032 at 25°C. From the data cited by Boyer,[25] it is found that a correction of about 0.0035 refractive index units should be added, giving a value of $n = 1.6067$. The Cauchy relation:

$$n = A + B/\lambda^2 + C/\lambda^4$$

was used to correct Vogel's data[16] for dispersion to obtain the refractive index of toluene and methyl ethyl ketone at 5460 Å: toluene, $n = 1.4979$ (5460 Å); methyl ethyl ketone, $n = 1.3781$ (5460 Å). The resulting values of dn/dc for polystyrene–toluene and polystyrene-methyl ethyl ketone are shown in Table IX together with the values found by Barrall, Cantow, and Johnson.[5] These are also plotted in Figure 2. Despite all the approximations, the trend of the calculated values of dn/dc is the same as the observed

TABLE IX
Observed and Calculated dn/dc for Polystyrene–Toluene and Polystyrene–Methyl Ethyl Ketone

$\bar{M}_n$	Specific volume v_2 ml/g	dn/dc in toluene, ml/g		dn/dc in methyl ethyl ketone, ml/g	
		Obs.	Calc.	Obs. (5)	Calc.
2,030	0.953	0.0985	0.0813	0.208	0.184
4,800	0.938	0.101	0.0902	0.210	0.191
10,300	0.932	0.102	0.0936	0.209	0.193
19,800	0.930	0.103	0.0950	0.213	0.1949
51,000	0.928	0.1065	0.0960	0.212	0.1947
97,200	0.9275	0.107	0.0963	0.214	0.1949
1,800,000	0.9268	0.109	0.0966	0.216	0.1951

values, and the relative change is greater for toluene (about 9%) than for methyl ethyl ketone (about 4%). This is due to the fact that the index of refraction of toluene (1.496) is closer to that of polystyrene (1.60) than that of methyl ethyl ketone (1.3814). As a result the difference between $R_2\rho_2$ and $R_1\rho_1$ is smaller for toluene than for methyl ethyl ketone, making the fractional change in dn/dc calculated from eq. (5) greater for toluene.

CONCLUSION

The observed changes in dn/dc with molecular weight in polyethylene, the n-alkanes, and low molecular weight polystyrene, may be explained by application of the Lorentz-Lorenz equation. Although absolute values of dn/dc are difficult to calculate without accurate values for indices of refraction, densities, and partial specific volumes, relative changes with molecular weight may be calculated if the change in refractive index or in density with molecular weight is known.

The discussions with Dr. M. G. Broadhurst and the suggestions by Dr. C. M. Guttman regarding the role of solute density in dn/dc are gratefully acknowledged.

References

1. J. D. Ingham and D. D. Lawson, *J. Polym. Sci. A*, **3**, 2707 (1965).
2. P. Rempp, *J. Chim. Phys.*, **54**, 421 (1957).
3. W. Heller and T. L. Pugh, *J. Polym. Sci.*, **47**, 203 (1960).
4. I. Zeigler, L. Freund, H. Benoit, and W. Kern, *Makromol. Chem.*, **37**, 217 (1960).
5. E. M. Barrall, II, M. J. R. Cantow, and J. F. Johnson, *J. Appl. Polym. Sci.*, **12**, 1373 (1968).
6. H. L. Wagner, to be published.
7. C. A. J. Hoeve, H. L. Wagner, and P. H. Verdier, papers of this series to be published.
8. Certificate SRM 1476, National Bureau of Standards.
9. A. K. Doolittle, *J. Appl. Phys.*, **22**, 1471 (1951).
10. R. Chiang and P. J. Flory, *J. Amer. Chem. Soc.*, **83**, 2857 (1961).
11. P. R. Swan, *J. Polym. Sci.*, **42**, 525 (1960).
12. M. J. Richardson, P. J. Flory, and J. B. Jackson, *Polymer*, **4**, 221 (1963).
13. G. N. Lewis and M. Randall, *Thermodynamics*, McGraw-Hill, New York, 1923.
14. J. Timmermans, *Physico-Chemical Constants of Pure Organic Compounds*, Elsevier, Amsterdam, 1965.
15. J. L. Lauer and R. W. King, *Anal. Chem.*, **28**, 1697 (1956).
16. A. I. Vogel, *J. Chem. Soc.*, **1943**, 638; found in J. R. Partington, *An Advanced Treatise on Physical Chemistry*, Vol. 4, Longman-Green, London, 1953.
17. C. J. F. Bottcher, *Theory of Electric Polarization*, Elsevier, New York, 1952.
18. W. Heller, *J. Phys. Chem.*, **69**, 1123 (1965).
19. W. Heller, *J. Polym. Sci.*, **4**, 209 (1966).
20. J. P. Bianchi, W. G. Luetzel, and F. P. Price, *J. Polym. Sci.*, **27**, 561 (1958).
21. K. Li, R. L. Arnett, M. B. Epstein, R. B. Ries, L. P. Bitler, J. M. Lynch, and F. D. Rossini, *J. Phys. Chem.*, **60**, 1400 (1956).
22. J. H. O'Mara and D. McIntyre, *J. Phys. Chem.*, **63**, 1435 (1959).
23. T. G Fox and P. J. Flory, *J. Appl. Phys.*, **21**, 581 (1950).
24. E. Jenckel and R. Hensch, *Kolloid-Z.*, **130**, 89 (1953).
25. R. H. Boundy and R. F. Boyer, Eds., *Styrene, Its Polymers, Copolymers and Derivatives*, Reinhold, New York, 1952.
26. J. E. Brown and P. H. Verdier, to be published.
27. H. L. Wagner and C. A. J. Hoeve, to be published.
28. C. J. Stacey and R. L. Arnett, *J. Polym. Sci. A*, **2**, 167 (1964).

Received November 5, 1970
Revised February 12, 1971

JOURNAL OF POLYMER SCIENCE: PART A-2 VOL. 9, 1777–1791 (1971)

Fold Surface of Polyethylene Single Crystals as Assessed by Selective Degradation. I. Ozone Degradation Method

D. J. PRIEST,* *H. H. Wills Physics Laboratory, University of Bristol, Royal Fort, Bristol BS8 1TL, England*

Synopsis

Ozone has been used as a selective oxidizing agent for degrading polyethylene single crystals at room temperature in order to confirm and extend results on surface structure obtained by use of fuming nitric acid at temperatures above 60°C. The surfaces of the crystals were rendered highly accessible to the ozone gas by preparing the crystalline material in a highly expanded form; the solvent in which the crystals were suspended was removed by sublimation from the solid state. The extent and nature of the reaction were studied by measuring the increase in weight and in density, by direct chemical analyses, and by making use of infrared spectroscopy and gel-permeation chromatography. It was found that the surfaces of the crystals are attacked at room temperature by ozone, with resulting chain scission, and the broad features of the chemical reaction were established. Some folded chains are found to be as long as the original thickness of the crystal, and once folds have been cut, continuing reaction shortens the chains. In the early stages of the degradation, during which most of the weight increase takes place, the density of the crystals increases, and the magnitude of the increase is that expected from the increase in weight alone, i.e., assuming no increase in effective volume.

INTRODUCTION

Selective degradation is an increasingly widely used technique in the study of polymer morphology.[1–3] Following up a large body of earlier work we are now presenting a coordinated systematic investigation as applied to polyethylene single crystals. The work is based on past experiences gained in these laboratories in this subject. It is a compendium of a variety of initially disconnected investigations which nevertheless converged to the same conclusions in the course of time. In doing so it mostly extends and partly modifies some of the earlier conclusions and in the course of it places several hitherto conflicting observations into a consistent framework hopefully setting a pattern for continued work in this subject. In the course of these studies new techniques were established and existing ones modified. Part I (the present paper) deals with the introduction of ozone as a degradation agent, Part II[4] with the modifications of the existing technique relying

* Present address: Reed Engineering and Development Services Ltd., Aylesford, Maidstone, Kent, England.

on nitric acid, and Part III[5] with the actual investigation on single crystals by the techniques covered by the preceding two papers. A systematic historical survey will be deferred to Part III.

Past degradation studies on polyethylene crystals[1–3] rely practically exclusively on fuming nitric acid acting at elevated temperatures (60°C or above). The origin of the work to be described in this paper was a search for a different selective oxidizing agent, mainly, as an initial objective, to provide confirmatory or additional evidence to that given by concentrated nitric acid. Some preliminary qualitative work[6] had shown that exposure of solvent-free polyethylene crystals to ozonized oxygen at room temperature caused their weight to increase. Apart from the intrinsic interest in pursuing this work, at the outset ozone seemed likely to offer the following advantages.

(a) It will work at room temperature, well below temperatures which might affect the structures to be studied; this has been shown by Beachell and Nemphos.[7]

(b) The chemical reaction should be simpler, since only oxygen atoms can be added to the polyethylene and because the reaction would be carried out without a liquid phase being present.

(c) Characteristically, treatment with concentrated nitric acid causes a loss in weight as degraded fragments are dispersed in the liquid. With ozone, the weight was seen to increase, which means that it is likely that products of degradation are retained and may be available for study. In any case, the different behavior could lead to new and interesting results.

(d) Ozone should be a milder degrading agent than hot concentrated nitric acid.

The results and conclusions presented in this paper bear out these expectations. In reading it, it should be borne in mind that the aim of the work was to arrive at information about the structure of the crystals rather than to study exhaustively the interaction of polyethylene with ozone. In this paper experimental methods are described in detail with initial results of the work; these are expanded and the major structural conclusions given in Part III.[5]

EXPERIMENTAL

For the reaction to proceed at its maximum rate, the surfaces of the crystals should be freely accessible to contact with the reactant gas, a situation which minimizes complications of interpretation due to long times of diffusion of gases to the reaction sites. The best way of achieving this was found to be to remove the solvent from the dilute suspension of crystals by sublimation at a temperature below its freezing point, thus eliminating the surface tension effects which draw the crystals into close contact when liquid is evaporated from a suspension. In what follows, this process will be given its usual name of freeze-drying, although, of course, water is not involved here. Subsequent experiments in which films of polyethylene were exposed to ozonized oxygen showed that the rate of reaction was negligible

compared with the rate of reaction with freeze-dried crystals. It is fortunate that *p*-xylene is a very suitable solvent, since its melting point is 13.2°C, while most previous work in this laboratory on polyethylene crystals has made use of xylene as a solvent (usually a mixture of the three isomers, *o*-, *m*-, and *p*-xylene).

Preparation of the Crystals

The linear polyethylene used was unfractionated Phillips Marlex 6009. A suspension of crystals (0.2 wt-%) in *p*-xylene was prepared by the self-nucleation technique;[8,9] a solution was precrystallized at 80°C, heated slowly from about 70°C to the seeding temperature (normally 101.5°C), a process which usually required about 5 hr, and crystallized at 85°C. The crystals so produced are largely monolayer truncated diamonds showing, when dried on a microscope slide, the usual lateral crease-mark; they measured about 6 × 4.5 μ and have been illustrated elsewhere.[8]

Freeze-Drying

The volume of the suspension was first reduced by centrifuging and decanting, typically from about 250 ml to about 70 ml (note that the centrifuge must be allowed to come to rest without deliberate braking, or deceleration forces will remix the sedimented crystals). The concentrated suspension was transferred to a flask and attached to a high vacuum system. The

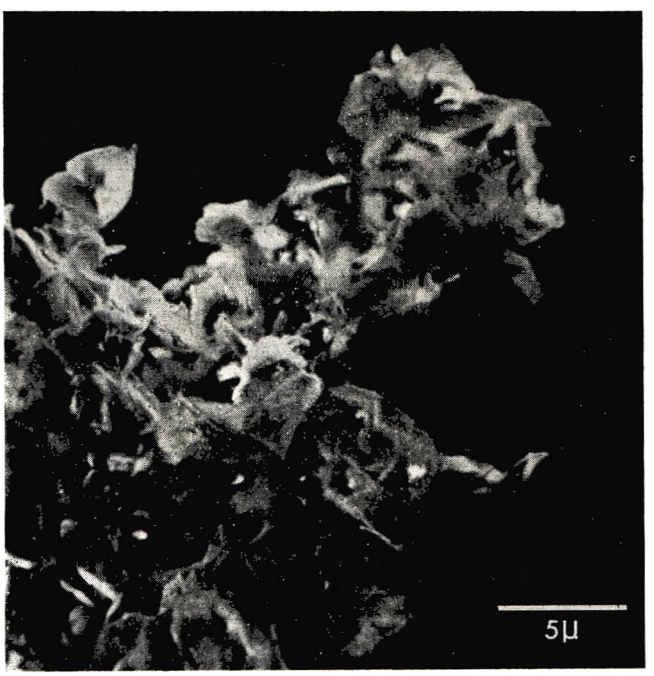

Fig. 1. Freeze-dried floc of polyethylene crystals grown at 85°C by the self-seeding procedure. Stereoscan micrograph.

flask was immersed in liquid air to freeze the *p*-xylene as quickly as possible so as to cause the least disturbance to the crystals. The system was then pumped for about 1 hr; the liquid air around the sample flask was then replaced by a mixture of ice and water, and an adjacent trap was cooled in liquid air. About 16 hr was usually allowed for the sublimation to ensure complete removal of the solvent, the final traces if any, being removed with the sample at room temperature. Before removing the flask dry air was admitted cautiously so as not to disturb the expanded crystal mass. A typical sample had a bulk density of approximately 1.5×10^{-2} gm/cm^3. Examination of the freeze-dried aggregate in a Cambridge Stereoscan scanning electron microscope at a magnification of about 1200× indicated that the crystal lamellae were separate; in places the characteristic hollow pyramidal structure could be seen (Fig. 1).

Treatment with Ozone

The ozonizer used was a modification of a published design.[10] It had two ozonizer tubes instead of three, and, for most of the work, was cooled by water instead of solid carbon dioxide, as this method was more convenient for prolonged experiments even at the expense of the amount of ozone produced. The transformer used gave 10 kV output at mains frequency (50 Hz). The whole system consisted of an oxygen cylinder fitted with a pressure reducing valve, a drying tower containing silica gel, a needle valve, (Edwards 951D), a flow meter, the ozonizer, the sample holder (see below), and two wash bottles containing aqueous potassium iodide solution (about 10% KI) to remove unused ozone. The amount of ozone produced was measured occasionally by first passing the gas into a solution of about 4 g potassium iodide in 200 ml water (with a little boric acid) at a flow rate of 100 cm^3/min for 10 min. The iodine produced was titrated with 0.1*N* sodium thiosulfate solution (1 ml 0.1*N* $Na_2S_2O_3 \equiv$ 2.4 mg ozone). Usually the oxygen contained 1 to 1.5 wt-% of ozone.

Tests and Analyses

Increases in Weight. In Figure 2 is shown the type of sample holder eventually adopted for measuring the increase in weight. Here the inner sample holder could be removed for weighing by special brass hooks. Owing to the low bulk density of the crystalline aggregate, a large holder is

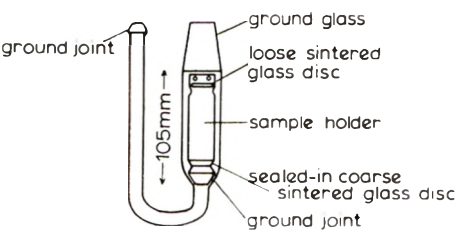

Fig. 2. Sketch of sample holder used for ozone treatment of polyethylene crystals.

required for a small weight of sample. The inner holder shown weighed about 20 g and held about 150 mg of sample. The maximum increase in weight of the sample was about 7% (i.e., about 10 mg), so great care was necessary in weighing. Initial experiments showed up a large buoyancy error due to slow diffusion of residual ozone and oxygen from the sample; the weight apparently drifted for some hours. This was corrected by gently drawing laboratory air through the sample (at about 200 cm^3/min) for about 0.5 hr. By these means reproducibility within 0.1 mg was achieved.

Infrared Spectroscopy. A sample (0.7–0.9 mg) was mixed thoroughly, but not ground, with about 0.5 g of previously dried and finely ground potassium bromide. The mixture was placed in a vacuum oven at about 60°C for 1–2 hr, then removed and pressed to a disk in the evacuated die. The spectra were recorded on a Unicam SP 100 spectrophotometer by using the rock salt prism monochromator.

Chemical Analysis of Oxygen Content. This was done by the Alfred Bernhardt Mikroanalytisches Laboratorium, Elbach über Engelskirchen, West Germany. Samples were despatched in sealed evacuated glass tubes.

Measurement of Density. Density was measured by means of a centrifugal flotation technique by use of an apparatus to be described elsewhere.[11]

Gel-Permeation Chromatography. Analyses were done on a Waters instrument; about 15 mg of the oxidized crystals was required, and was dissolved directly in the appropriate solvent. Details have been published elsewhere.[3,12]

RESULTS AND INTERPRETATION

Increase In Weight

The preliminary finding of Blundell and Keller[6] mentioned above was confirmed, and it was found that, in contrast to results obtained with concentrated nitric acid, the weight of the sample increased markedly on exposure to ozonized oxygen. Figure 3 shows graphs of the increase in weight, expressed as a percentage of the initial weight, plotted against cumulative time of treatment with ozone, for two samples of freeze-dried crystals. In both cases the weight is seen to rise to a maximum, suggesting saturation with oxygen. (Both samples of crystals were prepared and treated in the same way as far as possible. No explanation can be offered at present for the difference between them which appears both in the "saturation" value and in the rate of attack. However, the difference does not affect the interpretation of the results.)

The most elementary approach to explaining the increase in weight is to calculate the weight of oxygen in a dicarboxylic acid (the normal completely oxidized product; see below) having a length equal to that of a chain which traverses the single crystal once. The figures obtained, for a chain length of 150 Å as obtained from low-angle x-ray measurements, is 3.67%. The observed increases in weight, while not differing widely from this value, are clearly larger, suggesting degradation to an extent greater than that needed

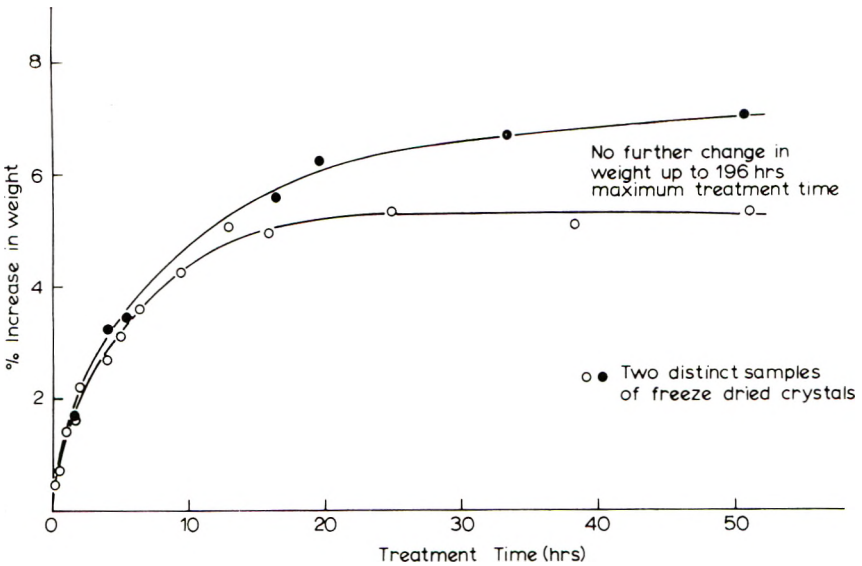

Fig. 3. Increase in weight of polyethylene crystals as a function of treatment time with ozone.

merely to saturate the basal surfaces with carboxylic acid groups. The edges of the crystals will be accessible to attack, but if the extent of reaction is assumed to be in proportion to the accessible area, the weight of oxygen absorbed by the edges would not exceed 0.1% and thus would not account for the discrepancy. Work to be described later, however will help to resolve this difficulty.

Change of Density

For our density technique the crystals were needed in suspension. It was found that freeze-dried crystals can be readily redispersed in a suitably compatible liquid; a dispersion in *p*-xylene should closely resemble the original suspension. This meant that it was possible to measure the density of the partially oxidized crystals in a way which allowed direct comparison with the undegraded ones which had a density of 0.98 by the same technique (unpublished work referred to in ref. 13). The result is shown in Figure 4, in which the density is seen to increase linearly with the increase in weight. Moreover, the line drawn is calculated from the value of density for the unoxidized crystals by assuming that the weight increases without an increase in volume. The good fit to the experimental results suggest that the oxygen may be filling voids in the structure which contributed to the original low density. The results of later work[4,5] suggest a structure in which such a mechanism could reasonably occur. Winslow et al.[14] have studied the change in density on oxidation of bulk polyethylene by oxygen gas at elevated temperatures. An example of their results is shown in Figure 5: the density showed two distinct rates of change as the oxidation

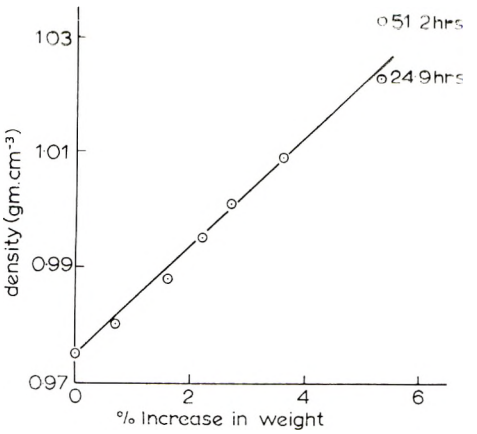

Fig. 4. Density of polyethylene crystals as a function of percentage weight increase in the course of ozone treatment.

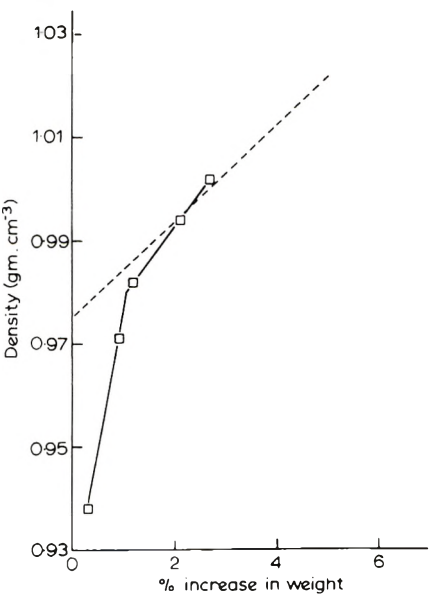

Fig. 5. Comparison of (- -) the results in Fig. 4 with (——) previous results of Winslow et al.[14] on the oxidation by oxygen of bulk polyethylene.

progressed. At the lower extents of oxidation, Winslow et al. supposed chemicrystallization to be taking place in the amorphous regions. The increase in density found in this work, also plotted in Figure 5, is seen to correspond, as expected, to the more highly crystalline part of Winslow's graph. The single rate of increase in density shows that there is no extensive rearrangement of the structure during most of the reaction, since an increment of oxygen absorbed at the early stages of reaction causes the same increase in density as an equal increment added when the oxygen content is

high. [However, this does not apply strictly after very long times of reaction. The point in Figure 4, which is off the line, represents such material (51.2 hr treatment, see Fig. 3). Results described in the next section show that the extent of reaction as measured by infrared spectroscopy has continued to increase.]

Chemical Analysis and Infrared Spectroscopy

In Figure 6 are plotted graphs of (a) the increase in infrared absorbance due to carbonyl groups at around 1712 cm^{-1} and (b) the increase in oxygen content as oxidation proceeds. (The infrared absorbance was corrected for slight variations in the weight of the sample by dividing by the absorbance at 2857 cm^{-1} due to C—H stretching vibrations. The ratio is denoted by A_{CO}.) Comparison with Figure 3 shows that after the time at which the weight increase levels out, both the oxygen content and A_{CO} continue to

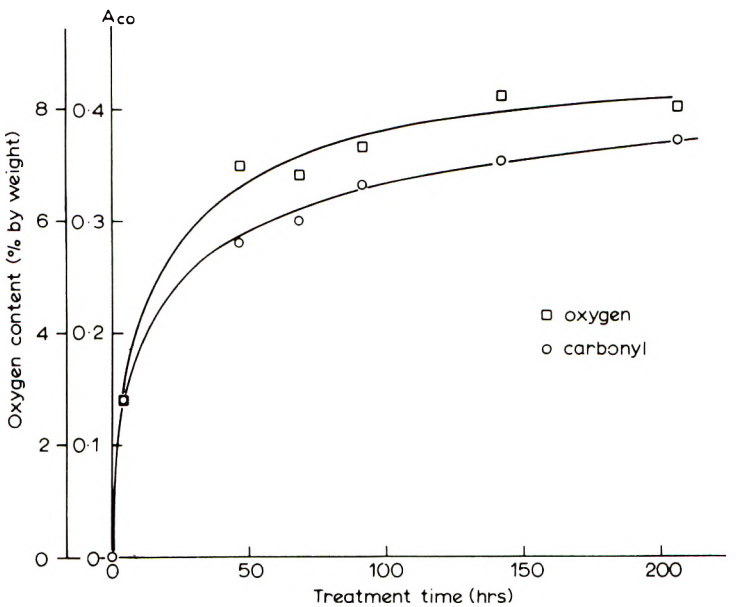

Fig. 6. Increase in oxygen content and infrared absorbance due to carbonyl groups (A_{CO}) as the oxidation proceeds. (No attempt has been made to match the oxygen content and A_{CO} scales).

rise up to the maximum times of treatment employed. This is more strikingly brought out by Figure 7, which shows that beyond 5% oxygen, the oxygen content increases while the weight stays constant. This means that, as might be expected, some material is being lost, probably as carbon dioxide and water vapor.[7] The fact that the increase in oxygen seems to compensate exactly the loss of weight seems remarkable. It may be due to the fact that the weight of one methylene group is very close to that of an oxygen atom.

The precise frequency of the carbonyl absorbance depends on the nature of the chemical grouping containing the carbonyl group, which may normally be an aldehyde, a ketone, an ester, an anhydride, or a carboxylic acid. Rugg, Smith, and Bacon[15] have recorded the infrared spectra of polyethyl-

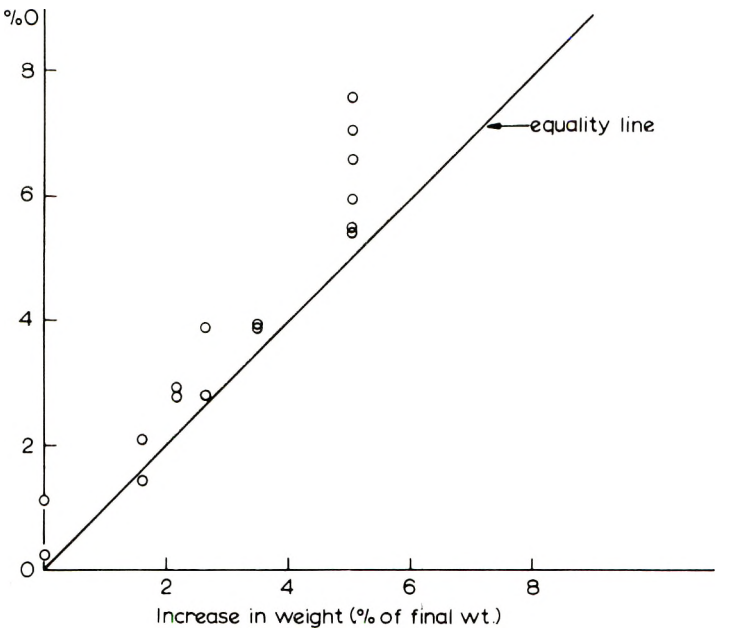

Fig. 7. Relation between increase in oxygen content and that of final percentage weight.

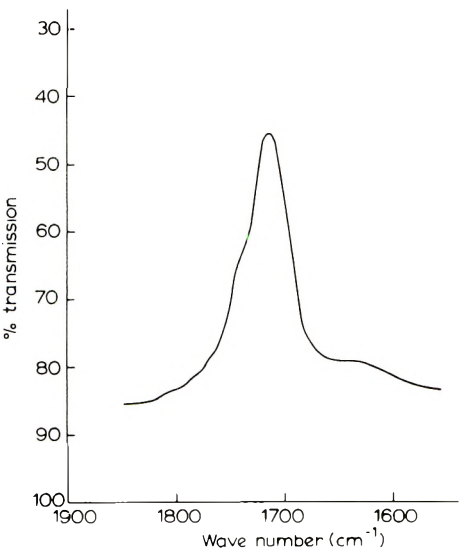

Fig. 8. Infrared spectrum showing the form of the absorption peak attributed to carbonyl groups.

ene mixed with various model compounds containing these groups, to simulate oxidized polyethylene. The infrared spectrum of the crystals degraded by ozone showed, in the relevant region, a single peak with a small shoulder on the high wavenumber side (see below) at all stages of the degradation. An example is shown in Figure 8. The frequency of this peak

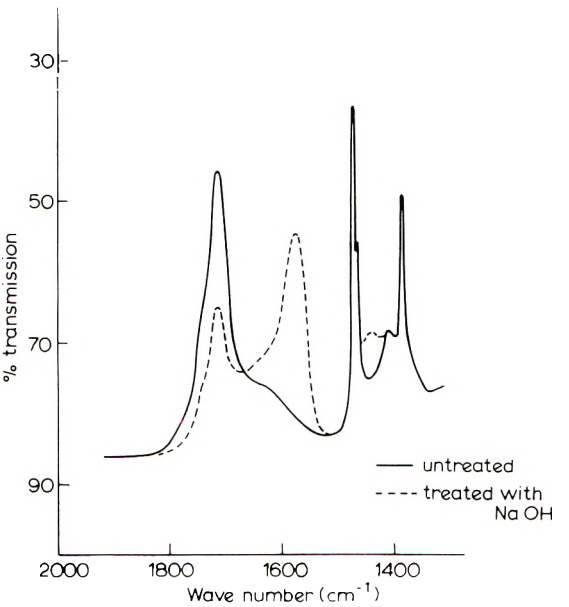

Fig. 9. Infrared spectrum showing the effect of treating the oxidized crystals with aqueous sodium hydroxide solution to form the sodium salt of the carboxylic acid.

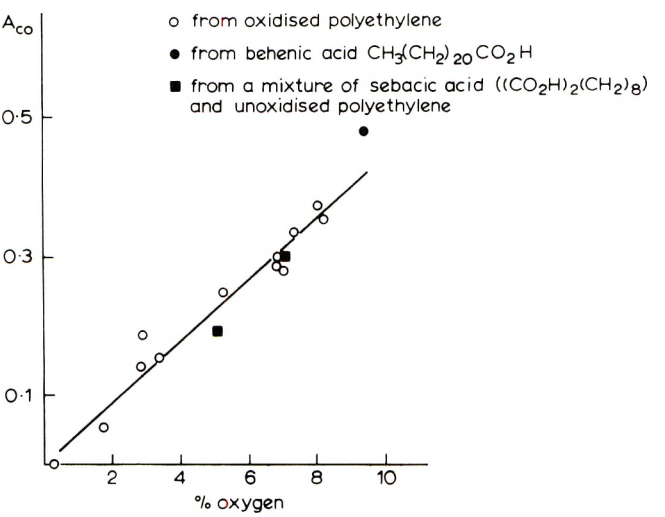

Fig. 10. Analyzed or calculated oxygen content plotted against the infrared absorbance due to carbonyl groups.

(1710 cm^{-1}) makes it most likely that the group is carboxylic acid, with some possibility of it being a ketone. Confirmation of the assignment to a carboxylic acid was obtained in the following way. After treatment of the degraded crystals with a dilute aqueous solution of sodium hydroxide the intensity of the carbonyl peak was greatly reduced (Fig. 9) and new peaks appeared at about 1400 and 1550 cm^{-1}; the effect is due to ionization of the carboxylic acid group, the new peak being due to symmetrical and antisymmetrical vibrations of $—CO_2^-$. The small peak remaining is at exactly the same frequency as the original large peak and so it probably represents carboxyl groups inaccessible to the alkali. Figure 10 shows a graph of analyzed oxygen content plotted against A_{CO} which includes points obtained from the spectra of two carboxylic acids. The linear relationship shows that initial small additions of oxygen produce the same intensity of carbonyl absorbance as equal increments of oxygen taken up late in the process. The situation is analogous to that of the increase in density (Fig. 4). (It should be noted that while the results of Figure 10 are in agreement with the assignment to carboxyl, this graph does not provide additional evidence because the extinction coefficient of ketone carbonyl is about the same as that for carboxylic carbonyl when expressed in terms of fractional oxygen content.[15])

Thus, evidence described so far indicates that with the polymer surfaces in this very accessible condition, as soon as a reaction is initiated at a given site, the oxidation rapidly proceeds to carboxylic acid. Initiation is slow by comparison, and its rate is governed simply by the number of sites remaining unattacked.

However, although this is probably correct in outline, there are no doubt complexities; hints of these are listed here.

The shoulder on the carbonyl infrared absorption peak, which has very roughly an absorbance of 5% of that of the main peak, indicates the presence of a small proportion of carbonyl groups other than carboxyl ones. This shoulder is present at all stages of the degradation, supporting the view that the basic reaction is the same throughout.

The precise frequency of the main carbonyl peak is about 10 cm^{-1} higher than those appearing in the spectra of model dicarboxylic acids. This is not sufficiently different to cast doubt on the clear evidence, from the ionization, for the presence of carboxylic acid predominantly; it may be due to a special environment of groups at the surface of the oxidized crystal.

A curious effect was found when remeasuring certain values of infrared absorbance on samples stored (in contact with the atmosphere) for long periods. This is shown in Figure 11. The increase in A_{CO} was not accompanied by a corresponding increase in chemically analyzed oxygen. In principle, the effect could be due to slow conversion of ozonides, formed at the occasional double bonds, into carboxyl, an effect observed recently in a definitive form in the course of ozone treatment of unsaturated polymers.[16] Nevertheless the effect in Figure 11 is too large: there are not sufficient double bonds for it. We have no further suggestion to make beyond plac-

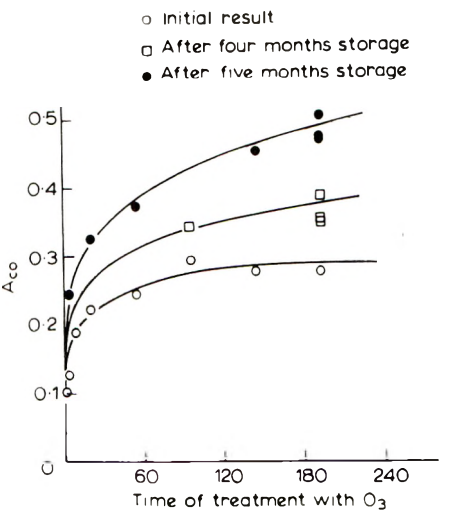

Fig. 11. Curves showing the apparent increase in infrared absorbance (carbonyl) with storage time of the oxidized crystals.

ing the effect on record. It should be noted that the results given above (Figs. 6–10) used values measured within a day or so of the treatment with ozone.

After long times of reaction the sample became slightly discolored to a very pale brown, suggesting more complex chemistry.

Gel-Permeation Chromatography

Measurement of the change in molecular weight distribution as degradation proceeded gave the same splitting into narrow bands as formed with degradation by concentrated nitric acid, but there are basic differences in detail. When extended and taken in conjunction with other new results obtained using nitric acid, these basic differences were eventually to contribute considerably to our idea of the structure of the surface layers of the crystal.

Figure 12 shows the appearance of a chromatogram after degradation with ozone. (A full sequence is given in the third paper in the series). The position of the main peak is found to correspond to a molecular length similar, but less than that of the thickness of the crystal (allowing for the tilt of the molecules), while that of the small peak corresponds to approximately twice that length. In nitric acid degradation, this "single traverse" which according to past work did not change significantly during the course of the degradation, has been associated with the true thickness of the crystal, the difference between it and the total thickness of the crystal being taken as readily degraded "amorphous" material.

On using ozone as the degrading agent, it was found that this single-traverse length decreased steadily during the degradation process (see, e.g., Fig. 10 of Part III[5] of this series); this clearly rules out a clear boundary

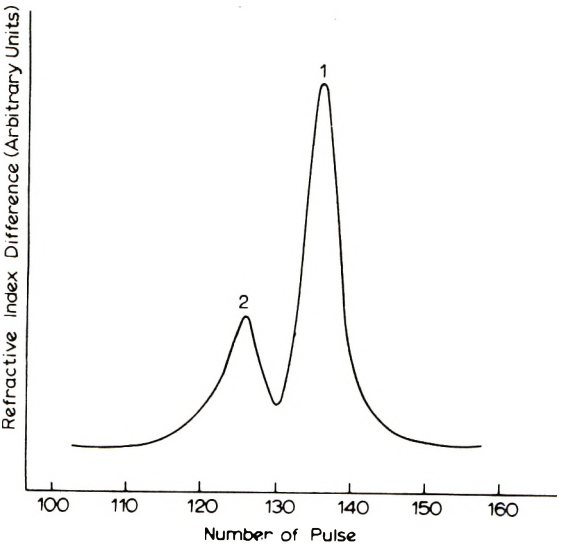

Fig. 12. Typical gel-permeation chromatogram of polyethylene single crystals in an advanced state of degradation with ozone. Degradation time 121 hr. Peaks 1 and 2 correspond to the single- and double-traverse lengths, respectively (see text).

between accessible and inaccessible layers within the crystal. These matters are dealt with in detail in Part III.[5]

Extraction of the Low Molecular Weight Products of the Degradation

The shortening of the traverse length as the degradation proceeds, coupled with the absorption of more oxygen than that required to "saturate" the surfaces, suggests that some oxidation products of low molecular weight were being formed which are not observed in the gel-permeation chromatogram. Corresponding products in the nitric-acid degradation would be dispersed in the liquid phase. The increase in weight observed here, as well as the high oxygen content, shows that the products are still, to a large extent, present in the degraded crystals.

Paraffinic dicarboxylic acids, $CO_2H—(CH_2)_n—CO_2H$, are appreciably soluble in water up to about $n = 5$. Above $n = 5$ there is still good solubility in diethyl ether. Some limited experiments on small samples were done in which the infrared spectrum was examined before and after extraction with water and diethyl ether. A marked reduction in A_{CO} was observed; this was approximately the same after extraction with both water and ether. According to Figure 10, the oxygen content after extraction was found to be approximately 4.0%, a figure which is near that of 3.67% calculated for a pure dicarboxylic acid with a chain length of 150 Å. In fact, of course, for the degraded material this figure will be in error, partly because the chains are now shorter (increasing the fractional oxygen content) and partly because not all the material is in the form of single traverses (decreasing the

fractional oxygen content). On use of the gel-permeation chromatograph to estimate these effects, a value of 3.62% oxygen is obtained.

In principle, it should be possible to calculate the mean chain length of the material extracted by using the decrease in thickness of the crystal (obtained from the x-ray and gel-permeation data) to give the hydrocarbon content and obtaining the oxygen content from the difference between the extracted and unextracted material. (The difference between the weight increase and the oxygen content of the unextracted crystals enables a correction to be made for the amount of carbon and hydrogen lost as carbon dioxide and water.) However, the low precision of most of the measurements, coupled with the use of three sets of differences, made the calculation highly inaccurate. One attempt yielded a value of 9 for the number of carbon atoms between the carboxyl groups, and this is clearly too high in view of the solubility requirements mentioned above. (From the known chemistry of oxidation of paraffins, it is most likely that after oxidation to a carboxylic acid, the carbon atom next to the carboxyl group will be attacked next in the chain-shortening process.[17])

CONCLUSIONS

At the close of this first phase of the study of degradation by use of ozone the following are the main points to have emerged.

At room temperature, the surfaces of polyethylene crystals, when rendered suitably accessible, are attacked by ozone with resulting chain scission. Analysis by gel-permeation chromatography suggested that some folded chains in the crystal are as long as the original thickness of the crystal (after allowing for the tilt) and showed that, once folds had been cut, attack continued in such a way as to shorten the chains, a finding to be expounded further in Part III of the series.[5]

In the early, relatively rapid stage of the degradation, the density of the crystals increases. The magnitude of the increase is that expected from the weight increase, assuming no increase in effective volume.

The broad features of the chemical reaction are a slow initiation stage, followed by a rapid oxidation principally to carboxylic acid with a small proportion of other, unidentified, carbonyl-containing groups plus the production of water-soluble carboxyl-containing fragments.

The results of extending the measurements to other temperatures, and the correlation with new results on degradation with nitric acid will be described in Part III[5] in connection with a detailed discussion of the consequences for the structure of polyethylene crystals.

The author wishes to thank Professor A. Keller for his help and encouragement, Dr. T. Williams for taking the GPC chromatograms and him and Professor I. M. Ward for their interest in their evaluation. He also wishes to acknowledge financial support by the Science Research Council.

References

1. R. P. Palmer and A. Cobbold, *Makromol. Chem.*, **74**, 174 (1964).
2. D. J. Blundell, A. Keller, and T. Connor, *J. Polym. Sci. A-2*, **5**, 991 (1967).
3. T. Williams, D. J. Blundell, A. Keller, and I. M. Ward, *J. Polym. Sci. A-2*, **6**, 1613 (1968).
4. A. Keller and Y. Udagawa, *J. Polym. Sci. A-2*, **9**, 1793 (1971).
5. A. Keller, E. Martuscelli, D. J. Priest, and Y. Udagawa, *J Polym. Sci. A-2*, **9**, 1807 (1971).
6. D. J. Blundell and A. Keller, unpublished data.
7. H. C. Beachell and S. P. Nemphos, *J. Polym. Sci.*, **21**, 113 (1956).
8. D. J. Blundell, A. Keller and A. J. Kovacs, *J. Polym. Sci. B*, **4**, 481 (1966).
9. D. J. Blundell and A. Keller, *J. Macromol. Sci., B2*, 337 (1968).
10. T. P. Whaley, *J. Chem. Educ.*, **34**, 94 (1957).
11. D. J. Priest, to be published.
12. F. C. Frank, T. Williams, and I. M. Ward, *J. Polym. Sci. A-2*, **6**, 1357 (1968).
13. A. Keller, *Progr. Repts. Phys.*, **31**, Part 2, 623 (1968).
14. F. H. Winslow, M. Y. Hellman, W. Matreyek, and S. M. Stills, *Polym. Eng. Sci.*, **6**, 273 (1966).
15. F. M. Rugg, J. J. Smith, and G. R. C. Bacon, *J. Polym. Sci.*, **13**, 535 (1954).
16. A. Keller and E. Martuscelli, *J. Macromol. Chem.*, in press.
17. F. Asinger, *Paraffins, Chemistry and Technology*, Pergamon Press, New York–London, 1968, p. 616.

Received January 21, 1971

JOURNAL OF POLYMER SCIENCE: PART A-2 VOL. 9, 1793–1805 (1971)

Fold Surface of Polyethylene Single Crystals as Assessed by Selective Degradation Studies. II. Refinements of the Nitric Acid Degradation Method

A. KELLER and Y. UDAGAWA, *H. H. Wills Physics Laboratory, University of Bristol, Bristol BS8 1TL, England*

Synopsis

Detailed critical examinations of three aspects of nitric acid treatment of polyethylene are reported. 1) The endgroups introduced by the nitric acid are examined. It is concluded that in samples degraded to a single-crystal traverse stage, carboxyl features only as endgroup, and conversely each chain-end is terminated by such a group. Consequently, the carboxyl content can be used for quantitative characterization of the cut chain length. The function and position of the nitro group remains unexplained. 2) The morphological selectivity of the nitric acid-induced degradation is scrutinized. It is concluded that the crystal core is attacked and thinned by the acid; the slowing down of the reaction is principally due to accumulation of reaction products. Accordingly, the usual distinction between a vulnerable amorphous layer and a resistant crystal core is not justified on the basis of such degradation experiments. It follows that meaningful structural information is obtained only when the relevant crystal properties are studied as a function of chain cutting, assessed from the molecular weight distribution (GPC), as opposed to that of degradation time alone. 3) The role of sample consistency and reagent strength has been examined. It is demonstrated that for the reaction to be sufficiently uniform throughout the sample for the results to be meaningful, the reaction rate has to be slow compared to the rate at which the reagent diffuses into the specimen. To realize these conditions, finely dispersed samples and weak reagents were found to be favorable

INTRODUCTION

As already stated, all past degradation studies on polyethylene relied on the action of fuming nitric acid. We have continued to employ this reagent in our studies of single crystals in addition to the more recently developed ozone technique described in the preceding paper.[1] In the course of extensive experimentation with nitric acid, considerable new information was obtained on the products of the chemical reaction, on the factors influencing the degradation, and on the potential and limitations of the technique. The present paper contains a selection from this material. The items selected are such as are sufficiently documented for a coherent presentation and at the same time are relevant to the principal investigation on the single crystals.[2] The following three subjects will be covered: (a) new information on the endgroups which are introduced by the nitric acid, (b) morphological selectivity of the reaction, (c) influence of sample consistency

and reagent strength. First, however, the general features of the experimentation will be briefly outlined.

EXPERIMENTAL

Samples and Degradation Methods

Polyethylene single crystals were Rigidex 50 grown at 85°C from xylene by conventional methods. Parts of the studies also utilized bulk material in pellet form. As in earlier studies, degradation was carried out in sealed glass tubes in a large excess of acid. In addition to the usually employed fuming nitric acid, diluted reagents were also employed. The most frequently used dilution was 82.5% acid obtained by appropriately diluting the stock reagent specified as 95%. The latter value was not specifically checked; consequently, the exact figures have only relative significance. Treatment temperature was usually 60°C.

Examination Methods

The degraded samples were investigated as regards lamellar thickness (long spacing) by low-angle x-ray diffraction, COOH and NO_2 group concentration by infrared spectroscopy, molecular weight distribution by GPC, and thermal measurements by DSC. The experimental procedures were identical to those described in the preceding paper.[1]

RESULTS

Endgroups

The first studies on nitric acid digestion of polyethylene established that the reaction introduces COOH and NO_2 groups.[3] The relative amounts of the two groups and their position along the chain however, remained unclarified. Chemical analysis for oxygen showed that the increase in oxygen correlates with other properties measured during degradation.[4] In particular, the oxygen content increased at a decelerating rate, reaching a constant value of about 5% which corresponds roughly to four oxygen atoms per chain traverse length through a lamella. As at that stage all folds were completely cut, this could be consistent with either a carboxyl or a nitro group (and possibly a mixture of both) at each chain end. The amount of nitrogen was also analyzed.[4] The nitrogen content increased very rapidly during the very first stage of the reaction to its maximum value of ca. 1% and stayed steady while the oxygen content continued to increase. It even decreased slightly at long treatment times. However, in view of the small amount of nitrogen and the large relative variation in the results in different samples, we did not attempt to interpret the data any further besides noting that correlation between nitrogen uptake and other measurements was not straightforward. The present work pursues these earlier studies.

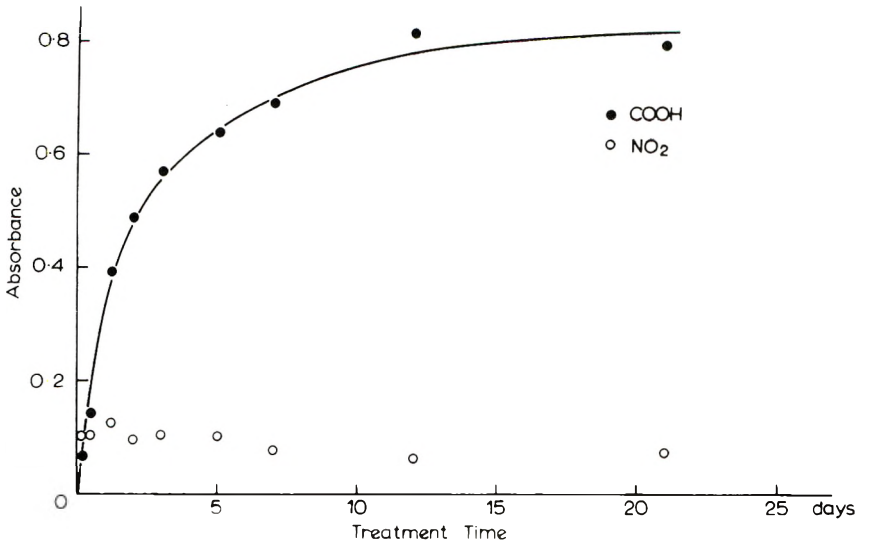

Fig. 1. Absorbances of the 1712 cm^{-1} carboxyl and 1557 cm^{-1} nitro infrared bands of nitric acid-treated polyethylene single crystals as a function of treatment time. The absorbances are normalized to the 1470 cm^{-1} methylene band, and the points for the nitro group have been scaled so as to make them directly comparable with those for the carboxyl group (see text).

In the course of the work COOH and NO_2 groups were measured quantitatively by infrared spectroscopy of the nitric acid-treated samples. The bands were: 1712 cm^{-1} for COOH and 1557 cm^{-1} for NO_2 content. The studies were carried out on two types of samples: (1) a given preparation followed as a function of degradation and (2) starting materials of different initial long periods compared in a state of degradation where all the folds were cut and the material consisted of single-traverse molecules only.[5,6]

Figure 1 shows the COOH and NO_2 content in a degradation series. The intensities of the COOH and NO_2 bands are expressed as normalized to the 1470 cm^{-1} CH_2 band. For comparing the COOH and NO_2 content quantitatively, the relative absorbances of the two bands were determined separately on model compounds. These were behenic acid and *n*-decoic acid for the carboxyl group and nitrodecane for the nitro groups. The latter was used as a liquid at room temperature. The ratio of the two extinction coefficients of nitro to carboxyl was close to unity, more precisely it was ca. 1.4. It seems reasonable to assume that the same ratio holds also for the longer chains of essentially similar compounds such as in our degradation products. The curve for the NO_2 group in Figure 1 has already been scaled according to this calibration so that the two curves in Figure 1 should give a correct representation of the relative amounts of the two groups in our degradation products.

It is seen that the carboxyl group content increases asymptotically to a limiting value while the nitro group rises first then levels off and decreases

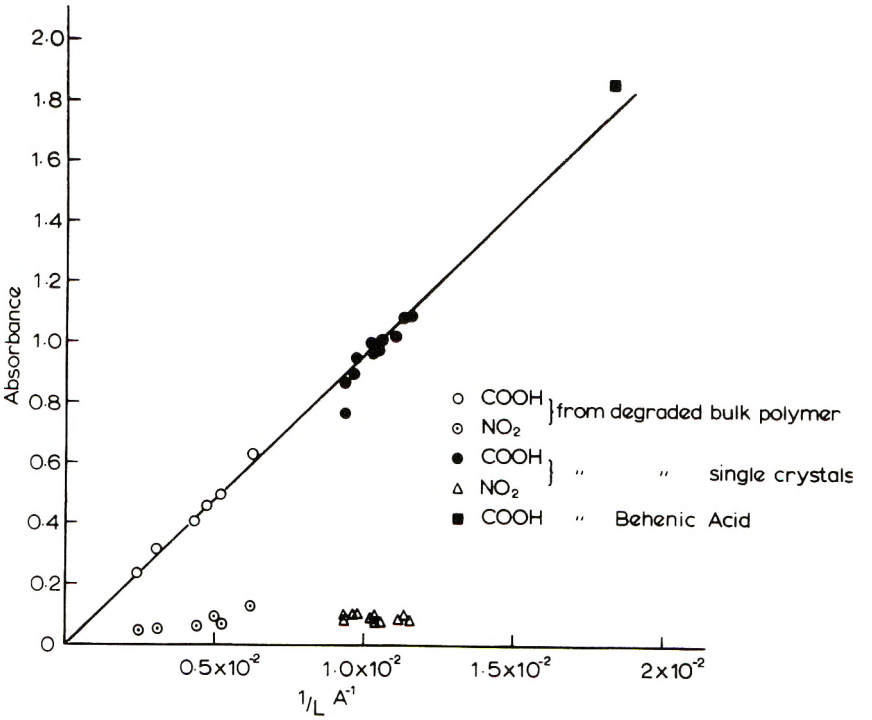

Fig. 2. Absorbances of the 1712 cm^{-1} carboxyl and 1557 cm^{-1} nitro infrared bands as a function of reciprocal x-ray long periods for different polyethylene preparations degraded to single-traverse lengths with nitric acid.

slightly thereafter, its concentration never exceeding $^1/_8$ of the final carboxyl. The relative trends of COOH and NO_2 groups found in these experiments directly by infrared spectroscopy is the same as indicated by the O and N analysis in the earlier work (Fig. 4 of ref. 4) and there stated with some reservation owing to the uncertainties in the nitrogen figures.

Samples having different original long spacings were degraded to the state where all the chains were of nearly identical length. This length of course corresponds to the single-chain traverse across the lamellae obtained when all the folds and ties are cut. This is manifest by the narrow single peak in the GPC chromatogram by which both the length of the chains and the sharpness of the distribution can be assessed.[6,7] As shown in previous studies,[5,6] the length of the corresponding chain traverse length relates to the long spacing of the undegraded material (it is usually 10–25% smaller). Accordingly, compounds with a variety of different and highly uniform length can be obtained by using appropriately chosen starting materials in order to cover a suitably wide range of chain lengths. Both bulk polymer and single crystals were used for our purposes. The long spacing variation in the bulk were achieved by different crystallization conditions. The full details are not immediately relevant for the present paper except for the final chain lengths which result from the degradation. The degradation

products from single crystals covered a lower range of chain lengths than those from the bulk. The origin of these samples and the differences between them will be apparent from the next section.

The COOH and NO_2 content is plotted against the reciprocal of the chain length in Figure 2. For the bulk samples the resulting L values were determined by GPC, for the single crystals by low-angle x-ray scattering (see next section); a point for a short-chain carboxylic acid (behenic acid) is also included. We see immediately that the COOH group content is inversely proportional to the chain length and extrapolates to zero for $L = \infty$. The NO_2 group content is practically constant throughout and shows no apparent correlation with chain length.

The foregoing is consistent with the picture that the chains are terminated by carboxyl groups and by these groups only, and conversely that all the carboxyl groups are at the end of the chain. Consequently, determination of the carboxyl content should give a quantitative measure of the number of folds cut, and in the stage when all the folds have been cut, of the number average molecular weight. In the case of a sharp distribution (as in our present samples) this figure should correspond closely to the molecular weight of a single chain-traverse. The function and position of the NO_2 groups however, remains unknown. The NO_2 does not seem to be quantitatively related to the degree of chain cutting nor to the number of chain ends. It appears, therefore, that it is an intermediary of the reaction and it may not even be at the end of the chain. While the problem of the NO_2 group may be important in its own right, at this stage of our knowledge, it does not seem to affect the structural deductions which can be reached about the polyethylene crystals; these seem to be accountable from the carboxyl group concentration alone.

Selectivity of the Reaction

Background. The underlying basis of all past degradation studies in aid of morphological investigations was the assumption that the amorphous, or in general, disordered material is digested while the lattice proper remains intact, or at any rate is degraded so slowly that these changes can be neglected on the time scale of the usual degradation.[5,6,8] In the case of single crystals in particular it was observed that the attack occurred predominantly along the basal surfaces proceeding surface downwards until it came to a halt at a certain well-defined depth. At this stage all folds were cut, the crystal consisting of straight chains being terminated by COOH groups (see preceding section). The surface layer thus removed was considered to represent the disordered material along the basal face of the crystal amounting usually to 10–25% of the total. This inference has been the starting point for all further speculations on the structure of the crystal lamellae. As will be seen, this underlying assumption will now be questioned.

The amount of layer thinning can be assessed by a variety of means.[4–8] The first direct assessment was made by following the changes in lamellar thickness by means of low-angle x-ray scattering.[4] The same information

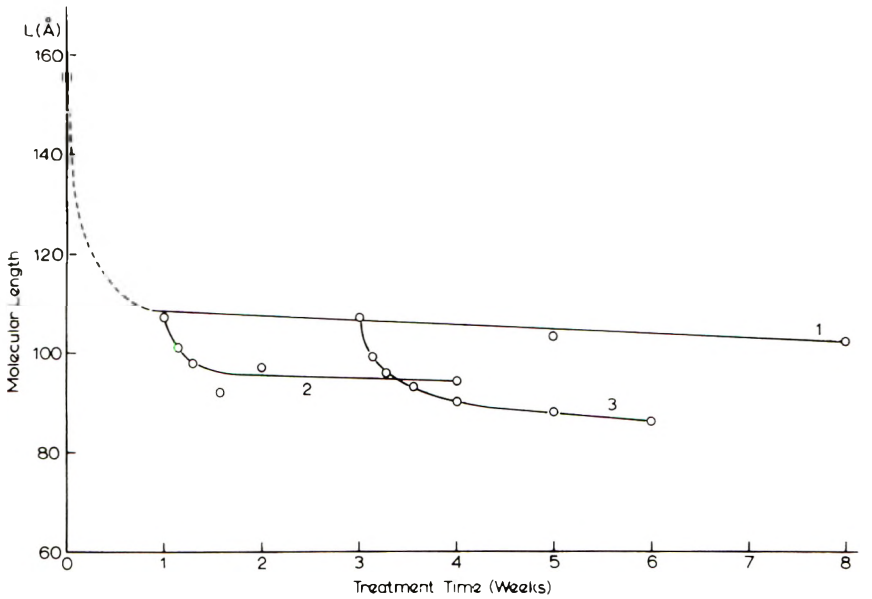

Fig. 3. Single-traverse lengths in highly degraded polyethylene single crystals, assessed by low-angle x-ray scattering, as a function of treatment time with nitric acid. For all except zero time, which corresponds to the fold length (corrected for chain inclination), the polymer is entirely in single-traverse form: (*1*) a continuous degradation; (*2*) and (*3*) samples were removed from the nitric acid at times corresponding to the common points along (*1*), were washed and resuspended in fresh nitric acid. Points along (*2*) and (*3*) correspond to these resuspended samples.

could also be obtained on a molecular level by measuring the molecular weight of the degradation products. Following some preliminary data by viscometry,[8] this could be most definitively achieved by means of GPC analysis.[5,6]

In this part of the paper we shall primarily rely on information obtained by low-angle x-ray scattering. While straightforward in principle, the method is seriously handicapped by the fact that the distinct low-angle maxima disappear or become greatly blurred and masked by continuous scattering in the course of the degradation.[4] For this reason, the original investigation required especially well oriented mats. Even in this case, the reflections disappeared during the initial stages of the reaction. When they reappeared later they were more diffuse and at least partially masked by continuous scattering. They became eventually unmeasurable as the reaction proceeded to very long times. For this reason, in the past the long spacing could only be followed over a limited range of degradation.

New Experiments. In the present studies we followed layer thicknesses up to very long times of degradation. This was made possible by the fact that at these stages the chains consisted of single traverses, and as assessed by GPC, were of highly uniform length. Even if after degradation the reflections were obscured (probably due to irregular layer-to-layer contact),

they reappeared again in sharply defined form when the degraded crystals were dissolved and recrystallized from a mixture of xylene and ethanol. As the newly formed crystals contain only single traverses, the molecular length could be determined from the long spacing. As assessed from wide-angle x-ray photographs, the molecules were perpendicular to the lamellar surfaces, hence the long spacing should give the molecular length directly. This contrasts with the original undegraded starting material where the chains were at 30° to the mat normal. Curve *1* in Figure 3 shows the molecular lengths as a function of degradation time obtained in this way. The point at zero time corresponds to the single traverse length in the chain-folded structure with chain inclination accounted for. All other samples were sufficiently degraded to contain single chain traverses only. Intermediate stages, such as are recorded in Figure 4 of ref. 5, were of no interest for the present.

We see that there is a large drop in fold segment length when going from the undegraded material to the single-traverse degradation product. This is the stage which has been studied previously and interpreted in terms of fold cutting and removal of the amorphous layer surface. We see that there is a slow but perceptible reduction in chain length over much prolonged degradation. This was noted previously, but the effect was considered negligible compared with changes during the first period of degradation and consequently did not affect the distinction between a highly vulnerable surface layer and a resistant crystal core. A very slow prolonged attack of the crystal nevertheless had to be admitted and allowed for when defining the intrinsically disordered layer thickness from these expeiments (see extrapolation in Fig. 4 of ref. 4).

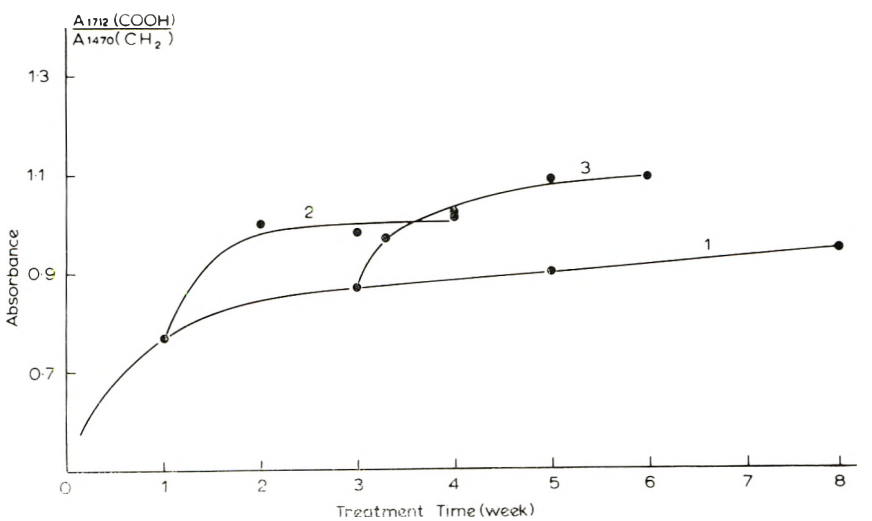

Fig. 4. Normalized absorbances of the 1712 cm^{-1} infrared carboxyl band of samples represented by points along the curves in Fig. 3.

In addition to reproducing the earlier findings and extending them to longer times we now performed some further experiments. Samples already degraded to single-traverse lengths were subjected to renewed degradation in fresh reagent after having been washed in water and acetone and dried in a vacuum oven. Curves *2* and *3* in Figure 3 show two such series starting from samples already degraded for 1 and 3 weeks, respectively. We see that in both cases there is a rapid initial decrease in the long period, hence in the chain length, leveling off gradually on prolonged treatment time. Figure 4 shows the COOH concentration corresponding to the three curves in Figure 3. It is apparent by inspection that the decrease in chain length correlates with the increase of the carboxyl concentration. A similar correlation is revealed on comparing the melting points (Fig. 5).

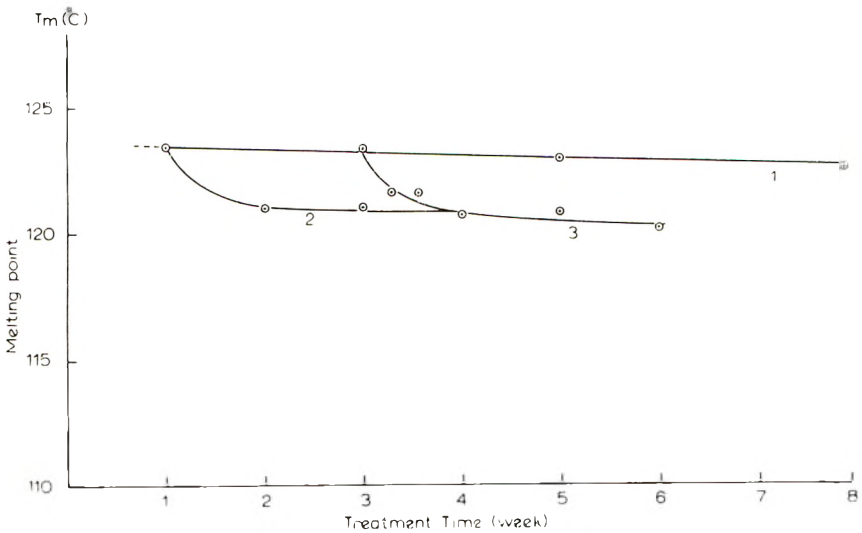

Fig. 5. Melting points of samples represented by points along the curves in Fig. 3.

Discussion. As in the single-traverse dicarboxylic acid crystals we have no more amorphous material in the usual sense, the immediate implication of the curves in Figures 3–5 is that the crystal itself can be attacked and thinned down by the acid at a rate much faster than was suspected, in fact at a rate comparable with the attack on the original chain-folded crystals. It will be apparent therefore, that it is of no significance to define a structural discontinuity in the crystals on the basis of where the digestion stops or slows down drastically, as this boundary can be shifted at will by changes in experimental conditions. It will be obvious that this removes the foundation on which past distinction between amorphous and crystalline portions rest, at least as assessed by selective degradation studies. This does not exclude that such a distinction may still be possible by smaller changes in the rate of layer-thinning, but this can certainly not be obtained from a sin-

gle curve but would require a new and complete analysis involving constant renewal of reagent and removal of reaction products.

It was shown in the previous section that the cut ends contain carboxyl groups, or conversely that such groups are situated at chain ends. In fact, the group of points in Figure 2 at high COOH content, hence at low L values were taken from series such as curves *2* and *3* in Figures 3 and 4. Accordingly, not only the end products of the fold cutting, but also those of the continued cutting of the dicarboxylic acids obey the relationship in Figure 2, i.e., the inverse proportionality between COOH concentration and chain length. This in turn means that dicarboxylic acids themselves are being shortened from the chain end downwards, in the course of which the terminating COOH is always removed while a new one is introduced at the end of the shortened chain. It is most likely that it is the methylene group adjacent to the terminal carboxyl group which is always attacked.[9] The melting point changes fall in line with this picture (Fig. 5). As no further carboxyl groups are introduced into a given chain the melting points in Figure 5 should correspond to those of a series of dicarboxylic acids of decreasing length.

The next question is the cause of the slowing down of the attack and its speeding up on renewed treatment. The most obvious suggestion that the reagent is exhausted cannot be maintained. First, the nitric acid is always used in large excess, secondly, the effect does not depend in any systematic way on the proportion of polymer to acid under our experimental conditions. The decisive procedure is the washing and drying of the sample before renewal of the degradation which indicates that the reaction slows down because of accumulation of reaction products at the crystal face. This effect was not pursued further.

It will be apparent that the above results remove the significance of the plotting as a function of time of molecular length, layer thickness, or any other property which is affected by the degradation, at least as far as structural conclusions are to be drawn from such plots. Clearly we need a time-independent measure of how far the reaction has proceeded. In the important stage before all the chains are converted to single-traverse dicarboxylic acids such a measure is the number of folds that has been cut i.e. $(1 - p)$ in ref. 10). The fractional amount P_1 of material present in the form of single traverses, readily obtainable from GPC chromatographs, combined with the well supported assertion that the cutting of folds occurs randomly, provides a direct measure for this degree of fold cutting.[10] In the light of the new findings this plotting of the relevant quantities versus P_1 or $1 - p$ instead of time becomes imperative. Such plotting was already used in Part I[1] and during some of the preceding work,[11] to some extent motivated by findings now presented and known to us at the time. The most important plot proved to be the length L of the single traverse obtained from the final GPC peak position against P_1, to be used extensively in the material to follow.

Effect of Sample Consistency and Acid Strength

It became evident in the course of many experiments that the accessibility of the sample, the strength of the acid and the temperature of the degradation treatment affected the results, e.g., the plots of single-traverse chain length versus degree of fold cutting (P_1). Once the importance of these variables was recognized, it influenced the design of the experiments and the evaluation of the data. At this point the effect of the acid strength and the sample consistency will be demonstrated on a bulk specimen. As regards single crystals some examples will be given in the following paper (Part III),[2] including some instances of the effect of the temperature, as the presentation of these data here would anticipate the main discussion on the fold structure of single crystals.

The bulk sample which should serve here as an example for the principle conclusions was Rigidex 50, as obtained in pellet form. It was used for three series of degradation experiments: series x, in the original pellet form with the use of 95% acid; series y, thin shavings from these pellets with the 95% acid; and series z, shavings as in series y but with 82.5% acid. The pellets were about 2 mm in size. The shavings were obtained by cutting with a razor blade by hand; the average thickness was 200 μ.

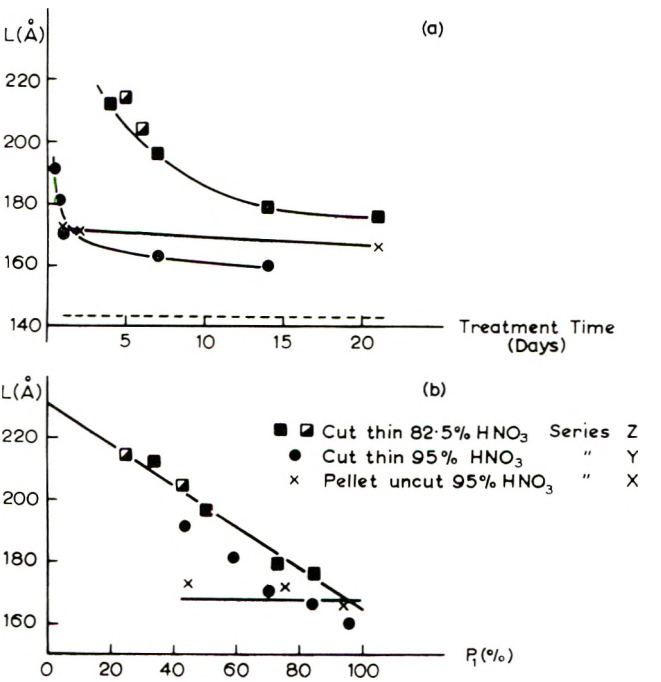

Fig. 6. Single-traverse lengths—as assessed by GPC as a function of (*a*) treatment time and (*b*) the degree of chain cutting for nitric acid-treated samples of polyethylene in finely cut and massive form for two acid concentrations. The fully and half filled squares correspond to two separate experimental series.

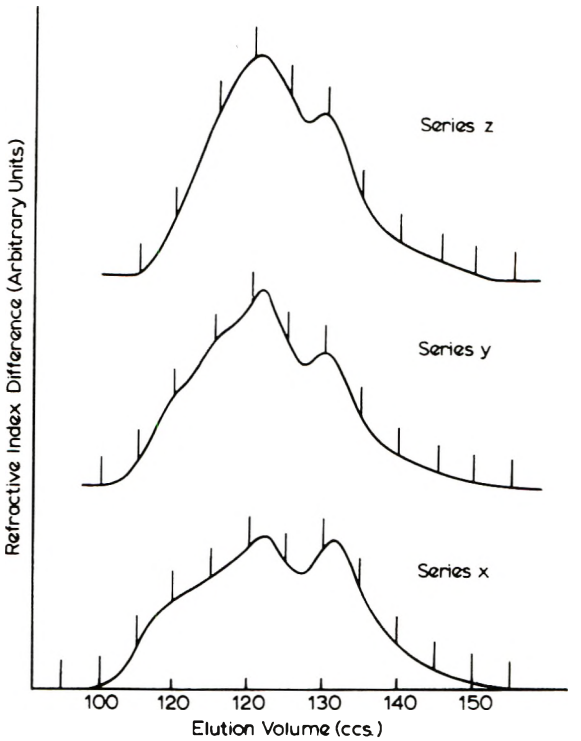

Fig. 7. GPC chromatograms for the three series of sample represented in Fig. 6 at the stage of degradation where P_1 is close to 40% for each. Low elution volumes correspond to high molecular weights.

Figure 6 shows the single-traverse length versus degradation time and P_1. It is immediately obvious that the three sets of experiments yield different results; the effect of the two kinds of plotting (Figs. 6*a*, 6*b*) can also be usefully compared. Concentrating on the more significant plot, Figure 6*b* (see above), we see that for series x the single-traverse peak corresponds to much shorter chain length than for the rest and changes little in position after its first appearance. For series z the single-traverse length decreases approximately linearly from a value not much smaller than the original long spacing of 218 Å. Extrapoation to $P_1 = 0$ would yield 230 Å, which relates to the measured long spacing if it is assumed that the chains are inclined at an angle of 18° to the lamellar normals. This is very plausible, as it is exactly the chain obliquity established in quenched polyethylene during earlier studies[12] (the pellets were originally obtained by quenching). Thus we see that series z gives a gradual decrease of the chain-traverse length from the value it is likely to have in the undegraded material. It coincides with series x only at very advanced stages of degradation. Series y is intermediate between series x and z but closer to series z. Similar results have also been obtained on branched bulk polyethylene in the course of these experiments.

The fact that finely dispersed samples give different results than massive specimens indicates that diffusion must play an important role. It would be expected, therefore, that the attack is less homogeneous throughout the massive sample. The fact that the more finely dispersed samples of series z leads to a sensible extrapolation gives confidence that the attack in those samples is not far from being uniform throughout. The influence of acid strength is understandable in this light. Weak acid reacts more slowly; hence the concentration gradient throughout the sample due to finite diffusion time has time to even out appreciably before the reaction is far advanced. Obviously the important factor is the ratio of reaction rate and penetration rate. For homogeneous attack this ratio has to be small. This can be achieved either by reducing the reaction rate through weakening the acid (or reaction temperature) or by increasing the penetration rate by making the sample interior more accessible. The safest method of course is to change both factors simultaneously. As will be seen in the following paper, this was done in the more detailed work on single crystals.[2]

Support for these views and also indications of the reason for the particular difference observed in the three samples will be apparent from Figure 7. These are three chromatograms taken from series x, y, and z in Figure 6, so chosen as to correspond to the same P_1 value (identical fraction of single-traverse material) obtained when the peaks are appropriately separated.[6] Two features are apparent: first, the molecular distribution of the material outside the single traverse peak is different in the three samples; most obviously it stretches towards increasingly higher molecular weight in the sequence z, y, x. This confirms the increasing inhomogeneity of the attack for more massive samples and stronger acids as anticipated. Clearly in case of less complete penetration more material is left comparatively unaffected, hence with long chain length, at the same stage of overall fold cutting. This implies, however, that in those portions of the sample, which have been fully exposed to acid the degradation must have proceeded further than it would have done in case of homogeneous degradation so as to yield the same overall number of single traverses (P_1). As by Figure 6 the length of such single traverse chains itself should decrease continuously during continued exposure to acid—a new finding at variance with some earlier statements (see below)—we would expect the single-traverse length to have been shortened more in the peripheral regions of the inhomogeneously degraded sample than it would have been in the sample uniformly degraded at the same overall degree of fold cutting (P_1). This in fact is the second effect apparent from Figure 7, where the single traverse peak is at increasingly higher elution volume, i.e., at shorter chain length, in the sequence z, y, x.

It is this last point which finds expression in the lower L values for series z—and to a lesser extent y—for the same P_1. In the extreme case of series x the final L value has been practically reached at a stage when much of the material is still undegraded; hence the apparent invariance of the single-transverse peak position. This invariance was the conclusion (erroneous, as it turns out) of the earlier scouting work on this topic where the importance of all these factors was not yet recognized.[6,13] The dotted horizontal

line in Figure 6 in fact gives the value of the invariant single-traverse peak from the report of Williams et al.[15] It is below series x but displays same trend. The analogous comparison with earlier work for single crystals will be shown in the next paper.[2] It must be emphasized that the presentation of this material and other studies from this laboratory does not follow chronological order. Some work to be published in the meantime has already taken cognizance of these factors. Thus the new detailed study on the bulk material by Ward and Williams[14] utilized thin films and obtained continually decreasing L versus P_1 curves such as in Figure 6. The purpose of the present section is to demonstrate an explicit example of why differences between the new and earlier results have arisen, how they were recognized, and how the errors are to be minimized in future work.

In conclusion we may take a wider view of the development of the nitric acid-degradation technique. The technique, as discovered originally,[3] served to disperse massive samples for morphological studies, and this required drastic degradation. For this purpose the attack could be considered as homogeneous even in comparatively thick samples and with the strongest acid. This, however, cannot be maintained any longer when more subtle effects concerning the molecular weight distribution, particularly during the initial stages, are being studied in specific detail. This holds particularly in the case of single crystals which are already in a dispersed state and where accordingly the study of the molecular weight distribution is the principle purpose of the degradation experiment.

We wish to thank Dr. T. Williams for performing the GPC analysis throughout most of this work and providing guidance in the evaluation of the results. We are obliged to Professor I. M. Ward for his association with parts of this project.

References

1. J. D. Priest, *J. Polym. Sci. A-2*, **9**, 1777 (1971).
2. A. Keller, E. Martuscelli, J. D. Priest, and Y. Udagawa, *J. Polym. Sci. A-2*, **9**, 1807 (1971).
3. R. P. Palmer and A. Cobbold, *Makromol. Chem.*, **74**, 174 (1964).
4. J. D. Blundell, A. Keller, and T. Connor, *J. Polym. Sci. A-2*, **5**, 991 (1967).
5. J. D. Blundell, A. Keller, I. M. Ward, and I. J. Grant, *J. Polym. Sci. B*, **4**, 781 (1966).
6. T. Williams, D. J. Blundell, A. Keller, and I. M. Ward, *J. Polym. Sci. A-2*, **6**, 1613 (1968).
7. T. Williams, Y. Udagawa, A. Keller, and I. M. Ward, *J. Polym. Sci. A-2*, **8**, 35 (1970).
8. A. Peterlin and G. Meinel, *J. Polym. Sci. B*, **3**, 1059 (1965).
9. F. Asinger, *Paraffins, Chemistry and Technology*, Pergamon Press, Oxford-London, 1968, p. 616.
10. I. M. Ward and T. Williams, *J. Polym. Sci. A-2*, **7**, 1585 (1969).
11. D. M. Sadler, T. Williams, A. Keller, and I. M. Ward, *J. Polym. Sci. A-2*, **7**, 1819 (1969).
12. A. Keller and S. Sawada, *Makromol. Chem.*, **74**, 190 (1964).
13. T. Williams, A. Keller, and I. M. Ward, *J. Polym. Sci. A-2*, **6**, 1621 (1968).
14. T. Williams and I. M. Ward, *J. Polym. Sci. A-2*, in press.

Received January 21, 1971

JOURNAL OF POLYMER SCIENCE: PART A-2 VOL. 9, 1807–1837 (1971)

Fold Surface of Polyethylene Single Crystals as Assessed by Selective Degradation Studies. III. Application of the Improved Techniques to Single Crystals

A. KELLER, E. MARTUSCELLI,* D. J. PRIEST,† and Y. UDAGAWA, *H. H. Wills Physics Laboratory, University of Bristol, Bristol BS8 1TL, England*

Synopsis

Previous studies on selective degradation of polyethylene single crystals with fuming nitric acid have been extended, both by using acid of lower concentration which gave better control over the degradation, and by resorting to ozone as an oxidizing agent which among others enabled the degradation temperature to be conveniently lowered. The molecular weight distribution was followed by gel-permeation chromatography in the course of degradation. Complete consistency between these different methods has been established, modifying some of the previous conclusions reached by this method. The principal feature which emerges is that we have a distribution of fold lengths. The largest straight fold stems can stretch across nearly the entire layer defined by the low-angle x-ray period, while there is a continuous distribution of shorter folds terminating deeper down in the crystals. The limiting depth at which the number of terminating folds becomes negligible can be identified and quantitatively assessed. The method of analysis is described, and individual data are discussed in detail. This picture of a fold surface layer containing essentially adjacently reentrant folds of uneven length agrees with quite recent results on other related chain-folded systems (annealed crystals, short chains, bulk structures) obtained in these laboratories and thus appears to be of general validity. The consequences of the model for our picture on polymer crystals in particular on the nature of the "amorphous" component, are discussed.

INTRODUCTION

The nature of the fold surface in polyethylene single crystals is currently a central topic for the understanding of polymer crystallization. In the first instance it is important for the understanding of the structure of single crystals and the molecular process of chain folding. More generally, it provides a good starting point for the elucidation of how disordered material can coexist with crystallinity in a semicrystalline polymer, as in the present case of a single chain-folded crystal layer this disorder (or amorphous con-

* Present address: Laboratorio Di Ricerche Su Tecnologia dei Polmeri e Reologia, Consiglio Nazionale delle Ricerche, 80072 Arco Felice, Napoli, Italy.

† Present address: Reed Engineering and Development Services Ltd., Aylesford, Maidstone, Kent, England.

tent) must be located within the confines of a geometrically defined single crystal.[1,2] One of the most specific approaches to this problem is provided by selective chemical degradation by means of strong oxidizing agents. Some aspects of these have been dealt with in the two preceding papers.[3,4] Here, the history of past studies as applied to polyethylene single crystals will be summarized, to be followed by an account of the new investigations.

Degradation studies so far have revealed the following facts. The crystals are digested surface downwards. In the first place this was revealed by loss of material[5–7] and more directly by direct observation of layer thinning by low-angle x-ray diffraction.[7] In the course of time, this layer thinning comes to a halt or at any rate becomes very slow. At the same time, the degree of crystallinity of the remaining material increases, as assessed by various methods (this assessment is not always as clear-cut as it seems because of the chemical modification of the cut chains[8]), and the chain mobility decreases. It was concluded therefore that less ordered material, possibly some form of amorphous material which is present along the crystal surfaces, is removed. The observation that the digestion proceeding surface downwards comes to a halt has been interpreted in this light, namely that the disordered material is much more vulnerable to the degradation than the crystal. Accordingly degradation would come to a halt at a depth where the disordered layer ceases and the crystal starts (Fig. 1). The depth of the amorphous layer estimated in this way amounts to 10–15 Å along each fold surface of the usual crystal. It may be stated at this stage that the results of the preceding paper[4] invalidate this latter conception as far as they remove the justification of a boundary between amorphous and crystalline strata distinguished by vulnerability and resistance to the oxidizing agent, respectively. (If there is a difference this would be a matter of a rather more subtle distinction in rates than by the criterion of reactivity or nonreactivity on the time scale of our experiments).

The study of the molecular weight distribution by gel-permeation chromatography (GPC) in the course of degradation had the following important information to add.[9,10] Distinct peaks developed in the course of the acid attack at the lower molecular weight end of the distribution. The peak at the lowest molecular weight (peak 1) corresponded to a chain length somewhat less than the layer thickness (allowing for chain inclination when required). This reduced length agreed well with the thickness of the thinned crystal layer as assessed by low-angle x-ray scattering. It was concluded that it corresponded to a single chain traverse through the crystalline core of the layer. The second peak (in sequence of increasing molecular weight, peak 2) was found to correspond to twice the chain length appropriate to peak 1, within an error of $\pm 5\%$, and was thus interpreted as due to a double traverse fragment of a chain-folded structure. A third peak in the chromatogram could have corresponded to a triple or quadruple, or possible combination of both traverse lengths, but owing to poorer resolution in that instrumental range, particularly in the early stages of the degradation where it appeared, was not followed up further.

At first it was noted that the peak positions did not change during degradation, only the relative height of the peaks: peak 1 became gradually more intense at the expense of the others, until it was the only one to remain. As the apparently constant position of peaks 1 and 2 corresponded to single and double traverses pertaining to the thinned crystal layer, it appeared that they represented the chain-folded structure within the crystalline core of the layer. The closely 1:2 ratio of the traverse lengths, coupled with the sharpness of the peaks—observed in the later stages of the degradation when the peaks were most clearly defined—was obviously due to the small amount of material within the folds themselves and was hence attributed to sharp, adjacently reentrant folds.[10] (For the peak-width measurements the chromatograms had to be corrected for the broadening caused by the carboxyl groups at the cut chain ends.[11])

This picture fitted into the structure concept embodied by Figure 1. It significantly added to it by showing that the core itself does contain folds which must be adjacently reentrant and sharp, and consequently that the assumed disordered layer is not the unique site of the folds. Or conversely, that at least a significant portion of the folds is not associated with the disordered material identified by the degradation procedure. However, the nature of the disordered portions remained unrevealed by this technique; in any case it is washed away and possibly completely degraded in the process.

It became gradually apparent that the above results and interpretations are not unique in every respect. One of the first indications of this emerged

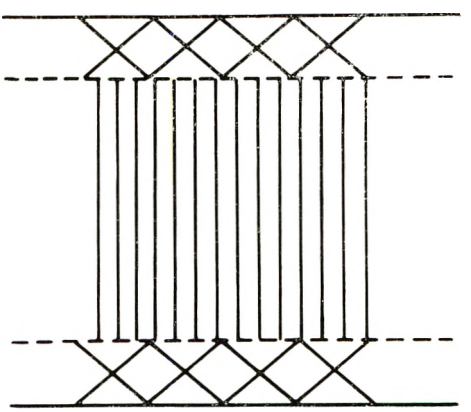

Fig. 1. Schematic representation of the existing concept of a single crystal lamella. The central region represents the crystalline core, the vertical lines the chains within the lattice (they could also be inclined). This is bordered by two surface layers containing disordered material (represented by X's). Previous digestion results with nitric acid seemed to confirm this division as the acid attack was believed to proceed to the broken line and not farther. According to past digestion work most folds were supposed to terminate at the broken line; the nature of the disordered material was left unspecified. By other views, the folds themselves would make up the disordered layer. (Not to scale.)

in the course of the development of the ozone technique. As mentioned in Part I,[3] the peaks within the chromatograms did not stay at a constant position—which, according to the above interpretation, corresponds to the thickness of the crystal core—but shifted together towards lower molecular weights in the course of degradation accompanied by the usual changes in peak heights. This immediately suggests that there is no unique core containing the regularly folded layer. It was clearly unsatisfactory that two different oxidation methods should show such a difference in trend, as it throws doubt on the uniqueness of the results obtained by such drastic interference with our system.

But even with the nitric acid technique a different picture started to emerge when applied to the study of crystals where the fold length has been increased by annealing.[12] Among a variety of observations, perhaps the most significant one was the shift of the peak positions during the degradation reaction. Both peaks 1 and 2 shifted together to lower molecular weight with an unaltered ratio close to 1:2, while the height of peak 1 increased and 2 decreased, until peak 1 alone was left. It was inferred that there must be a distribution of folds down to a considerable depth of the crystal and the "buried" folds are gradually exposed to the acid as the layers are thinning. The thickness of such a layer of buried folds was found to be proportional to the thickness increment due to annealing. Significant as this conclusion appeared, it set a double pattern of degradation behavior: one for unannealed, the other for annealed crystals. Further, there seemed to be no continuity between the disordered layer superposed on the folded crystal core (as in Figure 1) in the unannealed single crystals and the layer containing buried folds in the annealed crystals, a problem which became particularly apparent when considering only slightly annealed crystals with a small fold-length increase.

The present work is aimed at clearing up these inconsistencies and gaps in our existing picture and establish a unified pattern. For this purpose, more extensive use was made of the ozone degradation method, and the earlier work on the nitric acid degradation was repeated and extended with the improvements of the method described in the previous paper.[4]

EXPERIMENTAL

Single crystals were obtained by precipitating linear polyethylene Marlex 6009 from 0.1 and 0.5% xylene solution under isothermal conditions. Two crystallization temperatures were used 70 and 85°C. The resulting fold lengths as assessed by low angle scattering were 109 and 135 Å, respectively.

The preparations were of two kinds. At first the usual multilayer type was used, obtained by dissolving the polyethylene at temperatures near the boiling point of xylene before cooling to the crystallization temperature. For most of the work, predominantly monolayer crystals were employed, obtained by the self-seeding method described elsewhere.[13,14] The original purpose of using these two preparation methods was to distinguish between

effects caused by close adhesion of layers and by possible interlamellar material, from effects associated with the surface of an individual layer.

After precipitation the sediment was either filtered and dried in the usual way, giving rise to the familiar mat or cake, or was freeze-dried,[3] producing a highly flocculant crystal aggregate. As described above, freeze-drying was essential for the ozone treatment to ensure even penetration by the ozone. Presently, the effect of the freeze-drying procedure was also tested for the nitric acid treatment. Further essential details will be given in connection with the individual experiments.

The degradation methods included treatment with nitric acid and ozone. Both methods, with their latest modifications, have been described in the preceding papers. Present treatment conditions were as follows. With nitric acid, 60°C treatment temperature was adopted. The acid was used in two concentrations: 95% (nominal) and 82.5%. The ozone treatment was carried out at three degradation temperatures: 0, 23 (room), and 60°C.

The GPC measurements were carried out with a Waters chromatograph. A 2 ml portion of 0.2 wt-% solution in *o*-dichlorobenzene was used for each measurement which was carried out at 130°C. A series arrangement of five columns of upper porosity rating of 1.5×10^5, 3×10^4, 1×10^3, 800, and 350 Å was employed. An impurity peak which appears at about 100 ml after the sample peaks was used to standardize the peak positions.

The peaks were separated by the procedure described in previous publications.[10,15] Their positions, measured in terms of elution volume, could then be converted into molecular weights, and following this, into molecular lengths by means of a previously established calibration procedure[15] applied repeatedly throughout the previous works. The width of the peaks was also measured and expressed in terms of molecular weight spread by means of a resolution calibration[11] which takes into account the broadening due both to instrumental factors and to the carboxyl endgroup. Both the identification of the peak positions and even more so that of the peak width, becomes increasingly less accurate at the early stages of the degradation.

As previously, the degradation is defined in terms of the area ratio of peak 1 (single traverse) to the rest of the chromatogram, to be denoted as P_1 in what follows. This is a direct measure of the degree of fold cutting which, as shown previously, follows a random-attack (depolymerization into fold segments) model,[16] a point to be tested again in the course of this work. Use of P_1 eliminates the time as a variable in presenting the results. Time as variable will only be reported where the rates as such are to be referred to.

As the studies with ozone and nitric acid were pursued as different projects to begin with, they will be best presented separately.

RESULTS

Nitric Acid

A typical chromatogram series is shown by Figure 2. As seen, it follows the usual pattern of peak development reported previously.[9,10,17]

Rates

The progress of the degradation can be assessed from Figures 3*a*, 4*a*, and 5*a*, where P_1 is plotted as a function of time. Both curves level off, the 95% curve approaching 100% P_1 while the 82.5% remains much below for the times employed. We have seen[4] that the leveling off itself has no direct structural significance, as curves can be made to rise again by washing the crystals and newly exposing them to acid. From the practical point of

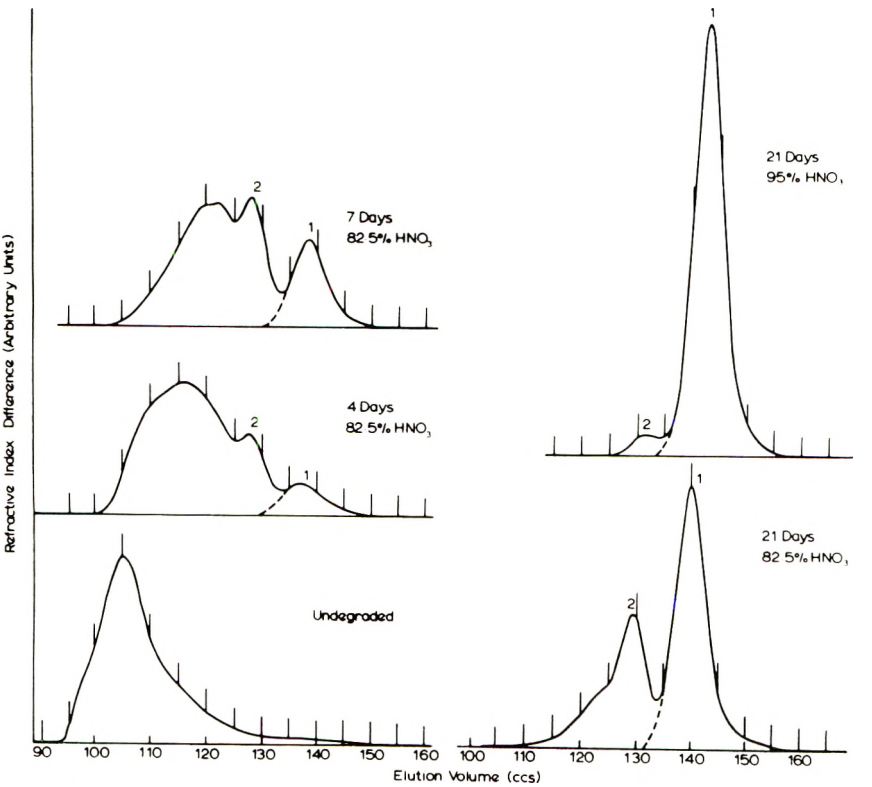

Fig. 2. GPC chromatograms of nitric acid-degraded monolayer single crystals grown at 85°C in stages of increasing degradation. Increasing elution volume corresponds to decreasing molecular weight. Single-traverse and double-traverse peaks are marked by 1 and 2, respectively.

view, however, the curves in Figures 3*a*, 4*a*, and 5*a* mean that a full degradation series from $P_1 = 0$ to $P_1 = 100\%$ cannot be readily carried out in a continuous manner with 82.5% acid within a reasonable time. Therefore, the results to be presented below (Figs. 3*c*, 4*c*, 5*c*) contain a combination of the 95% and 82.5% degradation series to be justified by the overlap and continuity of the series.

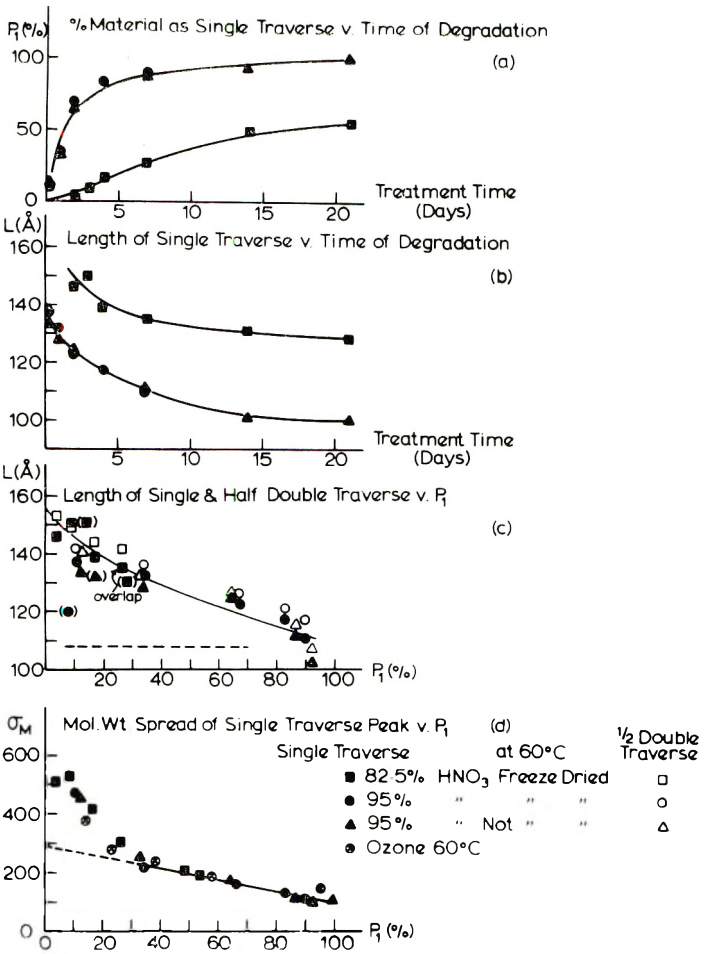

Fig. 3. Nitric-acid degradation series of monolayer crystals grown at 85°C as analyzed by GPC. P_1 is the percentage of material within single traverse peaks of the chromatograms; L is the length of chain corresponding either to single-traverse or half-double-traverse peak position in the chromatograms; σ_M is the standard deviation of the single-traverse lengths in terms of molecular weight from the width of the chromatogram peaks. A key to all points is given in Fig. 3*d*. The points in brackets in (c) are from earlier exploratory series and the interrupted horizontal line refers to ref. 10 (for details see text).

Chromatogram Peak Positions as a Function of Degradation

This is the principal aspect of the work. The peak positions will be expressed in terms of chain length L through the appropriate calibration curve which also takes into account the carboxyl nature of the end group. The chain lengths corresponding to peaks 1 and 2 will be referred to as L_1 and L_2 respectively. Figures 3*b*, 4*b*, and 5*b* show L_1 as a function of time; Figures 3*c*, 4*c*, and 5*c* contain L_1 and $^1/_2 L_2$ as a function of P_1. The latter plot will be our principal concern.

It will be stated at this stage that the definitive results were only obtained after sample preparation and treatment conditions had been standardized. As was stated in the preceding paper,[4] the fuming nitric acid (95%) usually employed gave peak positions at lower L values than the diluted acid during the early stages of attack. This was attributed to inhomogeneous attack throughout the sample owing to the fact that the diffusion time could not be neglected in comparison to the rate of reaction. In order to reduce the effect of finite diffusion time and thus obtain agreement between the results with different dilutions, greater attention was paid to preparation of samples. It was found that all the results could be made to coincide when monolayer crystals were used in freeze-dried form. However, in the case of multilayer crystals filtered under standard conditions, the variability with acid strength in the early stages of degradation could be greatly reduced, even if not quite removed, when the following precautions were taken. The dried mat was broken up manually into a powder as fine as possible. Then the preparation was soaked in the 95% acid at room temperature for 24 hr, after which the temperature was raised to that chosen for the degradation. This treatment ensures that the acid diffuses into the sample completely at a temperature at which the reaction rate is very slow. Accordingly, when the reaction is accelerated by subsequent raising of the temperature it will be uniform throughout the sample. In this way consistency between all samples and treatment conditions could be obtained. The individual experiments leading up to these conclusions, due to one of us (Y.U.), will not be described in detail, only the results where all the variables were already brought under control. A few selected points of other curves are nevertheless included in Figure 3*c* so as to illustrate how discrepancies were gradually removed.

Crystals Grown at 85°C (Monolayers). Here (Fig. 3*c*), both freeze-dried and non-freeze-dried monolayer samples were used. Four points selected from more extensive work on multilayers, carried out before the nitric acid technique was refined, are also included for comparison.

General trend. The principal feature is the continuous decrease of L with P_1. This is contrary to the earlier work[10] where the peak position was reported to be constant during the fold cutting process. This constant L value of the previous work on similar crystals found at the same temperature is shown by the horizontal dashed line in Figure 3*c*. We see that the present points lie much above this line throughout most of the degradation, converging to it at high P_1. Figure 3*c* also contains a point (●) obtained in the course of the present investigations on multilayer crystals with 95% acid without the special precautions listed above. We see that it corresponds to a much lower L, and in fact comes close to the dashed horizontal line. Two points obtained on the same multilayer preparation but with 82.5% acid (■) are also included and are in fact seen to follow the line with the rest of the points obtained on monolayers. We believe that the low L with strong acids at small P_1 is attributable to inhomogeneous attack on the grounds laid out above.

The effect of lower L values for the 95% acid in the early stages of degradation is still detectable in the present monolayer preparation but in a much reduced form and more so in the samples not freeze-dried, which again is in agreement with expectations. In either case, the lowering of the L values is now so small that it does not obscure the general trend of a continuous decrease. Nevertheless, it is still sufficiently apparent to illustrate this error source.*

Relation of peak positions. Figure 3*c* shows further that the single and double traverse lengths decrease together, both in a continuous fashion. In first approximation L_1 and $^1/_2L_2$ are nearly identical. Closer inspection, however, reveals that the $^1/_2L_2$ values lie systematically above those of L_1, the difference being about or within 5%.

Extreme L values. The extreme values of L_1 are of special interest. As no peak determination can be made close to $P_1 = 0$, the starting value can be only assessed by a somewhat uncertain extrapolation. In Figure 3*c* the curve drawn through the points extrapolates to around 155 Å. As the points at smallest P_1 values are subject to larger errors in the peak separation procedure in the chromatograms, a more detailed curve fitting would not be profitable without individual weighting of the points which will not be attempted.

The lowest value of L_1 lies between 100 and 110 Å. Fixing of the exact end point is made difficult by the fact that rapid changes in L_1 still occur between P_1 and 90 and $P = 100\%$, which is equivalent to saying that a very small double-traverse peak persists with comparatively small changes in height during continued layer thinning.

Peak widths. The peak width (Fig. 3*d*) is expressed in terms of standard deviation σ_M of the molecular weight. As already stated, these measurements are most precise at higher P_1. Here the peaks are sharp as σ_M is 100 (i.e., 67% of the material within the peak, with a maximum at 1000, is within a molecular weight spread of 100). However, the peaks broaden when going towards lower P_1. This broadening is in two stages: a linear portion with a gradient of about -2 down to $30 < P < 35$, and then a sudden upswing towards the lowest P_1 values. The significant increase in σ_M is beyond doubt even if the exact values themselves became increasingly uncertain in this range of the degradation.

Crystals Grown at 70°C. With the equivalence of monolayer and multilayer preparations for the present purposes virtually established, at least

* It is to be noted that lowering of the degradation temperature to room temperature in the case of the preceding work on multilayer crystals with 95% acid [point (▲) is a single illustration of a more extensive study] also reduced the discrepancy as compared with the corresponding 60°C point but did not raise L quite to the level of the 82.5% curve, although the rate at room temperature is about one third of that at 60°C for 82.5% acid. Further, it is noteworthy that point (▲) coincides with that obtained on monolayer crystals treated at 95°C with special measures to reduce diffusion. It appears therefore that there could be an intrinsic difference in the degradation with 95% acid, even rates apart, and that the small gap between the 95% and 82.5% curves cannot be completely closed.

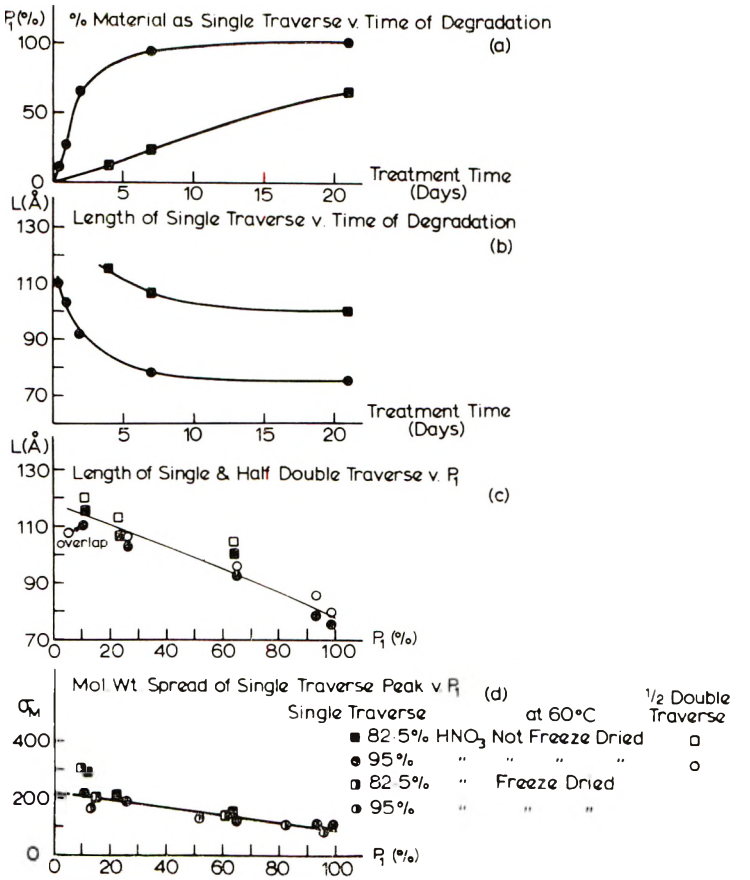

Fig. 4. Nitric acid-degradation series of multilayer crystals grown at 70°C as analyzed by GPC. A key to all points is given in Fig. 4*d* which combines points from Figs. 4 and 5.

under the appropriate experimental conditions, the less laborious multilayer preparations were used for further work. Two series are shown (Figs. 4 and 5); one employed freeze drying, the other did not, (but the sample was soaked in the acid at room temperature first).

General trend. The general trend is the same in both series and agrees with that in Figure 3, i.e., continuous decrease of L with P_1. The points with 95% acid are again somewhat below those obtained with 82.5% acid, in line with previous experience. However, rather inexplicably, at low P_1, the freeze-dried sample showed the biggest difference in this respect. This underlines the sensitivity of the earliest stages of the degradation to possibly fortuitous factors when using strong acid.

Relation of peak positions. It is seen that the half-double traverse is again close to the single traverse length all through. Again, the former is consistently slightly larger, the excess being again around or within 5% in general.

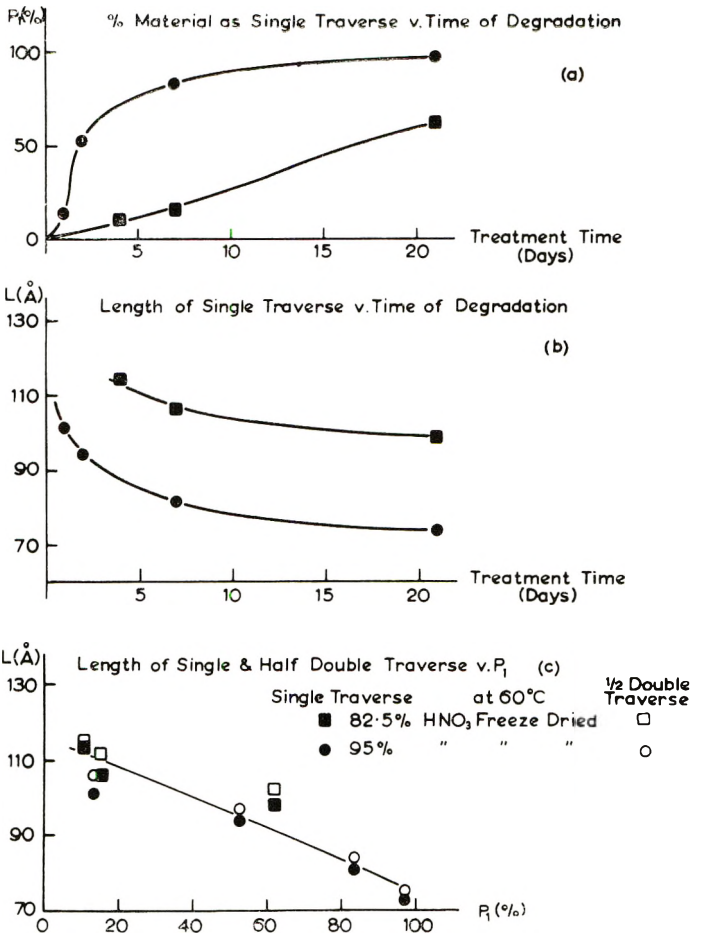

Fig. 5. Nitric acid-degradation series of freeze-dried multilayer crystals grown at 70°C as analyzed by GPC. A key to all points is given in Fig. 5*d*.

Extreme L_1 *values.* The maximum L_1 is again subject to uncertainties of extrapolation. The highest single traverse reading corresponds to 115 Å. If extrapolation is justified this could be increased to 120 Å. The lowest L value is in the range of 75 Å. Thus the difference between the extremes should be around 55 Å.

Peak widths. As above, the peak widths (Fig. 4*d*) are expressed in terms of the standard deviation in molecular weight of peak 1. There is again a general linear narrowing of the peak during degradation but the effect is smaller. Thus the maximum change in σ_M at the extremes of P_1 values is a factor of 2, at the most 3, The lowest σ_M value is again 100 the highest appears to be 200, or 300 when the two 82.5% points for lowest P_1 are included. The large upswing of the curve below $P_1 = 30$ (when proceeding towards diminishing P_1 values) is certainly absent. Whether the 82.5% points (as opposed to the 95%) at $P_1 = 11\%$ is indicative of such an upswing

is difficult to say because of the uncertainty of measurement at such low P_1 values. If it is, it is of small magnitude and at a lower P_1 value than in Figure 3.

Ozone

The separate origin of the ozone work necessitated some departures in the method of data display, which should be of no consequence for the content.

The samples were all monolayer preparations crystallized by the self-seeding technique at 84.5°C. The temperature of dissolution T_s[13] was 101.3°C. (For the present purposes we consider the 84.5°C as equivalent to the 85°C used in the nitric acid work.)

The technique has been described previously.[3,18] Hence it will only be added that the present measurements have been extended to two different temperatures (60°C and 0°C) in addition to the room temperature runs. The run at 60°C served to achieve an overlap with the nitric acid work, that at 0°C served to slow down the reaction in the hope to make it more discriminating.

The experiments at temperatures different from room temperature were carried out by immersing the sample-containing vessel in a bath kept at the appropriate temperature and by preheating or precooling the ozonized gas

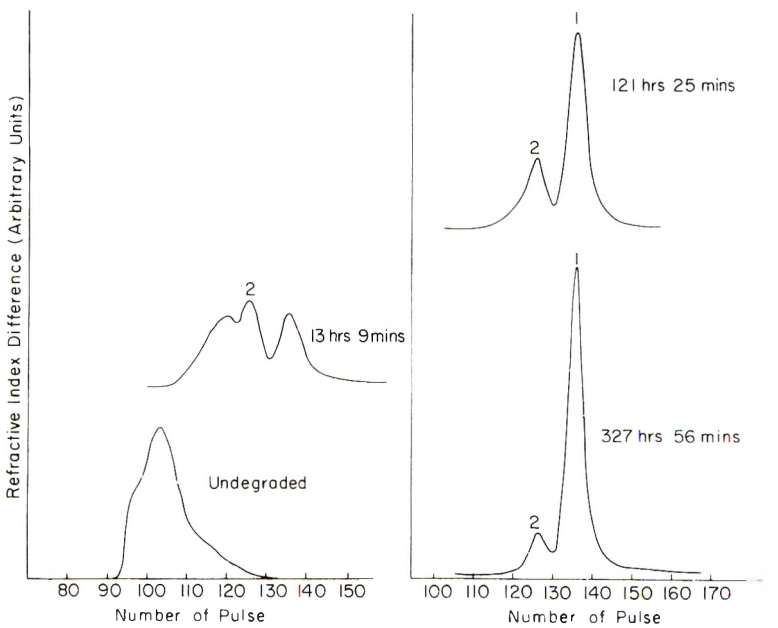

Fig. 6. GPC chromatograms of ozone-degraded monolayer single crystals grown at 85°C. Increasing number of pulses correspond to increasing elution volume, hence decreasing molecular weight. Single-traverse and double-traverse peaks are marked by 1 and 2, respectively.

before reaching the specimen. The latter was achieved by leading the gas through a coil immersed in an appropriately thermostated bath.

A typical chromatogram series is shown by Figure 6. It is very similar to that obtained with nitric acid degradation, displaying the characteristic peaks, increasingly so with increasing degradation.

Verification of Random Scission

It has been proposed[16] that the fold-cutting process can be considered as a random "depolymerization" with the single traverse length as the "monomer." Then if we denote the degree of polymerization by p, and if random scission held, this should be uniquely expressible in terms of the fraction or ratio of any x-mer, in keeping with a random distribution. Thus with P_1 and P_2 as fractions of monomer and dimer, respectively (fractional areas of first and second chromatogram peaks), we have

$$p = 1 - \sqrt{P_1} \tag{1}$$

$$p = P_2/2P_1 \tag{2}$$

by the usual formalism of, e.g., condensation polymerization,[19] applied specially to the problem of fold cutting.[16]

It follows further that

$$P_2 = 2P_1(1 - \sqrt{P_1}) \tag{3}$$

Thus one should be able to test the assumption of random scission by eq. (3),[16] i.e., by expressing P_2 in terms of P_1, both directly measurable from our chromatograms.

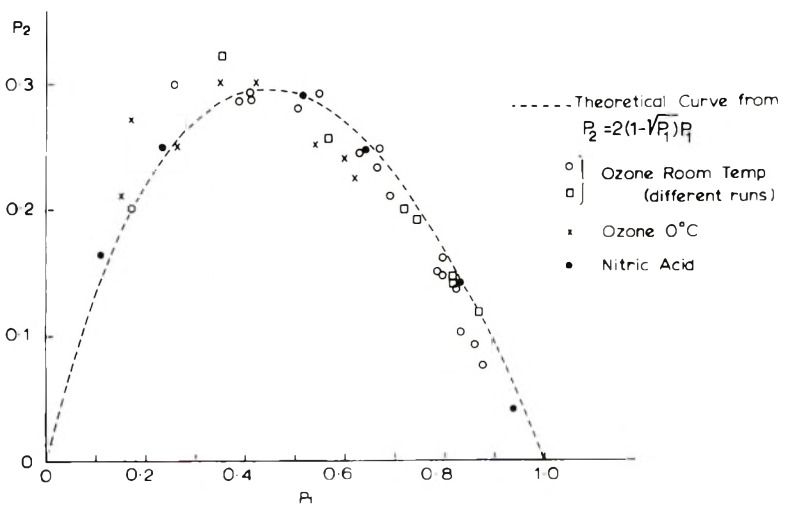

Fig. 7. Fractional amount P_2 of material within double-traverse peak as a function of fractional amount P_1 of material within single-traverse peak for three ozone and one nitric-acid degradation series. The theoretical relation from the random-scission model[16] is indicated.

This has been attempted in Figure 7. We see that agreement between theory and experiment and between the different experiments is satisfactory from about $P_1 = 0.3$ or $P_1 = 0.4$ upwards. There are three isolated points which depart from the theoretical curve particularly at lower P_1 while others still follow the theoretical curve closely down to $P_1 = 0.15$. Bearing in mind that the measurements themselves become less accurate at low P_1, we can regard the overall picture of random scission as being satisfactorily obeyed to serve as a guide for the present considerations. A few points from the nitric acid work are also added to demonstrate the equivalence of the two methods in this particular respect. (Applicability of random scission to nitric acid degradation has been demonstrated more fully previously.[16])

Rates

The results are displayed in Figure 8. Here the logarithm of the fraction of uncut sites, denoted by p, is plotted against the square root of time. Following the earlier described procedure,[16] p is expressed by eqs. (1) and (2) to provide also a further test of the random-scission model. We see immediately that p values arrived at by the two methods are closely similar and consistent with random distribution of traverse lengths, hence the underlying random-scission model.

The curves can be subdivided in two linear portions of differing slopes, the slope of the first portion being steeper. The discontinuity itself is of no special significance, as it has become so prominent through the $\sqrt{t}$ scale adopted. What is significant is that the reaction slows down, an effect also noted previously.[16] As the slowing down could be due to a variety of

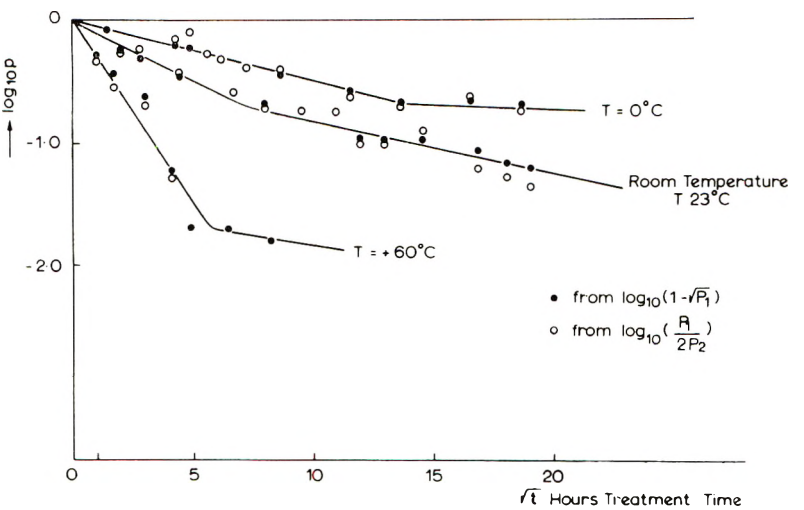

Fig. 8. Relation between the degree of chain cutting as assessed from P_1, and separately from the ratio of P_1 to P_2 on the basis of the random-scission model[16] for monolayer single crystals formed at 85°C, degraded by ozone at three different temperatures.

sources (see the nitric acid case[4]), we attach importance only to the initial slope obtained from the log p versus t plots (plot on t scale not illustrated here). Assuming that in the first stages the rate of reaction is proportional to the concentration of uncut folds, one can calculate the reaction rates and the activation energy of the degradation reaction.

The rates are at 0°C, 0.009 hr^{-1}; at 23°C, 0.035 hr^{-1}; at 60°C, 0.080 hr^{-1}. As is to be expected, the rates increase rapidly with temperature. From this temperature dependence an activation energy of 6 kcal/mole is obtained.

Chromatogram Peak Positions as a Function of Degradation

The results at 0, 23, and 60°C are shown by Figures 9, 10, and 11. Figures 9*a*, 10*a*, and 11*a* show L as a function of time, and Figures 9*b*, 10*b*, and 11*b* give L as a function P_1 (the information on the dependence of P_1 on time

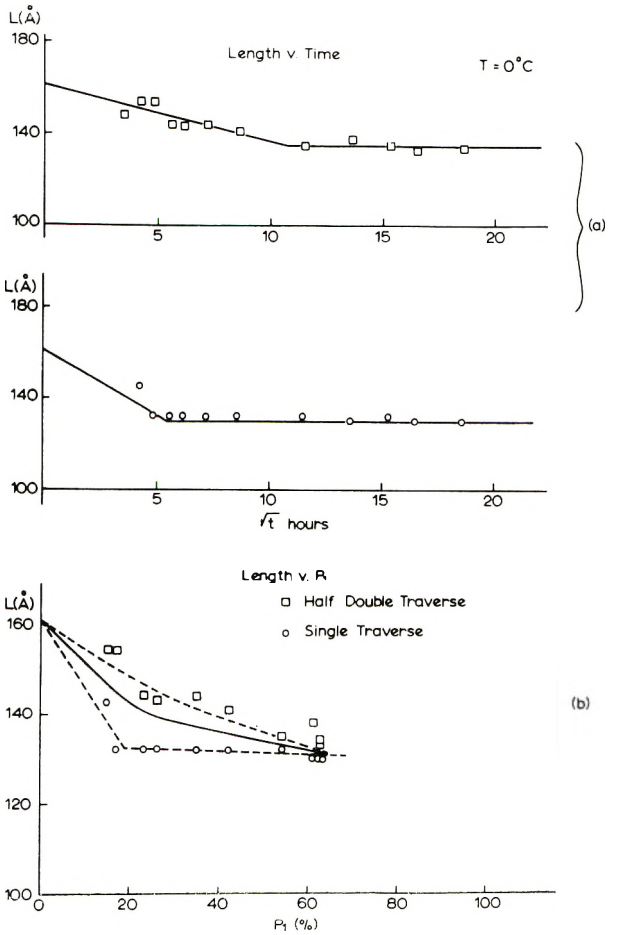

Fig. 9. Ozone-degradation series of monolayer single crystals grown at 85°C as analyzed by GPC. Degradation temperature was 0°C. A key to all points is given in Fig. 9b.

is contained in Fig. 8). As in the case of the nitric acid treatment, both L_1 and $^1/_2L_2$ are displayed. The 23°C series is partly a repetition and partly a continuation of the experiments in Part I.[3] The 60°C series provides a direct comparison with the nitric acid degradation work.

General Trend. The principal trend is the continuous decrease of L with P_1. Only at 60°C could the degradation be followed up to $P_1 = 100\%$. As the temperature was lowered, only a progressively smaller P_1 range could

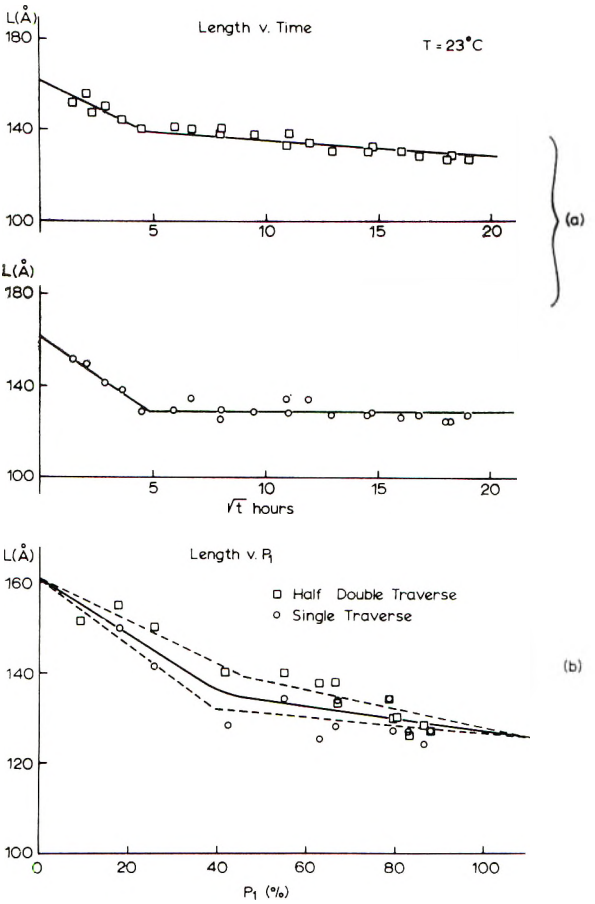

Fig. 10. Ozone-degradation series as in Fig. 9. Degradation temperature was 23°C (room temperature).

be covered within a practicable time scale owing to the decrease in rate. However, as far as mapped, the curves obtained at the three different temperatures are closely similar. Some small differences in detail however, do exist and will be commented on below. The major trend also agrees with that found with nitric acid. Figure 12 shows a composite plot containing points both from the nitric acid and ozone treatment on what are virtually the same specimens. The points featuring on it are taken from Figures 3*c*,

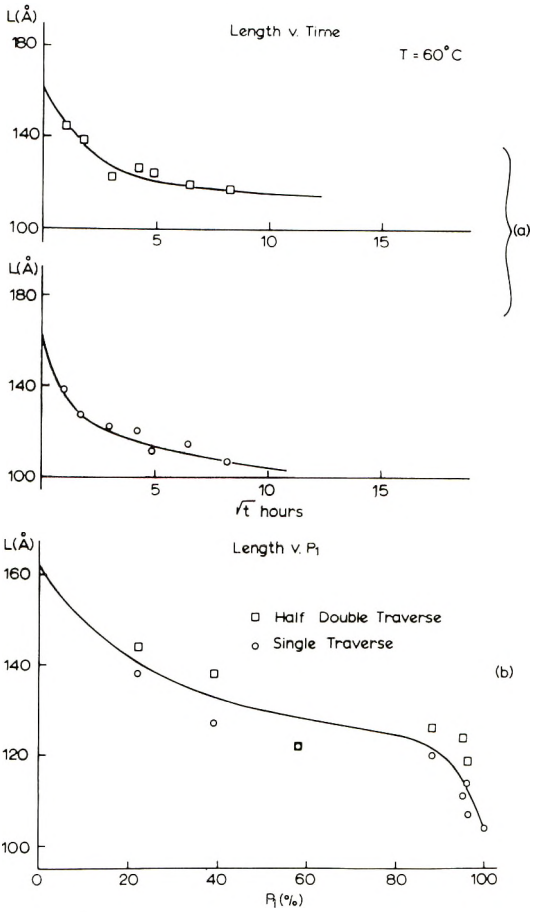

Fig. 11. Ozone-degradation series as in Fig. 9. Degradation temperature was 60°C.

10*b*, and 11*b*. The points all fall about the same line (with two points for 23°C ozone treatment slightly above the rest).

Relation of Peak Positions. Values of L_1 and $\frac{1}{2}L_2$ again agree closely, although the latter is again consistently somewhat larger. Closer inspection, however, reveals a systematic difference, particularly pronounced at the lower reaction temperatures. Consider Figure 9*b*. Here there is a very sizeable difference between L_1 and $\frac{1}{2}L_2$ at $P_1 = 17\%$. This difference gradually diminishes towards high P_1 values, becoming insignificant at $P_1 = 50\%$. This arises from the fact that L_1 decreases much more rapidly to begin with (as a function of P_1 and not in terms of time!) but remains practically constant thereafter, while L_2 decreases less rapidly but continues to do so after the decrease of L_1 has practically ceased. There is only one pair of points for P_1 values below $P_1 = 17\%$ (where the difference is maximum) in Figure 9; but from this it appears that the two points might converge again towards still smaller P_1 as they would have to if $\frac{1}{2}L_2$ decreased more slowly and L_1 more rapidly to begin with.

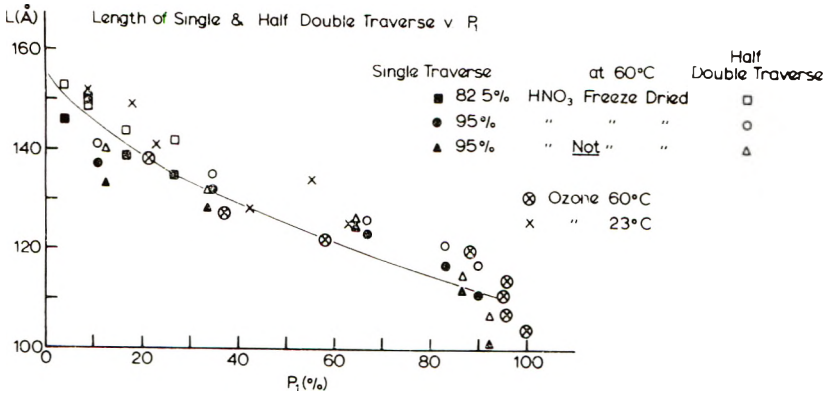

Fig. 12. Plot as in Fig. 3c showing correspondence between points obtained by nitric acid and ozone degradation.

The same trend is displayed by Figure 10. Here the maximum difference between the L_1 and $^1/_2L_2$ is smaller, but because of the wider P_1 range the convergence at both high and low P_1 values is more evident. However, because of the greater uncertainties the low P_1 region would need more detailed examination.

Extreme *L* Values. The highest single-traverse length is 152 Å; extrapolation to $P_1 = 0$ leads to 155 Å $< L_1 <$ 160 Å. As can be seen from Figure 11, L_1 is 104 Å for $P_1 = 100\%$. Thus we have a maximum difference in traverse lengths (not layer thickness, as chain inclination is not allowed for) of about 50 Å. This agrees closely with what has been found with nitric acid degradation on similar samples. This of course follows from the agreement between the two techniques as already demonstrated in Figure 12.

Peak Widths. The σ_M values for 60°C are entered in Figure 3*d* (the trend for the other two temperatures is closely similar). We see that the σ_M values are nearly coincident with those obtained for the 85°C crystals with nitric acid. Thus the spread is small at and close to $P_1 = 100$, there is a steady linear rise towards smaller P_1 values up to $P_1 \approx 30\%$, where there is a sudden surge to much higher σ_M values when going to still smaller P_1.

DISCUSSION

Methods

Before discussing the structural implications it is essential to note the reproducibility and consistency which has been achieved experimentally (Fig. 12). The use of strong oxidizing agents is a very drastic interference with the system, and the possibility of artifacts has to be carefully scrutinized, particularly when quantitative conclusions are to be drawn. It is significant therefore that two such different experimental procedures as the degradation with nitric acid and ozone could be made to give identical re-

sults by appropriate standardization of the sample preparation and degradation procedures. It is clear that the key factor is the combination of sample accessibility and reduction of reagent strength. It is apparent that fuming nitric acid, which was developed for disintegration of the bulk in aid of morphological studies,[20] is unnecessarily drastic for the present purposes, even at 60°C which is lower than generally applied[5,6,17] and that diluted reagents are more appropriate. It is true that with special precautions the fuming nitric acid treatment (95% acid) could be brought in line with the other methods, but even so a small discrepancy at the early stages of degradation remained (e.g., low L values in Fig. 3). As this could not be removed by lowering of the temperature, which otherwise slows down the attack, only by dilution of the acid, it may be a characteristic of the strong acid as such and not caused purely by the high reaction rate.

The lowered reactivity has also been achieved by the alternate route of ozonization. While experimentally it is a cleaner method, it is particularly demanding on standardization of sample preparation owing to its strong diffusion dependence. For this reason it is inapplicable to the bulk. Under the conditions used, ozone reacted faster at 60°C than 82.5% nitric acid, and the rate decreased more slowly with temperature, enabling experimentation down to 0°C. It is noteworthy that the activation energy of 6 kcal/mole obtained from the temperature dependence of the rates is commensurate with the 9 kcal/mole found in more conventional studies of ozone action on bulk polyethylene by the entirely different technique of infrared spectroscopy.[21]

General Trend

The principal qualitative feature is, as in the earlier studies,[9,10,17] development of a peaked distribution of the molecular weight (Figs. 2, 6). The differences now found do not invalidate the previous argument that the lowest molecular weight peak corresponds to a single-chain traverse, the second lowest to a double-chain traverse in the originally chain folded structure. In what follows peaks 1 and 2 will be referred to accordingly.

The important general trend observed with all methods and on all samples is the gradual decrease of the traverse lengths during degradation. Apart from minor differences at 0°C (Fig. 9), to be commented on below, the chain length corresponding to the double-traverse peak is close to twice that of the single traverse throughout. In the first place, this justifies its assignment as a double traverse. Secondly, the maintenance of this ratio throughout the fold-cutting implies that both single and double traverse shorten simultaneously, while the increase of the single traverse peak area at the expense of the double traverse peak implies that the folds are being continually cut. These observations suggest the following interpretation: the folds are of unequal stem lengths, i.e., the folding portions are located at varying depths within the crystal interior. The oxidizing agents cut those folds which are close to the fold surface first, producing single, double, and higher traverse lengths, depending on where the nearest cut is along the opposite crystal

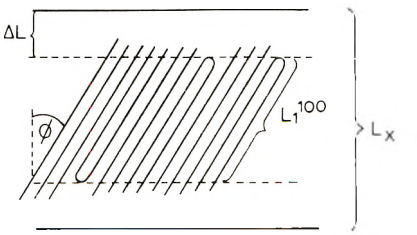

Fig. 13. Diagram of a crystal lamella defining the quantities determined by our experiments. L_x is the lamellar periodicity (measured by x-rays). The broken line defines the deepest level of buried folds at a depth ΔL; L_1 is the corresponding fold-stem length and ϕ its inclination. These quantities are not drawn to scale.

face. Those chain ends resulting from this cutting which protrude above its neighbors are accessible to attack from the side and thus will be shortened to the level of the environment. In this way folds at a lower level are progressively exposed and cut, and the process repeats itself as deep down as there are buried folds. When this level is reached, peak 2 disappears and all the material is in the form of peak 1 representing the single traverse, i.e., $P_1 = 100\%$. Essentially the same deductions have already been made previously in the case of annealed crystals from basically similar evidence,[12] i.e., simultaneous shift of single- and double-traverse lengths to lower values in the course of degradation. At the time, this distinguished the crystals which were annealed from those as grown, as in the latter the traverse length appeared to be constant at that stage of our knowledge (see Introduction).

Thickness of Buried Fold Layer

In the light of the foregoing the following quantities characteristics for the single-crystal system can be defined: L_x which, as before, is the layer periodicity measured by x-rays, L_1^{100} the length corresponding to the single traverse peak at $P_1 = 100$. If ϕ is the angle of chain inclination (Fig. 13), the thickness of the defect-free core is $L_1^{100} \cos \phi$. This defines

$$\Delta L = (L_x - L_1^{100} \cos \phi)/2$$

as the depth down to which submerged folds can be found in detectable quantities, i.e., defines the layer thickness which contains terminating folds. It is to be noted that L_x represents only an average repeat period, hence may also include an interlamellar gap trapping solvent etc. if such is present, while L_1 measures an intrinsic molecular parameter.

The average molecular tilt has been investigated in great detail for crystals grown at 90°C.[22] This was found to be 30°. Present tests based on the split of the 200 arcs in the wide angle pattern of oriented mats[22] suggests that at 85°C this inclination is lower, amounting to 25°. With L_1^{100} in the range 100–105 Å this yields, by eq. (3), $\Delta L \approx 45$ Å. For crystals grown at 70°C, ϕ is normally considered to be close to 90°. Nevertheless, according to earlier studies[22] there should be an inclination of 18° which disappears on the sedimentation of individual crystal layers by virtue of their mode of

collapse when viewed in isolation on a substrate. This small inclination, however, is likely to persist when crystals are sedimented in mass and is almost certainly to be present in the freeze-dried sample. By taking L_1^{100} close to 75 Å eq. (3) gives $\Delta L \approx 40$ Å. This is somewhat smaller than the value for the 85°C crystals. Whether the 5 Å difference is significant, i.e., whether there is a variation of ΔL with fold length, would require a more detailed examination of the exact endpoint at $P_1 = 100\%$ and the chain inclination in each case.

The maximum L_1 value detectable in the chromatogram is also of interest. For the 85°C grown crystals this is close to 150 Å. Allowing for a ϕ value of 25°, this would correspond to a layer thickness of 129 Å and by taking $\phi = 30°$ it would be 135 Å. In either case, it is in the range of L_x measured by x-rays in the undegraded state. In case of crystals grown at 70°C, the highest L_1 value is close to 115 Å. Again, on allowing for a chain inclination of 18°, this yields a layer thickness of 109 Å which is equal to the L_x value of 109 Å obtained by x-rays. All this suggests that the largest L_1 values correspond to an appropriately inclined straight-chain traverse through the entire lamellar thickness as assessed by x-rays. In other words, we have straight-fold stems which traverse the entire lamella, hence actual fold portions which are confined to the uppermost lamellar surface, as opposed to bulging folds which give rise to disordered chain portions spreading to an appreciable depth into the lamellar interior. This interpretation assumes that only straight stems contribute to L_1 and if there are large loose parts left after fold-cutting these are removed. Apart from general plausibility this assumption is strongly supported by the practically complete agreement between L_x and $L_1/\cos\phi$ at smallest P_1.

Ratio of Single- to Double-Traverse Lengths

As already stated the double-traverse length (L_2) is close to twice L_1 throughout the degradation. This is in agreement with the earlier work.[10] Nevertheless, inspection of Figures 3, 4, and 11 shows that $^1/_2L_2$ is systematically slightly above L_1. In most cases this difference is around or within 5% and even within smaller limits at high P_1 values. This is within or close to error limits specified in ref. 10. Hence, the presently found small excess of $^1/_2L_2$ does not conflict with the earlier assignment, which took $2L_1$ and L_2 as equal; it is merely a refinement of those results, particularly in the high P_1 region.

On the Cutting of Ends and Folds

However, as already commented on, the difference between $^1/_2L_2$ and L_1 becomes appreciably larger at low degradation temperatures, and this at low or intermediate P_1 (Figs. 9 and 10). This behavior arises from a steeper initial decrease in the L_1 values rather than from higher L_2 values as compared with the corresponding results at higher temperatures. This must mean that once the chains are cut, the cut ends shorten in preference to the cutting of new folds. This would have the result that at a given P_1 value

(which is a measure of folds cut) the single traverse length has suffered a greater proportional shortening due to this continued end-cutting than has the double-traverse length.

This picture, in the first place forced on us by results such as in Figures 9 and 10, is not as *ad hoc* as it may appear. It is established from standard ozone oxidation studies that the carbon atom adjacent to a carboxyl group is a preferred site for reaction with ozone, as compared with chain scission elsewhere along the methylenic chain.[23] Accordingly we could consider our layer-thinning to consist of two different reactions: (1) cutting of the methylenic chain anywhere along the chain, which in our case would correspond to cutting of the fold, giving rise to a terminating carboxyl group, (2) shortening of the carboxyl-terminated chain by attack on the methylenic group adjacent to the carboxyl. According to the foregoing such a distinction has been noted before.[23] What we note from our results in addition is that, at high enough temperatures, the rates of these two reactions are indistinguishable. But as the temperature is lowered, shortening of the carboxyl-terminated chain becomes faster relative to cutting of the methylenic chain, and thus the two reactions can be distinguished (in other words, the attack becomes more selective). Note that the foregoing remarks refer to relative rates, the overall rate of both reactions is very much reduced at the low temperatures (Fig. 8) and that we compare at equal P_1 and not equal times. This implies, of course, that at the low temperatures the methylenic groups in the chain interior are more resistant, even when in the fold, than when adjacent to a carboxyl group.

On Sharp versus Loose Folds

Previously the nearly 2:1 traverse ratio was taken as evidence for sharply defined, adjacently reentrant folds.[10] Later this was qualified insofar as it was strictly valid only for a narrow molecular weight distribution within the peaks.[11] This qualification was required because by cutting of large, loose, nonadjacently reentrant folds statistically, assuming that most of the resulting loose ends are retained, the maxima of the peaks would still satisfy the 2:1 traverse ratio but the peaks would be correspondingly broadened. To clear up this point, the molecular-weight spread corresponding to the peaks was determined by means of the newly constructed resolution calibration, and was found sufficiently narrow for adjacently reentrant, sharp folds.[11] However, this assessment was made at high P_1 values. In our present formulation this means that sharply adjacent reentry was, strictly speaking, only verified in the case of folds which were buried deep down in the crystal.

We see from Figures 3*d* and 4*d* that the molecular weight distribution is broader at lower P_1. This reduces the strength of the above conclusion about the sharpness and adjacent reentry of the folds in the earlier stages of the degradation. In our present picture this corresponds to folds closer to the mean lamellar surface as defined by x-rays. Even so, the requirement of a narrow peak for adjacently reentrant sharp folds is likely to be an unduly stringent one. As stated, it is based on retention of long, residual, loose ends after fold-cutting. It follows from the foregoing that if such are

present to begin with, they are likely to be removed by the acid in preference to cutting of new folds. Further, the peaks are broadest at the lowest P_1 values. Here the traverse lengths (taken as the length of the chain fragments) is close to the lamellar thickness, allowing for chain obliquity. If there is much looseness, and this is retained, the fragment length would be longer; but this is not observed.

It follows that correlation of peak broadening—while the peak maxima retain their closely 2:1 ratio—with fold looseness need not be unique, and in fact it is questionable whether such a broadening is evidence *in itself* for a loose fold structure. Nevertheless, the model of an increasing amount of fold looseness as the layer surface is approached from the crystal interior is at least compatible with the observed broadening of tbe peaks with decreasing P_1.*

When examining the actual figures for the molecular weight spread we see that there is a major difference between the 70°C and 85°C samples. The spreads are similar for $P_1 = 100$ but increase less steeply for the 70°C crystals. In fact, for P_1 up to 10–20%, the increase is only within a factor of 2; hence, even when taking the peak width as a measure of fold looseness, one need not depart significantly from an adjacently reentrant sharp fold structure reaching up close to the top surface of these crystals. There is a considerably larger increase in the spread for the 85°C crystals where in addition to the steeper linear increase there is a sudden surge below $P_1 = 30\%$. It is to be remembered that about 12% of the material remains uncrystallized at 85°C and, unless removed by filtration, crystallizes with a different fold length on cooling. As the corresponding material would deposit at the crystal periphery or in the form of overgrowth layers, it would be more accessible, and thus the folds within it could be cut in greater numbers during the early stages of degradation. When added to the fragments belonging to the rest of the crystal, this would lead to a spreading of the peak at a stage where the complete resolution of the peak, hence detailed assessment of the peak shapes is inaccurate in any case. This hypothesis should be amenable to direct test which, however, was not carried out during the present work.

Irrespective of differences between 70 and 85°C crystals, an upswing at very low P_1 values is indicated for both. This is at least consistent with the possibility of an increase of the number of loose-fold elements at the surface itself.

The Crystal Lamella in the Light of the New Results

Nature of the Defective Surface Layer

Pooling the foregoing considerations, the following picture emerges. We have a lamellar core with straight chains and a lattice which can be re-

* Departure from the 2:1 traverse ratio such as is apparent from Figure 9 need not affect the argument as in these cases it is the single traverse which is shorter and not the double traverse which is longer than observed under different circumstances. As stated above, we attribute this to an additional shortening of the single traverse and not to large amounts of excess material in the double traverse.

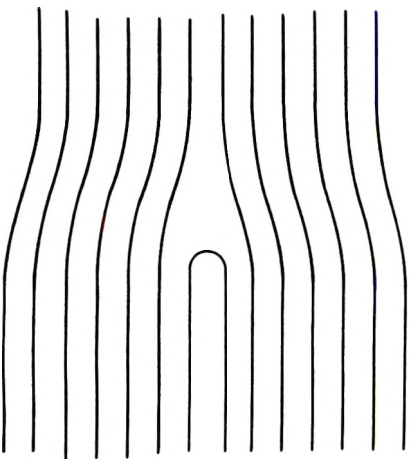

Fig. 14. Crystal defect due to a single fold buried deep inside the crystal.

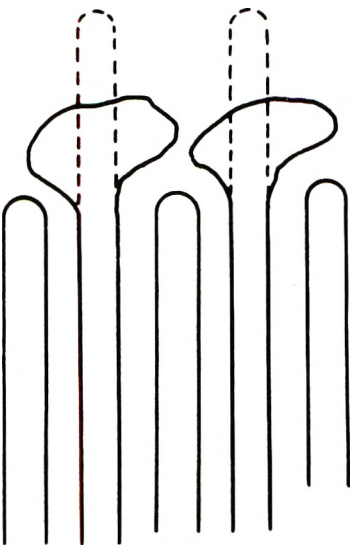

Fig. 15. Bulging out of folds due to several folds terminating at a lower level around them. The dotted lines show the straightened form of the bulging folds.

garded for the present discussion as perfect. Going outward toward the crystal surface from this fold free interior there will be found an increasing number of terminating folds. There may be no sharp boundary, but we may define a level where folding becomes detectable by our test. (This is defined at the depth ΔL in Fig. 13.) As we go farther outward more and more straight stems will terminate in the form of folds. Irrespective of structural details, this model implies a gradual reduction in density as more and more of the traversing stems are being removed. It is clear that at some stage the mean amorphous density will be attained. It will be ap-

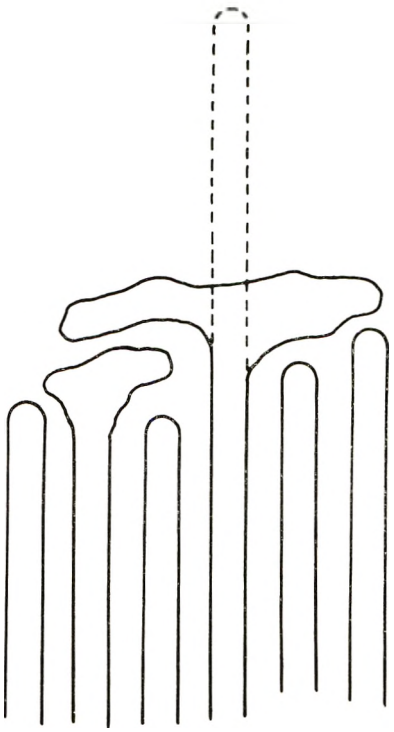

Fig. 16. Attempt to illustrate how a single, isolated fold protrusion would spread out in a disordered fashion onto its surrounding fold environment.

parent from the structural considerations to follow that this amorphous density will be maintained, even when still further folds are withdrawn.

The remaining step is to account for the consequences of fold termination in structural terms. In what follows the pertinent structure elements will be enumerated and sketched individually: there will be no attempt to piece them together into a model lamella. It is recognized that this can be done speculatively in a number of ways, but information is lacking as to the choice of specific details.

Figures 14–17 present schematic two-dimensional representations of various elements envisaged to constitute the fold surface when going outwards from the crystal interior. Each class is shown individually; their combination is not attempted.

An isolated fold within the crystal interior (Fig. 14) will constitute only a defect, namely a row vacancy or a dislocation, without affecting the essentially crystalline character of the material around it. As the number of such folds within the lamellar interior increases, the question arises of how the material will spread over the larger volume which becomes available to it. It can retain the lattice with uniformly distributed defects only up to a certain limit. Beyond that it will either have to break up into comparatively perfect crystal blocks with gaps between them, which will essentially

take up the extra volume, or spread evenly over this volume and become equivalent to amorphous material. In terms of individual, adjacently reentrant folds (Fig. 15) should serve as an illustration. The folds will bulge out, taking up an essentially disordered configuration. Still longer folds forming more isolated fold protrusions will not stay straight but will lie down in a disordered form on folds terminating at a lower level around them (Fig. 16) irrespective of whether these lower lying folds are sharp and regular or already loose, essentially "amorphous" as in Figure 15. It is obvious that

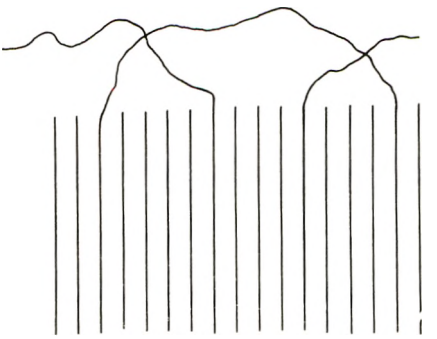

Fig. 17. A nonadjacently reentrant loose fold and examples of a short and long 'hair' overlying the rest of the fold surface, which is to be visualized as consisting of adjacently reentrant folds as in Figs. 14–16 but not drawn out here.

although unevenness of the fold surface measured by the straightened state of the folds may increase further at the outermost levels of the lamella, the overall density will not be further reduced because the protruding folds will fill up the volume lying between them by spreading out laterally in a disordered fashion.

Perhaps the really important point of distinction is the stage where the chains acquire an appreciable component lying along the basal face of the crystal, as opposed to being only perpendicular or at a specified large angle to it, which is the orientation characterizing the chains within the lattice.*

* It was brought to our attention by Professor E. W. Fischer that the exact analysis of low-angle x-ray intensities[24,25] precludes gradual transition between layers of high and low electron density with the transition region comparable or not much narrower than the layer of low electron density, i.e., there must be a comparatively sharp division into a high- and a low-density phase. Clearly the present model of uneven fold lengths must satisfy requirements such as set up by different criteria. It will be apparent that even if we said that the number of terminating folds increases in a continuous fashion towards the crystal surface this will only produce a gradual density decrease if the crystal lattice is otherwise retained but with increasing amount of imperfection and/or gradually increasing lattice spacing. It is likely that the amorphous density will not be approached gradually by the introduction of crystal imperfections and ensuing expansion of the lattice, because there will not be sufficient entropy gain to compensate for loss of enthalpy. Hence it can be expected that, below a certain density, the lattice collapses into what from the point of view of densities would correspond to an amorphous phase. Thus, in effect, a comparatively sharp boundary could exist within the confines of the present model.

The folds have been drawn essentially as adjacently reentrant. As is apparent, say, from Figure 14, this will be a necessity for folds which are buried within the crystal interior purely by considerations of chain packing geometry: without major gaps within the lattice they cannot connect non-adjacent positions. This situation will pertain to a diminishing extent up to near the top surface of the layer. However, close to the top surface remote reentry could readily occur. Here, and only here, could we have a structure which resembles the often quoted switchboard.[26] This uppermost layer could also accommodate loose chain ends and long hairs (Fig. 17).

Accordingly, there would be a whole spectrum of defects and disorder within the surface layer responsible for the crystallinity deficiency of chain-folded single crystals, from lattice defects deep in the interior to loose hairs at the surface. As regards their origin they fall in two basic categories. First and chiefly, defects due to the fluctuations of the fold-length alone. These comprise the types shown schematically by Figures 14–16. Secondly, what we consider misplaced or missing chain deposition resulting in large nonreentrant loops and loose hairs at the very top (Fig. 17). By this classification, the former would be intrinsic, the latter accidental (see below). At this stage two questions need attention: the particular depth of the disorder (ΔL) and secondly the contribution of each kind of disorder to the conventionally measured crystallinity deficiency.

Depth of Disorder (ΔL)

When allowing for chain inclination, the present work gives figures of 40–45 Å i.e., ΔL is 20–23 Å per lamellar surface. At first sight this seems to be a greater thickness than has ever been suggested. However, it needs recalling that the innermost stratum (such as in Fig. 14) may correspond only to a very small crystallinity deficiency and may contribute very little, if any at all, to the "amorphous" content of conventional amorphous-crystalline ratio determinations. Thus the depth specified on the latter basis would not be identical with our ΔL. The possible dependence of ΔL on various factors would require separate study. Even so, the marginally lower value (in view of the errors involved) for 70°C crystals, as compared with 85°C in the present work suggests a dependence on crystallization temperature or rather on L_x (x-ray layer thickness) itself. If confirmed, this would be at least in qualitative agreement with such a dependence observed in annealed crystals previously[12] when this dependence was associated solely with the fold-length increment due to the annealing. Such dependence on L_x has also emerged in concurrent work on the bulk[27,28] (where also σ_M is linearly related to L which again is in accord with our results, such as in Figs. 4*d* and 5*d*). If in single crystals ΔL did really depend on L_x, the uniqueness of such a dependence would be important to establish; in particular, whether say heat treatment or storage, such as in itself would not affect L_x, would alter ΔL. The important implications of such a possibility have been raised elsewhere.[29,30]

Disorder Type and Amorphous Content

The closest guide we have in this respect are our experiments with very short chains.[31–34] As such chains may only fold once or twice, there is no chance for a representative amount of loose nonreentrant loops and hairs (Fig. 17) (see also extensive works by Skoulios and collaborators on bulk materials with the same implication.[35]) Nevertheless, as assessed by conventional methods, such crystals are again only 80–85% crystalline. Also, frequently such crystals display interfacial dislocation networks, which imply crystallographic continuity when passing from one layer to the next in bilayer or multilayer crystals, and this would preclude a true amorphous surface layer, even in a lamella such as shown in Figures 15 and 16. However, it was deduced that the dislocation networks are due to the intermeshing of the fold stems from one layer, with the gaps due to submerged folds or chain ends in the next, ensuring the required crystallographic continuity. Clearly at the localities where this occurs, loose folds as in Figure 15 would straighten out while becoming part of the joint lattice formed by the two superposed layers. Uneven fold length is implicit in the model as here presented, and in fact was verified by the same kind of degradation experiment and deductions (simultaneous shifts of peak 1 and 2 with 1:2 ratio maintained)[32] as feature in the present work. In fact, these investigations were all concurrent and independently led to the same conclusion. Accordingly, the sizeable crystallinity deficiency in these particular crystals must be due to defects caused by buried folds along with no or little contribution from amorphous material proper.

It follows, therefore, that the layer of buried folds alone can cause all the familiar symptoms of deficient crystallinity in single crystals. It is questionable, therefore, whether "amorphous" material such as is shown in Figures 15 and 16 is strictly necessary; and if it is, how much of it. The large nonadjacently reentrant loops and loose hairs (Fig. 17) are certainly not required. No doubt if present, they will make their own contribution. Thus we conclude, that a large portion of the crystallinity deficiency is intrinsic to single crystals as it is associated with the unevenness of the folds which in turn seems to be an intrinsic feature of chain-folded crystallization. Whether this unevenness could be reduced by subsequent rearrangement with the appropriate consequences for the crystallinity values, as has been suggested elsewhere,[29] would require separate attention.

Correspondence with Swelling Experiments

It has been reported in a different investigation[30] that the lamellar periodicity, as assessed by low-angle x-ray diffraction, could be increased reversibly by swelling agents. As the crystal proper does not swell the effect was attributed to the surface layer. The same effect was inferred previously from electron microscope studies of the surface topography of means by gold decoration[1,2,36] which, while qualitative, directly identified the crystal surface as the site where the changes due to the swelling agents occur. Now,

for expansion to take place on swelling there have to be loose chains which have a sizeable component along the lamellar surface. (Clearly, folds as in Fig. 14 cannot expand upwards any further.) By the present model such chains can only be expected at the uppermost regions of the fold surface, either in the form of adjacently reentrant loose loops (Fig. 16) or, even more, in that of nonadjacently reentrant large loops and long hairs which are envisaged to cover the fold surface as the result of misplaced or interrupted deposition of long enough molecules (Fig. 17). Indeed, it was found that short molecules,[30] and particularly such as give rise to interfacial dislocations,[36] show practically no swelling effect by any of the above tests while still exhibiting about 15% crystallinity deficiency.

We see, therefore, that the swelling tests are capable of identifying that uppermost portion of the disordered layer formed by comparatively long molecules, which can be considered as truly amorphous in the sense that the chains take up a random configuration. However, the existence of such a layer is not necessary for the usually observed crystallinity deficiency of single crystals; for this can be due to fold-length fluctuations alone.

Relevance to General Studies on Polymer Degradation

The present results produced agreement between different degradation methods under variety of circumstances. In addition to serving the structural study of polymer crystals they could also be of value for investigations directed at the degradation process as such, as it follows that by discriminating between morphological features the degradation in itself will depend on the morphology. Improved understanding of the former, as hopefully provided by the present work, should provide an improved basis for the latter. In any event, the present studies established very sensitive criteria of how and when sample consistency and consequent diffusion-controlled effects influence the results. This in itself is an important preliminary of any degradation work on solid polymers.

CONCLUSIONS

A structure pattern has been established which seems to embrace most known facts about the fold surface of polymer single crystals prepared from a variety of materials under a variety of circumstances. The picture of fluctuating fold lengths, embodying structure features from crystal defects to loose amorphous material in appropriate sample types, falls in line with most theoretical ideas and a variety of experimental observations. Undoubtedly its relevance to the full spectrum of other investigations on the fold-surface problem, including the measurements of the absolute x-ray intensities in the low-angle regions[24,25] still need assessing.

However, we believe that the significance of the present work lies more in its forward-looking than retrospective nature. Namely, it provides concrete indications for further exploration. Thus is established (together with preceding[19] and other concurrent works[27,28] concrete structural parameters

of the fold surface which can be quantitatively assessed by experiment. Among these are the depth ΔL of the layer containing buried folds, the distribution of terminating folds as a function of depth (a potential inherent in the chromatograms but not yet evaluated), and distinction between different types of disorder within the layer such as principally provided by the combination of degradation and swelling experiments. What we consider as most encouraging is that the structural ideas embodied by the model are proving to be fruitful for new lines of work where, as in the current studies on polyamides,[37] they lead to even more conspicuous consequences.

Our thanks are due to Dr. T. Williams for his actively contributing to the GPC work at the earlier stages and for transmitting his experience, without which the present work would not have been possible. We wish to thank Professor I. M. Ward for his association with parts of the project and general interest.

References

1. A. Keller, *Repts. Progr. Phys.*, **31**, part 2, 623 (1968).
2. A. Keller, *Kolloid Z. Z. Polym.*, **231**, 386 (1969).
3. D. J. Priest, *J. Polym. Sci. A-2*, **9**, 1785 (1971).
4. A. Keller and Y. Udagawa, *J. Polym. Sci. A-2*, **9**, 1799 (1971).
5. A. Peterlin and G. Meinel, *J. Polym. Sci. B*, **3**, 1059 (1965).
6. A. Peterlin, G. Meinel, and H. G. Olf, *J. Polym. Sci. B*, **4**, 399 (1966).
7. D. J. Blundell, A. Keller, and T. Connor, *J. Polym. Sci. A-2*, **5**, 991 (1967).
8. A. Keller and Y. Udagawa, *J. Polym. Sci. A-2*, **8**, 19 (1970).
9. D. J. Blundell, A. Keller, I. M. Ward, and I. J. Grant, *J. Polym. Sci. B*, **4**, 781 (1966).
10. T. Williams, D. J. Blundell, A. Keller, and I. M. Ward, *J. Polym. Sci. A-2*, **6**, 1613 (1968).
11. T. Williams, Y. Udagawa, A. Keller, and I. M. Ward, *J. Polym. Sci. A-2*, **8**, 35 (1970).
12. D. M. Sadler, T. Williams, A. Keller, and I. M. Ward, *J. Polym. Sci. A-2*, **7**, 1819 (1969).
13. D. J. Blundell, A. Keller, and A. J. Kovacs, *J. Polym. Sci. B*, **4**, 481 (1966).
14. D. J. Blundell and A. Keller, *J. Macromol. Sci.*, **B2**, 337 (1968).
15. F. C. Frank, I. M. Ward, and T. Williams, *J. Polym. Sci. A-2*, **6**, 1357 (1968).
16. I. M. Ward and T. Williams, *J. Polym. Sci. A-2*, **7**, 1585 (1969).
17. F. H. Winslow, M. Y. Hellman, W. Matreyek, and R. Salovey, *J. Polym. Sci. B*, **5**, 89 (1967).
18. A. Keller and D. J. Priest, *J. Macromol. Sci.*, **B2**, 479 (1968).
19. C. Tanford, *Physical Chemistry of Macromolecules*, Wiley, New York, 1961.
20. R. P. Palmer and A. Cobbold, *Makromol. Chem.*, **74**, 174 (1964).
21. H. C. Beachell and S. P. Nemphos, *J. Polym. Sci.*, **21**, 113 (1956).
22. D. C. Bassett, F. C. Frank, and A. Keller, *Phil. Mag.*, **8**, 1753 (1963).
23. F. Asinger, *Paraffins, Chemistry and Technology*, Pergamon Press, London–New York, 1968, p. 616.
24. E. W. Fischer, *Kolloid Z. Z. Polym.*, **231**, 458 (1969).
25. E. W. Fischer, H. Goddar, and G. F. Schmidt, *J. Polym. Sci. B*, **5**, 619 (1969).
26. P. J. Flory, *J. Amer. Chem. Soc.*, **84**, 2857 (1962).
27. I. M. Ward and T. Williams, private communication, *J. Polymer Sci.*, in press.
28. T. Williams, Ph.D. Thesis, Bristol 1969.
29. J. D. Hoffman, J. I. Lauritzen, E. Passaglia, G. S. Ross, L. J. Frolen, and J. J. Weeks, *Kolloid Z. Z. Polym.*, **231**, 564 (1969).

30. Y. Udagawa and A. Keller, *J. Polym. Sci., A-2*, **9**, 437 (1971).
31. D. M. Sadler and A. Keller, *Kolloid Z. Z. Polym.*, **239**, 641 (1970).
32. D. M. Sadler and A. Keller, *Kolloid Z. Z. Polym.*, **242**, 1081 (1970).
33. A. Keller and Y. Udagawa, *J. Polymer Sci. A-2*, in press.
34. L. D'Ilario, A. Keller, and E. Martuscelli, *J. Polymer Sci. A-2*, in press.
35. J. R. Arlie, P. Spegt and A. Skoulios, *Makromol. Chem.*, **104**, 212 (1967).
36. D. M. Sadler, unpublished data.
37. E. D. T. Atkins, A. Keller, and D. M. Sadler, *J. Polymer Sci. A-2*, in press.

Received January 21, 1971

JOURNAL OF POLYMER SCIENCE: PART A-2 VOL. 9, 1839–1850 (1971)

Steady Flow and Dynamic Viscosity of Branched Butadiene–Styrene Block Copolymers

GERARD KRAUS, F. E. NAYLOR, and K. W. ROLLMANN,
Phillips Petroleum Company, Bartlesville, Oklahoma 74004

Synopsis

Steady flow and dynamic viscosities were determined for symmetrical linear and star-branched block copolymers of butadiene and styrene above their upper (polystyrene) glass transition. Block structures examined were B-S-B, (B-S-)$_3$, S-B-S, (S-B-)$_3$ and (S-B-)$_4$. At constant molecular weight and total styrene content viscosities were greater for polymers terminating in styrene blocks, irrespective of branching. Branching decreased the viscosity of either polybutadiene-terminated or polystyrene-terminated block polymers, compared at equal $\bar{M}_w$. However, comparisons at equal block lengths showed that the length of the terminal blocks, not the total molecular weight, governs the viscoelastic behavior of these polymers to a surprisingly good approximation. This unusual result is rationalized in terms of the two-phase domain structure of these polymers, which persists to a significant degree in the melt. Below the glass transition of the polystyrene blocks the effects of branching were masked by differences in the morphology of the domain structure unrelated to branching.

INTRODUCTION

Several years ago, Kraus and Gruver[1] showed that the steady-flow Newtonian melt viscosity of narrow distribution, star-branched polybutadienes is smaller than that of linear polybutadienes below a certain molecular weight, (i.e., the theoretical prediction[2]) but that the reverse is true at high molecular weights. This behavior has since been confirmed by others, not only for polybutadiene,[3,4] but also for polystyrene, where the "cross-over" occurs at much greater molecular weights.[5] Coupled with the large limiting zero-shear viscosity, there is an increase in shear response of the branched polymer. In randomly branched, broad-distribution polymers the behavior is complex, but numerous instances of increased melt viscosity attributable to long-chain branching have been demonstrated.[6–9]

The rheological behavior of butadiene–styrene block polymers is dominated by their two-phase domain structure, which persists in the melt,[10–12] i.e., at temperatures exceeding the glass transition T_g[3] of the polystyrene domains. Since the association of polystyrene blocks into domains represents a type of physical branching (B-S and B-S-B block polymers) or crosslinking (S-B-S and S-B-S-B . . . block polymers), the effects of additional chemical branching are not predictable. In the present paper we describe the effects of symmetrical star-branching on the viscoelastic behavior of narrow-distri-

bution butadiene–styrene block polymers of the following structures: BSB, $(BS-)_3$, SBS, $(SB-)_3$, and $(SB-)_4$.

EXPERIMENTAL

Polymer Preparation

All reactions were conducted in cyclohexane solvent (Phillips olefin polymerization grade) which had been dried by countercurrent nitrogen flow through an activated alumina column. Butadiene (Phillips special purity) was dried by flashing through an activated alumina column at about 70°C. Styrene (Dow polymerization grade) was dried by distillation from CaH_2. Reaction vessels were beverage bottles, stored in a hot-air oven at 70°C. *sec*-Butyllithium was obtained as a 15% solution in *n*-heptane from Foote Mineral Co. Reaction temperature was 70°C. The reactions were short-stopped with isopropanol containing 1 phr of antioxidant (Ionol). Polymers were recovered by isopropyl alcohol coagulation.

Linear S-B-S Polymers. Half the styrene and all the butyllithium were added to the solvent (780 phm) in capped 26-oz bottles, and the monomer was allowed to polymerize for 30 min. Next all the butadiene was charged. After 45 min the remaining styrene was added and polymerization con-

TABLE I
Polymer Description and Characterization[a]

Polymer	Structure	Free polystyrene, %	$[\eta]$, dl/g[b]	$M_t/1000$[c]	$\bar{M}_w/1000$[d]	$\bar{M}_n/1000$[d]
A	BSB	0	0.62	48	51	44
B	"	0	1.00	91	97	78
C	"	0	1.34	154	154	116
D	$(BS-)_3$	0	0.73	72	77	63
E	"	0	1.10	136	148	113
F	"	0	1.66	231	216	155
G	SBS	1.0	0.76	56	54	48
H	"	1.6	0.81	71	82	72
I	"	1.8	1.06	91	99	88
J	$(SB-)_3$	1.8	0.99	115	135	111
K	"	2.5	1.16	115	159	124
L	"	1.9	1.22	136	165	132
M	"	1.0	1.28	150	146	115
N	"	2.0	1.34	167	171	139
O	"	1.5	1.49	187	177	139
P	$(SB-)_4$	2.5	1.14	154	173	148
Q	"	1.9	1.13	181	156	127

[a] All polymers contain 30% styrene by weight.

[b] In tetrahydrofuran at 25°C.

[c] Target "kinetic" moecular weight. Calculated from initiator cocentration, corrected for estimated catalyst-poison level. Coupling assumed 100% efficient.

[d] GPC, exclusive of free polystyrene.

tinued to quantitative conversion (30 min) at which point the reaction was shortstopped.

Branched S-B-S Polymers. Styrene and butyllithium were added to bottles containing cyclohexane (790 phm). After 30 min butadiene was added and polymerized for 30 min. The requisite coupling agent,[13] PCl_3 for trichain and $SiCl_4$ for tetrachain polymers, was introduced, and the coupling reaction allowed to proceed for 30 min. Gel-permeation chromatograms indicated narrow molecular weight distributions with very minor amounts of polystyrene and uncoupled styrene–butadiene block polymer.

B-S-B Polymers. Butadiene and butyllithium were added to bottles containing cyclohexane (786 phm). After 30 min styrene was charged and reacted for 30 min. A small amount of butadiene (1 phm) was added to facilitate coupling. Methyltrichlorosilane or dimethyldichlorosilane was added as the coupling agent and allowed to react for 30 min. Coupling was less efficient than in the preparation of S-B-S block polymers; 10–25% butadiene–styrene block polymer remained. This was removed by fractional precipitation of branched product from toluene by slow addition of isopropanol.

Polymer characterization data are shown in Table I.

Molecular Weight Determination

Weight-average and number-average molecular weights of all polymers were determined by gel-permeation chromatography and dilute solution viscometry, by making use of a "universal" GPC calibration of hydrodynamic volume, $M[\eta]$, versus eluent volume. The molecular weights obtained were in good agreement with expectations based on initiator level and coupling stoichiometry in most instances.

Physical Measurements

Melt viscosities were determined by capillary rheometry by using established techniques. Both the "entrance" and Rabinowitsch corrections were applied to all data.[14]

Dynamic measurements were carried out with a Vibron Viscoelastometer (Toyo Measuring Instruments Co., Tokyo, Japan). A special sample holder, similar to the one described by Erhardt et al.,[15] was used for shear measurements. As a check on the validity of the shear measurements a

TABLE II

Frequency, Hz	$\log\lvert G^*\rvert$, dyne/cm²		tanδ	
	This work	Ferry[17]	This work	Ferry[17]
3.5	7.05	6.97	0.090	0.095
11	7.07	7.00	0.035	0.066
35	7.10	7.03	0.050	0.050
110	7.12	7.05	0.041	0.043

polybutadiene of $\bar{M}_w$ = 510,000, which had been investigated in detail by Ferry and associates,[16,17] was examined at 25°C. Characterization data are given in Table II.

The agreement between laboratories using different equipment must be considered satisfactory.

RESULTS AND DISCUSSION

Viscoelastic Behavior in the Melt ($T > T_g^s$)

Between 100 and 160°C all polymers, with the exception of some of the lowest molecular weight samples, exhibited strongly non-Newtonian flow over the entire range of shear rates, $0.5 < \dot{\gamma} < 50$ sec^{-1}. Similarly, dynamic viscosities showed a strong frequency dependence in the range of angular frequency from 22 to 690 radians/sec. Since the objective of this study was to ascertain the effects of branching and block sequence at equal shear rate (or frequency) and comparable molecular weight or block length, the steady-flow viscosity η, the dynamic viscosity $|\eta^*|$, and tanδ were found at $\dot{\gamma}$ = 1 and 10 sec^{-1}, or ω = 10 and 100 radians/sec, respectively. This involved interpolation (in some cases short extrapolation) of plots of the various viscoelastic functions versus log $\dot{\gamma}$ or log ω. The results are displayed in Table III.

Figures 1 and 2 illustrate graphically the relationships between viscosity, block sequence and branching for block polymers containing 30% styrene at 130°C and $\dot{\gamma} = \omega$ = 10 sec^{-1}. The same general behavior is observed at other temperatures and shear rates or frequencies. It is immediately obvious that, at equal molecular weight, the viscosity of a block polymer with terminal styrene blocks exceeds that of a polymer with terminal bu-

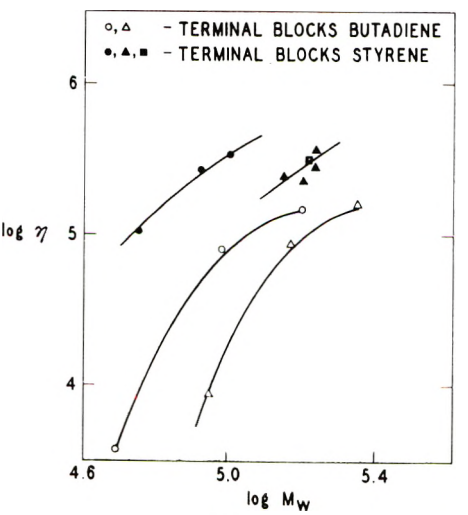

Fig. 1. Steady flow viscosity at 130°C, $\dot{\gamma}$ = 10 sec^{-1}: (○,●) linear polymers; (△,▲) trichain; (■) tetrachain.

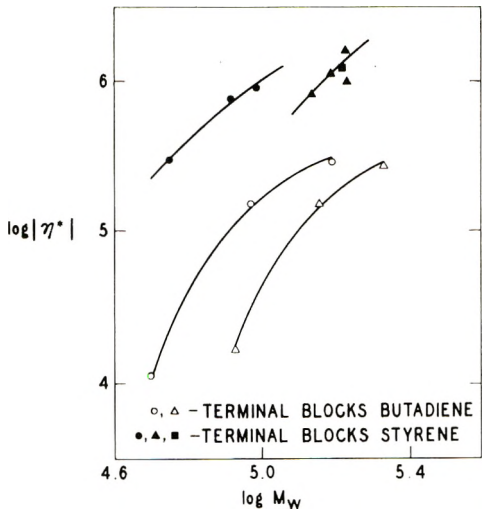

Fig. 2. Dynamic viscosity at 130°C, ω = 10 rad/sec: (○,●) linear polymers; (△,▲) trichain; (■) tetrachain.

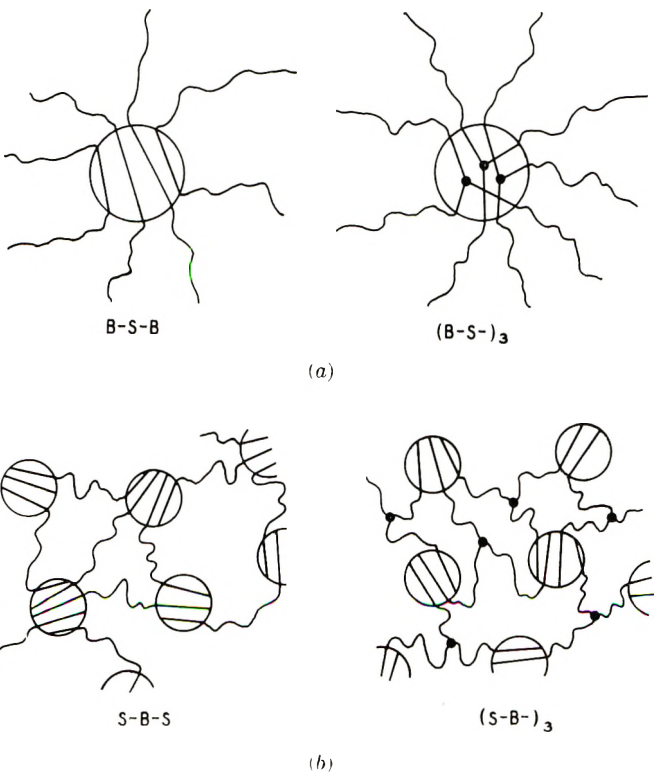

Fig. 3. Schematic representation of domain structures: (*a*) polymers terminating in butadiene blocks; (*b*) polymers terminating in styrene blocks.

TABLE III
Steady Flow and Dynamic Viscosity Data[a]

Polymer	Structure	$\bar{M}_w/1000$	Temp, °C	$\eta \times 10^{-5}$, poise		$\lvert\eta^*\rvert \times 10^{-5}$, poise		tanδ	
				$\gamma = 1$	$\gamma = 10$	$\omega = 10$	$\omega = 100$	$\omega = 10$[b]	$\omega = 100$
A	BSB	51	130	0.052[c]	0.048	0.107	0.062	1.2	1.3
			160	0.030[c]	0.0295	0.059	0.029	1.2	1.3
B	"	97	130	3.0	0.83	1.54	0.44	0.74	0.54
			160	1.8	0.64	0.73	0.21	0.78	0.58
C	"	154	130	7.6	1.55	2.9	0.55	0.36	0.34
			160	6.8	1.29	1.63	0.33	0.38	0.37
D	$(BS-)_3$	77	130	0.100[c]	0.093	0.163	0.080	1.0	1.2
			160	0.042[c]	0.042	0.076	0.038	0.66(?)	1.2
E	"	148	130	4.0	0.90	1.65	0.44	0.72	0.51
	"		160	2.6	0.75	0.83	0.21	0.71	0.56
F	"	216	130	8.8	1.74	2.8	0.53	0.33	0.31
			160	—	—	1.74	0.35	0.31	0.35
G	SBS	54	130	1.3	1.03	3.1	0.63	0.51	0.29
			160	0.30[c]	0.28	1.05	0.34	1.10	0.53
H	"	82	130	9.8	2.8	6.9	1.04	0.32	0.20
			160	2.3	1.35	3.0	0.66	0.66	0.30

I	"	99	130	25.5	3.3	8.8	1.29	0.165	0.155
			160	12.0	3.0	4.9	0.71	0.30	0.17
J	$(SB-)_3$	135	130	15.8	2.5	8.0	1.25	0.20	0.20
			160	9.2	1.8	4.4	0.66	0.35	0.21
K	"	159	130	14.5	2.3	11.6	1.68	0.19	0.17
			160	7.6	1.5	6.1	0.93	0.32	0.22
L	"	165	130	20.9	3.9	10.5	1.72	0.19	0.17
			160	12.5	2.0	5.4	0.78	0.21	0.16
M	"	146	130	—	—	10.8	1.70	0.18	0.19
			160	—	—	6.8	0.94	0.21	0.15
N	"	171	130	27.0	3.0	17.0	2.45	0.16	0.18
			160	17.0	2.6	9.6	1.38	0.18	0.13
O	"	177	130	—	—	11.0	1.62	0.17	0.17
			160	—	—	6.2	0.82	0.14	0.13
P	$(SB-)_4$	173	130	17.2	3.6	11.8	1.70	0.18	0.18
			160	10.2	1.7	7.1	1.01	0.32	0.20
Q	"	156	160	—	—	3.9	0.60	0.32	0.19

[a] All polymers contain 30% styrene by weight.
[b] Obtained by extrapolation.
[c] Newtonian viscosity.

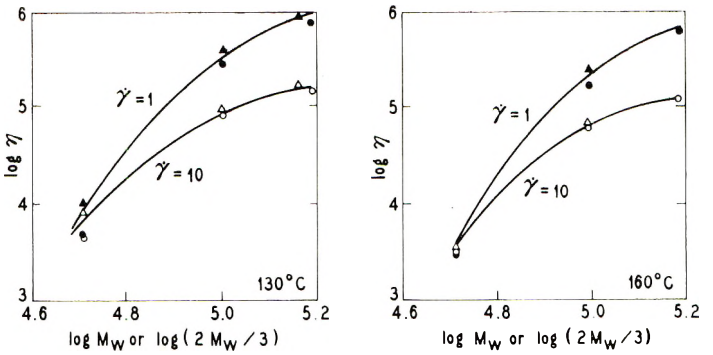

Fig. 4. Steady flow viscosity of polymers terminating in butadiene blocks compared at equal butadiene block length: (○,●) linear polymers; (△,▲) trichain.

tadiene blocks, and that, for either type of block arrangement, the branched polymers have the lower viscosities. These trends are the same for steady flow and dynamic viscosity. Additionally, comparison of Figures 1 and 2 shows that $\eta \neq |\eta^*|$ when $\dot{\gamma} = \omega$, the disparity being greater for block polymers terminating in styrene.

Figure 3 shows a schematic drawing of the various block polymer molecules, as they are imagined to exist in a melt with domain structure. We note that polymers terminating in butadiene blocks resemble multichain polymers of high functionality of branching, whether or not they are also branched chemically. If the domain size is unaffected by an occasional branch point and if the polymer flows with little disruption of the polystyrene domains, then the viscosity might be expected to be primarily a function of the butadiene block length and not the molecular weight of the whole polymer. On the other hand, polymers with terminal styrene blocks cannot undergo steady flow without some disruption of the domains. The effective molecular weight of the flowing molecules will depend on the ease with which polystyrene blocks are extracted from the domains. This, in turn, will depend on the length of the styrene blocks. In the following we show that the observed behavior is, indeed, consistent with these qualitative considerations.

Polymers Terminating in Butadiene Blocks. The length of the butadiene block, M_b, in units of molecular weight is

$$M_b = Mw_b/n_b \tag{1}$$

where M is the molecular weight of the whole polymer, w_b is the weight fraction of butadiene, and n_b is the number of butadiene blocks per molecule. Equal values of M_b are achieved at equal w_b when the molecular weight of a trichain block polymer is $^3/_2$ that of the linear B-S-B polymer. Since our polymers are of narrow molecular weight distribution, a comparison of linear and tribranched polymers at $\bar{M}_w$ and $2\bar{M}_w/3$, respectively, represents approximately equal butadiene block lengths. Figures 4, 5, and 6 show η,

$|\eta^*|$, and tanδ, compared in this manner at several conditions. While the agreement is not perfect, particularly at the lowest molecular weight, there seems little doubt that butadiene block length and not total molecular weight of the block polymer is the principal factor in the viscoelastic response of linear and branched B-S-B melts.

Polymers Terminating in Styrene Blocks. The length of the styrene blocks M_s is

$$M_s = Mw_s/n_s \tag{2}$$

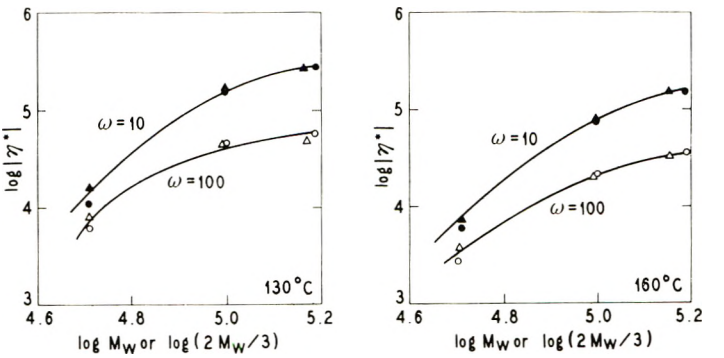

Fig. 5. Dynamic viscosity of polymers terminating in butadiene blocks compared at equal butadiene block length: (○,●) linear polymers; (△,▲) trichain.

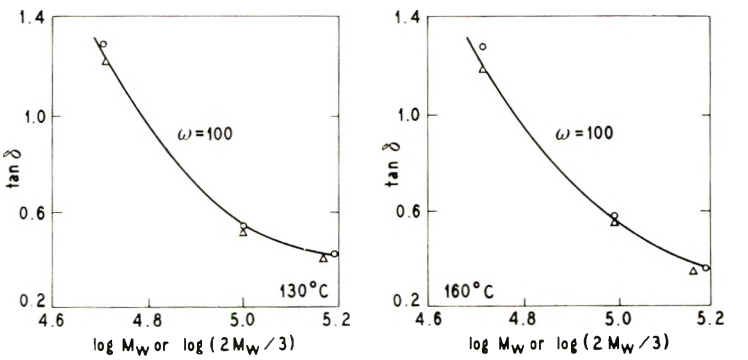

Fig. 6. Loss tangent of polymers terminating in butadiene blocks compared at equal butadiene block length: (○) linear polymers; (△) trichain.

where w_s is the weight fraction of styrene in the block polymer, i.e., after correction for free polystyrene. By the above argument a comparison at approximately equal styrene block length is achieved by comparing properties at M_w (linear) and $2M_w/n_s$ (branched). Figures 7–9 show the results. They exhibit considerably more scatter than Figures 4–6 but show no systematic trends contradicting the hypothesis that styrene block length is the primary variable governing the viscoelastic behavior of these polymers.

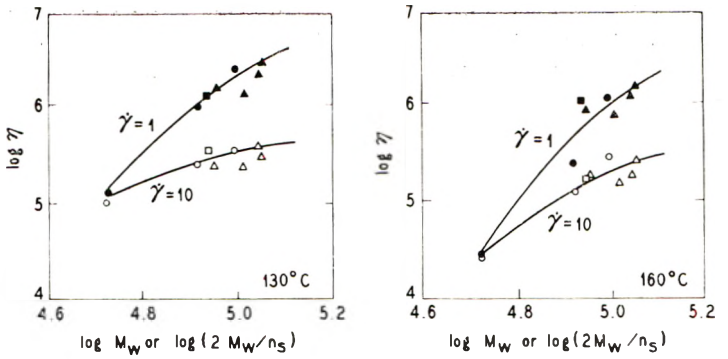

Fig. 7. Steady flow viscosity of polymers terminating in styrene blocks compared at equal styrene block length: (○,●) linear polymers; (△,▲) trichain: (□,■) tetrachain.

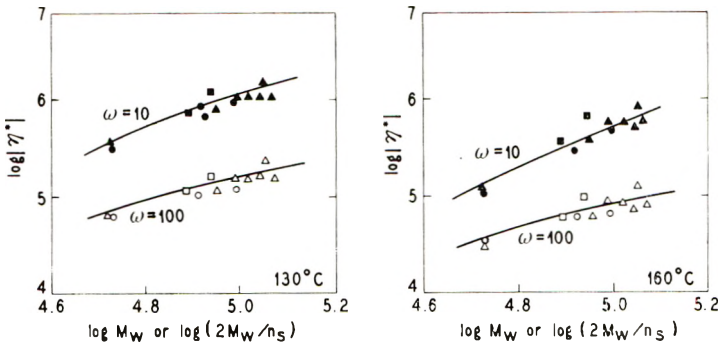

Fig. 8. Dynamic viscosity of polymers terminating in styrene blocks compared at equal styrene block length: (○,●) linear polymers; (△,▲) trichain; (□,■) tetrachain.

The intrinsic effects of the branch points in the butadiene center block appear to be small and are not revealed clearly by the data.

The persistence of the domain structure in the melt is shown very clearly by the loss tangents of Figure 9. At 130°C, even short styrene blocks suffice to produce networks with relatively low loss, but not at 160°C. When the block length is large, tanδ is smaller at the higher temperature, but this does not indicate a higher storage modulus, for $G' = \omega|\eta^*|(1 + \tan^2\delta)^{-1/2}$ and $|\eta^*|$ dominates G'. Thus the network deteriorates with rising temperature at all block lengths, but does so more rapidly when the blocks are short. At 160°C, where the network becomes increasingly imperfect, the effect of the branch point becomes apparent in somewhat lower values of tanδ. For polymers terminating in butadiene blocks (Fig. 6), which cannot form networks, tanδ is much larger and $|\eta^*|$ is smaller, so that G' is very much smaller, as expected.

Steady Flow versus Dynamic Viscosity. Whereas in homopolymers and random copolymers $|\eta^*|$ and η usually have similar numerical values[18] when compared at $\omega = \dot{\gamma}$, in the polymers of the present study $|\eta^*|$ is always

greater than η. We attribute this, in part, to the disruption of the domain network structure which must occur in steady flow, but not necessarily in small amplitude oscillations. Table III shows that $|\eta^*|/\eta$ tends to be less for polymers terminating in butadiene blocks, for which disruption of the domain structure is not a prerequisite for steady flow.

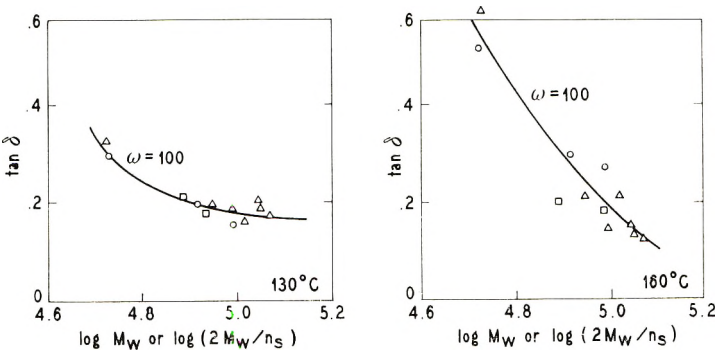

Fig. 9. Loss tangent of polymers terminating in styrene blocks compared at equal styrene block length: (○) linear polymers; (△) trichain; (□) tetrachain.

Block Polymers of Higher Styrene Content. Several polymers containing 40% styrene by weight were prepared and examined in the manner described above. The effects of branching on their viscoelastic behavior were in all respects similar to those found in the 30% styrene series.

Viscoelastic Behavior Below T_g^s

In polymers with terminal styrene blocks of equal length the effect of branching below T_g^s should be primarily a reduction in the effective polybutadiene network chain length. This should lead to an increase in G' and a decrease in tanδ. However, on comparison of polymers I, J, and P between 25 and 100°C, it was found that results depended strongly on the morphology of the domain structure, which dominated the effects of branching. One of the manifestations of morphology was the observation of tensile storage moduli, which exceeded the corresponding shear moduli by a factor larger than 3. This was even more pronounced in block polymers containing 40% styrene, where $E'/3G'$ ratios as high as 12 were observed at 25°C. The ratio dropped rapidly in passing through T_g^s. These observations pertain to molded polymer films; when films were cast from solution in toluene, a good solvent for both blocks, the ratio $E'/3G'$ was more nearly equal to unity. Branching had no discernible effect on this behavior. It is believed that the disparity between E' and $3G'$ arises from the formation of interconnected polystyrene domains leading to network-like structures of glassy polystyrene throughout the rubbery matrix. Details of this phase of the work will be described elsewhere.

CONCLUSION

The melt rheology of linear and star-branched block polymers of butadiene and styrene follows laws which are entirely different from those applying to homopolymers or random copolymers. The effects of branching are minor when the polymers are compared at equal lengths of the terminal block sequences.

References

1. G. Kraus and J. T. Gruver, *J. Polym. Sci. A*, **3**, 105 (1965).
2. F. Bueche, *J. Chem. Phys.*, **40**, 484 (1964).
3. V. L. Folt, *Rubber Chem. Technol.*, **42**, 1294 (1969).
4. B. L. Johnson, H. E. Adams, F. C. Weissert, and K. Farhat, *Proc. Internat. Rubber Conf.*, McLaren, London, 1968, pp. 29–43.
5. R. Suzuki and A. J. Kovacs, paper presented at 4th IUPAC Microsymposium on Macromolecules, Prague, September 1969.
6. V. C. Long, G. C. Berry, and L. M. Hobbs, *Polymer*, **5**, 517 (1964).
7. G. Kraus and J. T. Gruver, *Advances in Polymer Science and Technology, (Soc. Chem. Ind. Monograph No. 26)*, Soc. Chem. Ind., London, 1967, p. 30.
8. R. P. Chartoff and B. Maxwell, *J. Polym. Sci. A-2*, **8**, 455 (1970).
9. R. A. Mendelson, W. A. Bowles, and F. L. Finger, *J Polym. Sci. A-2*, **8**, 105 (1970).
10. G. Kraus and J. T. Gruver, *J. Appl. Polym. Sci.*, **11**, 2121 (1967).
11. K. R. Arnold and D. J. Meier, *J. Appl. Polym. Sci.*, **14**, 427 (1970).
12. U. Bianchi, E. Pedemonte, and A. Turturro, *Polymer*. **11**, 268 (1970).
13. R. P. Zelinski and C. F. Wofford, *J. Polym. Sci. A*, **3**, 93 (1965).
14. W. Philippoff and F. H. Gaskins, *Trans. Soc. Rheol.*, **2**, 263 (1958).
15. P. F. Erhardt, J. J. O'Malley, R. G. Crystal, paper presented at New York American Chemical Society Meeting, September 1969; *Polym. Preprints*, **10**, No. 2, 812 (1969).
16. R. H. Valentine, J. D. Ferry, T. Homma, and K. Ninomiya, *J. Polym. Sci. A-2*, **6**, 479 (1968).
17. R. H. Valentine, PhD Thesis, University of Wisconsin, 1967.
18. F. Bueche, *Physical Properties of Polymers*, Interscience, New York, 1962, pp. 218–222.

Received March 10, 1971

JOURNAL OF POLYMER SCIENCE: PART A-2 VOL. 9, 1851–1869 (1971)

NMR Observations of Drawn Polymers. VIII. Doubly Oriented Nylon 66*

HEINZ G. OLF, *Camille Dreyfus Laboratory, Research Triangle Institute, Research Triangle Park, North Carolina 27709*

Synopsis

A wide-line NMR study of chain segmental motion in nylon 66 has been made on a rolled sheet having "double orientation." In this sheet the crystallite c axis, i.e., the molecular chain axis, is oriented preferentially along the roll direction, and the crystallographic (010) plane lies predominantly parallel to the roll plane, or the plane of the sheet. The direction of the applied magnetic field with respect to the sheet is characterized by two angles, the polar angle γ subtended by the roll direction and the magnetic field, and an azimuthal angle ϕ. NMR spectra were taken at various values of the angles γ and ϕ and at three temperatures -196°C, 20°C, and 180°C. The second moments of the absorption spectra taken at 180°C were compared with theoretical predictions of second moments based on two models for the high-temperature segmental motion (called the α_c process) in crystalline regions of nylon 66. One model consists of rotational oscillation with amplitude δ of segments around their axes. The second model is denoted 60° flip-flop motion and consists of rotational 60° jumps of the segments around their axes between two equilibrium sites with the possibility that the segments also oscillate with a general amplitude δ around each site. The experimental results are consistent with fairly large amplitudes δ, in which case both models approach the limiting case of full segment rotation. For this reason the experiments do not allow a distinction between the two models. From the second moments at -196°C and 20°C the decrease in second moment due to the low temperature segmental motion, the γ process, is obtained. This motion occurs in noncrystalline regions of nylon 66 and is found to cause a decrease in second moment which is strongly dependent on the two angles γ and ϕ, implying double orientation of the noncrystalline segments. It is suggested that at low temperatures the noncrystalline segments become immobilized in sites dictated by the crystallite orientation through the extensive hydrogen bonding known to exist in nylon 66.

INTRODUCTION

The usefulness of wide-line nuclear magnetic resonance (NMR) in studies of structural aspects and of molecular motion in nonpolymeric crystalline solids depends on the availability of large single crystals of these materials.[1] Crystalline polymers cannot as a rule be obtained as single crystals large enough for NMR work, and this results in a loss of information. As a remedy, a single crystal can be approximated by using samples, e.g. fibers, having a preferred orientation (texture). Semicrystalline polymers are readily

* Presented in part at the Meeting of the American Physical Society, Dallas, Texas, March 1970.

obtained as fibers in which the macromolecular chain is preferentially aligned parallel to the fiber axis, with rotational symmetry around the fiber axis. Several studies have already been made of the dependence of the NMR absorption on the alignment angle of the fiber axis with respect to the applied magnetic field.[2-21] In this way more detailed information can be obtained on the often highly anisotropic chain segmental motions than would be available with unoriented samples.

Here we report NMR results on a rolled nylon 66 sheet having a texture hereafter referred to as "double orientation." As will be described in greater detail below, this texture is characterized by a preferential alignment of the molecular axes along a certain direction, as in a fiber, but in addition a crystallographic plane [in nylon 66 the (010) plane] is predominantly parallel to the plane of the sheet. This texture represents a closer approach to a single crystal than does a fiber, and work on the doubly oriented film was undertaken with the hope that it might be possible to distinguish between different molecular mechanisms proposed for the high-temperature segmental motion, which has been called the α_c process,[22] in crystalline regions of nylon 66. Such a distinction was not possible in a previous NMR study involving fibers.[22]

Specifically, two models of segmental motion for the high-temperature α_c motional process will be examined by using the second moment of the NMR absorption. The models are (1) rotational oscillation around the chain axis and (2) a motion called 60° flip-flop. The latter is similar to a motion proposed by Brill[23,24] and by Schmidt and Stuart.[25] An individual crystalline segment of unspecified length is thought to perform rotational jumps of 60° around its chain axis between two equilibrium sites. One site is familiar from the room-temperature triclinic crystal structure determined by Bunn and Garner,[26] in which the molecules form the well-known two-dimensional network of hydrogen bonds. According to Schmidt and Stuart,[25] a second equilibrium site can be occupied at elevated temperatures, where the lattice becomes pseudohexagonal, and they suggest that the molecules then form a three-dimensional network of hydrogen bond.[25]

Both models, which have been discussed at length previously,[22] appear to be consistent with the available experimental evidence, notably with NMR results on nylon 66 fibers. Theoretical predictions of the NMR second moment, based on the two motional models, will be compared to experimental second-moment data on the doubly oriented sheet in an attempt to distinguish between these models. Some observations concerning the low-temperature segmental motion, or the γ process, will also be discussed.

Following Slichter's paper of 1955,[27] numerous accounts of wide-line NMR work on nylon 66 have appeared in the literature.[13,14,22,28-43]

THEORETICAL

The crystallite orientation in the doubly oriented nylon 66 sheet is assumed ideal, in other words all the crystallite c axes, or molecular axes, are assumed parallel to the roll direction and all the crystallographic (010)

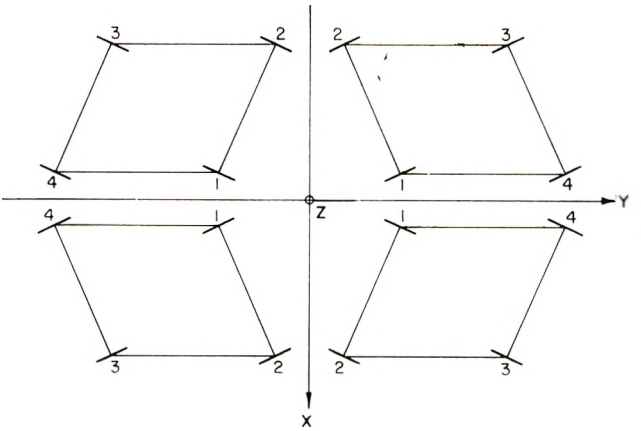

Fig. 1. Four positions of the nylon 66 unit cell consistent with ideal double orientation in a projection along the chain axis. The planes of the zigzag chains are indicated.

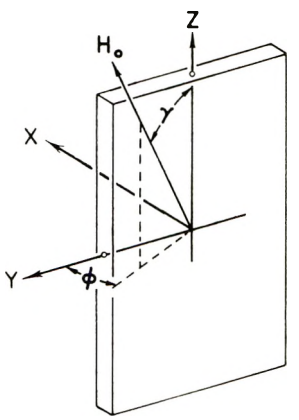

Fig. 2. Direction of the NMR magnetic field with respect to the system XYZ, fixed in the rolled sheet, is characterized by the angles γ and ϕ (see text).

planes, in which the molecules lie hydrogen-bonded to one another, are taken parallel to the roll plane. Keeping in mind that the unit cell of nylon 66 has a center of symmetry (space group $P\bar{1}$), one realizes that the unit cell can assume four different orientations which are consistent with the symmetry elements of the rolled sheet. These are indicated in Figure 1 along with a coordinate system XYZ which is fixed in the sheet. The Z axis is parallel to the molecular axis or the roll direction, and the YZ plane is parallel to the (010) plane or the roll plane.

The direction of the applied magnetic field with respect to the system XYZ can be specified by the angle γ subtended by the roll direction or Z axis and the magnetic field and the azimuth ϕ as indicated in Figure 2.

The general expression for the second moment,

$$S = KN^{-1} \sum_{j>k=1}^{N} \left\langle \frac{3\cos^2\theta_{jk} - 1}{r_{jk}^3} \right\rangle_t^2 \qquad (1)$$

which has been given by Van Vleck[44] and others[45–48] can be readily applied

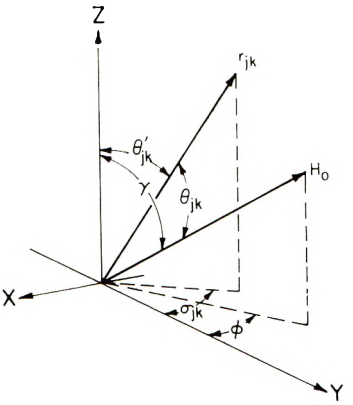

Fig. 3. Definition of some angles used in the text.

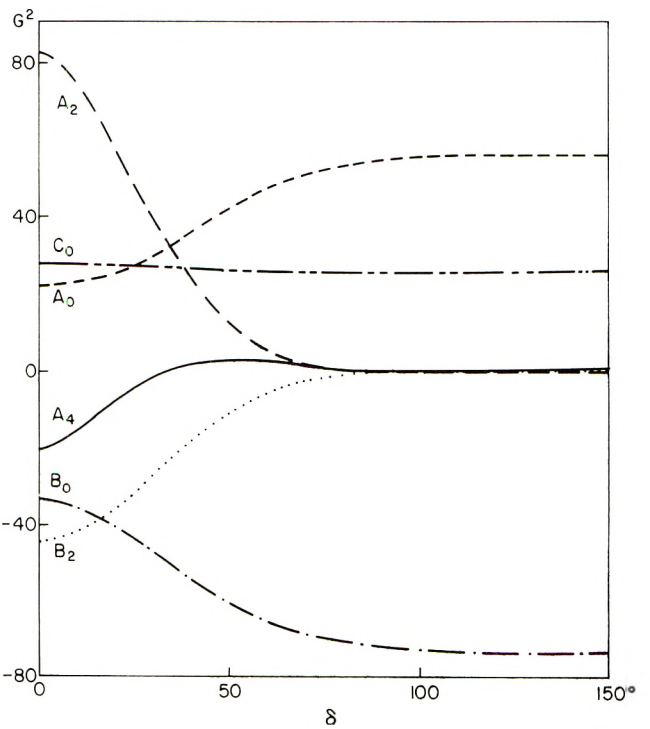

Fig. 4. Variation of the constants A, B, and C of eq. (2) with amplitude δ of rotational oscillation. (———) A_4, (– –) A_2; (- -) A_0; (· · ·) (B_2); (–·–) B_0; (— - - —) C_0.

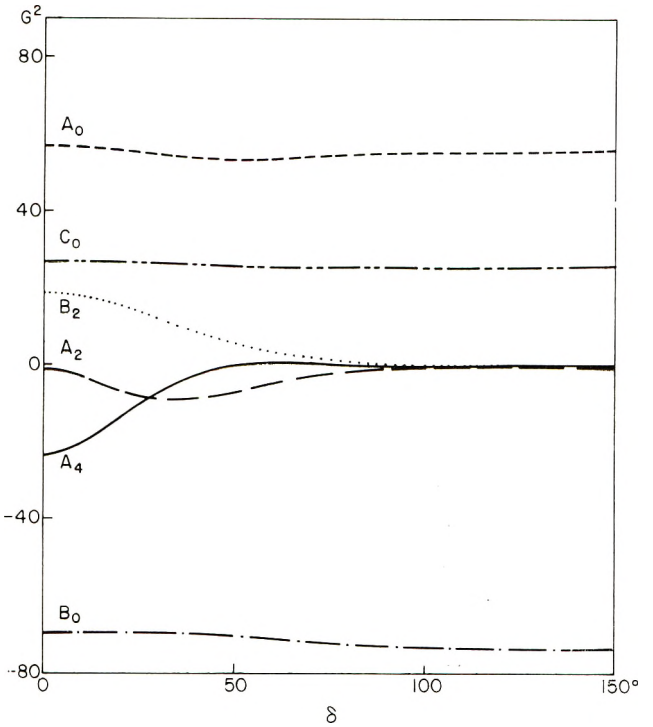

Fig. 5. Variation of the constants A, B, and C of eq. (2) with amplitude δ of oscillation in the case of 60°-flip-flop motion. Key as in Fig. 4.

to such a sheet. In eq. (1), K is a constant characteristic of the nuclear magnetic dipole–dipole interaction[44] and N is the number of nuclei taken into account. As is shown in Figure 3, $\mathbf{r}_{jk}$ is the vector connecting proton j with proton k, θ_{jk} is the angle between $\mathbf{r}_{jk}$ and the magnetic field $\mathbf{H}_0$, θ_{jk}' is the angle between the Z axis and $\mathbf{r}_{jk}$, and σ_{jk} is an azimuthal angle measured in the XY plane. Also indicated in Figure 3 are the angles γ and ϕ, which have already been defined (Fig. 2). Upon replacing θ_{jk} in eq. (1) by using the relation

$$\cos\theta_{jk} = \cos\theta_{jk}' \cos\gamma + \sin\theta_{jk}' \sin\gamma \cos(\sigma_{jk} - \phi)$$

and after some further manipulation, one arrives at the following expression for the second moment of a rolled nylon 66 film,

$$S(\gamma,\phi) = \sin^4\gamma(A_4 \sin^4\phi + A_2 \sin^2\phi + A_0) + \sin^2\gamma(B_2 \sin^2\phi + B_0) + C_0 \quad (2)$$

The parameters A, B, and C are independent of γ and ϕ. They can be calculated on the basis of the known structure of nylon 66 for different molecular motions according to expressions given in the appendix.

These results will now be used to predict theoretically the second moment $S(\gamma,\phi)$ in the presence of either of the two motions, rotational oscillation or

60°-flip-flop motion. The nylon 66 chain molecules are assumed to perform these motions as rigid rods, that is, we neglect chain torsion. For the present purposes this simplification is not serious, as will be seen later. The rotational oscillation is assumed to occur around the chain axis with amplitude δ. The 60° flip-flop motion consists essentially of 60° rotational jumps of chain segments around their axis between two equilibrium sites. To be realistic we further admit oscillation of amplitude δ about each equilibrium site. This brief description may suffice here, as a more detailed account has been given in Part VII.[22] The variation of the six constants A_0, A_2, A_4, B_0, B_2, and C_0 with the motional amplitude δ is given in Figures 4 and 5 for rotational oscillation and 60°-flip-flop motion, respectively. These parameters determine, in conjunction with eq. (2), the angle-dependent second moment $S(\gamma,\phi)$ of the rolled nylon 66 sheet.

It should be noted that although eq. (2) has been derived for ideal double orientation, it will be valid in the same form when a more general crystallite orientation exists, such as in the rolled nylon 66 sheet used in this work. In this case, however, the parameters A, B, and C are no longer defined by the simple expressions given in the appendix but are also dependent on orientation parameters.

By averaging the second moment of a doubly oriented sheet, eq. (2) over the azimuthal angle ϕ, one obtains the second moment in the case of fiber symmetry,

$$S(\gamma) = \sin^4\gamma[(3/8)A_4 + (1/2)A_2 + A_0] + \sin^2\gamma[(1/2)B_2 + B_0] + C_0 \quad (3)$$

where γ is now the alignment angle between fiber axis and magnetic field. Finally, the average of eq. (3) over γ yields the second moment of an unoriented, isotropic sample, sometimes called the powder-average second moment,

$$S = (1/15)(3A_4 + 4A_2 + 8A_0) + (1/3)(B_2 + 2B_0) + C_0 \quad (4)$$

EXPERIMENTAL

Sample

The rolled sheet of nylon 66 was kindly supplied by Dr. H. W. Starkweather, Jr., of E. I. du Pont de Nemours & Company, Inc. The x-ray photographs taken with the incident beam parallel to the roll direction showed very good double orientation both at room temperature and at 180°C. The x-ray intensity maximum at small angles indicates the presence of a long period of 82 Å along the roll direction.

The density of the sheet as determined by the flotation method in a mixture of toluene and tetrachloroethylene was 1.139 g/cm^3. This corresponds to a crystalline mass fraction α_m of 0.50, on the basis of the density values of Starkweather and Moynihan[49] for crystalline and noncrystalline nylon 66.

NMR Measurements

The proton NMR absorption was measured with a Varian DP-60 spectrometer. Calibration and evaluation procedures and steps taken to prevent saturation effects have been described elsewhere.[11,50] The application of wide-line NMR to polymeric solids has been discussed, for example, in the review article by Powles.[51]

Prior to the measurements the samples were dried in a vacuum ($<10^{-4}$ torr) at 100°C.

The manner in which the two angles γ (alignment angle between roll direction and magnetic field) and ϕ (azimuthal angle) were varied is described below. First, rectangular specimens were cut from the rolled sheet with definite angles ζ between the roll direction and the long axis of the rectangle which will be called the sample axis (Fig. 6). Several of these pieces were

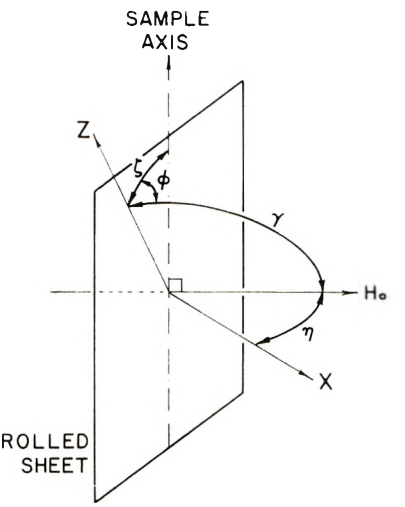

Fig. 6. Relation between the experimentally given angles ζ, η, and the angles γ, ϕ, defined in Fig. 2. The sample axis and the Z axis lie in the plane of the rolled sheet; the X axis is normal to the sheet.

inserted into an opening cut in a Teflon-rod sample holder so that the sample axis was directed parallel to the rod axis. By turning the rod around its axis the angles γ and ϕ are varied over a certain range which depends on ζ. The situation is illustrated in Figure 6 where the magnetic field is directed horizontally and the sample axis vertically. In addition to the angles γ, ϕ, and ζ which have already been defined, the angle η subtended by the X axis (the normal to the rolled sheet) and the magnetic field is shown: η measures the rotation of the sheet around the sample axis. The desired angles γ and ϕ are related to the experimentally given angles ζ and η through the equations

$$\cos\gamma = \sin\zeta \sin\eta \tag{5}$$

$$\cos\phi = \cos\zeta \sin\eta(1 - \sin^2\zeta\sin^2\eta)^{-1/2} \tag{6}$$

RESULTS

NMR spectra were obtained at three temperatures, −196°C, 20°C, and 180°C, and at various values of the angles γ and ϕ. The angle settings at which spectra were taken are indicated by the points in Figure 7. The points along a curve with constant ζ were covered with one sample, and hence nine samples were required to obtain measurements at the nine different values of ζ in the range from 0° to 90°. It is apparent from Figure 7 that the measurements cover the $\gamma\phi$ plane fairly evenly.

The second moments determined from the spectra are shown in Figure 8 as functions of the angle η at the nine different values for ζ. The angular coordinates (ζ,η) were converted to (γ,ϕ), by using eqs. (5) and (6), and thus the experimental second moments were given as functions of γ and ϕ. By a least-squares procedure the theoretical eq. (2) was fitted to the 82 second moments measured at each temperature, to yield the values for the parameters A, B, and C given in Table I. The curves shown in Figure 8 have been calculated by using these values, and the overall fit of the curves to the experimental points is seen to be quite good.

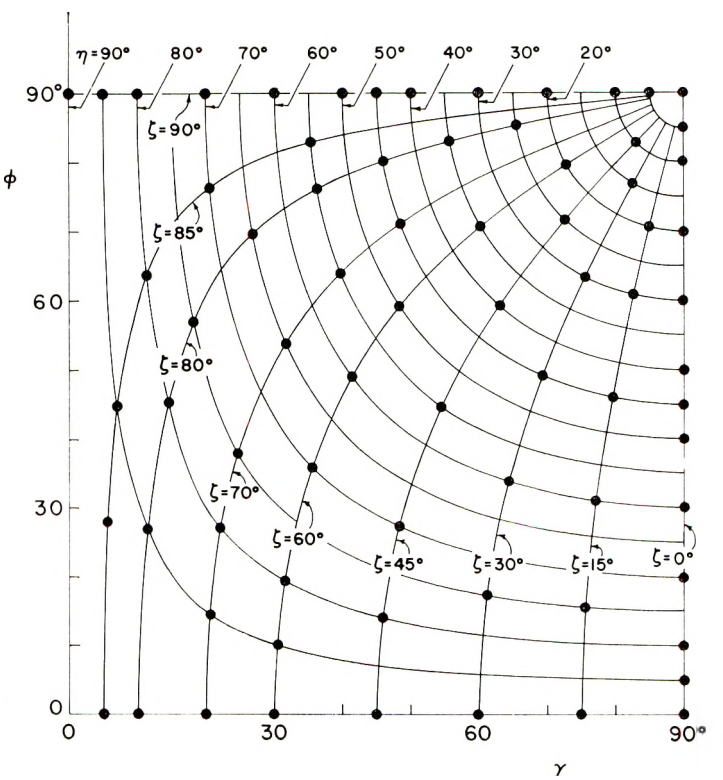

Fig. 7. Measurements of the NMR second moment were made at the values of γ and ϕ indicated by the points in the $\gamma\phi$ plane.

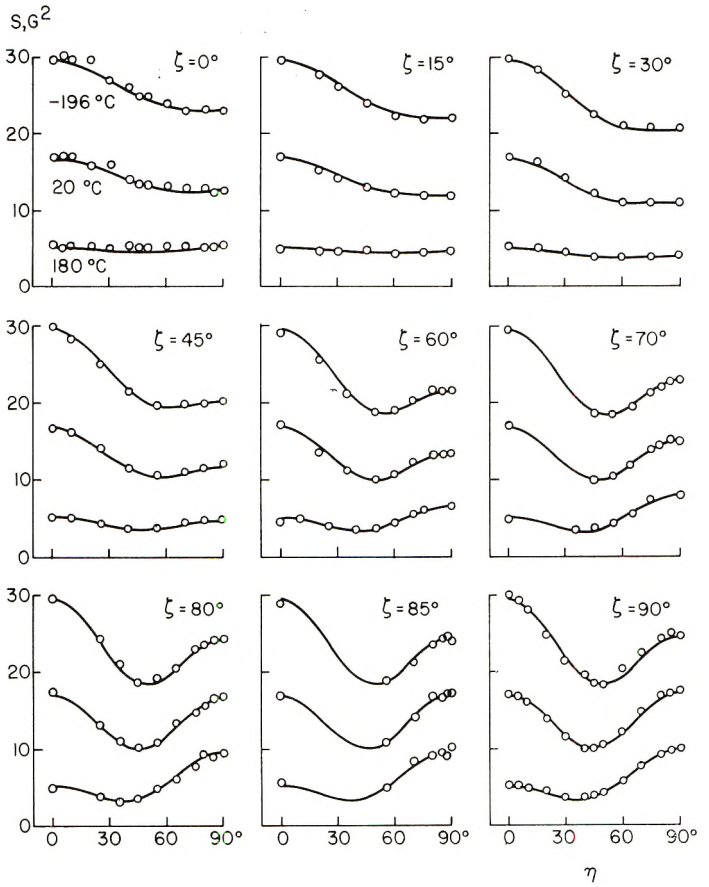

Fig. 8. Second moment measured as a function of the experimentally given angles ζ and η at -196°C (upper curves), 20° (central curves), and 180°C (lower curves).

A comment on the choice of temperatures ($-196°$, 20°, and 180°C) is in order. It is well known that a narrowing of the NMR spectrum and a concomitant decrease in second moment take place when a molecular motion attains frequencies on the order of 10^4–10^5 Hz. Second-moment analysis, as it now stands, can deal with two extreme cases. One is the low frequency limit or rigid lattice case, where motional frequencies fall below 10^4 Hz; in this case the time average over the motion, indicated in eq. (1), must not be performed. The other extreme case is the limit of fast motion, where the frequencies are greater than 10^5 Hz; here, the time average in eq. (1) must be taken. At motional frequencies in or near the range 10^4 to 10^5 Hz, however, the second moment is of doubtful significance.

Experimentally the frequency of a motional process is often varied by changing the temperature, as has been done in this work. It is important that the temperatures be chosen so as to correspond to frequencies in the two extremes mentioned above, lest second-moment analysis become illusory.

From previous work on the entire temperature dependence of second moment in nylon 66 it is inferred that the temperatures chosen here satisfy this condition.[22] The leveling out of the second moment to a plateau at

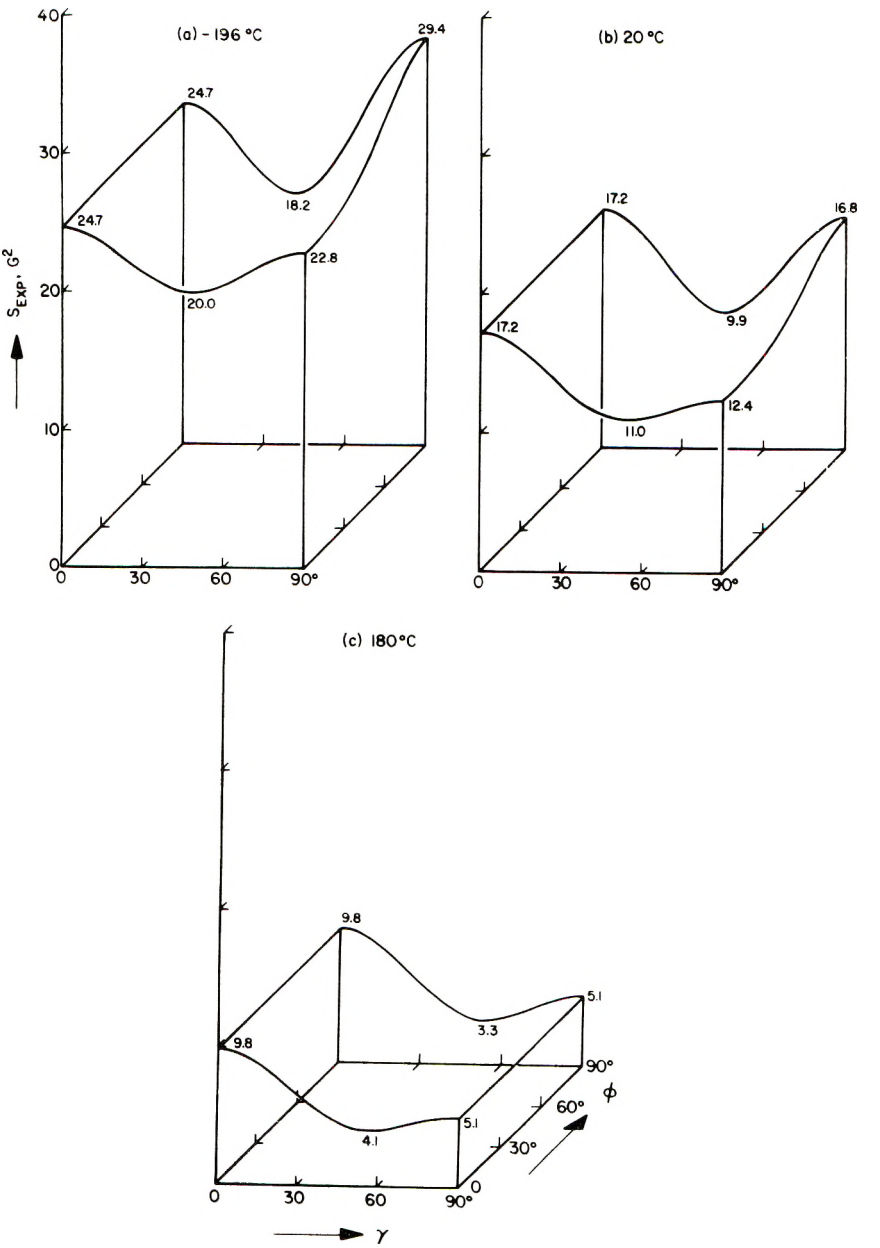

Fig. 9. Experimental (total) second moments as a function of the angles γ and ϕ in three-dimensional representation. The curves shown were obtained according to eq. (2) with the least-squares estimates of the constants A, B, and C given in Table 1: (*a*) −196°C; (*b*) 20°C; (*c*) 180°C.

TABLE I
Least-Squares Estimates of the Constants in Equation (2)

	−196°C	20°C	180°C
A_4	5.2	4.2	1.2
A_2	14.6	10.7	2.6
A_0	14.7	13.5	11.4
B_2	−13.2	−10.5	−3.8
B_0	−16.6	−18.3	−16.1
C_0	24.7	17.2	9.8
Powder-average second moment[a]	22.0	12.4	4.8
Standard deviation[b]	0.40	0.30	0.20

[a] Calculated from the above constants and eq. (4).

[b] Calculated according to $\sqrt{\Sigma\epsilon^2/(n-6)}$, where ϵ is the deviation of the measured second moments from the least-squares fit of eq. (2) and n is the number of measurements (82).

about −196°C is indicative of the rigid lattice condition, especially since the experimental second moment agrees well with the theoretical rigid-lattice second moment.[22] Toward higher temperatures, the second moment initially decreases owing to the γ process, until another plateau is reached at 20°C; this shows that the low-temperature γ process is fully activated and that the high temperature motions, the α_a and the α_c processes, have not yet begun.[22] The two latter motions cause a second-moment decrease which commences at about 100°C and terminates in a plateau at temperatures around 180°C, indicating full excitation of all motional processes.[22]

Comparison of the experimental second-moment data with theoretical predictions for different motional models will be made by using three-dimensional representations of the second moment $S(\gamma,\phi)$ as a function of the angles γ and ϕ. The experimental results appear in Figs. 9*a* to 9*c*, where the data points have been left out for the sake of clarity. The surface $S(\gamma,\phi)$ is represented in these figures by the curves of intersection with

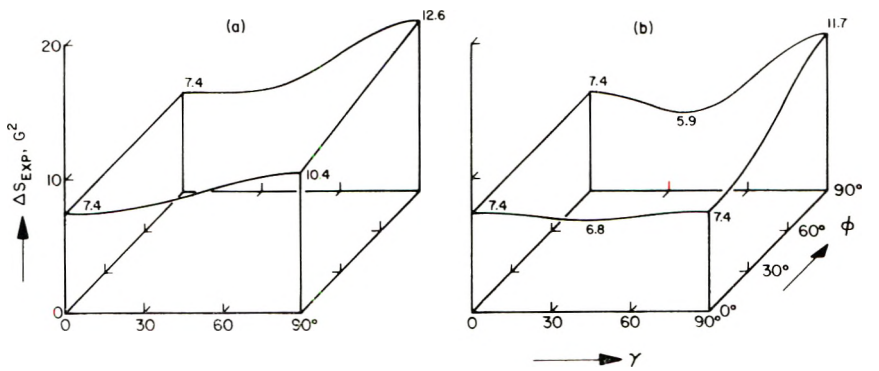

Fig. 10. Experimental decrease of the second moment: (*a*) between −196°C and 20°C and (*b*) between 20°C and 180°C.

the four planes $\gamma = 0°$, $\gamma = 90°$, $\phi = 0°$, and $\phi = 90°$. Also shown is the experimental decrease of the second moment between $-196°C$ and $20°C$ in Figure 10*a*, and between $20°C$ and $180°C$ in Figure 10*b*.

DISCUSSION

Theoretical predictions for 60° flip-flop motion are shown in Figures 11*a* to 11*c*, where the cases $\delta = 0°$, $\delta = 20°$, and $\delta = 47°$ have been chosen. The latter value is an estimate obtained in Part VII.[22] Predictions for rotational oscillation appear in Figures 12*a* to 12*c* with $\delta = 20°$, $\delta = 59°$,[22] and $\delta = \infty$ which corresponds to full rotation.

At $-196°C$, NMR-active motions are thought to be frozen out, so the second moments measured at that temperature (Fig. 9a) can be compared to the theoretical rigid-lattice second moments in Fig. 13. The qualitative features of the second-moment surfaces in Figures 9*a* and 13 are rather similar. However, in the experimentally determined surface the peaks are not as high and the valleys not as low as in the theoretical surface; this is a consequence of the ideal orientation assumed in the calculations, while the distribution of crystallite orientations and the existence of noncrystalline regions in the samples cause a certain averaging out of these features.

Next, we consider the decrease of the experimental second moment which occurs between $-196°C$ and $20°C$ (Fig. 10*a*). It has been shown recently that this decrease is due to thermally activated segmental motion, commonly referred to as the γ process,[22] in noncrystalline regions. As is readily apparent from Figure 10*a*, this decrease in second moment depends on both γ and ϕ. The dependence on γ is not surprising since a similar effect has been observed in fibers of nylon 66.[22] If the decrease in second moment of the doubly oriented sheet is averaged over the angle ϕ by making use of eq. (3) one obtains in fact a dependence on γ which is nearly identical to that found in fibers. This dependence is due partly to a preferential orientation of noncrystalline segments along the fiber axis[22] or, in the present case, along the roll direction. Secondly, it is due to the anisotropic nature of the segmental motion involved in the γ process, which probably consists of rotational modes around the segment axes.[22] The dependence of the decrease in second moment on ϕ (Fig. 10*a*) is a new observation and indicates that even noncrystalline segments are doubly oriented.

The following explanation is offered for this observation. When the noncrystalline segments become immobile at low temperatures it is assumed that they come to rest in positions dictated by hydrogen bonds. Since hydrogen bonding in nylon 66 is known to be extensive even in noncrystalline regions, it is conceivable that the double orientation of the crystallites is communicated to some extent to the noncrystalline segments via the hydrogen bonds. Conversely, when these doubly oriented noncrystalline segments are mobilized and undergo rotation at temperatures with fully activated γ process, the greatest decrease in second moment is expected to occur when both γ and ϕ are equal to 90°; this is evident when the theoretical

predictions of second moment for a doubly oriented rigid lattice in Figure 13 are compared with those for the case of full rotation in Figure 12*c*. This, of course, is the condition actually observed in Figure 10*a*.

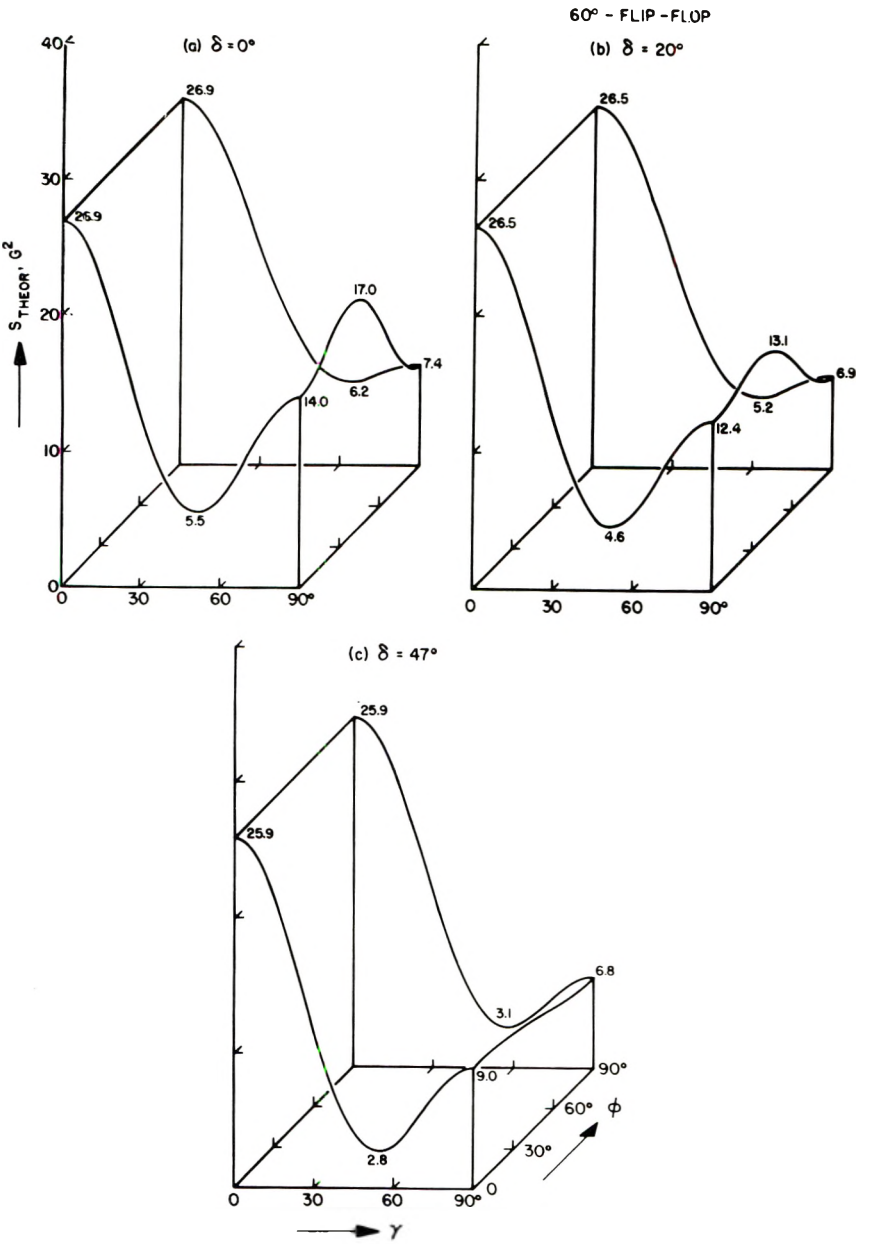

Fig. 11. Theoretical predictions of the NMR second moment of nylon 66 having ideal double orientation: the case of 60° flip-flop motion in the high-temperature pseudo-hexagonal lattice with (*a*) $\delta = 0°$; (*b*) $\delta = 20°$; (*c*) $\delta = 47°$.

The suspicion might arise that thermal lattice expansion, which undoubtedly is highly anisitropic in nylon 66, could account for these observations and therefore invalidate the above conclusions. Such suspicion is

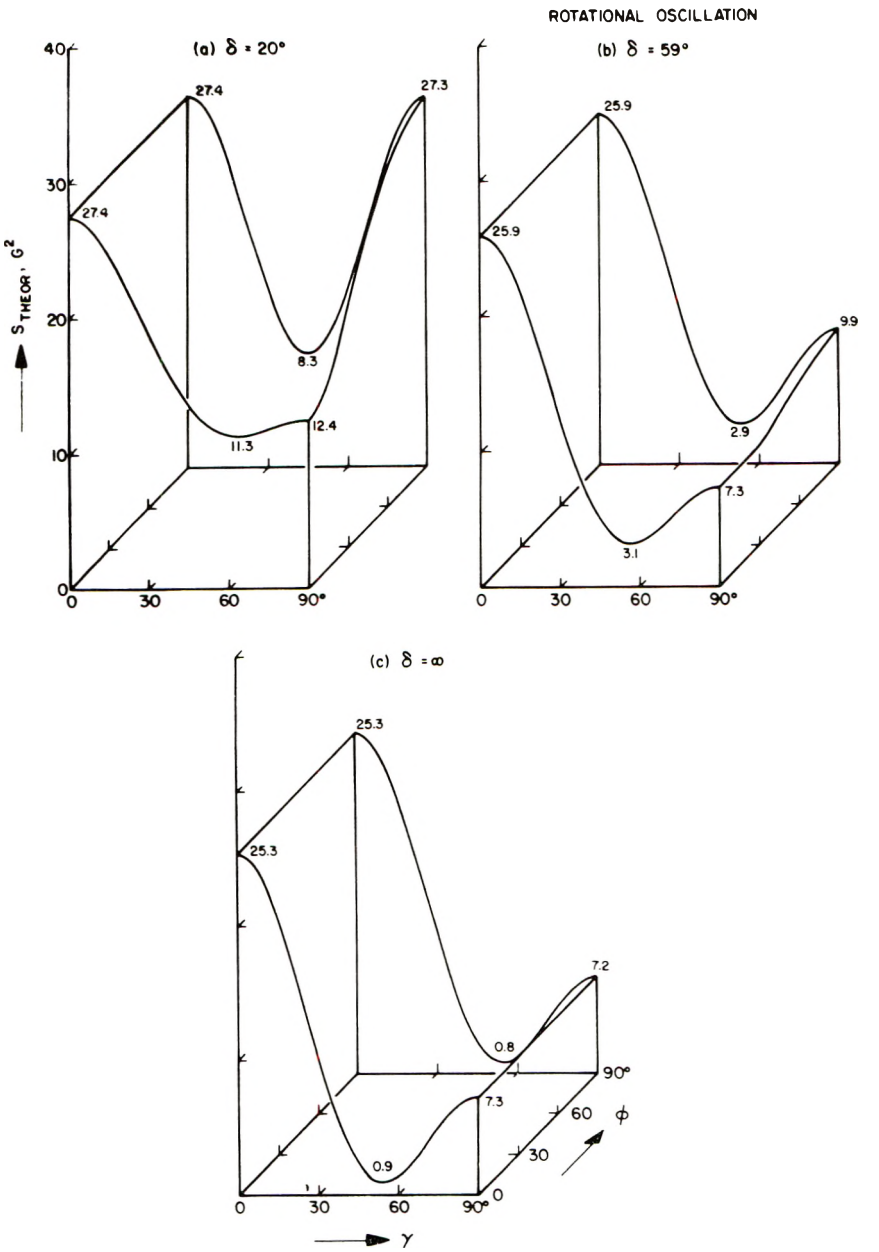

Fig. 12. Nylon 66 with ideal double orientation: theoretical predictions of the NMR second moment in the presence of rotational oscillation in the high-temperature pseudo-hexagonal lattice: (*a*) $\delta = 20°$; (*b*) $\delta = 59°$; (*c*) $\delta = \infty$ (full rotation).

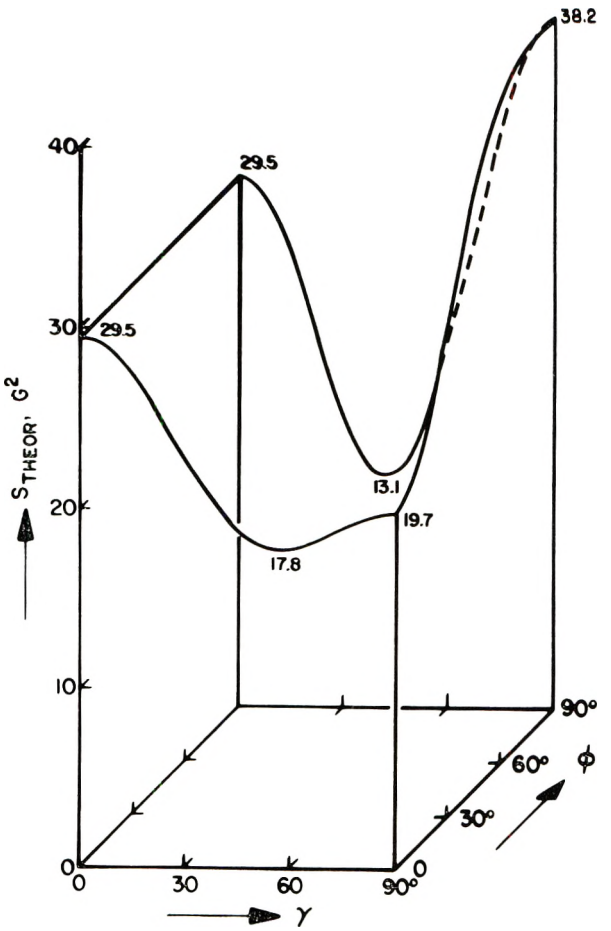

Fig. 13. Nylon 66 with ideal double orientation: theoretical NMR second moment for the low-temperature triclinic rigid lattice.

unfounded, as is shown by Figure 14, where the second-moment decrease due to expansion from a rigid low-temperature triclinic lattice to a rigid high-temperature pseudohexagonal one is plotted versus γ and ϕ. It is apparent that the resulting dependence on ϕ at $\gamma = 90°$ is in fact slightly reversed from the experimentally observed dependence.

In the temperature range between 20°C and 180°C two motional processes are activated; the α_a process, which consists of micro-Brownian motion in noncrystalline regions, and the α_c process, which corresponds to segmental motion in crystalline regions. Both motions contribute to the decrease in second moment shown in Figure 10*b*. For a quantitative discussion of the α_c process this overall decrease of second moment is therefore not suitable. The second moment data at 180°C, however, are more readily interpreted in terms of motion in crystalline regions. As in Part III,[22] we recognize the fact that because of the micro-Brownian motion the second-

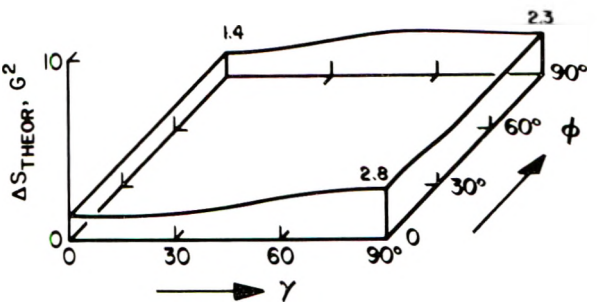

Fig. 14. Nylon 66 with ideal double orientation: theoretical decrease of the NMR second moment due to expansion from a low-temperature triclinic lattice to a high-temperature pseudohexagonal lattice.

moment contribution from noncrystalline regions must be both small and nearly independent of the angles γ and ϕ at 180°C. The angle dependence observed at that temperature (Fig. 9*c*) should therefore be characteristic of the crystalline regions and will now be discussed with respect to segmental motions present there.

As a starting point let us consider the following two motions both of which were recently found to be in agreement with NMR data on nylon 66 fibers: rotational oscillation of amplitude $\delta = 59^\circ \pm^{40^\circ}_{15^\circ}$, and 60° flip-flop motion with oscillation amplitude $\delta = 47^\circ \pm^{40^\circ}_{15^\circ}$. In the case of fiber symmetry these motions with amplitudes 59° and 47°, respectively, gave rise to nearly identical dependences of second moment on the alignment angle γ and were therefore indistinguishable.[22] With a doubly oriented sheet, however, these motions do result in different predictions of the second moment as a function of the angles γ and ϕ, as shown in Figures 12*b* and 11*c*. The main difference lies in the dependence of the second moment on ϕ where $\gamma = 90°$. Explicitly, rotational oscillation implies that

$$S(\gamma = 90°, \phi = 0°) = 7.3 \text{ G}^2$$

and

$$S(\gamma = 90°, \phi = 90°) = 9.9 \text{ G}^2$$

while 60° flip-flop with $\delta = 47°$ implies the opposite dependence, namely

$$S(\gamma = 90°, \phi = 0°) = 9.0 \text{ G}^2$$

and

$$S(\gamma = 90°, \phi = 90°) = 6.8 \text{ G}^2$$

This theoretically predicted difference between the two motions raised the hope that a distinction could be made experimentally and motivated the present study. Comparing the experimental results obtained at 180°C (Fig. 9*c*) with these predictions (Figs. 11*c* and 12*b*), one realizes that the dependence of second moment on ϕ, found experimentally when $\gamma = 90°$, is

negligibly small and intermediate between the predictions for the two motions considered, thus agreeing with neither.

The lack of dependence on ϕ in the experimental data is possibly due to the nonideal double orientation of the sample which leads, of course, to a certain averaging out of the angle dependence of the second moment. On the other hand, the experimentally observed anisotropy in second moment at 180°C (Fig. 9*c*) is generally consistent with full rotation of the crystalline chain segments around their axes, the case treated in Figure 12*c*. It is suggested, therefore, that chain rotation accounts best for the observations. In actuality there will be large-amplitude oscillation rather than full chain rotation, of course. Figures 4 and 5 show that the parameters A, B, and C which determine the second moment practically approach the values characteristic of chain rotation at oscillation amplitudes close to 100°. This is in fact consistent with the earlier estimate[22] of $\delta \approx 59^\circ {}^{+40^\circ}_{-15^\circ}$.

Left out of this discussion entirely is chain torsion, although it is known to be involved in the motion in crystalline regions at 180°C.[22] The effect of torsion, however, is mainly to decrease the second moment at $\gamma = 0°$; it scarcely affects the second moment at $\gamma = 90°$ where the features of interest are. For the present semiquantitative discussion chain torsion is, therefore, of no consequence.

CONCLUSIONS

The second moment data on doubly oriented nylon 66 reported here allow the following conclusions.

(1) The onset of segmental motion in noncrystalline regions at low temperature (γ process) causes a decrease of second moment which depends on both the alignment angle γ and the azimuthal angle ϕ. This implies that the noncrystalline chain segments are doubly oriented when they become immobile at low temperatures.

(2) The angle dependence of the second moment at 180°C is essentially given by the crystalline regions and should therefore be interpretable in terms of segmental motion in crystalline regions, i.e., the α_c process. The experimental angle dependence is well accounted for by full rotation. In practice this means fairly large oscillation amplitudes, close to 100° or greater. This estimate is consistent with one recently derived from measurements on nylon 66 fibers.[22]

APPENDIX

The quantities A, B, and C in eq. (2) can be expressed as follows:

$$A_4 = KN^{-1}\Sigma[(M_{2jk} - M_{3jk})^2 - M_{5jk}^2]$$

$$A_2 = KN^{-1}\Sigma[2(M_{1jk} - M_{2jk})(M_{2jk} - M_{3jk}) + (M_{4jk}^2 + M_{5jk}^2 - M_{6jk}^2)]$$

$$A_0 = KN^{-1}\Sigma[(M_{1jk} - M_{2jk})^2 - M_{4jk}^2]$$

$$B_2 = -KN^{-1}\Sigma[2(M_{2jk} - M_{3jk})(M_{1jk} - M_{7jk}) + (M_{4jk}^2 - M_{6jk}^2)]$$

$$B_0 = KN^{-1}\Sigma[-2(M_{1jk} - M_{2jk})\cdot(M_{1jk} - M_{7jk}) + M_{4jk}^2]$$

$$C_0 = KN^{-1}\Sigma(M_{1jk} - M_{7jk})^2$$

The summation signs stand for the double sum $\sum_{j>k=1}^{N}$ N is the number of protons taken into account; and K is a constant.[1,44] The definitions of the seven time averages occurring in these expressions are given below:

$$M_{1jk} = 3\left\langle \frac{\cos^2\theta_{jk}'}{r_{jk}^3} \right\rangle_t$$

$$M_{2jk} = 3\left\langle \frac{\sin^2\theta_{jk}'}{r_{jk}^3}\cos^2\sigma_{jk} \right\rangle_t$$

$$M_{3jk} = 3\left\langle \frac{\sin^2\theta_{jk}'}{r_{jk}^3}\sin^2\sigma_{jk} \right\rangle_t$$

$$M_{4jk} = 3\left\langle \frac{\sin 2\theta_{jk}'}{r_{jk}^3}\cos\sigma_{jk} \right\rangle_t$$

$$M_{5jk} = 3\left\langle \frac{\sin^2\theta_{jk}'}{r_{jk}^3}\sin 2\sigma_{jk} \right\rangle_t$$

$$M_{6jk} = 3\left\langle \frac{\sin 2\theta_{jk}'}{r_{jk}^3}\sin\sigma_{jk} \right\rangle_t$$

$$M_{7jk} = \left\langle \frac{1}{r_{jk}^3} \right\rangle_t$$

Financial support of this work by the Camille and Henry Dreyfus Foundation is gratefully acknowledged.

References

1. A. Abragam, *The Principles of Nuclear Magnetism*, Clarendon Press, Oxford 1961.
2. L. H. Meyer, Thesis, Univ. of Illinois, 1953.
3. W. P. Slichter, *J. Polym. Sci.*, **24**, 173 (1957).
4. D. W. McCall and W. P. Slichter, *J. Polym. Sci.*, **26**, 171 (1957).
5. D. Hyndman and G. F. Origlio, *J. Polym. Sci.*, **39**, 556 (1959).
6. D. Hyndman and G. F. Origlio, *J. Appl. Phys.*, **31**, 1849 (1960).
7. D. Hyndman and G. F. Origlio, *J. Polym. Sci.*, **46**, 259 (1960).
8. K. Yamagata and S. Hirota, *Rept. Progr. Polym. Phys. Japan*, **5**, 236 (1962).
9. A. Peterlin and H. G. Olf, *J. Polym. Sci. B*, **2**, 409 (1964) (Part I).
10. A. Peterlin and H. G. Olf, *J. Polym. Sci. B*, **2**, 769 (1964) (Part III).
11. H. G. Olf and A. Peterlin, *J. Appl. Phys.*, **35**, 3108 (1964) (Part IV).
12. A. I. Koltsov and M. W. Volkenstein, *Vysokomol. Socdin.*, **7**, 250 (1965).
13. H. G. Olf and A. Peterlin, *Structure of Drawn Polymers*, Technical Report AFML-TR-67-6 to the Air Force Materials Laboratory, 1966.
14. P. E. McMahon, *J. Polym. Sci. A-2*, **4**, 639 (1966).

15. J. B. Lando, H. G. Olf, and A. Peterlin, *J. Polym. Sci. A-1*, **4**, 941 (1966).
16. A. Peterlin and H. G. Olf, *J. Polym. Sci. A-2*, **4**, 587 (1966) (Part V).
17. H. G. Olf and A. Peterlin, *Makromol. Chem.*, **104**, 135 (1967) (Part VI).
18. V. J. McBrierty and I. M. Ward, *J. Physics D*, **1**, 1529 (1968).
19. H. G. Olf and A. Peterlin, *J. Polym. Sci. A-2*, **8**, 753 (1970).
20. H. G. Olf and A. Peterlin, *J. Polym. Sci. A-2*, **8**, 771 (1970).
21. H. G. Olf and A. Peterlin, *J. Polym. Sci. A-2*, **8**, 791 (1970).
22. H. G. Olf and A. Peterlin, *J. Polym. Sci. A-2*, **9**, 1449 (1971).
23. R. Brill, *J. Prakt. Chem.*, **161**, 49 (1943).
24. R. Brill, *Makromol. Chem.*, **28/29**, 294 (1956).
25. G. F. Schmidt and H. A. Stuart, *Z. Naturforsch.* **13a**, 222 (1958).
26. C. W. Bunn and E. V. Garner, *Proc. Roy. Soc.* (London), *A***189**, 39 (1947).
27. W. P. Slichter, *J. Appl. Phys.* **26**, 1099 (1955).
28. W. P. Slichter, *J. Polym. Sci.*, **35**, 77 (1959).
29. A. E. Woodward, R. E. Glick, J. A. Sauer, and R. P. Gupta, *J. Polym. Sci.*, **45**, 367 (1960).
30. R. E. Glick, R. P. Gupta, J. A. Sauer, and A. E. Woodward, *J. Polym. Sci.*, **42**, 271 (1960).
31. K. H. Illers and R. Kosfeld, *Makromol. Chem.*, **42**, 44 (1960).
32. D. J. Shaw and B. A. Dunnell, *Can. J. Chem.*, **39**, 1154 (1961).
33. D. W. Jones, *Polymer*, **2**, 203 (1961).
34. R. P. Gupta, *J. Phys. Chem.*, **65**, 1128 (1961).
35. D. W. Jones, *J. Polym. Sci.*, **59**, 271 (1962).
36. D. W. McCall and E. W. Anderson, *Polymer*, **4**, 93 (1963).
37. S. N. Zhurkov and E. A. Yegorov, *Dokl. Akad. Nauk SSSR*, **152**, 1155 (1963).
38. Y. Sekita and K. Kawasaki, *Repts. Progr. Polym. Phys. Japan*, **7**, 283 (1964).
39. R. E. Glick and R. C. Phillips, *J. Polym. Sci. A*, **3**, 1885 (1965).
40. P. E. McMahon, *J. Polym. Sci. B*, **4**, 75 (1966).
41. P. E. McMahon, *J. Polym. Sci. B*, **4**, 43 (1966).
42. P. E. McMahon, *J. Polym. Sci. A-2*, **4**, 501 (1966).
43. P. F. Dismore and W. O. Statton, in *Small Angle Scattering from Fibrous and Partially Ordered Systems* (*J. Polym. Sci. C*, **13**), R. H. Marchessault, Ed., Interscience, New York, 1966, p. 133.
44. J. H. Van Vleck, *Phys. Rev.*, **74**, 1168 (1948).
45. H. S. Gutowsky and G. E. Pake, *J. Chem. Phys.*, **18**, 162 (1950).
46. E. R. Andrew and R. A. Newing, *Proc. Phys. Soc.* (London), **72**, 959 (1958).
47. E. R. Andrew, A. Bradbury, and R. G. Eades, *Nature*, **182**, 1659 (1958).
48. E. R. Andrew and G. J. Jenks, *Proc. Phys. Soc.* (London), **80**, 663 (1962).
49. H. W. Starkweather and R. E. Moynihan, *J. Polym. Sci.*, **22**, 363 (1956).
50. H. G. Olf and A. Peterlin, *Kolloid-Z. Z. Polym.*, **215**, 97 (1967).
51. J. G. Powles, *Polymer*, **1**, 219 (1960).

Received January 11, 1971
Revised April 5, 1971

JOURNAL OF POLYMER SCIENCE: PART A-2 VOL. 9, 1871–1885 (1971)

Study of Compositional Distribution in a Styrene–Methyl Acrylate Copolymer by Means of Density-Gradient Centrifugation

A. NAKAZAWA* and J. J. HERMANS, *Chemistry Department, University of North Carolina, Chapel Hill, North Carolina 27514*

Synopsis

Several samples of a copolymer were examined by means of equilibrium centrifugation in a density gradient. The results for the samples without compositional distribution (homogeneous polymers) were used to determine the relation between the chemical composition and the distance from the center of rotation. For one of the homogeneous polymers a quantitative analysis of the schlieren curve was made in order to show the kind of accuracy that can be achieved. For the inhomogeneous polymer it was found that the schlieren curve could, in principle, be described quantitatively by the assumption that fluctuations in composition are independent of fluctuations in molecular weight, but on this basis the average square of the fluctuations in composition is more than four times smaller than the value derived from chromatographic data. A more satisfactory explanation of the experimental results is provided by assuming a linear correlation between average molecular weight and composition, but it is not claimed that this is necessarily the only model that explains the data.

Introduction

The determination of compositional distribution in polymers is a problem of long standing, and although progress has been made recently, few of the experimental techniques known can be considered as fully established. Light scattering[1–4] gives only limited information and has not been applied very frequently. Fractionation by precipitation and by dissolution is difficult and time-consuming. Most promising at present are the results of thin-layer chromatography, which was applied successfully by Inagaki and co-workers.[5–11]

A method that has been explored little is density-gradient centrifugation. This method is suggested immediately by the fact that each polymer species tends to move towards the position where its buoyant density is matched by the density of the solvent. Polymer molecules that differ in composition will therefore tend to collect at different positions in the density gradient. Qualitative studies of compositional distribution and of ste-

* Present address: Institute for Chemical Research, Kyoto University, Uji Kyoto-Fu, Japan.

reoregularity on the basis of density gradient centrifugation have indeed been carried out by several authors.[12-14] The only attempt to apply this method in a quantitative fashion seems to have been made by Ende and Hermans[15] in a study of a styrene–iodostyrene copolymer.

The present work is an additional quantitative study, which was made to establish both the utility and some of the limitations of the method. Our starting point is an approximation previously derived[16,17] for the contribution of the polymer to the refractive index in density-gradient centrifugation at equilibrium:

$$F(x) = (\lambda/\pi)^{1/2} \int_0^\infty dM \int_{-\infty}^\infty d\epsilon M^{1/2} f(M,\epsilon) \exp\{-\lambda M(x - \epsilon/b)^2\} \quad (1)$$

Here x is the distance from some arbitrary origin, where the density of the solvent is ρ^*, say. Equation (1) expresses the fact that polymer molecules with buoyant density $\rho^* + \epsilon$ will collect in a gaussian band around a point at distance ϵ/b from the origin chosen, b being the density gradient in the liquid. The quantity λ is given by

$$\lambda = \omega^2 r_0 b/2\rho^* RT$$

where ω is the rotational speed and r_0 the distance between the center of rotation and the origin $x = 0$. Finally, $f(M,\epsilon)dMd\epsilon$ is the weight of polymer that has a molecular weight between M and $(M + dM)$ and a buoyant density between $\rho^* + \epsilon$ and $\rho^* + \epsilon + d\epsilon$. In reality, $f(M,\epsilon)$ in eq. (1) should be multiplied by a function $s(\epsilon)$ which determines the contribution of the polymer to the refractive index.[16,17] However, when the fluctuations are small, we make no large error in treating $s(\epsilon)$ as a constant.

It is convenient to introduce new variables

$$\begin{aligned} P &= \lambda M \\ \epsilon/b &= w \end{aligned} \quad (2)$$

and to replace $f(M,\epsilon)$ by $f(P,w)$. In schlieren optics, the experimental quantity is

$$g(x) = -dF/dx \quad (3)$$

and it has been shown[16,17] that moments of the function $g(x)$ are related to moments of the distribution function $f(P,w)$. We quote here the theoretical results that will be used.

Averages $\langle\psi\rangle$ of a function $\psi(P,w)$ are defined by the equation

$$\langle\psi\rangle \int_0^\infty dP \int_{-\infty}^\infty dw f(P,w) = \int_0^\infty dP \int_{-\infty}^\infty dw \psi(P,w) f(P,w) \quad (4)$$

Moments S_n^+ and S_n^- of $g(x)$ are defined by

$$\begin{aligned} S_n^+ &= \int_0^\infty dx x^n g(x) \\ S_n^- &= \int_{-\infty}^0 dx (-x)^n g(x) \end{aligned} \quad (5)$$

If powers of w higher than the second are neglected, we have the relations:[15]

$$\pi^{1/2}S_n^+/A = \Gamma\left(\frac{n+2}{2}\right)\langle P^{(1-n)/2}\rangle + n\Gamma\left(\frac{n+1}{2}\right)\langle P^{(2-n)/2}w\rangle + (n-1)\Gamma\left(\frac{n+2}{2}\right)\langle P^{(3-n)/2}w^2\rangle \quad (6)$$

$$\pi^{1/2}S_n^-/A = -\Gamma\left(\frac{n+2}{2}\right)\langle P^{(1-n)/2}\rangle + n\Gamma\left(\frac{n+1}{2}\right)\langle P^{(2-n)/2}w\rangle - (n-1)\Gamma\left(\frac{n+2}{2}\right)\langle P^{(3-n)/2}w^2\rangle \quad (7)$$

Here Γ is the gamma function and

$$A = S_1^+ - S_1^- \quad (8)$$

A is proportional to the integral over $F(x)$ from $-\infty$ to $+\infty$ and is therefore proportional to the total amount of polymer present. It will be convenient to consider also

$$\begin{aligned} U_n &= (S_n^+ + S_n^-)/A \\ V_n &= (S_n^+ - S_n^-)/A \end{aligned} \quad (9)$$

We have, by definition, $V_1 = 1$. Note that in the previous papers,[15] where it was tacitly assumed that $F(x)$ was normalized, eqs. (6) and (7) were written for S_n rather than S_n/A.

It must be remembered that eq. (1) and all its consequences are valid only when theta conditions prevail. As a rule this will not be true for all polymer species simultaneously; it is therefore necessary to determine the ratios S_n/A for a number of initial polymer concentrations and to extrapolate the results to zero polymer content. This eliminates effects of nonideality.

Samples Used

A number of styrene–methyl acrylate copolymers were kindly put at our disposal by Prof. Inagaki, Kyoto University. They were prepared by Matsuda, Yamano, and Kamiyama at the Research Laboratory of Sekisui Chemical Co., Ltd. Details of the polymerization and some solution properties have been described by Matsuda et al.[5] The samples have been further characterized by Inagaki et al.[6] Some of their results are shown in Table I.

The samples SM25, SM40, SM50-1, and SM76-1 had negligible compositional distribution, the first three because the conversion was low, the last one because it was an azeotropic copolymer, i.e., it had been made under conditions in which the polymer composition does not vary with degree of conversion.

The compositional distribution in sample SM35H has been measured by means of thin-layer chromatography,[6] and the results have been given in

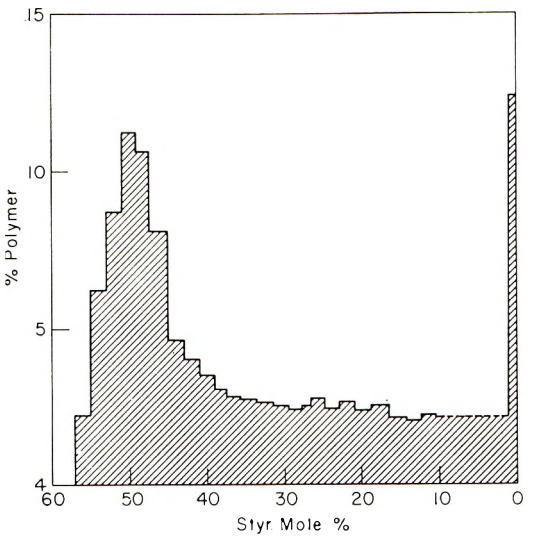

Fig. 1. Compositional distribution in sample SM35H as derived from thin-layer chromatography (from Fig. 7 of Inagaki et al.[6]). (Redrawn by permission of the copyright owner.)

tabular and graphical form (see Ingaki et al.[6]). The figure is shown here as our Figure 1, for later comparison. The peak at 0% styrene corresponds to about 11 wt-% of polymer that is almost pure PMA. The occurrence of this fraction in a copolymer is not unexpected when the degree of conversion is high.[7] From Table VII of Inagaki et al.[6] one calculates an average styrene mole fraction 0.36, in good agreement with the value (0.34) determined by elementary analysis. For reasons which will become clear later, we have also calculated from that table a measure for the variance (see below).

The number averages mentioned in Table I were determined by us by osmometry in a Hewlett-Packard high-speed osmometer.

TABLE I
Conversion in Polymerization, Styrene Content, and Viscosity-Average and Number-Average Molecular Weights of the Samples Used

Sample	Conversion, %	Styrene, mole %	$\bar{M}_v \times 10^{-4}$	$\bar{M}_n \times 10^{-4}$
PMA	20.0	0	80.0	—
SM25	6.1	25.8	14.5	—
SM40	2.2	42.5	17.0	—
SM50-1	3.5	52.7	14.5	—
SM76-1[a]	15.3	77.6	11.1	7.3[b]
SM35H	97.8	34.2	38.9	16.5

[a] Azeotropic copolymer.
[b] $\bar{M}_w = 13.4 \times 10^4$.

Technical

The search for a suitable theta solvent proved to be very time-consuming. After many trials, samples PMA, SM25, SM40, SM50, and SM35H were investigated at 26.5°C in a mixture of 30 vol-% methyl ethyl ketone (MEK), 13 vol-% 1,2-dibromo-1,1-difluoroethane, 29.4 vol-% isopropanol, and 27.6 vol-% dichlorooctafluorocyclohexene-1. It was established by osmometry that the second virial coefficient in this solvent mixture was zero at 26.45°C.

The densities and refractive indices of the solvents used are listed in Table II. MEK and dibromodifluoroethane are solvents for the polymer, while isopropanol and dichlorooctafluorocyclohexene are nonsolvents.

TABLE II
Densities ρ and Refractive Indices n of Solvents Used at 25°C

Solvent	ρ, g/cm^3	n
Methyl ethyl ketone	0.7995	1.3761
1,2-Dibromo-1,1-difluoroethane	2.2116	1.4457
Isopropanol	0.7810	1.3747
Dichlorooctafluorocyclohexene	1.719	1.367

Sample SM76-1 required a different solvent mixture, made by mixing 53.8 vol-% MEK, 17.6 vol-% 1,2-dibromo-1,1-difluoroethane, 17.2 vol-% isopropanol, and 11.4 vol-% dichlorooctafluorocyclohexene-1; temperature 31°C. Here again, this temperature was established by means of osmometry (at 27, 30, and 35°C).

Centrifugation was carried out in a Spinco model E ultracentrifuge with a temperature control unit and with the use of schlieren optics and phase plate. Fluctuations in rotor speed were less than 0.5%. We employed Spinco 12-mm double-sector cells, filled Epon, with a plane quartz window and a 1° negative wedge window. One of the sectors was filled with the solvent mixture, so that each schlieren curve appears superimposed on a base line due to the solvent mixture. The schlieren photographs were enlarged 10 times and traced by means of a Nikon universal contour projector (Nippon Kogaku Co.). For the analysis of the curves we refer to Ende.[18] We developed a Fortran IV(G) program to speed up the calculation of the moments, using an IBM-360 computer for the calculations. These moments showed a negligible dependence on the initial concentration of the polymer. However, at low polymer concentration the data scatter considerably. We estimate the possible error in the extrapolated values to be of the order of 10%.

Density-Gradient Centrifugation of Sample SM76-1

Density-gradient centrifugation was carried out at 31°C at a rotor speed of 40,500 rpm. The schlieren curves had the customary shape for polymers without compositional distribution, but they will be used to demonstrate

TABLE III
Extrapolated Values of $-S_n^-/A$ and S_n^+/A for Sample SM76-1

	Moments, cm^{n-1}							
	$n = 3$	$n = 2.5$	$n = 2$	$n = 1.5$	$n = 1$	$n = 0.5$	$n = 0$	$n = -0.5$
$-S_n^-/A$ (exptl)	0.0137	0.031	0.072	0.18	0.48	1.39	4.40	15.3
S_n^+/A (exptl)	0.0146	0.033	0.078	0.19	0.51	1.47	4.58	16.5
S_n/A (calcd)[a]	0.0174	0.034	0.078	0.18$_5$	0.50	1.46	4.73	17.5

[a] The calculated values were determined on the assumption that P_0 in eqs. (10) and (11) is equal to 36.0.

some of the characteristics of the curves and the practical limitations of the method.

The extrapolated moments are shown in Table III. As can be seen from eqs. (6) and (7), when there is no compositional distribution we should find $S_n^+ = -S_n^-$. Table III shows that this is only approximately true: S_n^+ is consistently somewhat larger than $-S_n^-$. This lack of symmetry could in principle be due to a small compositional distribution or to a distribution of stereoregularity which is a special type of compositional distribution. However, a very similar disagreement between theoretical and experimental results has been observed in earlier work[19] and has been attributed to shortcomings of the theory. It sets obvious limitations to the quantitative evaluation of the data and must be kept in mind when we discuss the results obtained with sample SM35H.

To compare the experimental moments with theoretical expectations, we approximate the molecular weight distribution by an equation of the Schulz-Zimm type:

$$f(P) = \frac{1}{\Gamma(s+1)} \frac{P^s}{P_0^{s+1}} e^{-P/P_0} \tag{10}$$

where s and P_0 are constants. On this assumption we have

$$\langle P^k \rangle = \Gamma(s+k+1) P_0^k / \Gamma(s+1). \tag{11}$$

Now, from the ratio 1.84 between weight average and number average in sample SM76-1, it follows that for this sample $s = 1.19$. If this is used in eqs. (6) and (7), it is found that reasonable agreement between experimental and calculated moments can be achieved by assuming that $P_0 = 36$. The agreement is relatively poor when $n = 3$, but this is not unexpected when we remember that the higher moments are strongly affected by errors in the tails of the schlieren curve. All in all the agreement between experimental and calculated moments in Table III must be considered as fairly representative of the accuracy that can be obtained.

Density-Gradient Centrifugation of PMA, SM25, SM40, SM50-1, and SM35H

These were all done at 26.5°C in the solvent mixture mentioned above at a centrifugal speed of 36,000 rpm. The schlieren curves for the first four samples had normal shape. The curve obtained in the case of SM35H is shown in Figure 2. Qualitatively it is in good agreement with the results of thin-layer chromatography (Fig. 1). The peak at distance 6.81 cm from the center of rotation is at the same position as that found for PMA. We have also measured the position of zero refractive index gradient in the single peaks of samples SM25, SM40, and SM50-1. The results are plotted in Figure 3, which relates position r_0 in the cell to styrene mole fraction m in the polymer.

For a quantitative evaluation of the results with SM35H we took the origin $x = 0$ at the position r_0^* which, in the absence of compositional dis-

TABLE IV

Extrapolated Experimental Moments S_n^+ and S_n^- from Schlieren Curve for Sample SM35H and U_n and V_n Calculated from the S_n

	Moments, cm^{n-1}							
	$n = 3$	$n = 2.5$	$n = 2$	$n = 1.5$	$n = 1$	$n = 0.5$	$n = 0$	$n = -0.5$
S_n^+/A	0.012	0.027	0.062	0.146	0.363	1.01	3.36	17.8
S_n^-/A	−0.024	−0.053	−0.115	−0.269	−0.636	−1.51	−3.30	−2.0
U_n	−0.012	−0.026	−0.053	−0.123	−0.273	−0.50	0.06	15.8
V_n	0.036	0.080	0.177	0.145	1	2.52	6.66	19.8

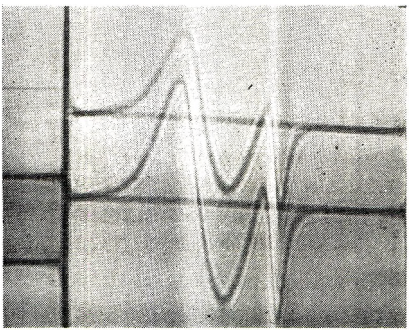

Fig. 2. Schlieren curve for sample SM35H.

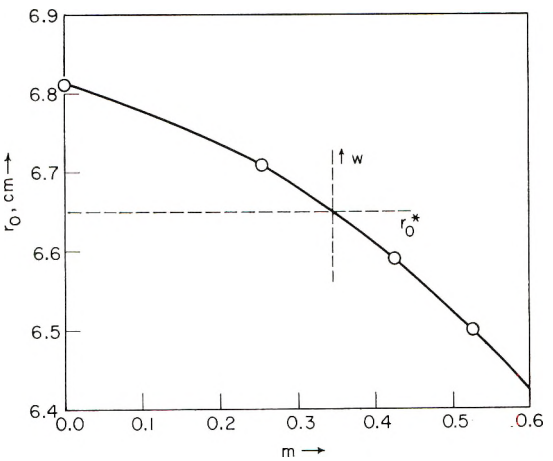

Fig. 3. Position of zero refractive index gradient vs. molar content of styrene in samples PMA, SM25, SM40, and SM50-1.

tribution, would correspond to the overall composition of this sample, 34.2%. This means that the quantity w defined in eq. (2) should result in an average value $\langle w \rangle = 0$ for this sample. We will later make a comparison also between the experimental and the expected value of $\langle w^2 \rangle$. The expected value was calculated from the data given by Inagaki et al.[6] (their Table VII) Figure 3 being used to convert values of styrene mole fraction m to values of w. This leads to the result $\langle w^2 \rangle = 0.012$ cm^2.

The moments about the origin so chosen are listed in Table IV, along with the corresponding values of U_n and V_n [eq. (9)]. It is noted that the experimental values of $S_{-1/2}{}^+$ and $S_{-1/2}{}^-$ may contain a relatively large error, because although the integral over $s^{-1/2}g(x)$ converges, the function $x^{-1/2}g(x)$ becomes infinite at $x = 0$.

Discussion of the Results for SM35H

We observe, first of all, that according to eqs. (6), (7), and (9), we should have

$$U_0 = 0$$

and

$$U_2 = 2\langle w \rangle$$

The first condition is met approximately: S_0^+ and S_0^- differ by only 2%. The second condition would require that $U_2 = 0$, because our choice of origin $x = 0$ was such that the average fluctuation in composition was zero. From the value of U_2 in Table IV we would conclude, however, that $\langle w \rangle = -0.026$ cm. The corresponding error in terms of average mole fraction styrene is only 4%. This discrepancy is of the same order of magnitude as that found in earlier work with a styrene–iodostyrene copolymer,[15] where the difference between the expected and the experimental value of $\langle w \rangle$ was 0.02 cm. It demonstrates once again that the accuracy of the method is limited.

In the previous study[15] the data were interpreted on the assumption that fluctuations in molecular weight are independent of fluctuations in composition. This is *a priori* very unlikely, but it is nevertheless instructive to see what happens when this assumption is made. It means that the averages in eqs. (6) and (7) become

$$\begin{aligned} \langle P^k w \rangle &= \langle P^k \rangle \langle w \rangle \\ \langle P^k w^2 \rangle &= \langle P^k \rangle \langle w^2 \rangle \end{aligned} \tag{12}$$

We can estimate $\langle P^k \rangle$ on the basis of eq. (11), where now we take $s = 0.735$. This is based on the fact that the viscosity average is always rather close to the weight average, so that $\bar{M}_w/\bar{M}_n$ for sample SM35H is equal to 2.36. If these assumptions are used in eqs. (6) and (7) and the results are substituted in eq. (9), we obtain the results given in Table V where, for the sake of convenience, we wrote

$$\begin{aligned} P_0^{1/4} &= p \\ \langle w \rangle &= \alpha \\ \langle w^2 \rangle &= q \end{aligned} \tag{13}$$

As can be seen in this table, the advantage of U and V over S^+ and S^- is that when the assumption of eq. (12) is made, the U do not contain $\langle w^2 \rangle$ and the V do not contain $\langle w \rangle$.

It was found by trial and error that a fairly good fit could be obtained with P_0 near 48, $\langle w \rangle$ about -0.03 and $\langle w^2 \rangle$ about 0.003. We then wrote $P_0 = 48(1 + g)$; $\langle w \rangle = -0.03(1 + u)$; $\langle w^2 \rangle = 0.003(1 + v)$, linearized the equations in Table V with respect to g, u, and v and found the best values of g, u, and v by the method of least squares.[20] This led to the final "best" values $P_0 = 45.0$; $\langle w \rangle = -0.029$; $\langle w^2 \rangle = 0.0027$. Table V shows that the agreement between the calculated and the experimental data is good, the only exception being the value of V_3, where the error is about 30%.

It must be noted however that the value required for $\langle w^2 \rangle$ is 0.0027, which is more than four times lower than the value derived from the thin layer chromatography data. We consider this discrepancy large enough to reject

TABLE V
Equations Obtained from Equations (6), (7), and (9) on the Basis of the Assumption (12)[a]

	Calcd	Exptl		Calcd	Exptl
$U_3 = 3.360\ \alpha/p^2$	−0.015	−0.012	$V_4 = 2.040/p^4 + 3.000\ q$	0.053	0.036
$U_{2.5} = 2.506\ \alpha/p$	−0.028	−0.026	$V_{2.5} = 1.394/p^3 + 2.442\ pq$	0.097	0.080
$U_2 = 2\alpha$	−0.058	−0.053	$V_2 = 1.22/p^2 + 1.386\ p^2q$	0.192	0.177
$U_{1.5} = 1.662\ \alpha p$	−0.125	−0.123	$V_{1.5} = 1/p + 0.572\ p^3q$	0.413	0.415
$U_1 = 1.386\ \alpha p^2$	−0.270	−0.273	$V_{0.5} = 1.110\ p - 1.102\ p^5q$	2.53	2.52
$U_{0.5} = 0.994\ \alpha p^3$	−0.50	−0.50	$V_0 = 1.386\ p^2 - 3.088\ p^6q$	6.78	6.66
$U_{-0.5} = 4.41\ \alpha p^5$	14.9	15.8	$V_{-0.5} = 1.988\ p^3 - 7.400\ p^7q$	18.9	19.8

[a] The values calculated are found when we insert $P_0 = 45 (p = 2.59)$; $\langle w \rangle = \alpha = -0.029$; $\langle w^2 \rangle = q = 0.0027$.

the assumption in eq. (12), but at the same time it must be admitted that the agreement shown in Table V reveals a serious shortcoming of the density gradient centrifugation method. If we had not had independent information concerning the value of $\langle w^2 \rangle$, we might have considered the agreement as acceptable, and we would then have "derived" the wrong value of $\langle w^2 \rangle$ from our data.

In the present case, however, we do know the value of $\langle w^2 \rangle$, and the question arises whether we can make use of this knowledge to get more information concerning our sample. When we reject eq. (12), we must in some way try to account for the fact that fluctuations in degree of polymerization are correlated with those in composition. There are several ways of doing this, but we do not want to use more than three adjustable parameters and have therefore tried the following approach. We assume that the distribution over molecular weight and composition is

$$f(P,w) = \frac{1}{\Gamma(s+1)} \frac{P^s}{P_0^{s+1}} e^{-P/P_0} g(w) \tag{14}$$

where $g(w)$ is an arbitrary function, which is normalized:

$$\int_{-\infty}^{\infty} g(w)dw = 1 \tag{15}$$

while also P_0 is a function of w. This means that we assume a Schulz-Zimm type distribution for each composition individually, but the average molecular weight for this distribution is a function of composition. In general we must also expect that the width of the distribution (which is determined by s) is a function of w, but we assume s to be independent of w for the sake of simplicity and because we want to keep the number of adjustable parameters to a minimum. As a first approximation we try a linear relationship between P_0 and w,

$$P_0 = Q(1 + \beta w) \tag{16}$$

If in eq. (4) we use eq. (14), the integration over P gives

$$\langle P^k \rangle = \frac{\Gamma(s+k+1)}{\Gamma(s+1)} \int_{-\infty}^{\infty} P_0^k g(w)dw \tag{17}$$

Here P_0^k, according to eq. (16), may be written

$$P_0^k = Q^k[1 + k\beta w + {}^1/_2 k(k-1)\beta^2 w^2 \ldots] \tag{18}$$

but it must be remembered that eqs. (6) and (7) were derived on the assumption that powers of w higher than the second may be neglected. To be consistent with this approximation we should also truncate the expansion in Eq. (18) after the term with w^2, so that eq. (17) becomes

$$\Gamma(s+1)\langle P^k \rangle = \Gamma(s+k+1)Q^k[1 + k\beta\langle w \rangle + {}^1/_2 k(k-1)\beta^2\langle w^2 \rangle] \tag{19}$$

TABLE VI

Equations Derived from Equations (6), (7), and (9) on the Basis of Equations (19)–(21)[a]

	Calcd	Exptl		Calcd	Exptl
$U_3 = 3.360(\alpha - {}^1/_2\beta q)/\xi^2$	−0.011	−0.011	$V_3 = 2.040(1 - \alpha\beta + \beta^2 q)/\xi^4$	0.060	0.036
$U_{2.5} = 2.506(\alpha - {}^1/_4\beta q)/\xi$	−0.023	−0.026	$V_{2.5} = 1.384(1 - {}^3/_4\alpha\beta + {}^{21}/_{32}\beta^2 q)\xi^3$	0.100	0.080
$U_2 = 2\alpha$	−0.052	−0.053	$V_2 = 1.122(1 - {}^1/_2\alpha\beta + {}^3/_8\beta^2 q)/\xi^2$	0.193	0.177
$U_{1.5} = 1.662(\alpha + {}^1/_4\beta q)\xi$	−0.118	−0.123	$V_{1.5} = 1.005(1 - {}^1/_4\alpha\beta + {}^1/_{32}\beta^2 q)/\xi$	0.417	0.415
$U_1 = 1.386(\alpha + {}^1/_2\beta q)\xi^2$	−0.266	−0.273	$V_{0.5} = 1.110(1 + {}^1/_4\alpha\beta - {}^3/_{32}\beta^2 q)\xi$	2.70	2.52
$U_{0.5} = 0.994(\alpha + {}^3/_4\beta q)\xi^3$	−0.508	−0.50	$V_0 = 1.386(1 + {}^1/_2\alpha\beta - {}^1/_8\beta^2 q)\xi^2$	8.10	6.66
$U_{-0.5} = -4.41(\alpha + {}^5/_4\beta q)\xi^5$	15.4	15.8	$V_{-0.5} = 1.998(1 + {}^3/_4\alpha\beta - {}^3/_{32}\beta^2 q)\xi^3$	28.0	19.8

[a] The calculated values follow when we insert $\xi = 2.40$ ($Q = 33.2$); $\alpha = \langle w \rangle = -0.026$; $q = \langle w^2 \rangle = 0.012$; $\beta = -1.20$.

By the same procedure we find

$$\Gamma(s + 1)\langle P^k w\rangle = \Gamma(s + k + 1)Q^k[\langle w\rangle + k\beta\langle w^2\rangle] \tag{20}$$

$$\Gamma(s + 1)\langle P^k w^2\rangle = \Gamma(s + k + 1)Q^k\langle w^2\rangle \tag{21}$$

This enables us to express the moments of the schlieren curve in terms of the parameters Q, β, $\langle w\rangle$, and $\langle w^2\rangle$. As before, we take $s = 0.735$ and consider the functions U_n and V_n defined by eq. (9). The resulting equations are given in Table VI, where

$$\begin{aligned} Q &= \xi^4 \\ \langle w\rangle &= \alpha \\ \langle w^2\rangle &= q \end{aligned} \tag{22}$$

Although our procedure introduces an additional parameter β in eq. (16), this does not increase the number of adjustable quantities, because we will take q as given by the results of thin-layer chromatography, namely, $q = \langle w^2\rangle = 0.012$ cm^2. Table VI shows that good agreement between experimental and calculated data can be achieved if we take $Q = 33.3$, $\langle w\rangle = -0.026$, and $\beta = -1.20$. The agreement is poor for V_3 and for $V_{-0.5}$, but it has already been mentioned that the moments S_n^+ and S_n^- are not very reliable when $n = -0.5$, and that relatively large errors can result from the tails of the schlieren curve when n is large. The agreement with almost all the other moments is considerably better than the experimental error, and this means that the agreement for V_3 and $V_{-0.5}$ could, if desired, be improved somewhat at the cost of a less perfect agreement in the other moments, by a slightly different choice of the parameters. It is not considered worthwhile, however, to pursue this further, because several simplifying assumptions were made in the theory, so that complete agreement cannot be expected anyway; nor do we claim that the interpretation given is the only possible one.

Conclusion

Our attempts to give a quantitative explanation of the moments of the schlieren curve for sample SM35H have revealed a somewhat ambiguous situation. The moments can be represented with reasonable accuracy by the theoretical equations for a sample in which the fluctuations in molecular weight are independent of those in composition, but the numerical value of the variance in composition comes out less than one fourth of the value derived from the thin-layer chromatography data. This discrepancy can be removed by assuming a linear correlation between the chemical composition and the average molecular weight. Making use of some reasonable approximations, this second method leads to an equally acceptable interpretation, and the variance in composition is now in complete agreement with the results of thin layer chromatography.

This shows that density-gradient centrifugation alone is not a reliable method to obtain quantitative results concerning the distribution over

molecular weight and composition, but that it can be used to yield additional information in those cases in which independent data exist. It is not claimed, however, that the interpretation given is the only possible one. Equally good agreement can probably be achieved on the basis of other assumptions.

This work was supported by the National Science Foundation under Grant GU 2059.

References

1. W. H. Stockmayer, L. D. Moore, Jr., M. Fixman, and B. N. Epstein, *J. Polym. Sci.*, **16**, 517 (1955).
2. W. Bushuk and H. Benoit, *Can. J. Chem.*, **36**, 1616 (1958).
3. M. Leng, C. Strazielle, and H. Benoit, *J. Chim. Phys.*, **60**, 501 (1963).
4. V. Y. Eskin, A. L. Izyumnikov, Y. D. Royozhkina, and Y. P. Vyrskii, *Polym. Sci. USSR*, **7**, 1310 (1965); *ibid.*, **9**, 591 (1967).
5. H. Matusda, K. Yamano, and H. Inagaki, *J. Polym. Sci. A-2*, **7**, 609 (1969).
6. H. Inagaki, H. Matsuda, and F. Kamiyama, *Macromolecules*, **1**, 520 (1968).
7. G. Markert, *Makromol. Chem.*, **103**, 109 (1967); *ibid.*, **109**, 112 (1967).
8. F. Kamiyama, H. Matsuda, and H. Inagaki, *Makromol. Chem.*, **125**, 286 (1969).
9. T. Miyamoto and H. Inagaki, *Macromolecules*, **2**, 554 (1969).
10. H. Inagaki, T. Miyamoto, and F. Kamiyama, *J. Polym. Sci. B*, **7**, 329 (1969).
11. H. Inagaki, *Bull. Inst. Chem. Res. Kyoto Univ.*, **47**, 196 (1969).
12. S. E. Bresler, L. M. Pyrkov, and S. Y. Frenkel, *Vysokomol. Soedin.*, **2**, 216 (1960).
13. R. Buchdahl, H. A. Ende, and L. H. Peebles, in *First Biannual American Chemical Society Polymer Symposium* (*J. Polym. Sci. C*, **1**), H. W. Starkweather, Jr., Ed., Interscience, New York, 1963, p. 153.
14. R. Buchdahl, H. A. Ende, and L. H. Peebles, in *First Biannual American Chemical Society Polymer Symposium* (*J. Polym. Sci. C*, **1**), H. W. Starkweather, Jr., Ed., Interscience, New York, 1963, p. 143.
15. H. A. Ende and J. J. Hermans, in *Macromolecular Chemistry, Paris 1963* (*J. Polym. Sci. C*, **4**), M. Magat. Ed., Interscience, New York, 1963, p. 513; *J. Polym. Sci. A*, **2**, 4053 (1964).
16. J. J. Hermans, *J. Chem. Phys.*, **38**, 597 (1963); in *First Biannual American Chemical Society Polymer Symposium* (*J. Polym. Sci. C*, **1**), H. W. Starkweather, Jr., Ed., Interscience, New York, 1963, p. 179.
17. J. J. Hermans and H. A. Ende, in *Newer Methods of Polymer Characterization*, B. Ke, Ed., Interscience, New York, 1964.
18. H. A. Ende, *Makromol. Chem.*, **88**, 159 (1956).
19. A. Nakazawa and J. J. Hermans, *Proc. Roy. Soc.* (*Amsterdam*), **B73**, 334 (1970).
20. A. W. Leissa and W. E. Clausen, *Fundamental Aspects of Fiber Reinforced Plastic Composites*, R. T. Schwartz and H. S. Schwartz, Eds., Interscience, New York, 1968, p. 35.

Received February 17, 1971
Revised April 12, 1971

JOURNAL OF POLYMER SCIENCE: PART A-2 VOL. 9, 1887–1905 (1971)

Time-Dependent Heat Capacity in the Glass Transition Region

STEPHEN M. WOLPERT,* ALEXANDER WEITZ, and BERNHARD WUNDERLICH, *Department of Chemistry, Rensselaer Polytechnic Institute, Troy, New York 12181*

Synopsis

Time-dependent, apparent heat capacities of glucose, poly(vinyl chloride), polystyrene, selenium, poly(methyl methacrylate), and poly(2,6-dimethyl-1,4-phenylene ether) in the glass transition region were determined by differential thermal analysis. The thermal history was set by linear cooling at rates between 0.007 and 160°C/min. Linear heating for analysis was carried out at rates between 0.3 and 600°C/min. Average activation energies of 52, 81, 90, 54, 77, and 108 kcal/mole, respectively, were evaluated by using the hole theory of glasses previously developed. Within experimental limitations all data could be described quantitatively by the theoretical expressions using only one parameter, the number of frozen-in holes, to describe the thermal history. Experimental and theoretical limitations are discussed.

Measurements of heat capacity of amorphous materials in the glass transition region show nonequilibrium effects due mainly to time-dependent configurational rearrangements of the molecules. At temperatures sufficiently below the glass transition T_g, the configuration is virtually frozen in, and the heat capacity of the glass behaves like an equilibrium property. Frequently, the heat capacity of glasses is similar to heat capacity of equilibrium crystals of chemically identical structures down to temperatures as low as 50°K. At temperatures sufficiently above T_g, the configurational rearrangements are so fast that their time dependence is not measurable, and an equilibrium heat capacity exists for the melt. The heat capacity contribution due to changes in mode of motion (such as vibrations changing to rotation or translation) is much smaller than that due to configurational rearrangements (such as hole formation) in the T_g region. This paper will be concerned with the time-dependent apparent heat capacity of six materials in the glass transition region: glucose ($C_6H_{12}O_6$), selenium (Se), poly(vinyl chloride) (PVC), polystyrene (PS), poly(methyl methacrylate) (PMMA), and poly(2,6-dimethyl-1,4-phenyl ether) (PPO).

Early observations of heat capacity as a function of time and temperature established that a maximum and a minimum can occur in the transition region of several organic, inorganic, and polymeric glasses.[1–5] Presently

* Present address: Polymers Department, Research Laboratories, General Motors Technical Center, Warren, Michigan 48089.

some quantitative data are available for poly(vinyl acetate),[6] polystyrene,[6–11] glucose,[9] polycarbonate,[12] poly(ethylene terephthalate),[10] poly(vinyl chloride),[13] poly(vinyl chloride-*co*-acetate),[13] and phenolphthalein.[11] Most of the measured data, however, are difficult to interpret and to compare because of different thermal histories and time variables as well as the inherent problems of accuracy in making time-dependent thermal measurements. The present investigation was undertaken as a followup of initial work on polystyrene[8] after a thorough analysis of the applicability of differential thermal analysis as a dynamic technique for measuring heat capacities.[14,15] In this research techniques were developed which allowed linear cooling between 0.007 and 160°C/min followed by linear heating between 0.3 and 600°C/min; these heating and cooling rates set the time scales for the present experiments.

The interpretation of the time dependent effects of the heat capacity in the glass transition region as a relaxation process was first given by Richards in 1936.[16] The thermodynamic basis for relaxation processes was reviewed by Davies and Jones.[17] For a cyclic process starting and ending in a point in the (possibly supercooled) equilibrium melt region, the conservation of energy requires:

$$\oint C_p dT = 0 \tag{1}$$

The integral over any cyclic path has to be zero, independent of time dependent processes and their direction. For a system cooled slowly through the glass transition region, followed by fast heating, the time-dependent

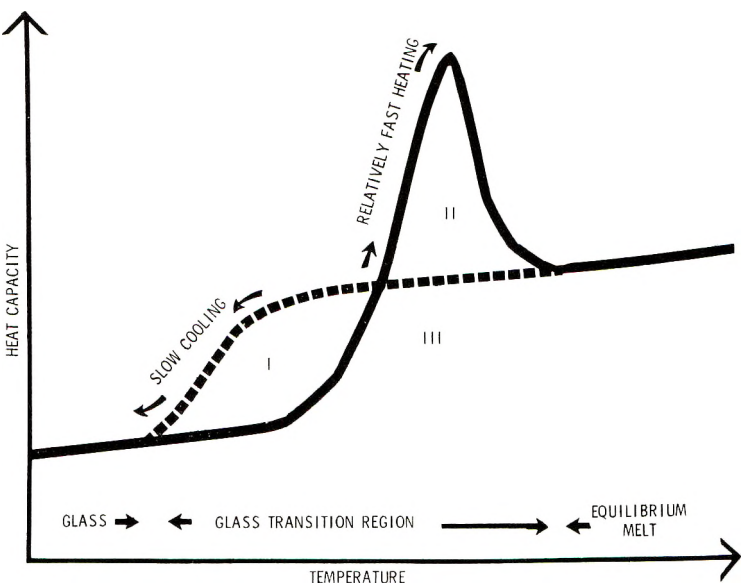

Fig. 1. Schematic drawing of the apparent heat capacity on slow cooling and subsequent faster heating.

heat capacity curves are illustrated schematically in Figure 1. Areas I + III must equal areas II + III, and therefore area I must also equal area II.

To describe the time-dependent apparent heat capacity in the transition region, nonisothermal kinetics must be used. Volkenshtein and Ptitsyn[18] derived the first expressions for the heat capacity effects from the first order approach of the "fraction of kinetic particles in the excited state" to equilibrium. Later, Wunderlich et al.[8] developed similar expressions based on the hole theory of liquids[19-21] and glasses.[22] Although more sophisticated theories have been developed recently, they have not yet lent themselves to detailed heat capacity analysis.[23-26] Therefore, the kinetic expressions based on the hole theory will be used in this paper. It will be shown that a simple set of parameters can describe the apparent heat capacity in the glass transition region over a wide range of heating aud cooling rates.

All equations used, were derived previously.[8] In summary, the equilibrium number of holes N^* is assumed to be described by:

$$N^* = (v_0/v_h) \exp\{-(\epsilon_h + pv_h)/RT\} \tag{2}$$

where v_0 and v_h are the molar volumes occupied by the molecules or repeating units and the holes, respectively. The excess energy of a hole over a no-hole sityation is ϵ_h. The symbols R, T and p have the usual significance. The first-order approach of the instantaneous number of holes N to equilibrium takes the form:

$$dN/dt = (1/\tau)(N^* - N) \tag{3}$$

where τ is the relaxation time governed by the activation energy for hole formation ϵ_j:

$$\tau = (A/T) \exp\{\epsilon_j/RT\} \tag{4}$$

The hole contribution to the apparent heat capacity $C_{p,h}'$ can finally be found by:

$$C_{p,h}' = \epsilon_h(\partial N/\partial T) \tag{5}$$

The final, partially integrated equation for the apparent heat capacity is:[8]

$$C_{p,h}' = [(\epsilon_h/q\tau) \exp\{-\phi\}]\left[N^*(T_a) - N_a + \int_{N^*(T_a)}^{N^*(T)} \exp\{\phi\} dN^*(T)\right] \tag{6}$$

with ϕ given by

$$\phi = \int_{T_a}^{T} (dT'/q\tau) \tag{7}$$

The symbols T_a and N_a are the initial temperature and number of holes; q represents the heating or cooling rate, dT/dt. More detailed discussions of the equations can be found in the literature.[18-20] The computer program to evaluate equation (5) has been given elsewhere.[15] A schematic drawing of the changes in contribution of holes to enthalpy H (proportional to the instantaneous number of holes, N) is given in the upper part of Fig-

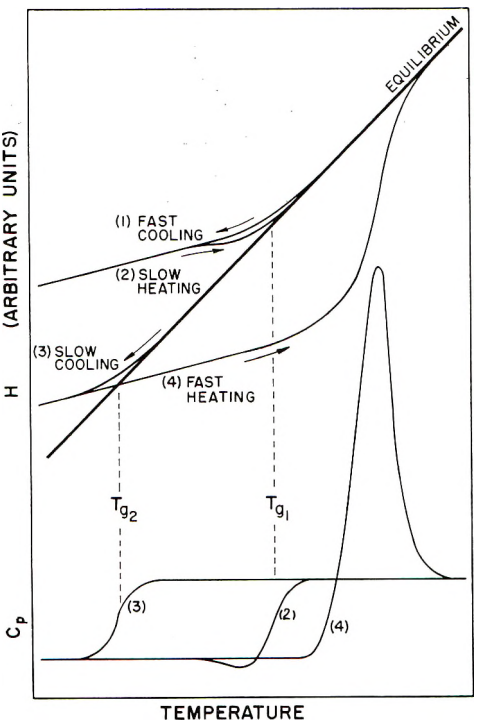

Fig. 2. Schematic drawing of changes of enthalpy and heat capacity on unequal cooling and heating.

ure 2 for various linear heating and cooling rates q. The lower part represents the apparent heat capacity as described by eq. (6). Curves (1) and (3) represent the behavior of rapidly and slowly cooled samples, respectively. The transition temperature is shifted to lower temperatures with slower cooling rates. Reheating the samples at similar rates leads to only slightly different curves on heating. Following fast cooling with slow heating as in curve (2) leads to a minimum in the heat capacity curve because of drift toward equilibrium before reaching the glass transition temperature previously observed on cooling. Following slow cooling with fast heating leads to the lost distinctive DTA curve,[8] which shows a maximum in the heat capacity due to inability of the system to achieve equilibrium at the glass transition temperature previously observed on cooling. This paper will be concerned mostly with the determination of the characteristic kinetic parameters of the chosen glasses from the peak in apparent heat capacity as measured by differential thermal analysis.

EXPERIMENTAL

Methods

The basic measuring instrument was a duPont 900 differential thermal analyzer, capable of heating rates between 2 and 100°C/min. Depending

on heating rate 4 mm (2–20°C/min) or 2 mm (above 20°C/min) glass capillaries were used as sample holders. For slower heating rates a motor driven linear potentiometer controlled the heating, and brass sample holders of about 8 mm internal diameter were used, as in the set-up described previously.[27] For heating rates up to 600°C/min, a special 1000-W cartridge heater was installed in the DTA block. Its output was set by a variable transformer. Without further control, nearly linear heating rates were obtained in these very fast heating experiments.

The temperature axis was calibrated by melting a large number of zone-refined organic chemicals. The reproducibility of their melting points was ±0.2°C. The absolute accuracy of the instrument is considered to be about ±0.3$_4$°C on the basis of the standard deviations from empirical calibration curves.[15] Practically no change in onset of melting was observed on changing heating rates in the ranges quoted above.

Slow cooling was usually accomplished by a linearly driven thermoregulator outside the DTA apparatus. The lower limit being set only by the patience of the experimenter. The lowest cooling rate reported in this research was less than 9°C/day. Experiments at faster rates were performed directly in the DTA set-up.

Samples were loaded as powder in the holders and then fused above the glass transition temperature. The thermocouple was thus molded into place. Samples which were cooled outside the DTA apparatus each had a separate thermocouple fixed in place. The special sample descriptions, preparations and measurements are given below.

Glucose. Anhydrous, crystalline, Fisher reagent-grade glucose was dried in vacuum at 90°C overnight. The dry crystals were melted in the sample holders to a clear liquid at 160–170°C which is below the dehydration temperature. By quenching in ice water glassy glucose was produced. The x-ray diffraction studies showed no crystallinity of the samples and no development of crystallinity on annealing for 12 hr at 55°C. Crystallization could be accomplished above 80°C, or, in case of presence of water, at room temperature. The glassy samples were heated to about 45°C to erase previous thermal history and impart reproducible starting conditions. Then the samples were linearly cooled to about 15°C at four different rates: 0.0067, 0.08, 1.4, and 5.1°C/min. Faster, nonlinear cooling was accomplished by quenching in liquid nitrogen, giving a rate of about 156°C/min in the glass transition region.

Poly(vinyl Chloride). The poly(vinyl chloride) (PVC) used in this research was supplied by Monsanto Chemicals Co. It was of the Opalon 660 type and is reported[28] to have the following properties: approximately 51% syndiotactic linkages, no plasticizer, stabilizer, or residual solvents, minor traces of water-soluble surfactants, and up to 0.2% water, about 8% crystalinity, molecular weight by gel permeation $\bar{M}_n$ = 48,000; $\bar{M}_w$ = 115,000. The polymer was supplied as a powder and used as such because it degraded at temperatures necessary for fusion. All samples were used only once. Thermal history was erased by cooling from 98°C at 0.082 and 0.0065°C/min.

Polystyrene. The polystyrene (PS) used in this research was supplied by Dow Chemical Co. (designation PS-37, S-5). The sample was identical to the polymer previously analyzed: $\bar{M}_n$ = 198,000; $\bar{M}_w$ = 357,000. Since similar measuring techniques were employed, the slow heating rate data from the previous study[8] are included in the present discussion. Data were collected after cooling from about 150°C at 0.65 and 0.018°C/min.

Selenium. The glassy selenium was prepared by quenching 99.999+% pure selenium from the liquid state. To check on possible differences of molecular length and ring-polymer ratio in the melt, quenching was started at 235, 350, 525, and 900°C. The selenium was sealed under vacuum in quartz or glass tubing and quenched from the chosen temperature by dropping into ice water. The thermal history other than chemical configuration was erased by reheating to about 50°C. Controlled cooling was then done at 0.0045, 0.028, 1.5, and 2.3°C/min. After cooling, all samples were stored at −15°C. Crystallization is known not to occur below 70°C in an unstrained condition. Our samples showed no evidence of crystallinity on the basis of x-ray diffraction.

Poly(methyl Methacrylate). Two poly(methyl methacrylate) (PMMA) samples were supplied by Rohm and Haas Co. They were obtained by free-radical polymerization and had 75% syndiotactic linkages. The molecular weights of the first sample were $\bar{M}_n$ = 19,400; $\bar{M}_w$ = 49,000. Considerable scatter of DTA data was observed when samples were exposed to ambient humidity. The effect of moisture was analyzed by erasing thermal history at 150°C and cooling at 0.083°C/min in water vapor-saturated, ambient, and $CaCO_3$-desiccated atmospheres. The effect of moisture is clearly evident in the change in peak temperature with humidity as illustrated in Figure 3. Other linear cooling rates of 0.0065 and 0.5°C/min were investigated only at ambient conditions.

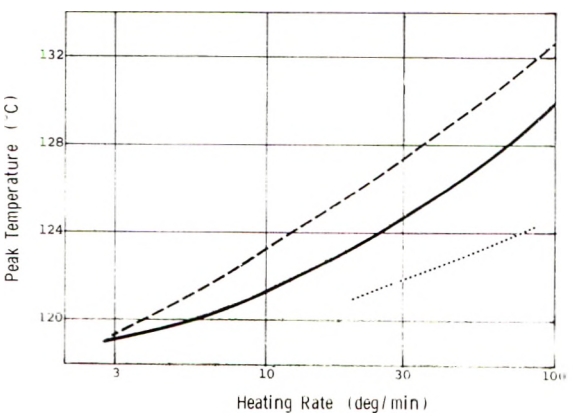

Fig. 3. Peak temperature of PMMA cooled at 0.083°C/min as a function of heating rate for different moisture contents: uppermost curve dried, middle curve ambient, lowest curve for sample in contact with 100% RH at room temperature.

A high molecular weight PMMA ($\bar{M}_n$ = 160,000; $\bar{M}_w$ = 322,000) of similar chemical structure was compared to the standard sample at varying cooling and heating rates. The entire transition region of the high molecular weight PMMA was uniformly shifted upwards by 2.4 ± 0.9°C (average and standard deviation of seven comparisons).

Poly(2,6-dimethyl-1,4-phenylene Ether). The sample of poly(2,6-dimethyl-1,4-phenylene ether) (PPO) was a production-grade powder with $\bar{M}_n$ = 26,000 and $\bar{M}_w$ = 58,000, as determined by gel-permeation chromatography in trichloroethylene at 55°C (polystyrene beads). The intrinsic viscosity was 0.46 dl/g in chloroform at 30°C, and the volatile content (which, for the most part, represents surface moisture and traces of residual toluene solvent) was 0.7%.

The material was dried at 100°C *in vacuo* for 24 hr to remove moisture and solvent.[29] Cells used were 2-mm and 4-mm diameter glass tubes. In each case, dried powdered PPO was filled into the tubes. To avoid oxidation of the sample, the preparation technique consisted of placing the sample cell complete for DTA, filled with PPO powder, into a container, evacuated to 0.3 mm of mercury. The whole assembly was then placed in an aluminum block which was preheated to 230°C. The temperature was subsequently slowly raised to about 240–250°C. At this temperature the viscosity of the material is sufficiently reduced to allow slow compression and fusion of the powder into a clear solid mass. The heating was continued to 270°C, where it was held constant for about 5 min to relieve any stresses from the compression procedure and to be sure all crystallites were melted (the melting point of PPO is 235°C). After this annealing, the apparatus was removed from the heating block and cooled in ambient air while still under vacuum. About 40 such samples were prepared. The cooled samples were stored in a desiccator until tested. For controlled cooling, the samples with their thermocouples were placed in a large Pyrex test tube, heated to 245°C in a silicone oil bath while nitrogen gas flowed through the tube. The two cooling rates for this investigation were 0.12 and 1.5°C/min.

RESULTS

Typical direct copies of DTA traces for glucose are shown in Figures 4–6. Figure 4 shows the shallow minimum in heat capacity (maximum in T_s-T_r) obtained on fast cooling followed by relatively slow heating. Figures 5 and 6 illustrate the change in DTA traces on heating a slowly cooled sample at various rates.

The DTA peak temperatures are shown in Table I as a function of heating rate. They could be shown to be a close representation of the true apparent heat-capacity-peak temperature,[14,15] almost completely unaffected by instrument lag with the mode of DTA used here. The relative peak height is calculated as the ratio of the peak height from the glassy baseline to the jump in baselines on going through the glass transition region. Its

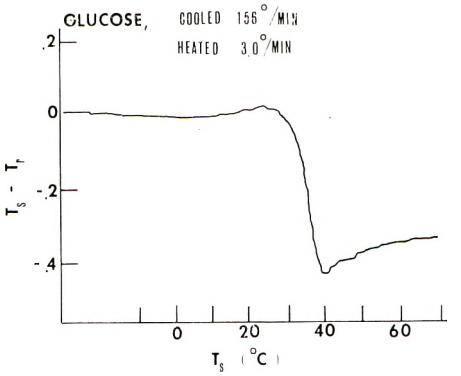

Fig. 4. DTA curve of glucose cooled rapidly and heated slowly. DTA temperature difference between sample and reference = $T_s - T_r$ in °C.

magnitude corresponds to the similarly defined apparent heat capacity ratio only at the lowest heating rates. Figure 7 shows the variation of measured relative peak height with heating rate for glucose. The larger peak heights found for slower prior cooling rates show more deviation from the expected straight line increases with heating rate. Model calculations have shown[14,15] that this type of deviation is to be expected in the equipment used. The absolute value of the peak height, expressed as apparent heat capacity ratio, fortunately does not enter as an important factor into a compound quantity Z, to be described below. A crude linear extrapolation of

TABLE I
DTA Peak Temperatures as Function of Heating Rate

Sample	Cooling rate, °C/min	Heating rate q, °C/min	Peak temperature, °C
Glucose	0.0067	2–100	$40.2 + 6.54 \log q$ (± 0.8)
Glucose	0.08	1–100	$37.6 + 6.76 \log q$ (± 0.9)
Glucose	1.4	3–100	$37.4 + 5.25 \log q$ (± 0.8)
Glucose	5.1	8–90	$35.4 + 7.45 \log q$ (± 1.0)
PVC	0.0065	2–98	$86.7 + 5.85 \log q$ (± 0.6)
PVC	0.083	2–98	$85.7 + 7.49 \log q$ (± 0.9)
PS	0.018	0.3–95	$105.2 + 6.30 \log q$ (± 0.8)
PS	0.65	1–85	$103.1 + 5.96 \log q$ (± 0.7)
Se (235)	0.028	12–98	$41.8 + 7.16 \log q$ ($+0.4$)
Se (350)	0.0045	1–98	$43.3 + 5.53 \log q$ (± 0.8)
Se (350)	0.028	11–98	$40.2 + 8.14 \log q$ (± 0.5)
Se (350)	1.5	2–80	$39.1 + 6.12 \log q$ (± 0.8)
Se (350)	2.3	20–98	$38.3 + 6.86 \log q$ (± 0.4)
Se (525)	0.028	5–98	$41.0 + 8.01 \log q$ (± 0.3)
Se (900)	0.028	20–96	$36.3 + 9.04 \log q$ (± 0.5)
PMMA	0.083	3–99	$114.4 + 8.92 \log q$ (± 0.8)
PPO	0.12	2–354	$216 + 9.29 \log q$ (± 1.3)
PPO	1.5	2–640	$217 + 7.95 \log q$ (± 1.6)

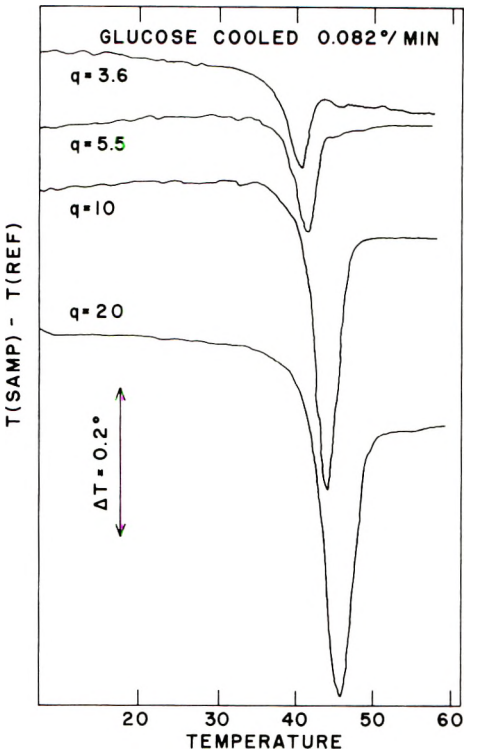

Fig. 5. DTA curve of glucose cooled at 0.082°C/min heated at 3.6–20°C/min. Temperature difference between sample and reference in arbitrary units.

the peak heights based on low heating rate trends was used when needed.

Table II lists some quantities derived from the DTA-curves. The meaning of Z needs some explanation. This quantity arises from the analysis of the apparent heat capacity peak as described by eq. (6) and given previously.[8] Setting dC_{ph}/dT equal to zero results in an approximately linear expression:

$$\log Z = \log A' + (B/T_p) \tag{8}$$

where

$$Z = (RT_p^3/q) - (\epsilon_h^2 N_h^* T_p/qh\Delta C_p),$$

where ΔC_p is the difference in heat capacity of the melt and the glass. The constant B is equal to $0.4343\epsilon_j/R$ and is an easy source of the activation energy of hole formation ϵ_j. The parameter A' is related to A in eq. (4).

Besides the experimental data listed in the Tables I and II, values for ϵ_h, v_h, v_0, and ΔC_p are necessary. As was shown previously,[30] these quantities are interrelated and can be computed from experimental data on ΔC_p, T_g, and the cohesive energy. For the present calculations, data from a recent

TABLE II
Data Derived from DTA as a Function of Heating Rate

Sample	Cooling rate, °C/min	log Z (T_p in °K)	A, min/°C	ϵ_j, kcal/mole
Glucose	0.0067	$(-37.36 + 14113/T_p) \pm 0.11$	6.64×10^{-43}	64.6
Glucose	0.08	$(-31.33 + 12059/T_p) \pm 0.12$	8.22×10^{-32}	55.2
Glucose	1.4	$(-21.19 + 8743/T_p) \pm 0.05$	1.57×10^{-26}	40.0
Glucose	5.1	$(-27.64 + 10699/T_p) \pm 0.02$	4.62×10^{-34}	49.0
PVC	0.0065	$(-40.49 + 17243/T_p) \pm 0.07$	4.01×10^{-46}	78.9
PVC	0.083	$(-43.84 + 18332/T_p) \pm 0.14$	1.69×10^{-49}	83.9
PS	0.018	$(-49.41 + 21702/T_p) \pm 0.01$	3.80×10^{-55}	99.3
PS	0.65	$(-39.57 + 17697/T_p) \pm 0.03$	3.27×10^{-45}	81.0
Se(235)[a]	0.028	$(-31.52 + 12292/T_p) \pm 0.05$	1.43×10^{-35}	56.0
Se(350)[a]	0.0045	$(-36.24 + 13871/T_p) \pm 0.11$	8.90×10^{-42}	63.5
Se(350)[a]	0.028	$(-26.37 + 10604/T_p) \pm 0.06$	8.63×10^{-32}	48.5
Se(350)[a]	1.5	$(-33.86 + 12877/T_p) \pm 0.10$	2.29×10^{-39}	58.9
Se(350)[a]	2.3	$(-26.24 + 10420/T_p) \pm 0.06$	1.18×10^{-31}	47.7
Se(525)[a]	0.028	$(-28.26 + 11247/T_p) \pm 0.04$	1.05×10^{-33}	51.5
Se(900)[a]	0.028	$(-22.46 + 9234/T_p) \pm 0.05$	8.08×10^{-28}	42.3
PMMA	0.083	$(-30.33 + 14760/T_p) \pm 0.08$	6.80×10^{-36}	67.6
PPO	0.12	$(-40.46 + 23852/T_p) \pm 0.12$	2.17×10^{-46}	109.5
PPO	1.5	$(-41.81 + 24393/T_p) \pm 0.14$	2.67×10^{-45}	106.4

[a] The number in parentheses gives the melt temperature in °C before initial quenching.

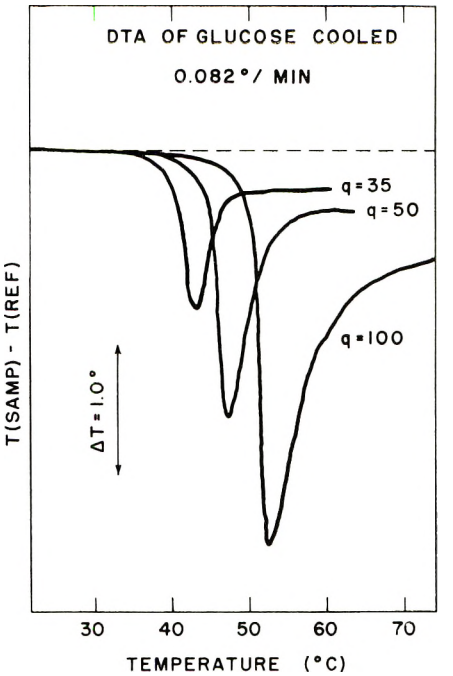

Fig. 6. DTA curve of glucose cooled at 0.082°C/min, heated at 35–100°C/min. Temperature difference between sample and reference in arbitrary units.

compilation[15,31–33] have been taken. The values are listed in Table III along with average values of ϵ_j.

TABLE III
Hole Parameters

Material	ϵ_j, kcal/mole	ϵ_h cal/mole	v_h cm/mole	ΔC_p, cal/°C-mole rep. unit
Glucose	52	1460	4.1	30.0
PVC	81	1070	10.3	4.4
PS	90	800	11.2	7.3
Selenium	54	1340	6.6	3.0
PMMA	77	1150	10.8	8.2
PPO	108	1880	18.1	6.9

DTA on cooling of PMMA at rates between 2 and 50°C/min gave for the temperature of half-freezing the following result:

$$\log q = 90.554 - 34710/T_g(\pm 0.8) \tag{9}$$

or

$$T_g = 383.3 + 4.23 \log q$$

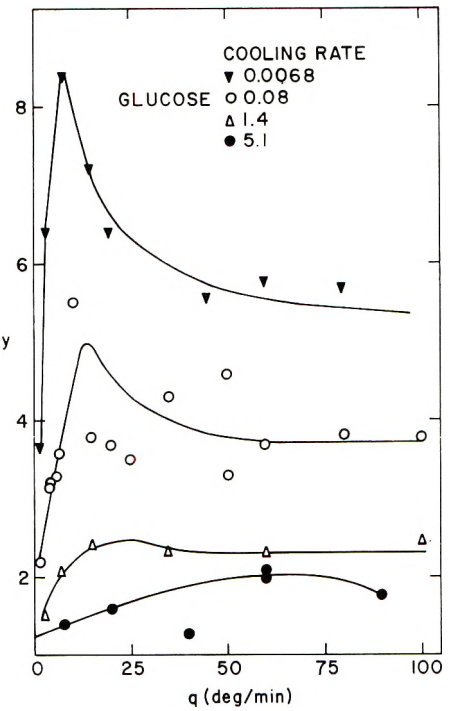

Fig. 7. Measured relative DTA peak height y of glucose cooled at the indicated rates as a function of heating rate. The initial slope increases as expected with increasing peak height (decreasing cooling rate).

This equation should be compared with results on PS derived previously:[8]

$$\log q = 92.463 - 34444/T_g(\pm 0.8) \tag{10}$$

or

$$T_g = 387.4 + 4.36 \log q$$

(where temperature is in degrees Kelvin, q in degrees-Celsius/minute) which indicates the close similarity of the two substances.

DISCUSSION

The glasses analyzed varied widely. Their transition temperatures ranged from 300 to 500°K; they included organic and inorganic macromolecules as well as glucose; they ranged from uncrystallizable atactic polymers to crystallizable molecules. Qualitatively all these glasses followed the behavior outlined in Figures 1, 2, and 4–6. Quantitatively their apparent heat capacities on linear temperature increase after linear cooling through the glass transition region can be described within the experimental accuracy by eq. (6).

A more detailed look at eq. (6) shows that it contains two independent variables, the heating rate q and the temperature T. Of the remaining six

material parameters v_0, v_h, ϵ_h, ϵ_j, A, and N_a, three (v_0, v_h, ϵ_h) are determined by independent equilibrium heat capacity measurements; two (ϵ_j and A) are derived from DTA heating experiments alone, while the initial number of holes N_a is determined by thermal history only. As long as thermal history consists of linear cooling, the present experiments show that a single parameter N_a suffices to describe the heat capacity. This one-parameter thermal history description can also be linked to the fictive temperature concept of Tool[1] by setting the initial hole number N_a equal to the equilibrium hole number at the fictive temperature T_x. A change in N_a changes only the magnitude of the apparent heat capacity:

$$dC_{p,h}'/dN_a = (\epsilon_h/q\tau) \exp\{-\phi\} \tag{11}$$

Equation (11) approaches zero above and below the glass transition region and has a maximum close to the peak temperature in $C_{p,h}'$. Since the heat capacity measurement by DTA is least accurate in the determination of peak height, this may be the reason for the perhaps surprisingly good fit of a one-parameter thermal history description. Further work in development of improved experimental techniques and comparison of different thermal histories is necessary.

The preexponential factor A and the activation energy ϵ_j determine the change in relaxation time with temperature [eq. (4)] and govern in turn the peak width (relaxation region) and peak position. Figures 8 and 9 illustrate the correspondence between calculation and experiment on two examples. The peak temperatures in these and other comparisons usually match within 1°C over the complete heating rate range analyzed. The experimental peak half-width in turn is always 0.5–3°C narrower. This fact indicates that a distribution of relaxation times as suggested previously[8] would not achieve better agreement with experiment; it could only broaden the calculated peaks further. An attempt to replace eq. (4) by a WLF-type temperature dependence of τ did not improve the fit and led to unreasonable relaxation times in the glass transition regions. Equation (4), in contrast, leads to relaxation times of the order of magnitude expected[34] in the glass transition region. At the low-temperature end of the apparent heat-capacity peak the product $q\tau$ is usually about 200°C; at the peak temperature $q\tau$ has decreased to 2.0°C; and at the high-temperature foot of the apparent heat-capacity peak, $q\tau$ is about 0.2°C.

The activation energy has been derived through eq. (8) and is listed for each cooling rate in Table II and for each substance averages are listed in Table III. The standard deviation of ϵ_j for each cooling rate is 10–15%, with larger ϵ_j found preferentially at lower heating rates and smaller ϵ_j found at higher heating rate range. The average activation energies of Table III derived from varying cooling rates, covering three orders of magnitude show a standard derivation of 13%. Between the different materials there is a definite, close-to-linear relationship between magnitude of average activation energy and glass transition temperature; the higher T_g, the larger is ϵ_j.

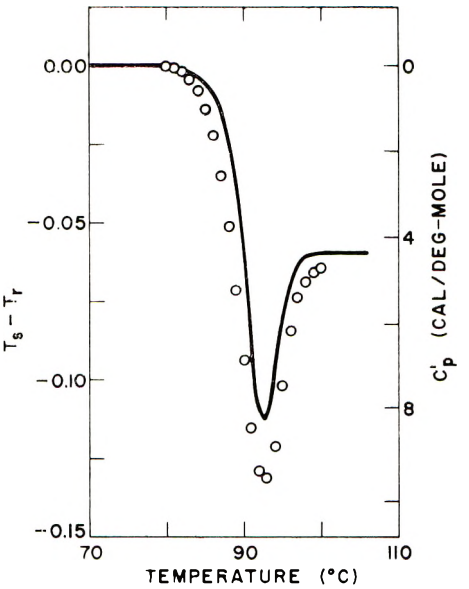

Fig. 8. Comparison of (——) a DTA curve and (O) apparent heat capacity values for PVC calculated by using eq. (6). Sample cooled at 0.083°C./min., heated at 30°C./min. Calculation based on $N^* = 4.56 \exp\{-1070/RT\}$, $\tau = (1.69 \times 10^{-49}/T) \exp\{83{,}900/RT\}$ $T_x = 367$°K. Temperature difference $T_s - T_r$ in °C.

A comparison of the average activation energies derived from different heat capacity measurements with those derived from mechanical and dielectric experiments in the same temperature range shows reasonable correspondence. For PMMA, Bueche[35] found from tensile creep experiments activation energies increasing from 125 to 210 kcal/mole in the temperature interval of 135–120°C which should be compared to the activation energy of 77 kcal/mole. Saito and Nakajima[36] made measurements of dielectric loss by a dc transient method. They found for PMMA at 125–120°C an activation energy of 105–95 kcal/mole. For PS the same authors found at 120–105°C an activation energy of 90–115 kcal/mole, compared to 90 kcal/mole found in this research. Dielectric loss measurements of Sommer[37] on PVC between 100 and 85°C led to an activation energy of 85–180 kcal/mole, compared to 81 kcal/mole. Finally, data on stress relaxation of amorphous selenium by Eisenberg and Tobolsky[38] between 53 and 40°C yielded activation energies between 50 and 65 kcal/mole, while the present study gave 54 kcal/mole. In general, then, the activation energies of dielectric and mechanical relaxation measurements agree reasonably well with ϵ_j. The hole model used for the description of the glass transition phenomena would distinguish between these two types of experiments as follows. The apparent heat capacity measurements are a measure of the establishment of a new hole equilibrium after a change in temperature on the transition region, while the dielectric and mechanical relaxation measurements are a measure of the isothermal rate of rearrangement of pre-existing holes fol-

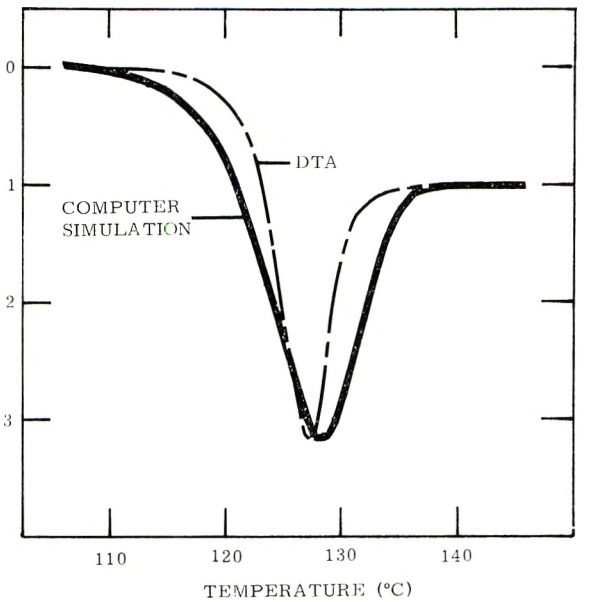

Fig. 9. Comparison of (- - -) a DTA curve and (——) apparent heat capacity for PMMA calculated by using eq. (6). Ordinate expressed in multiples of ΔC_p. Sample cooled at 0.0067°C/min, heated at 25°C/min. Calculation based on $N^* = 8.05 \exp\{-1150/RT\}$, $\tau = (1.52 \times 10^{-41}/T) \exp\{78{,}000/RT\}$, $T_x = 372$°K.

lowing an external disturbance. Since the two processes are related, the similarity in activation energies is gratifying.

The preexponential factor A is less suited for comparative discussion since it is obtained by a longer extrapolation of log Z to $1/T_p = 0$. Even small variations in slope lead to large fluctuations in A. Interpretation of A in terms of an activation entropy[21] requires a large positive value for the activation entropy. An activated state with a large positive activation entropy would have to involve a large number of mobile units in less dense packing than the average structure of the glass: Such a state is quite reasonable as an intermediate before hole formation.

Turning now to the particular glasses analyzed, the apparent heat capacity of glucose was analyzed by Ellerstein.[9] In his analysis he assumed that an "equilibrium" enthalpy H^* could be reached by cooling extremely slowly. This enthalpy H^* would be equal to the areas I + III in Figure 1. The kinetic parameters could then be obtained by determining point-for-point through the glass transition region:

$$C_p' = dH/dT = (H - H^*)^n/q\tau \qquad (12)$$

an equation similar to eq. (3), since $H - H^*$ should be proportional to $N - N^*$. For $n = 1$, τ has again the form of a relaxation time. Experimentally, Ellerstein found lower peak temperatures and activation energies for glucose. For example, on cooling at 0.625°C/min followed by heating

at 10°C/min. Ellerstein found a peak temperature of 32°C; a peak temperature of 43°C would be expected from this work. Corresponding activation energies are 33 kcal/mole, compared to 52 kcal/mole in this research. The explanation of this discrepancy is most likely the neglect of drying of the glucose before analysis by Ellerstein. Water is an effective plasticizer for glucose. In contrast to the glucose data, we find good agreement with Ellerstein's data on polystyrene: his activation energy of 99 kcal/mole corresponds favorably with our value of 90 kcal/mole.

Hentze[39] has shown that on long-time tempering of crystallizable polymers below the glass transition temperature, a second maximum in heat capacity develops on subsequent heating. This second maximum, which can coincide with the hysteresis maximum discussed here, has the properties of a first-order transition; it does not shift on measurement with different heating rates and also does not change its heat capacity peak area with heating rate. We found no indication of such a phenomenon, however, even our slowest heating rates may not have allowed sufficient time for such reorganization to occur. Similar claims of a latent heat of fusion by other authors[40–42] are less well documented and present most likely a wrong interpretation of the apparent heat capacity peaks presented here.

The effect of water on PMMA, as shown in Figure 3, is clearly that of a plasticizer. Only in the well-dried state is the peak temperature in the apparent heat capacity approximately linear with increasing log q. The changing slope of the samples containing water is most likely caused by the different degree of drying with varying heating rates. For this reason only data for dry samples are presented. Various ambient-condition results are tabulated elsewhere.[15] The data on the half-freezing temperature on cooling [eq. (9)] does not suffer from this difficulty since the samples are dried sufficiently in the molten region before cooling to the glass transition region.

The early measurements on polystyrene by Wunderlich et al.[8] agree well with the present experiments. In fact, some of their results were included in the data of Tables I and II. The activation energies quoted and their variation with cooling rate should be considered superseded by the present computations. Reasons for the small activation energies computed from the same data and the smaller variation with cooling rate were traced to the use of the uncorrected DTA peak heights in the earlier calculation and to the much smaller heating-rate available.

The selenium data must be interpreted in terms of the ring-chain equilibrium present in the melt before quenching. Literature data on ring concentration and number-average molecular weights of various authors are collected in Table IV. Assuming no chemical change to have occurred during quenching, each sample quenched from a different temperature should represent a chemically different entity. Figure 10 shows the peak temperatures as a function of the logarithm of heating rate of selenium samples quenched from four different temperatures and all cooled through the glass transition temperature at 0.028°C/min. Only the selenium quenched from

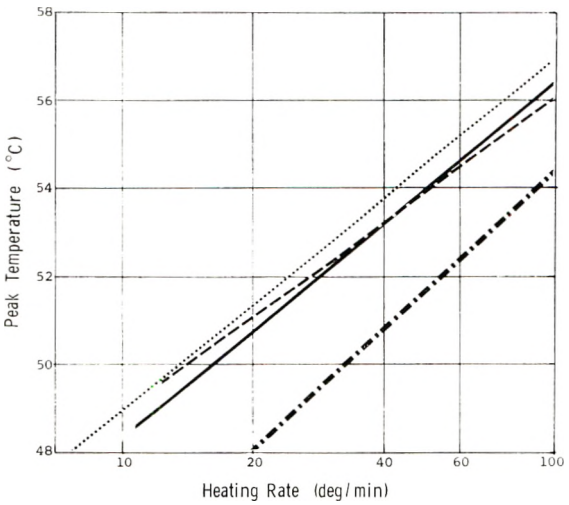

Fig. 10. Effect of melt temperature of selenium before quenching on the peak temperature of the apparent heat capacity on heating through the glass transition region at various rates. Melt temperatures before quenching: (- -) 235°C; (——) 350°C; (. . .) 525°C; (-·-) 900°C. After quenching, all samples were cooled at 0.028°C/min through the glass transition region to impart reproducible thermal history.

900°C shows a significant difference. A similar constancy in glass transition temperature on quenching between 270 and 500°C was shown by Eisenberg and Tobolsky.[47] One normally expects a decrease in glass transition temperature of polymers when the number of backbone chain atoms decreases below 800, a value probably only barely reached at 500°C, but certainly too high for the selenium melt at 900°C. Since the proportion of selenium rings also changes, one must conclude that rings and high molecular weight polymer have not too different glass transition temperatures. The lower glass transition region of the selenium quenched from 900°C could then be caused by a plasticizing of Se_8 rings by low molecular weight linear polymer.

TABLE IV
Glassy Selenium Structures

Quench temperature, °C	Ring concentration, wt-%[a]	Number-average chain length of polymeric selenium		
		b	c	d
235	62	210,000	—	98,000
350	74	34,000	—	9,000
525	86	(5,500)	(3,000)	160
900	(90)	—	(210)	—

[a] Data of Briegleb.[43]
[b] Data of Keezer and Bailey.[44]
[c] Data of Massen et al.[45]
[d] Data of Eisenberg.[46]

This research was supported by a grant from the National Aeronautics and Space Administration and by The Armstrong Cork Company.

References

1. A. Q. Tool and C. G. Eichlin, *J. Amer. Ceram. Soc.*, **14**, 276 (1931); *J. Res. Natl. Bur. Stand.*, **6**, 523 (1931).
2. G. S. Parks and S. B. Thomas, *J. Amer. Ceram. Soc.*, **56**, 1423 (1934).
3. A. G. Obald and R. F. Newton, *J. Amer. Chem. Soc.*, **59**, 2495 (1937).
4. R. O. Davies and G. O. Jones, *Proc. Roy. Soc.* (London), **A217**, 26 (1953).
5. A. Otsubo, T. Haseda, and E. Kanda, *Sci. Rep. Inst. Tohoku Univ.* **A2**, 216 (1955).
6. M. V. Vol'kenshtein and Yu. A. Sharanov, *Vysokomol. Soedin.*, **3**, 1739 (1961); *Sov. Phys. Solid State*, **5**, 429 (1963); *ibid.*, **6**, 992 (1964).
7. H. Martin and F. H. Müller, *Makromol. Chem.*, **75**, 75 (1964).
8. B. Wunderlich, D. M. Bodily, and M. H. Kaplan, *J. Appl. Phys.*, **35**, 95 (1964).
9. S. M. Ellerstein, *J. Phys. Chem.*, **69**, 2471 (1965); *Fourth Cellulose Conference* (*J. Polym. Sci. C*, **2**), R. H. Marchessault, Ed., Interscience, New York, 1964, p. 111.
10. M. Ikeda, *Kobunshi Kagaku*, **25**, 87 (1969).
11. E. B. Petrie, *Bull. Am. Phys. Soc.*, **14**, 424 (1969).
12. D. J. David, *Polym. Preprints*, **7**, 262 (1965) Phoenix, Ariz.
13. P. V. McKinney and C. R. Foltz, *J. Appl. Polym. Sci.*, **11**, 1189 (1967).
14. S. M. Wolpert and B. Wunderlich, Proceedings of the 3rd ICTA, Davos Switzerland Aug. 1971.
15. S. M. Wolpert, Thesis, Department of Chemistry, Rensselaer Polytechnic Institute, Troy, N. Y, 1970.
16. W. T. Richards, *J. Chem. Phys.*, **4**, 499 (1936).
17. R. O. Davies and G. O. Jones, *Adv. Phys.*, **2**, 370 (1953); *Proc. Roy. Soc.* (Loudon) **A217**, 26 (1953).
18. M. V. Vol'kenshtein and O. B. Ptitsyn, *Zh. Tekhn. Fiz.*, **26**, 2204 (1956); (Engl. Transl.) *Soviet Phys.-Tech. Phys.*, **1**, 2138 (1957).
19. H. Eyring, *J. Chem. Phys.*, **4**, 283 (1936).
20. J. Frenkel, *Kinetic Theory of Liquids*, Clarendon Press, Oxford, 1946.
21. S. Glasstone, K. J. Laidler, and H. Eyring, *The Theory of Rate Processes*, McGraw-Hill, New York, 1941.
22. N. Hirai and H. Eyring, *J. Appl. Phys.*, **29**, 810 (1958); *J. Poly . Sci.*, **37**, 51 (1959).
23. R. F. Boyer, *Rubber Chem. Technol.*, **36**, 1303 (1963).
24. M. G. Goldstein, *J. Chem. Phys.*, **39**, 3369 (1963).
25. M. G. Goldstein, in *Modern Aspects of the Vitreous State*, J. D. Mackenzie, Ed., Vol. 3, Butterworths, Washington, 1964.
26. M. C. Shen and A. Eisenberg, in *Progress in Solid State Chemistry*, H. Reiss, Ed., Vol. 3, Pergamon Press, Oxford, 1966.
27. B. Wunderlich and D. M. Bodily, in *Thermal Analysis of High Polymers* (*J. Polym. Sci. C*, **6**), B. Ke, Ed., Interscience, New York, 1964, p. 137.
28. L. E. Rademacher, private communication (1968).
29. F. E. Karasz, H. E. Bair, and J. M. O'Reilly, *J. Polym. Sci. B*, **3**, 561 (1965).
30. B. Wunderlich, *J. Phys. Chem.*, **64**, 1052 (1960).
31. S. M. Wolpert and B. Wunderlich, to be submitted.
32. B. Wunderlich and H. Baur, *Fortschr. Hochpolym. Forsch.*, **7**, 151 (1970).
33. B. Wunderlich and L. D. Jones, *J. Macromol. Sci.-Phys.*, **B3**, 67 (1969).
34. W. Kauzmann, *Chem. Rev.*, **43**, 219 (1948).
35. F. Bueche, *J. Appl. Phys.*, **26**, 738 (1955).
36. S. Saito and T. Nakajima, *J. Appl. Polym. Sci. A*, **2**, 93 (1959).
37. W. Sommer, *Kolloid Z.*, **167**, 97 (1959).
38. A. Eisenberg and A. V. Tobolsky, *J. Polym. Sci.*, **61**, 483 (1962).

39. G. Hentze, *Kolloid-Z. Z. Polym.*, **231**, 434, 617 (1969).
40. E. W. Merrill and D. A. Gibbs, *Chem. Eng. News*, **41**, 41 (Sept. 23, 1963).
41. P. V. McKinney and C. R. Foltz, *J. Appl. Polym. Sci.*, **11**, 1189 (1967).
42. M. I. Kashmiri and R. M. Holsworth, *J. Paint Technol.*, **41**, 167 (1969).
43. G. Briegleb, *Z. Physik. Chem.*, **A144**, 321, 340 (1929).
44. R. C. Keezer and M. W. Bailey, *Mater. Res. Bull.*, **2**, 185 (1967).
45. C. H. Massen, A. G. L. M. Weijts, and J. A. Poulis, *Trans. Faraday Soc.*, **10**, 317 (1964).
46. A. Eisenberg, *J. Polym. Sci. B*, **1**, 33 (1963).
47. A. Eisenberg and A. V. Tobolsky, *J. Polym. Sci.*, **46**, 19 (1960).

Received February 8, 1971
Revised March 26, 1971

NOTES

On the Determination of Polymer Crystallinities from Thermal Measurements

In two recent papers, a general method of determining the absolute crystallinities of polymer samples without isolation or prior characterization of either the crystalline or amorphous phases is proposed.[1,2] It is assumed that a given polymer can be described by a two-phase model in which the heat capacities of the amorphous and crystalline phases are additive and in which the measured enthalpies are proportional to the mass fractions of crystalline material, that is,

$$mC^{b} = m_{c}C_{c} + m_{a}C_{a}^{b} \tag{1}$$

$$mC^{s} = m_{c}C_{c} + m_{a}C_{a}^{s} \tag{2}$$

and

$$m^{s} = \Delta H/\Delta H_{f} \tag{3}$$

where C is the measured heat capacity, ΔH is the measured heat of fusion, ΔH_f is the heat of fusion of completely crystalline polymer, the subscripts c and a refer to the pure crystalline and amorphous phases, and the superscripts b and s to data taken above and below the glass temperature, T_g. For two samples of the same weight it is shown algebraically that the respective masses of crystalline and amorphous material in each are given by equations of the form

$$m_{c_1} = mA(1 - B)/(A - B) \tag{4}$$

$$m_{a_1} = mB(A - 1)/(A - B) \tag{5}$$

where

$$A = (\Delta H_1 - \Delta H_{c_1})/(\Delta H_2 - \Delta H_{c_2})$$

$$B = (C_1^{s} - C_1^{b})/(C_2^{s} - C_2^{b})$$

and the subscripts 1 and 2 designate the samples. Thus, the technique requires only calorimetric measurements of the heat capacities of two samples of different, but unspecified, crystallinities above and below T_g and of their heats of crystallization and fusion.

The apparent simplicity of this experiment makes it appear attractive for the determination of the absolute crystallinities of many polymers in which poor solubility, unknown crystal structure, or overlapping melting and degradation temperatures make traditional calorimetric, dilatometric, and diluent techniques unacceptable.

The experiments described below were carried out on commercial poly(ethylene terephthalate), $[\eta]^{22°C} = 0.62$. The polymer can be readily quenched or crystallized to various degrees and, in the amorphous state, shows a large heat capacity change at T_g. Furthermore, it appeared that PET with its relatively stiff, sterically hindered chains would provide a material of good structural contrast to the polymers which had been investigated (polydimethylsiloxane and polybutadiene). Finally, published density and heat of fusion data offered viable alternate methods of determining sample crystallinities.

Samples of PET were crystallized from the melt by slow cooling to various levels of crystallinity. In each case densities were measured in an H_2O–KI density-gradient column to ± 0.001 g/cm^3. Th heat capacity and enthalpy data were taken on a Perkin-Elmer DSC-1b differential scanning calorimeter. Scans were made at 20°C/min over a temperature range of −80°C to 300°C. Sapphire calibration standards were used to determine the absolute heat capacities of the samples and the linearity of the DSC traces. Heats of crystallization and fusion were determined graphically, and the heat capacity changes at T_g were calculated by extrapolation as described by Yagfarov.[2] After melting, each sample was quenched in liquid nitrogen and rerun to determine $\Delta C_p(T_g)$ for the amorphous material. The identical values obtained for the heats of crystallization and fusion in the quenched specimens showed that such quenching provided completely amorphous samples.

Initially, the mass-fraction crystallinity m_c was calculated for several samples directly from the enthalpy and density data by using the eqs. (3) and (6).

$$m_c = \rho_c(\rho - \rho_a)/[\rho(\rho_c - \rho_a)] \tag{6}$$

Since at least two sets of crystalline and amorphous densities and several heats of fusion for the perfectly crystalline polymer were available, the calculations were carried out for different published values. The calculated crystallinities appear in Table I.

TABLE I
Comparative Mass-Fraction Crystallinities Calculated from Enthalpy, Density, and Heat Capacity Data

	Sample 1	Sample 2	Sample 3	Sample 4
ΔH, cal/g (measured)	0.71	4.8	7.3	9.3
ρ, g/cm^3 (measured)	1.338	1.357	1.363	1.385
m_c [from eq. (3)]				
ΔH_f = 30.0 cal/g[a]	0.02	0.16	0.24	0.31
ΔH_f = 20.7 cal/g[b]	0.03	0.23	0.36	0.45
ΔH_f = 28.1 cal/g[c]	0.02	0.17	0.26	0.34
ΔH_f = 11.5 cal/g[d]	0.06	0.42	0.64	0.81
ΔH_f = 30.7 cal/g[e]	0.02	0.16	0.24	0.30
m_c [from eq. (6)]				
ρ_c = 1.455 g/cm^3[f]; ρ_a = 1.335 g/cm^3[f]	0.02	0.14	0.18	0.32
ρ_c = 1.498 g/cm^3[g]; ρ_a = 1.337 g/cm^3[g]	0.01	0.20	0.25	0.41
m_c[h]	0.07	0.39	0.46	0.77

[a] Data of Dole.[3]
[b] Data of Rybnikar.[4]
[c] Data of Smith and Dole.[5]
[d] Data of Edgar and Ellery.[6]
[e] Data of Kirshenbaum.[7]
[f] Data of Daubeny et al.[8]
[g] Data of Kilian et al.[9]
[h] Method of Yagfarov.[2]

Of the literature values those of Smith and Dole[6] and of Daubeny, et al.[8] are probably the most accurate and widely accepted. The data of Edgar and Ellery[6] and Rybnikar[4] are obtained from copolymer data by using Flory's theory[10] and are almost certainly too

low because of the neglect of high surface free energies resulting from small crystallite size.

The values in the last section of Table I were calculated from the measured heat capacities and enthalpies by using Yagfarov's method. Significantly, the m_c values calculated in this way are almost twice those calculated from the best density and enthalpy data. This is in sharp contrast to the results reported for polydimethylsiloxane and polybutadiene. Since generally good agreement in m_c values calculated independently from density, enthalpy, and x-ray studies has been found,[11] the above discrepancies suggest that the additive, two-phase model employed in such calculations cannot be generally extended to describe variations in $\Delta C_p(T_g)$ with m_c as has been proposed. Yagfarov's statement[2] that the lack of two-phase additivity does not affect the accuracy of his method is, in fact, contradicted by his original assumptions. The nonlinear variation in $\Delta C_p(T_g)$ with m_c has been reported elsewhere in the literature.[12-15]

Wunderlich has shown for polyethylene that the heat capacities of samples of different crystallinity show increasing deviations from additivity with increasing temperatures above T_g and with decreasing crystallinity.[12,13] The behavior has been ascribed to changes in the defect structure of crystalline regions and is manifested primarily as a change in slope in the C_p versus T curve. It has also been noted for BPA polycarbonate[14] and for poly(ethylene terephthalate)-sebacate copolymers[15] that the heat capacity changes at T_g are not linearly proportional to the observed crystallinities of these materials. Würstlin[16] has suggested that in these cases, at low levels of crystallinity, microcrystallites may restrict the length and mobility of the amorphous segments and reduce ΔC_p at T_g. If such an analysis is correct, one would expect a rise in T_g, although no such effect was observed in our work. It seems certain, however, that when even small amounts of crystalline material are present in PET, mobility in the amorphous regions is severely restricted. A comparison of this polymer with polydimethylsiloxane and polybutadiene suggests that this effect may be substantially magnified by increased chain stiffness and steric requirements. Experiments to determine the dependence of $\Delta C_p(T_g)$ on chain flexibility in other aromatic polyesters are planned.

In conclusion, it appears that the technique of determining polymer crystallinities by using the combination of heat capacity and enthalpy data is not generally applicable and can give very large errors in some polymer systems. Unfortunately, it is not clear from Yagfarov's work that his method is even acceptable for PDMS and polybutadiene since no attempt is made to cross-correlate his m_c values with those calculated by alternate methods. Until this is done, the reliability of these studies is in serious doubt.

References

1. M. Sh. Yagfarov, *Vysokomol. soedin.*, **A10**, 1267 (1968).
2. M. Sh. Yagfarov, *Vysokomol. soedin.*, **A11**, 1195 (1969).
3. M. Dole, *J. Polym. Sci.*, **19**, 347 (1956).
4. F. Rybnikar, *Chem. Listy*, **52**, 1042 (1958).
5. C. W. Smith and M. Dole, *J. Polym. Sci.*, **20**, 37 (1956).
6. O. B. Edgar and E. Ellery, *J. Chem. Soc.*, **1952**, 2633.
7. I. Kirshenbaum, *J. Polym. Sci. A*, **3**, 1869 (1965).
8. R. DeP. Daubeny, C. W. Bunn, and C. J. Brown, *Proc. Roy. Soc.* (London), **A226**, 531 (1954).
9. H. G. Kilian, H. Haboth, and E. Jenckel, *Kolloid-Z.*, **172**, 166 (1960).
10. P. J. Flory, *J. Chem. Phys.*, **17**, 223 (1949).
11. F. W. Billmeyer, *Textbook of Polymer Science*, Interscience, New York, 1966, p. 1962.
12. B. Wunderlich, P. Sullivan, T. Arakawa, A. B. Dievan, and J. F. Flood, *J. Polym. Sci. A*, **1**, 3581 (1963).
13. B. Wunderlich and H. Baur, *Fortschr. Hoch. Forsch.*, **7**, 151 (1970).

14. J. M. O'Reilly, F. E. Karasz, and H. E. Bair, in *Thermal Analysis of High Polymers* (*J. Polym. Sci. C*, **6**), B. Ke, Ed., Interscience, New York, 1963, p. 109.
15. M. Dole, *Kolloid-Z.*, **165**, 40 (1959).
16. H. A. Stuart, *Die Physik der Hochpolymeren*, Berlin-Göttingen-Heidelberg, 1955, p. 648.

S. Y. Hobbs
G. I. Mankin

Polymer Chemistry Branch
Research and Development Center
General Electric Company
Schenectady, New York 12301

Received February 5, 1971
Revised April 5, 1971

Concentration of Radicals in γ-Irradiated Poly(ethylene Terephthalate)

Several earlier ESR studies of γ-irradiated poly(ethylene terephthalate) (PET) have been reported,[1–8] and at least two radical species have been identified.[7,8] Two major products of radiation damage are radicals I and II.

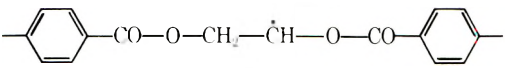

Radical I

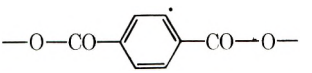

Radical II

Radical II can be separated from radical I by heat treatment at 150°C, where radical I decays. The relative concentrations of these radicals were of interest as part of a study concerned with the relative stability of polymers to ionizing radiation.

Previously it was reported[4,8] that radical I constitutes 95% of the radical concentration in the crystalline regions of biaxially oriented PET film. Radical II and an unidentified

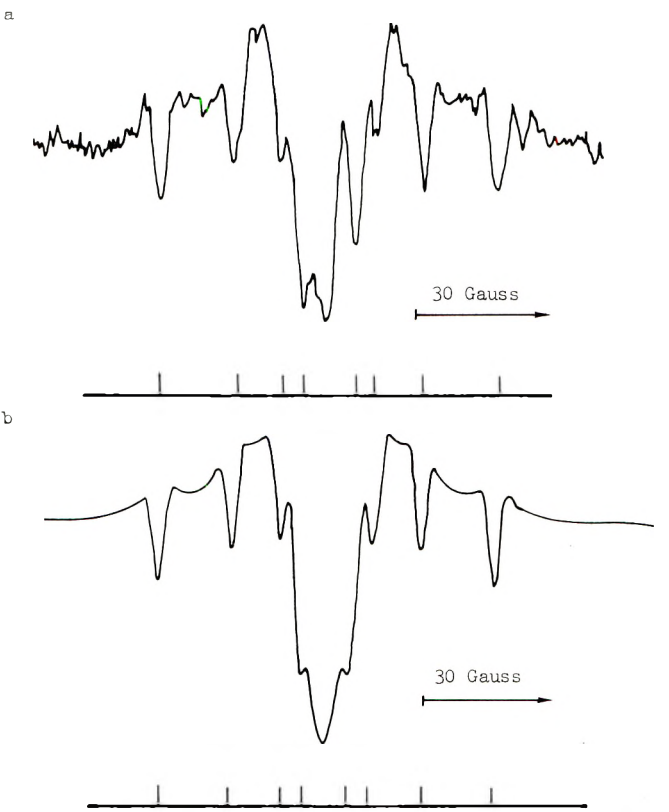

Fig. 1. Second-derivative ESR spectrum of γ-irradiated PET with surface of film perpendicular to H_0: (*a*) observed; (*b*) computer-generated.

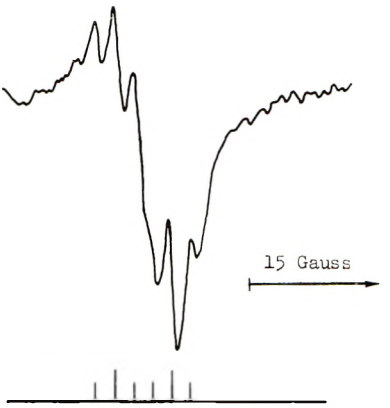

Fig. 2. ESR spectrum of PET after heating sample at 150°C. Surface of film perpendicular to H_0.

radical (radical III) accounted for the remaining 5%. Measurements at this laboratory indicate that radical I accounts for only 1–2% of all radicals in the gross polymer. For a polymer approximately 50% crystalline these results imply vastly different trapping efficiencies (G values) for the amorphous and crystalline regions.

All the samples were prepared from biaxially oriented film (duPont Mylar; crystallinity 40–50%) of 1 mil thickness (2.54×10^{-3} cm) which was cut into strips and placed in quartz tubes and then evacuated at 10^{-6} torr for 12 hr. The samples were then sealed in the tubes under vacuum and exposed to γ-radiation from a ^{60}Co source at a dose rate of 1.6 Mrads/hr at 35°C. Total doses ranged from 5 to 100 Mrads. ESR spectra of the irradiated samples were obtained with a Varian V4502 ESR spectrometer.

A second-derivative absorption spectrum of γ-irradiated film (dose = 30 Mrads) is shown in Figure 1*a*. The spectrum was obtained with the surface of the film perpendicular to the external magnetic field H_0. The spectrum consists of eight lines due to radical I and a single broad component superimposed on the eight lines. The splittings for the eight lines are 17, 29, and 34 gauss as previously reported.[8] Figure 1*b* is the computed spectrum, which was calculated by superimposing the idealized spectrum of radical I with its eight lines of equal intensity and a spectrum consisting of one broad line due to radical II with unresolved hyperfine structure. The slight discrepancy between the observed and computer-generated spectrum is probably due to a trace of unidentified radicals, possibly radical III.

Since computer simulation indicated that the spectrum is largely a superposition of eight lines from radical I and a broad central peak from radical II, the relative concentrations of the two radicals were obtained by double integration of the first-derivative spectrum. The total concentration was obtained from the integrated intensity of the entire spectrum and the concentration of radical I was measured from the integrated intensity of one of the outer lines of the octet. The octet signal from radical I accounted for 1–2% of the total integrated intensity.

The double integration was performed numerically by a method which approximates the first moment of the first-derivative spectrum and involves an error of less than 5%.[9] Since only relative concentration measurements were made, none of the experimental difficulties associated with absolute concentration measurements were encountered; and care was taken to avoid saturation of one radical species at the expense of another.

When the sample of Figure 1 was heated at 150°C for 1 hr, the spectrum in Figure 2 was observed with the film surface perpendicular to H_0. At other orientations, no hyperfine structure was observed and only a singlet with halfwidth of about 20 gauss was observed. This spectrum is probably due to radical II trapped in the oriented crystalline

regions of the polymer (the radicals in the amorphous regions presumably decaying at 150°C) and consists of six lines with splittings of 5 and 15 gauss.

Radical II has also been observed in samples exposed to low doses of γ-radiation (6–10 Mrad). Figure 3 shows a spectrum of PET film exhibiting no trace of radical I

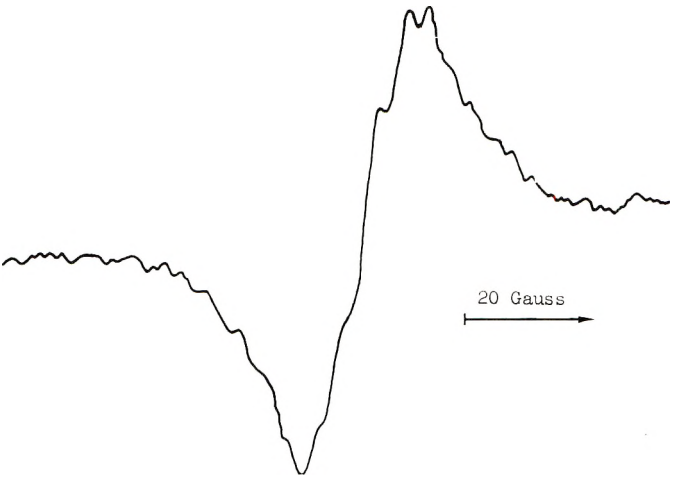

Fig. 3. ESR spectrum of PET after a dose of 6 Mrads. Surface of film perpendicular to H_0.

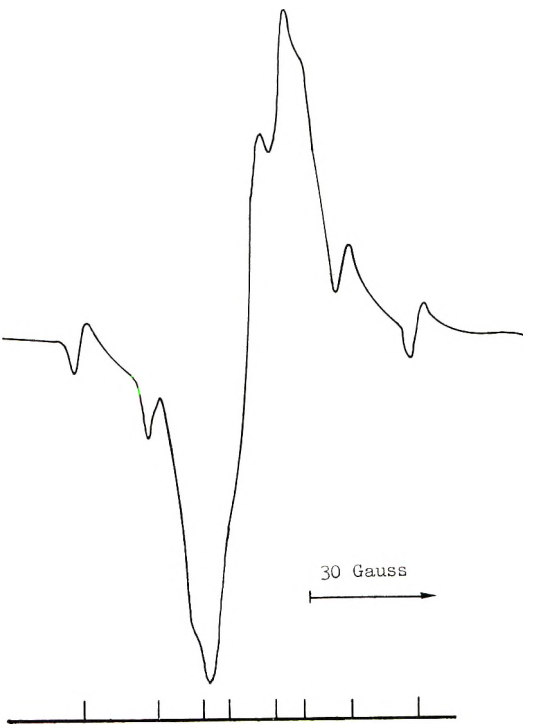

Fig. 4. Observed spectrum of PET after a total dose of 50 Mrads. Surface of film perpendicular to H_0.

after a dose of 6 MRad. This first-derivative spectrum was obtained with the surface of the film perpendicular to H_0. In this sample, as opposed to the heat-treated sample of Figure 2, there is a large concentration of radical II in the amorphous regions of the polymer where the radicals are randomly oriented. Thus the hyperfine structure was not resolved even in the perpendicular orientation. The fact that no signal was detected from radical I at this low dose implies different trapping efficiencies for amorphous and crystalline regions, an observation which has been previously reported.[10]

Upon further exposure to γ-radiation (dose >50 Mrads) the spectrum of Figure 4 was obtained. Here the eight-line spectrum of radical I is present but its concentration does not exceed 2%.

If radical I accounts for 90% of the radicals in the crystalline regions and radical II accounts for 98% of the radicals in the gross polymer, then the logical consequence of there results is that radical I is contained almost exclusively in crystalline regions and radical II almost exclusively in amorphous regions. Previous results have indicated that radical II is the most abundant species in amorphous regions.[4] However, another implication is that the G values for the amorphous regions are at least an order of magnitude larger than for the crystalline regions. Slight differences of G values at low doses have been reported; however such large differences have not been observed.[10]

The author is indebted to N. T. Wakelyn for providing the values for the degree of crystallinity.

References

1. S. Ohmiski, Y. Ikeda, M. Kashiwagi, and I. Natta, *Polymer*, **2**, 119 (1961).
2. Z. Kuri and H. Ueda, *J. Polym. Sci.*, **50**, 349 (1961).
3. Y. Hama, S. Okamoto, and N. Tamura, *Repts. Progr. Polym. Phys. Japan*, **7**, 351 (1964).
4. D. Campbell and D. T. Turner, *J. Polym. Sci. A-1*, **5**, 2199 (1967).
5. J. Sobue, Y. Tabata, and M. Hiroaka, *Kogyo Kagaku Zasshi*, **64**, 372 (1961).
6. J. R. Chapman, Ph.D. Thesis, Vanderbilt Univ., 1967.
7. K. Araki, D. Campbell, and D. T. Turner, *J. Polym. Sci. B*, **3**, 993 (1965).
8. D. Campbell, K. Araki, and D. T. Turner, *J. Polym. Sci. A-1*, **4**, 2597 (1966).
9. S. J. Wyard, *J. Sci. Instr.*, **42**, 769 (1965).
10. D. Campbell, L. K. Montieth, and D. T. Turner, *J. Polym. Sci. A-1*, **8**, 2703 (1970).

Robert S. Rogowski

NASA, Langley Research Center
Hampton, Virginia 23365

Received November 30, 1970
Revised March 25, 1971

Effect of Halogen Ring Substitution and Crazing on the Polystyrene δ Peak

INTRODUCTION

Polystyrene exhibits a small pronounced low temperature dynamic mechanical damping peak known as the δ peak. For atatic polystyrene this peak has been reported by a number of workers in the 35–50°K region,[1–5] depending on frequency. In addition, the dielectric properties of polystyrene and some polychlorostyrenes in this temperature region have been reported,[6] in which a dielectrically active peak is found in the same position as the mechanical peak for polystyrene. This does suggest some motion of the slightly dipolar phenyl groups. The latter workers also found that poly-*p*-chlorostyrene exhibited a more intense dielectric absorption peak than polystyrene in the same temperature region, which indicates the phenyl group is at least undergoing a wagging motion, but does not eliminate the possibility of a torsional motion as well.

To obtain further insight into the molecular motion involved in this temperature region we have investigated the dynamic mechanical properties of poly-*p*-chlorostyrene and poly-*p*-bromostyrene and the corresponding *meta* compounds from 4 to 250°K. In these polymers the inertia and/or the molecular environment of the phenyl side group will be different from that in polystyrene. A highly crazed sample of polystyrene was also investigated to observe the effect of crazes on the δ peak.

Experimental and Results

The four polyhalostyrenes were produced by thermal polymerization. These polymers were purified by precipitation from benzene solution by methanol addition. After drying they were redissolved in benzene and then freeze-dried. Polymer specimens were molded between plates on a press and then allowed to cool slowly form 40°C above their T_g to minimize thermal stresses. The crazed polystyrene sample was prepared by immersion in methanol for one week. It was then removed, wiped dry and then dipped in commercial hexane (Skelly solvent B) for a second, removed, and the solvent was allowed to evaporate off.[6]

The freely vibrating reed apparatus was used to determine the dynamic mechanical properties of these polymers; the experimental procedure is similar to that described in a previous publication.[1]

The results are shown in Figures 1–3. The two poly-*p*-halostyrenes have an absorption peak in the 40–43°K temperature range (Figs. 1 and 2) (ca. 5 cps), similar to polystyrene. (It should be noted that δ peaks are broad flat peaks, hence the exact positions of T'_{max} are difficult to determine very accurately.) There does, however, appear to be no significant shift in the position of the δ peak. The intensities of these peaks and the general backgrounds below 100°K are similar for all three polymers with the exception of the polystyrene peak[4] which is 5/3 times higher than the other two peaks. The latter exception may be due to different polymerization conditions in producing this polymer, resulting in a slightly different microstructure.[3] When the position of the chlorine or bromine atom is shifted from the *para* to the *meta* position on the phenyl ring the damping peaks are shifted to the 10–15°K (ca. 5 cps) temperature range (Figs. 1 and 2) (this is in agreement with reported dielectric peak positions of the polychlorostyrenes[6]), and their intensities and the corresponding general background are a factor of, two to three times lower. (The other undulations in the damping background can be associated with experimental scatter with the exception of a small peak at 90°K for poly-*p*-bromostyrene.) In addition, the latter two polymers have a higher modulus at 4°K than the poly-*p*-halostyrenes and polystyrene, indicating better packing. The intensity of the δ peak at 37°K (6.9 cps) for crazed polystyrene is 20% lower than that of uncrazed polystyrene. In addition it should be noted that for each peak there is an associated drop in modulus on the low temperature side.

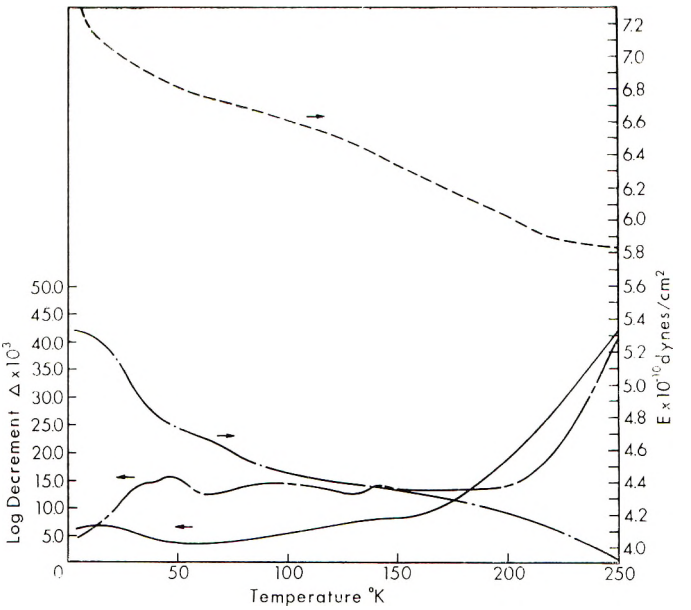

Fig. 1. Logarithmic decrement for poly-*p*-chlorostyrene (— - —) and (——) poly-*m*-chlorostyrene and Young's modulus for (- -) poly-*p*-chlorostyrene and (--) poly-*m*-chlorostyrene as functions of temperature.

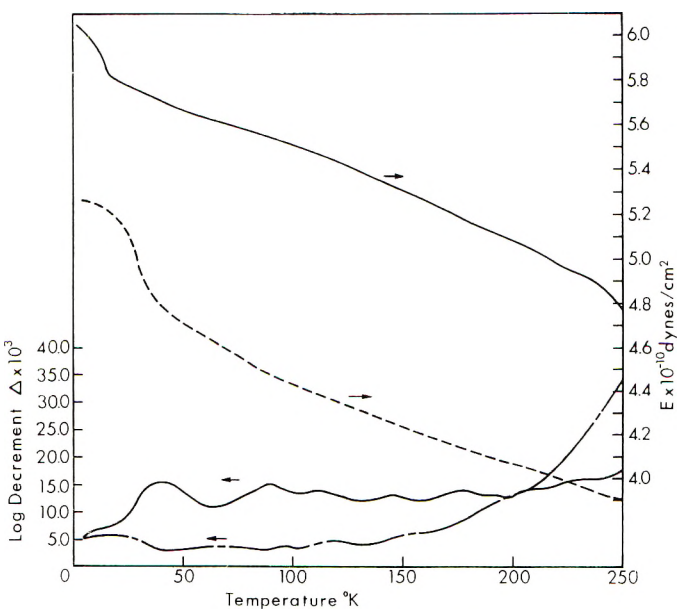

Fig. 2. Logarithmic decrement for (——) poly-*p*-bromostyrene and (— - —) poly-*m*-bromostyrene and Young's modulus for (–) poly-*p*-bromostyrene and (——) poly-*m*-bromostyrene as functions of temperature.

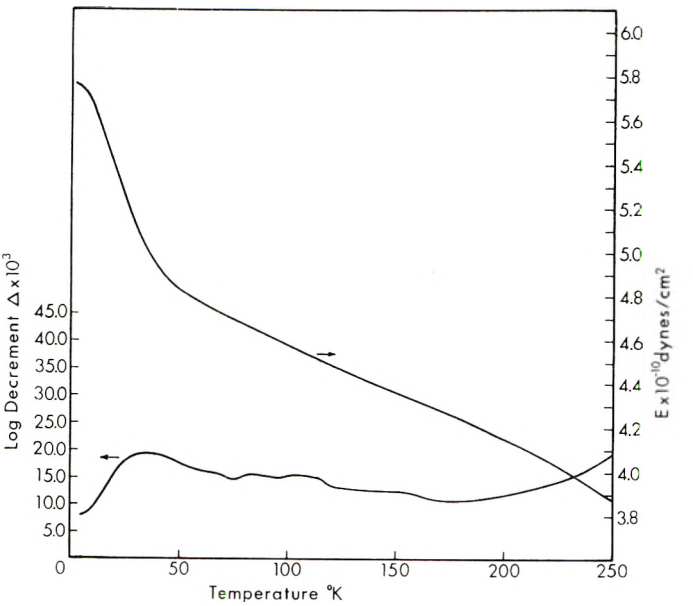

Fig. 3. Logarithmic decrement and Young's modulus for crazed polystyrene as functions of temperature.

Discussion

The δ peak position with halogen substitution has been explained by the coupling of the torsional and wagging modes of the phenyl ring.[7] However, birefringence measurements on SBR elastomers indicate that torsional oscillations of the phenyl side groups are even severely restricted at room temperature.[8] If such motions take place at such low temperatures, therefore, it would seem plausible that they occur at a few defect points in the amorphous matrix where free volume is available. This would explain the relatively low intensity of the δ peak. In addition, the authors have shown that only a very small number of toluene molecules need be present in the matrix to eliminate the δ peak completely,[9] again indicating motion at defect points. To identify a particular absorption peak with a certain type of defect within the material would be an extremely difficult task and would require a detailed knowledge of the chain conformations, tacticity, and packing. Data are available in the literature on the chain dimensions of some of the polyhalostyrenes; however, there is unfortunately little agreement among dipole moment, light scattering, viscosity,[10] and also birefringence[11] measurements in dilute solutions. The nature of the molecular mechanism causing energy absorption at these defect points can have a number of possible explanations from the known facts in addition to that suggested by McCammon, et al.:[7] (1) the breaking of intermolecular forces prior to phenyl group motion; (2) wagging of phenyl side group independently of main chain; and (3) cooperative small main chain–phenyl side group motions. The first two mechanisms seem unlikely, as the position of the δ peak on the temperature scale does not appear to be noticeably shifted for the styrene, *p*-chlorostyrene, and *p*-bromostyrene polymer series, where the intermolecular forces and the phenyl wagging inertia are both modified. Hence the third proposal seems more likely with the energy absorption process primarily occurring in the main chain and the motion of the phenyl side group a secondary effect, as doubling the mass of the latter has no significant effect on the temperature position of the peak. The energy absorption process could be similar to that described by Anderson and Bommel[12] to explain the 35°K (66,000 cps) peak in

fused silica, in which it is assumed there are two nearly equivalent states near the minimum energy conformation of the main chain bond, and a stress wave will bias one of the states with respect to the other causing a lag in returning to the equilibrium ratio.

The lowering of the intensity of the δ peak with crazes could be explained by the fact that orientation of polystyrene[3] reduces the δ peak intensity. Hence it is reasonable to assume that oriented material within the crazes, where primarily the stress will be concentrated, is responsible for the decreased intensity. However it should be noted that solvent crazing may leave residual solvent in the polymer, which could easily decrease the intensity of the δ peak.[9]

We would like to thank Dr. Ray Wetton for supplying us with the polyhalostyrenes.

This work was supported by Advanced Research Projects Agency Contract No. N00014-67-C-0218, under Office of Naval Research.

References

1. K. M. Sinnott, *J. Appl. Phys.*, **29**, 1433 (1958).
2. J. M. Crissman and R. D. McCammon, *J. Acoust. Soc. Am.*, **34**, 1703 (1962).
3. V. Frosini and A. E. Woodward, *J. Polym. Sci. A-2*, **7**, 525 (1969).
4. R. Buchdahl, R. J. Morgan, and L. E. Nielsen, *Rev. Sci. Instr.*, **41**, 1342 (1970).
5. S. Miller III, M. Tomozawa, and R. K. MacCrone, *Physics of Non-Crystalline Solids, III*, Sheffield, Oct., 1970.
6. L. E. Nielsen, *J. Appl. Polym. Sci.*, **1**, 24 (1959).
7. R. D. McCammon, R. G. Saba, and R. N. Work, *J. Polym. Sci. A-2*, **7**, 1721 (1969).
8. R. J. Morgan, Ph.D. Thesis, Manchester University, 1968.
9. R. J. Morgan, L. E. Nielsen, and R. Buchdahl, in preparation.
10. T. M. Birshtein and O. B. Ptitsyn, *Conformation of Macromolecules*, Interscience, New York, 1966, pp. 10, 14.
11. M. V. Volkenstein, *Conformational Statistics of Polymeric Chains*, Interscience, New York, 1963, p. 430.
12. O. L. Anderson and H. E. Bommel, *J. Ceramic Soc.*, **38**, 125 (1955).

R. J. Morgan
L. E. Nielsen
R. Buchdahl

Materials Research Laboratories
Washington University
St. Louis, Missouri 63130

Received February 15, 1971
Revised April 2, 1971

The *Journal of Polymer Science* publishes results of fundamental research in all areas of high polymer chemistry and physics. The *Journal* is selective in accepting contributions on the basis of merit and originality. It is not intended as a repository for unevaluated data. Preference is given to contributions that offer new or more comprehensive concepts, interpretations, experimental approaches, and results. Part A-1 *Polymer Chemistry* is devoted to studies in general polymer chemistry and physical organic chemistry. Contributions in physics and physical chemistry appear in Part A-2 *Polymer Physics*. Contributions may be submitted as full-length papers or as "Notes." Notes are ordinarily to be considered as complete publications of limited scope.

Three copies of every manuscript are required. They may be submitted directly to the editor: For Part A-1, to C. G. Overberger, Department of Chemistry, University of Michigan, Ann Arbor, Michigan 48104; and for Part A-2, to T. G Fox, Mellon Institute, Pittsburgh, Pennsylvania 15213. Three copies of a short but comprehensive synopsis are required with every paper; no synopsis is needed for notes. Books for review may also be sent to the appropriate editor. Alternatively, manuscripts may be submitted through the Editorial Office, c/o H. Mark, Polytechnic Institute of Brooklyn, 333 Jay Street, Brooklyn, New York 11201. All other correspondence is to be addressed to Periodicals Division, Interscience Publishers, a Division of John Wiley & Sons, Inc., 605 Third Avenue, New York, New York 10016.

Detailed instructions on preparation of manuscripts are given frequently in Parts A-1 and A-2 and may also be obtained from the publisher.

Selected Titles for the Polymer Scientist

REAGENTS FOR ORGANIC SYNTHESIS

Volumes 1, 2, and 3

VOLUME 1—*By LOUIS F. FIESER and MARY* FIESER, *both of Harvard University*

"*Reagents for Organic Synthesis* is well on the way to becoming the reference book of choice for everyone concerned with techniques of synthesis in organic chemistry."—*Science*

1967 1,457 pages illus. $29.00

VOLUME 2—*By* MARY FIESER *and* LOUIS F. FIESER

"Volume 2 . . . should be added to the library of anyone involved In chemical, physical, or biological research."

. . *American Journal of Pharmaceutical Education*

1969 538 pages Illus. $17.50

When Volumes 1 and 2 are purchased together, the set price is $40.00

VOLUME 3—*By* MARY FEISER *and* LOUIS F. FIESER

1971 832 pages (approx.) illus. In Press

TECHNIQUES OF POLYMER SYNTHESES AND CHARACTERIZATION

Second Edition

By DIETRICH BRAUN, *Deutsches Kunststoff-Institute,* HAROLD CHERDRON, *Farbwerke Hoechst AG Kunststoff-Forschung, and* WERNER KERN, *Organisch-Chemisches Institut der Univ. Mainz*

Techniques of Polymer Syntheses and Characterization includes detailed descriptions of almost 100 well worked-out experiments, with their accompanying theoretical interpretation. As such, it enables the reader to learn about syntheses, reactions, and characterizations of macromolecular substances within the framework of studying preparative organic chemistry at the post-graduate level.

1971 300 pages (approx.) $17.95

MACROMOLECULAR REVIEWS

Volumes 4 & 5

Edited by A. PETERLIN, *Research Triangle Institute, North Carolina;* M. GOODMAN, *Polytechnic Institute of Brooklyn;* S. OKAMURA, *Kyoto University, Japan;* B. H. ZIMM, *Revelle College, La Jolla, California; and* H. MARK, *Polytechnic Institute of Brooklyn*

Continuing the theme of the first three volumes in the series, Volumes 4 and 5 present outstanding reviews of Important topics in polymer science. These topics reflect the most recent advancements in the field. However, Volumes 4 and 5 differ from the earlier volumes In that they have a soft binding and comprise Part D of the *Journal of Polymer Science,* with Board of Editors: H. Mark, C. G. Overberger, and T. G. Fox.

Volume 4: 1970 345 pages 17.50

Volume 5: 1971 325 pages (approx.) In Press

POLYMER STABILIZATION

Edited by W. LINCOLN HAWKINS, *Bell Telephone Laboratories, Inc., Murray Hill, New Jersey*

"The primary purpose of this book is to present a fundamental approach to the stabilization of polymers. In the chapters that follow, stabilization is discussed as it relates to each of the principal factors responsible for polymer deterioration."—*from the Preface*

1971 448 pages (approx.) 113 illus. $24.95

ORGANIC PEROXIDES

Volumes 1 and 2

Edited by DANIEL SWERN, *Temple University*

VOLUME 1—

". . . this first volume is a well-integrated, masterful work. . . There is no other recent published work in the field to which this volume can be compared."—*Choice*

1970 654 pages 70 illus. $31.50

VOLUME 2—

CONTENTS AND CONTRIBUTORS: *Hydroperoxides* —R. Hiatt. *The Chemistry of Hydroperoxides in the Presence of Metal Ions*—G. Sosnovsky and D. J. Rawlinson. *Metal Ion-Catalyzed Reactions of Hydrogen Peroxide and Peroxydisulfate*—G. Sosnovsky. *Formation of Organometallic Peroxides by Autoxidation*—Alwyn G. Davies. *Organic Peroxy Acids as Oxidizing Agents*—Daniel Swern. *Determination of Organic Peroxides by Physical, Chemical, and Colorimetric Methods*—R. D. Mair and R. T. Hall. *Physical Properties of Organic Peroxides*—Leonard S. Silbert. *Acyl Peroxides*—R. Hiatt.

1971 928 pages 59 illus. $39.95

FLUOROPOLYMERS

Edited by LEO A. WALL, *National Bureau of Standards, U. S. Department of Commerce*

Volume XXV in High Polymers

Editorial Board: H. Mark, P. J. Flory, C. S. Marvel, and H. W. Melville

Fluoropolymers critically reviews the synthesis, polymerization, and important physical properties of the family of polymers containing fluorine. It should be a particularly valuable volume for researchers and materials scientists interested in synthesizing new and known fluoropolymers, and for investigators seeking knowledge of the relationship between structure and chemical and physical properties.

1971 672 pages (aprox.) 149 illus. In Press

Prices subject to change without notice.

WILEY-INTERSCIENCE
a division of JOHN WILEY & SONS, Inc.
605 Third Avenue, New York, N.Y. 10016
In Canada: 22 Worcester Road, Rexdale, Ontario